Development of c-Met targeted chimeric antigen receptor T-cell immunotherapy for malignant pleural mesothelioma

Thayaparan, Thivyan

Awarding institution:
King's College London

Development of c-Met targeted chimeric antigen receptor T-cell immunotherapy for malignant pleural mesothelioma

THIVYAN THAYAPARAN, 1010643

SUBMITTED TO KING'S COLLEGE LONDON FOR THE AWARD OF DOCTOR OF PHILOSOPHY

CAR Mechanics Group, Research Oncology,
Division Of Cancer Studies, Faculty Of Life Sciences And Medicine,
King's College London

July 2016

Abstract

Malignant pleural mesothelioma (MPM) is an incurable cancer that commonly presents at an advanced stage. Although surgery, chemotherapy and radiotherapy treatment may be used, median survival from diagnosis is less than 12 months. Consequently, new therapeutic approaches are essential. Chimeric antigen receptors (CARs) are fusion molecules that couple the HLA-independent binding of a cell surface target to the delivery of a tailored T-cell activating signal. The receptor tyrosine kinase c-Met is overexpressed in >80% of MPM making it an attractive candidate for CAR T-cell immunotherapy. To target c-Met, three candidate CARs were developed named N28z, M28z and cM28z. All contained a CD28/CD3ζ endodomain fused to one of three stabilised peptides based on the N and K1 domains of hepatocyte growth factor, which is the only natural ligand for c-Met. Specificity and functionality of c-Met re-targeted CAR^+ T-cells was confirmed by co-cultivation with c-Met-expressing NIH 3T3 and MPM cell lines. This was indicated by target-dependent cytotoxicity and enhanced cytokine release (IL-2 and IFN-γ), when compared to appropriate controls. Anti-tumour activity of all three candidate CARs could be further enhanced by pre-treatment of tumour cells with poorly cytotoxic doses of chemotherapy (cisplatin and pemetrexed) or by co-incubation with the PD-1 blocker, pembrolizumab. No differences between function of the three candidate CARs were evident in these studies. To evaluate *in vivo* anti-tumour activity, an intraperitoneal MPM xenograft model was established that was amenable to monitoring using bioluminescence imaging. Candidate c-Met re-targeted CARs were co-expressed with the chimeric cytokine receptor, 4αβ, enabling IL-4 mediated, selective enrichment of CAR^+ T-cells. In mice with an established tumour burden, I found that cM28z/$4\alpha\beta^+$ T-cells were superior to other c-Met re-targeted or control T-cells in eliciting sustained disease control. Together, these findings demonstrate proof of concept for the utility of c-Met re-targeted CAR^+ T-cells to recognise and destroy mesothelioma tumour cells.

Table Of Contents

List Of Figures

List Of Tables

List Of Abbreviations

293T	Cell line derived from HEK293 cells that have been stable transfected with the SV40 T antigen
4αβ	IL-4Rα – IL-2/15Rβ chimeric cytokine receptor
aAPC	Artificial antigen presenting cells
AC	Adherent culture
ACD	Citrate Dextrose solution
ACT	Adoptive cell therapy
ADCC	Antibody dependent cell cytotoxicity
AICD	Activation induced cell death
ALL	Acute lymphoblastic Leukaemia
APC	Allophycocyanin
ATP	Adenosine triphosphate
BLI	Bioluminescent imaging
BSA	Bovine serum albumin
C	C terminal repeat
CA	Capsid
$CaCl_2$	Calcium Chloride
CAF	Cancer-associated fibroblast
CAIX	Carbonic anhydrase IX
CAR	Chimeric antigen receptor
CASP	Caspase
CALGB	Cancer and Leukaemia group B
CBD	Cell binding domain
CCR	Chemokine receptor
CD	Cluster of differentiation
CD44v6	CD44 exon variant 6
cDNA	Complementary DNA
CEA	Carcinoembryonic antigen
CH	Constant heavy
CIP	Calf Intestinal Alkaline Phosphatase
CLL	Chronic lymphocytic Leukaemia
cM28z	CAR comprised cdM2.2 D127N, CD28 and CD3ζ
cM4	Combined expression of cM28z and 4αβ
CMV	Cytomegalovirus
CO_2	Carbon Dioxide
CPDA	Citrate phosphatase dextrose adenine

CR	Complete response
CRP	C-reactive protein
CRS	Cytokine release syndrome
CRUK	Cancer Research UK
CSF-1	Colony-stimulating factor-1
CT	Computer-tomography
CTA	Cancer-testis antigen
cTCR	Chimeric T-cell receptor
CTL	Cytotoxic T-lymphocytes
CTLA	Cytotoxic T-lymphocyte-associated protein
CTP	Cytosine triphosphate
DAMP	Damage associated molecular pattern
DAP10	DNAX-activation protein-10
dATP	Deoxyadenosine triphosphate
DC	Dendritic Cells
DEAE	Diethyaminoethyl
dH2O	Distilled water
DMEM	Dulbecco's Modified Eagle Medium
DMSO	Dimethyl Sulfoxide
DNA	Deoxyribonucleic acid
dsDNA	Double stranded DNA
E.Coli'	*Escherichia Coli*
EBV	Epstein-Barr virus
EDTA	Ethylenediaminetetraacetic acid
EGF	Epidermal growth factor
EGFR	Epidermal growth factor receptor
EGFRvIII	Epidermal growth factor receptor variant III
ELISA	Enzyme linked immunosorbent assay
EORTC	European Organisation for Research and Treatment of Cancer
ErbB	Erythroblastosis oncogene B
ERK	Extracellular signal-regulated kinase
EtOH	Ethanol
FACS	Fluorescence activated cell sorting
FAK	Focal adhesion kinase
FAP	Fibroblast activation protein
FasL	Fas ligand
FBS	Foetal Bovine Serum
CS	Calf Serum
FcγR	Fc gamma receptor

FDA	Food and Drug Administration
ffLuc	Firefly Luciferase
FITC	Fluorescein isothiocyanate
FMS	Macrophage colony stimulating factor-1 receptor
Fra-1	Fos-related antigen 1
G	Gauge
Gab1	Grb2-associated binding protein 1
GALV	Gibbon-Ape Leukaemia Virus
GD2	Diasialoganglioside-2
Gen	Generation
GITR	Glucocorticoid-induced TNFR family related gene
GM-CSF	Granulocyte macrophage colony-stimulating factor
Grb2	Growth factor receptor-bound protein 2
GTP	Guanidine triphosphate
GvHD	Graft versus Host Disease
H	Hairpin
H29D	Human retroviral packaging cell line derived from HEK293 cells, expressing the MoMLV *gag-pol* genes and the VSVIG *env* gene
H_2O	Dihydrogen mono-oxide
H_2SO_4	Sulfuric acid
HCl	Hydrochloric acid
HCM	Human cardiac myocytes
HER	Human Epithelial Growth Factor Receptor
HEPES	4-(2hydroxethyl)-1-pierazineethanesulfonic acid
HGF	Hepatocyte growth factor
HIV	Human immunodeficiency virus
HLA	Human leukocyte antigen
HMGB1	High mobility group box 1
HRP	Horseradish Peroxidase
HS	Human serum
HSCT	Heamatopoetic stem cell transplant
HSPG	Heparin sulphate proteoglycans
hTERT	human telomerase reverse transcriptase
IC	Intracellular
ICAM	Intracellular adhesion molecule
ICOS	Inducible co-stimulatory
IDO	Indoleamine 2,3-dioxygenase
IFN	Interferon
Ig	Immunoglobulin

IL	Interleukin
i.p.	Intra-peritoneal
IPT	Imunoglobulin-plexin-transcription
IRES	Internal ribosome entry site
ITAM	Immunoreceptor tyrosine-based activation motif
i.v.	Intra-venous
JM	Juxtamembrane
K	Kringle
KCl	Potassium Chloride
KOH	Potassium hydroxide
LB	Luria Broth
LFA	Lymphocyte function associated antigen
LT	ffLuc and the red fluorescent protein, tdTomato
LTR	Long terminal repeat
LUC	Luciferase
M28z	CAR comprised M2.2 D127N, CD28 and CD3ζ
M4	Combined expression of M28z and 4αβ
mAb	Monoclonal Antibody
MAPK	Mitogen-activated protein kinase
MBS	Membrane Binding Solution
MeOH	Methanol
c-Met/MET	Mesenchymal-epithelial transition factor
$MgCl_2$	Magnesium Chloride
$MgSO_4$	Magnesium Sulphate
MHC	Major Histocompatibility Complex
MMP	Matrix metalloproteinases
MoMLV	Moloney murine leukaemia virus
MPM	Malignant pleural mesothelioma
mRNA	Messenger RNA
MSKCC	Memorial Sloan Kettering Cancer Centre
MSLN	Mesothelin
MTD	Maximum tolerated dose
MTT	3-[4,5-dimethylthiazol-2-yl]- 2,5I- diphenyltetrazolium bromide; thiazolyl blue
MUC	Mucin
MWS	Membrane Wash Solution
N28z	CAR comprised of Ik1, CD28 and CD3ζ
N4	Combined expression of N28z and 4αβ
NaCl	Sodium Chloride

NaOH	Sodium Hydroxide
NC	Nucleocapsid
NCAM	Neural cell adhesion molecule
NCI	National Cancer Institute
NEB	New England Biolabs
NHL	Non-Hodgkin's lymphoma
NIH	National Institutes of Health
NK-cells	Natural killer cells
NSCLC	Non-small cell lung cancer
NSG	NOD.Cg-Prkdc^{scid} Il2rg^{tm1wjl}/SzJ murine strain
NY-ESO	New York Oesophageal antigen-1
OR	Objective response
OS	Overall survival
PAC	Pancreatic adenocarcinoma
PBMCs	Peripheral blood mononuclear cells
PBS	Phosphate buffered saline
PCR	Polymerase Chain Reaction
PD-1	Programmed death-1
PD-L1	Programmed death-Ligand 1
PD-L2	Programmed death-Ligand 2
PE	phycoerythrin
PEI	Polyethylenimine
PerCP	Peridinin chlorophyll protein complex
PF	Progression-free
PFS	Progression-free survival
PG13	Murine retroviral packaging cell derived from NIH 3T3 fibroblasts, containing the MoMLV *gag-pol* genes and the GALV *env* gene
PI3K	phosphatidylinositol 3-kinase
PKC	Protein kinase-C
PLCγ	Phospholipase-Cγ
PR	Partial remission
PR	Partial response
PSCA	Prostate stem cell antigen
PSMA	Prostate specific membrane antigen
R	Receptor
r	Recombinant
RCR	Replication-competent retrovirus
RN	RetroNectin
RNA	Ribonucleic acid

ROI	Region of interest
ROR1	Receptor orphan tyrosine kinase receptor 1
RPM	Revolutions per minute
RPMI	Roswell Park Memorial Institute
RR	Response rate
SAE	Serious adverse event
SARS	Severe acute respiratory syndrome
s.c.	Subcutaneous
scFv	Single chain variable fragment
SCID	Severe combined immunodeficiency
SD	Stable disease
SD	Standard deviation
SEM	Standard error of the mean
SEMA	Semaphorin
SDS	Sodium dodecyl sulphate
SOC	Super optimal broth with catabolite repression
SPH	Serine protease homology domain
STAT	Signal transducer and activator of transcription
SV40	Simian virus 40
T1E	EGF/TGFα chimera
T28z	CAR comprised of T1E peptide, CD28 and CD3ζ
T4	Combined expression of T28z and 4αβ
T2A	*Thosea-asigna* virus 2A
TAA	Tumour associated antigen
TAM	Tumour associated macrophages
TBE	Tris-borate EDTA
TCR	T-cell receptor
tdTom	tdTomato
TGF	Transforming growth factor
TILs	Tumour infiltrating lymphocytes
TK	Tyrosine kinase
T_M	Melting Temperature
Tm	Transmembrane
TMB	Tetramethylbenzadine
TNF	Tumour necrosis factor
TNM	Tumour Node Metastasis
Treg	Regulatory T-cells
Tris-Cl	Tris-hydroxymethyl-amino methane
TSA	Tumour-specific antigen

T_{SCM}	Memory stem T-cell
tTa	Tetracycline-transactivator
UPenn	University of Pennsylvania
UT	Untransduced
V28z	CAR comprised of avb6-targeting peptide (abrogated binding activity due to scrambled amino acid sequence), CD28 and CD3ζ
V4	Combined expression of V28z and 4αβ
v/v	volume/volume
v/w	volume/weight
VEGF	Vascular endothelial growth factor
V_H	Variable heavy chain
V_L	Variable light chain
VSV-G	Vesicular stomatis virus G
w/v	weight/volume
WT	Wild type
WT-1	Wilm's Tumour antigen 1
Zap-70	Zeta-chain associated protein 70
βc	β-chain
γc	Common γ-chain

Acknowledgements

Firstly, I wish to express my sincere gratitude to my supervisor *Dr John Maher* for providing me with the opportunity to undertake this PhD and The British Lung Foundation for the generous grant. John, thank you for the continual support, advice and motivation. As you mentioned throughout, a PhD is character building and this incredible journey has definitely been a true testament. It has not always been straightforward but you have taught me to be more confident about my ideas and research, for which I am very grateful. Thank you for always making yourself available – your selfless time, energy and passion is inspirational. One could not have wished for a better mentor.

My sincere thanks also go to *Dr James Spicer* for the encouragement and opportunities you afforded me. The experience I gained presenting at International conferences such as British Thoracic Oncology Group and AACR were invaluable.

I am particularly grateful to *Ana* for teaching me everything when I first came to the lab. During those initial months, your mentorship and guidance gave me confidence to apply for this PhD studentship within an immensely exciting field of study. If you had not fought my corner – I would not be here today. Thank you for your constant support, advice, honesty and motivational words of wisdom – all with true Portuguese flair! *Lynsey* - "my G&T partner in crime" - thank you for all of the advice, support and friendship over the last three years.

Marc, it's fair to say I have been very fortunate to experience your omnipotent knowledge and work ethic first hand. Thank you for always taking the time to answer my many questions. Your advice and support has been greatly appreciated. *Nia*, to think the workplace may actually have been "boring", sorry normal, before you arrived! I am ever so thankful for all of your advice, motivation and critical analysis (much needed) throughout my PhD. I am also very grateful to you, Ana and Lynsey for all of the advice whilst writing this Thesis. *Tom*, thank you for your support during this PhD.

To all those (past and present) in the CAR Mechanics Group, Immuno-Engineering and BCBG, *Sophie*, *Antonella*, *May*, *Astero*, *Vincent*, *Erin*, *Daniella*, *Ben*, *Artemis*, *Mustafa*, *Michael*, *Fiona*, *Franco*, *Debbie*, *Prof Joy Burchell* and *Prof Joyce Taylor-Papadimitriou*. Thank you for all of your help and laughter, making the Research Oncology offices a fantastic place to work.

Sjoukje, you were simply inspirational when I first joined. Thank you for always being there, whenever needed, and for all of the advice and support you continue to provide. You have and always will be a true friend. *Bauke*, *Maarten* and *Christos* – my fellow iCell Therapeutics alumni – it has been a great ride. Working with you guys has brought much laughter and enjoyment throughout and I am fortunate to be able to count on such good friends as yourselves.

Adam, I am ever so grateful for your support and encouragement. You have always been ready and willing to help whenever required, no questions asked. *Sangeetha*, I am very grateful for your help and support throughout the writing of this thesis. Thank you.

Roseanna, where does one start. I would not have made it without your endless love and support. You have always been there for me throughout this PhD and I am eternally grateful. Thank you for everything. I know you will continue to do great during your PhD!

Last but not the least, I would like to thank my family: my parents and to my sister for their unconditional support throughout. I am truly blessed to have such a loving family – thank you. *Dhanusha*, I'm sure you'll be glad to see me finally finish studying and "get a proper job". *Mum* and *Dad*, I am forever grateful to you both for the sacrifices made to allow me to pursue my dream of attaining this Doctorate.

This thesis is dedicated to my parents
for their love, endless support
and encouragement.

CHAPTER 1 Introduction

1.1 Malignant mesothelioma

1.1.1 Epidemiology and Aetiology

Malignant mesothelioma is a devastating cancer that arises from the mesothelial cells lining the body cavities and is associated with high morbidity and mortality. In approximately 90% of cases, the disorder occurs in the pleural space (Figure 1-1). However, mesothelioma may also originate in the peritoneal cavity, pericardium or tunica vaginalis.

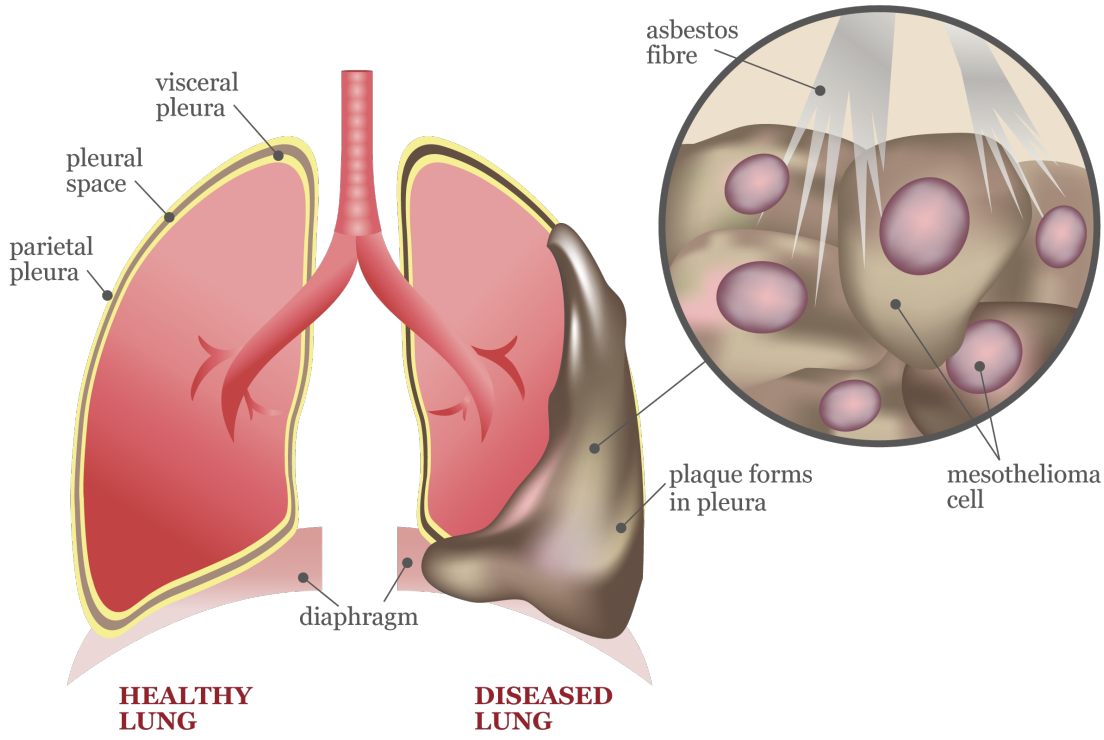

Figure 1-1. Comparison between healthy lung and malignant pleural mesothelioma lung.
Illustration comparing a healthy lung (left) with a diseased MPM lung (right). Inhalation of asbestos fibres results in chronic inflammation leading to development of MPM and plaque formation in pleura. Parietal pleura – outer layer, Pleural space – between the parietal pleura and visceral pleural, Visceral pleura – encompasses lungs. Adapted from [1].

The primary causative agent associated with the development of malignant mesothelioma is inhalation of asbestos fibres (80% attributable fraction [2]). Industrial use of asbestos was widespread in many countries during the twentieth century, until asbestos mining was banned during the 1980's and 1990's in most developed nations. However, it is still mined today in Russia, China, Brazil and Canada and is widely used both in these countries and other developing countries such as India. Additionally, concomitant smoking enhances the risk of malignancy in an asbestos worker, with a 60-fold increased risk of developing non-small cell lung cancer [3, 4]. Although asbestos workers are at highest risk of development of mesothelioma, family members are also at increased risk due to fibre exposure from primary clothing bought home.

There is a long latent period between asbestos exposure and the development of mesothelioma (average 30-40 years) [5]. Consequently, the incidence of mesothelioma continues to rise despite tighter regulation and decreased use of asbestos [6]. The UK mortality rate has increased from below 160 deaths in 1968 to more than 2000 deaths in 2005 [7] (Figure 1-2). It is predicted that the incidence of mesothelioma will peak in Europe between 2015 and 2020 [8, 9]. Within the United States of America, over 100,000 new cases of mesothelioma are predicted over the next four decades. For those countries still mining and using asbestos in large quantities, rates of mesothelioma are expected to continue increasing decades after its use is banned, however this is still yet to be implemented.

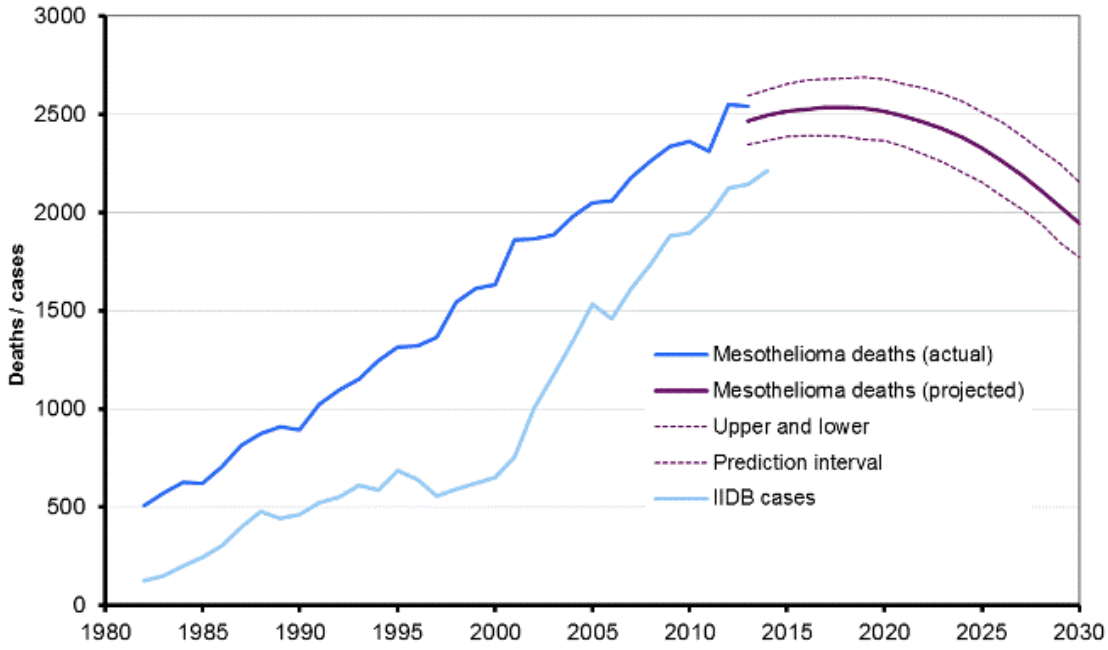

Figure 1-2. Mesothelioma in Great Britain: annual deaths and projected future deaths.
There were 2,538 mesothelioma deaths (2,123 males and 415 females) in Great Britain during 2013 with 2,548 deaths in 2012. Projected annual deaths are 2,500 annually for remainder of this decade. *IIDB, Industrial Injuries Disablement Benefit.*
From http://www.hse.gov.uk/Statistics/causdis/mesothelioma/index.htm (accessed May 21st, 2016)

Cancer risk is greatest following exposure to the needle-like asbestos fibres that constitute the amphiboles (sharp, rod-like), best exemplified by crocidolite (blue) and amosite (brown) asbestos. Although these forms of asbestos are rarely used today, serpentine or chrysotile asbestos (white) is still mined and used widely throughout many parts of the world and is also linked to induction of both mesothelioma and other cancers [10]. These fibres are typically found within brake linings, ships building and ceiling or pool tiles [4]. Thus, as exposure is work-related, mesothelioma is largely considered to be an occupational disease and because past exposure was more common in occupations with a predominantly male workforce, the current incidence of mesothelioma is higher in men.

Other risk factors for mesothelioma are less well understood but include underlying genetic background [11], radiation exposure (e.g. radiotherapy for other malignancies such as lung and breast cancer [12]) and exposure to non-asbestos mineral fibres, notably erionite [13]. Prior infection with the simian virus 40 (SV40), a DNA tumour virus, has also been implicated in disease development [5, 14, 15]. It is also established that patients who smoke and have been exposed to asbestos have a higher risk of

developing lung cancer [16]. More recently, concern has been raised about the potential genotoxicity of carbon nanotubes. These possess asbestos-like morphological features and are increasingly used in modern technologies and manufacturing processes [17, 18].

1.1.2 Molecular pathogenesis

Several molecular defects have been described in malignant mesothelioma cells (reviewed in [19, 20]). Mutation induced defects in the function of tumour suppressor genes are prevalent, notably affecting the *CDKN2A* gene (encoding $p16^{INK4a}$/ cyclin-dependent kinase inhibitor 2A and $p14^{ARF}$/ alternative reading frame), *NF2* (encoding neurofibromatosis type 2/ merlin) and the *BAP1* gene, which encodes for the BRCA1-associated protein-1 [20, 21]. In addition, aberrant activation of the Wnt pathway occurs in the majority of mesotheliomas, indicated by cytoplasmic accumulation of β-catenin [21]. Furthermore, multiple receptor tyrosine kinases (RTKs) are commonly over-active in mesothelioma cells, leading to enhanced signalling via the Ras-MAP (mitogen-activated protein) kinase and phosphatidylinositol 3-kinase pathways. Among a panel of 42 such receptors analysed, the c-Met and epidermal growth factor receptors (EGFR) are activated most frequently in this disease [22]. In addition, several other receptors are commonly upregulated in mesothelioma, including AXL, insulin-like growth factor-1 receptor, vascular endothelial growth factor receptor (VEGFR)-2, RON and other members of the ErbB family [23, 24].

In the majority of cases, mesothelioma is believed to originate as a result of chronic asbestos-induced serosal inflammation. The physico-chemical properties of amphibole asbestos in particular facilitate its deposition and long-term persistence in both the lungs and pleura. Several contributory immunopathological mechanisms have been described that may link asbestos exposure to mesothelioma development. Asbestos fibres are mutagenic and elicit DNA damage primarily from the release of reactive oxygen and nitrogen species, both by phagocytic and mesothelial cells [25]. Furthermore, asbestos triggers an inflammatory response, owing in large part to its ability to promote the release of the high-mobility group box 1 (HMGB1) protein [21].

HMGB1 is an example of a “damage-associated molecular pattern” (DAMP) molecule that acts as a potent inflammatory cue through at least two distinct mechanisms. First, HMGB1 activates a multi-protein complex termed the NLRP3 inflammasome, found within phagocytes, mesothelium and other cell types [26]. Inflammasome activation promotes the caspase 1-dependent maturation of interleukin (IL)-1β and IL-18. In turn, this triggers the subsequent release of a cascade of chemotactic, mitogenic and angiogenic factors, some of which have transforming properties when cultured with

mesothelial cells [27]. However, although NLRP3-deficient mice manifest a reduction in asbestos-induced lung pathology [21], they are not protected from asbestos-induced peritoneal mesothelioma [28]. A second action of HMGB1 is to instigate the release of tumour necrosis factor (TNF)-α. This provides NFκB-dependent survival signals to mesothelial cells, some of which may harbour an asbestos-induced mutational load [29, 30].

1.1.3 Clinical presentation

Although mesothelioma may present in various tissue types, over 90% of cases occur within the pleura, termed malignant pleural mesothelioma (MPM). Patients frequently present with symptoms of breathlessness and chest pain that is often insidious with the result that disease is often advanced at the time of diagnosis. Imaging modalities such as chest x-ray and computed tomography (CT) usually show evidence of pleural effusion and/ or irregular pleural thickening within the chest cavity. However, these features are not unique to MPM and a definitive tissue diagnosis is required.

Three major histological subtypes of mesothelioma have been described: epithelioid, sarcomatoid and biphasic. The epithelioid variant is most common (>50% in most series) and has a slightly better prognosis compared between tumours with sarcomatoid features. The sarcomatoid subtype is associated with the poorest prognosis and accounts for 10% of patients. As determined by histopathology, biphasic tumours comprise at least 10% of elements from both epithelioid and sarcomatoid tumours [31].

1.1.4 Diagnosis

Definitive diagnosis of malignant mesothelioma can be challenging and requires obtaining an adequate amount of tissue. Generally, this requires a pleural biopsy obtained by thoracoscopy or needle biopsy of pleural tissue under CT guidance, or more radically, at the time of open thoracotomy. However, tissue obtained during these procedures may be compromised by sampling error and small sample size. Initially haematoxylin and eosin (H&E) staining is required to detect characteristic morphological abnormalities consistent with a malignant process of the pleural lining. Due to the limited tissue collected, almost 25% of patients experience an under-classification in the correct histology [4].

Immunohistochemical staining is important to distinguish between mesothelioma and adenocarcinomas of lung origin or metastasis [32]. Biomarkers typically found within mesothelioma, such as calretinin – which is positive in mesothelioma with a reported sensitivity of 95% and specificity of 87% and thrombomodulin, with a 92% specificity (but less sensitive at 68%) help to discriminate this tumour from other differential

diagnoses [33]. The International Mesothelioma Interest Group (IMIG) established guidelines for diagnosing mesothelioma using a panel of histochemical markers (<80% sensitive) [32].

1.1.5 Staging

A number of staging systems have been used for mesothelioma over the years, almost exclusively pertaining to primary pleural mesothelioma [4]. Peritoneal mesothelioma does not have its own staging system. The oldest staging system is the Butchart system – which is still regularly used in certain countries. It is based upon a simple description of the extent of disease irrespective of histological subtype: pleural contained (Stage I), chest wall or mediastinal invasion (Stage II), peritoneal or diaphragmatic penetration (Stage III), or distant metastases (Stage IV).

The most practical and ubiquitously used system is the tumour-node-metastasis (TNM) protocol developed by IMIG (Figure 1-3) [34]. The American Joint Committee on Cancer also currently adopts this system as the accepted standard [35]. Most patients present with advanced disease that is usually considered unresectable.

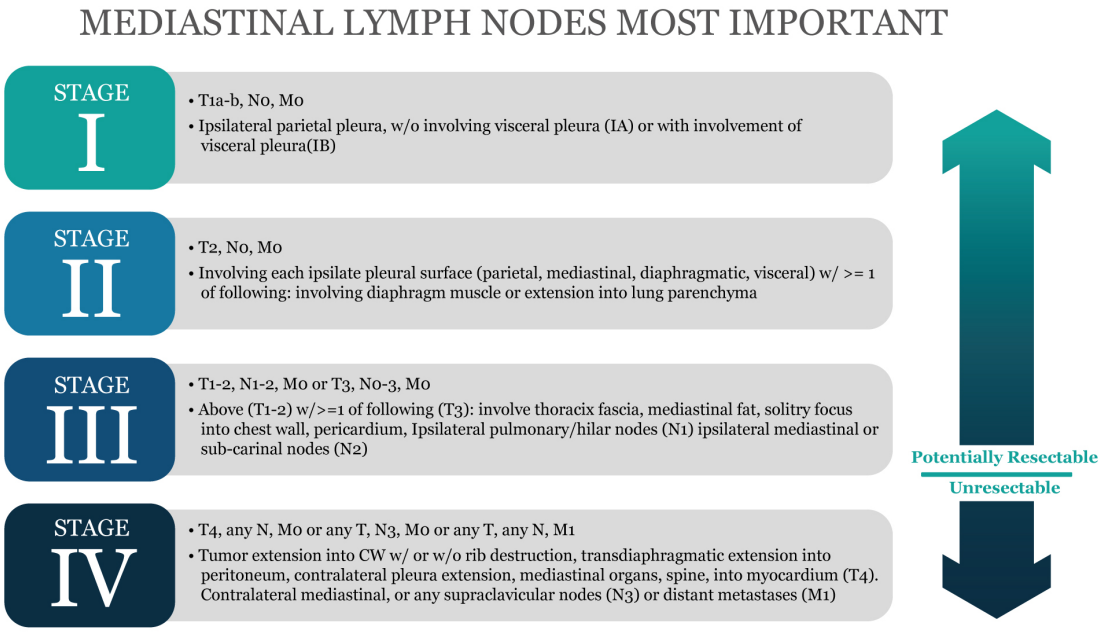

Figure 1-3. Tumour-node-metastasis staging system for mesothelioma.
Modified from [4].
Protocol developed by the International Mesothelioma Interest Group.

1.1.6 Prognostic factors

Prognostic factors affecting patient outcome have been determined from large multicentre trials [36]. Factors associated with poorer prognosis in patients with MPM include poor performance status, advanced stage of disease (e.g. stage III/IV), non-epithelioid histology, weight loss, anaemia, elevated lactate dehydrogenase, elevated white blood cell count and elevated platelet count. Subsequently, the European Organisation for Research and Treatment of Cancer (EORTC) and the Cancer and Leukaemia Group B (CALGB) developed three prognostic scoring methods [37, 38].

The effect of immune system status is increasingly studied to predict patient survival in many malignancies. A low lymphocyte count has recurrently been seen a number of advanced stage cancer patients, and is often associated with poor overall survival [39-41]. Monocytes are also prevalent immune cells in cancer and are recruited into tumours where they alter the tumour microenvironment, promoting tumour progression via local immune suppression and angiogenesis [42]. A high monocyte count has previously been reported as a poor prognosis factor in patients with solid malignancies [43-45]. Furthermore, a low lymphocyte-to-monocyte ratio (LMR), defined as the absolute lymphocyte count divided by the absolute monocyte count, is reportedly correlated to unfavourable prognosis within a multitude of cancers [46]. Two recent studies have reported the prognostic significance of LMR in patients with MPM. Yamagishi et al. studied 150 patients and observed that an elevated LMR was independently associated with increased overall survival (OS) [47]. Similarly, Tanrikulu et al., analysed 292 MPM patients and showed that a decreased LMR was associated with worse survival [48].

Several immune biomarkers have been investigated for their prognostic value in patients with MPM. Illustrating this, plasma Activin A has recently been linked to diagnosis and tumour volume in MPM and to poorer outcome in patients with epithelioid tumours [49]. Similarly, the immune checkpoint receptor CTLA-4 is relatively well characterised as a negative regulator of T-cell mediated immune response, and has recently been studied for its prognostic value in MPM. Roncellaet al., investigated CTLA-4 expression in MPM by immunohistochemistry (IHC), and soluble (s)CTLA-4 levels within sera and matched pleural effusions using ELISA from 45 patents [50]. A positive correlation was observed between pleural effusion (PE) sCTLA-4 levels and OS in MPM patients. This study was considerably smaller in cohort size than the previous studies detailed above however further experimental assessment will be required before both prognostic markers may be utilised within the clinic.

1.1.7 Treatment of mesothelioma: current standard of care to novel agents

The management of malignant mesothelioma remains controversial and at present, there is no known curative treatment for MPM. The role of radical surgery as part of multi-modality therapy has been promoted [51]. However, the incidence of post-operative morbidity is relatively high and survival benefit remains unproven [52]. Palliative combination chemotherapy using an anti-folate agent (pemetrexed or raltitrexed) in combination with cisplatin has been shown to prolong survival by a few months in suitable patients [53, 54]. However, only a minority of patients respond well to such therapy. Forms of immunotherapy have also been used to treat pleural mesothelioma with varying limited effects. Perhaps unsurprisingly, this form of treatment seems to be most active in patients with very early stage disease [55-57]. Molecular targeted therapy has also emerged as an interesting modality with further searches ongoing for therapeutic targets of interest [58-62]. Irrespective of management regimen, long-term control of malignant mesothelioma remains elusive and prognosis is generally poor with a median survival from presentation of 9 - 12 months [63].

1.1.7.1 Surgery

Eligible MPM patients may be offered two main surgical procedures, namely extrapleural pneumonectomy (EPP) or partial pleurectomy/decortication.

Extrapleural pneumonectomy is a major surgical procedure that entails radical excision of the entire lung, including visceral and parietal pleura, pericardium and diaphragm, followed by synthetic reconstruction. Usefulness of this surgical procedure is controversial, although it may benefit a small sub-group of fit patients with epithelioid histology, no evidence of extra-pleural nodal involvement and in whom negative surgical resection margins can be achieved [64]. Nonetheless, this extensive surgical procedure is associated with a high morbidity and mortality rate of 50% and 4% respectively [65] and current guidelines are that EPP should only be performed in the context of a clinical trial, in specialised centres as a part of a multimodality treatment regimen [66, 67]. No randomised trial has yet shown a survival benefit with EPP. The MARS (Mesothelioma and Radical Surgery) trial was established to define the role of EPP in the context of a trimodal therapy (either preoperative chemotherapy followed by postoperative hemithorax radiotherapy or to no EPP) [68]. Patients were assigned to EPP followed by post-operative hemithorax irradiation or no EPP surgery. The study ended with 50 patients accrued over a 3-year period (primary endpoint); however it was not significantly powered to analyse the effectiveness of surgery [69]. The results determined that due to the high morbidity associated with EPP, a trimodal therapy including EPP offers no benefit, thereby causing potential harm to the patient [52].

Partial pleurectomy or decortication can be defined as significant but incomplete resection of the pleural tumour and is often used to relieve an entrapped lung and/ or palliate control of chest wall pain. Though this form of surgery is not performed with curative intent, it plays a significant role in a sub-group of patients for symptom control.

1.1.7.2 Chemotherapy

Results published by Kao *et al.* in 2013 demonstrated that the majority of eligible mesothelioma patients pursue palliative therapy rather than aggressive surgery for disease management [70]. Despite extensive clinical research, only limited options involving combination chemotherapy have achieved a significant survival benefit for patients with MPM. Towards the end of the 20th century, it was accepted that a number of chemotherapy drugs achieved response rates of the order of 20% when administered as single agents, with no existing evidence at the time that combination chemotherapy offered any additional benefit [71]. In 2003, data from the EMPHACIS trial ("Evaluation of mesothelioma in a Phase III trial of pemetrexed with cisplatin") were published which caused a significant impact in medical management of this disease. EMPHACIS was a single blind international and multi-centre randomised controlled trial comprising 448 patients that compared the combination of pemetrexed (500mg/m^2) with cisplatin (75mg/m^2) to cisplatin alone (75mg/m^2), administered intravenously every 21 days [53]. The combination regimen was shown to significantly improve response rate (41% compared to 17% with single agent cisplatin), leading to an improvement in median survival from 9.3 to 12.1 months (hazard ratio (HR) 0.74, p = 0.0003). In addition, patients treated with the combination regimen demonstrated a statistically significant improvement in symptom control over 18 weeks, when compared with those who received cisplatin alone. Subsequently, van Meerbeeck *et al.* demonstrated that the combination of cisplatin plus ralitrexed improved median survival to 11.4 months, compared to 8.8 months for cisplatin alone [54]. As a result, the combination of cisplatin and pemetrexed is considered standard first-line systemic therapy for unresectable MPM, as recommended by the National Institute for Health and Care Excellence. This also constitutes standard recommended treatment in the adjuvant setting as part of combined modality treatment of resectable MPM disease [72].

Subsequent studies evaluating combination regimens including gemcitabine/platinum and vinorelbine/cisplatin have demonstrated response rates of 12-40% though, once more neither have shown significant benefit over active symptom control (ASC) [72]. The MSO1 trial, run by the Medical Research Council and British Thoracic Society, randomised 409 patients to either ASC, ASC and vinorelbine or ASC plus MVP (mitomycin, vinorelbine and cisplatin) with the combination of ASC plus vinorelbine resulting in a non-significant increase in median survival compared to either ASC alone

or ASC plus MVP (9.4 months compared to 7.6 or 7.8 months respectively; HR 0.81, p = 0.11) [73].

More recently, combinatorial strategies including targeted therapeutic agents have been evaluated in order to improve the response rate and outcome of first-line chemotherapy. The MAPS (Mesothelioma Avastin Cisplatin Pemetrexed Study) trial evaluated the combination of bevacizumab (15mg/kg for 6 cycles) plus cisplatin/pemetrexed for 6 cycles, followed by maintenance bevacizumab until the endpoint of disease progression was observed. Comparison was made with cisplatin/pemetrexed alone, which represented standard of care. A total of 448 patients were treated in this multicentre randomised phase II/ III French trial [74]. The median overall survival of patients enrolled in the triple treatment arm was 18.8 months, representing a 2.7 months increase in survival compared to the standard of care treatment arm (HR 0.76, p = 0.012). Patients who received triple therapy demonstrated a response rate of 14% and a 6-month disease control rate of 73.5%, compared with 43.2% in the control arm [75]. Furthermore, the benefit of triple therapy was not confined to patients in the best prognostic subgroups.

Despite these advances in medical management of MPM, the majority of patients fail to respond to these therapeutic approaches. Presently, there is no standard for second-line therapy available to those patients that are deemed suitable for further treatment. A number of studies with patients that did not receive pemetrexed as first line treatment have been conducted evaluating the use of pemetrexed, both as a single agent and in combination, however the benefits are limited [76, 77]. Furthermore, since the combination of pemetrexed and cisplatin is commonly given to those eligible as a standard first-line regimen, those eligible for pemetrexed as second-line treatment are few and far between.

1.1.7.3 Radiotherapy

The role of radiotherapy for the treatment of MPM is limited. This form of treatment has shown little benefit in reducing chest wall masses or alleviating pain. Furthermore, due to the extensive nature of the disease there is high risk of toxicity to the underlying lung [78] and responses are often of a transient nature. Data from a phase II study in which high dose hemithorax radiation was administered following EPP demonstrated low loco-regional recurrence [79] and a study looking at the role of intensity-modulated radiotherapy (IMRT) after EPP has achieved good local control, but with severe pulmonary toxicity [80].

1.1.7.4 Novel approaches: Targeted therapy and Immunotherapy

Despite the lack of driver mutations identified for targeted therapy within MPM, the resistance of this disease to conventional treatments has meant that a multitude of targeted agents have been trialled in patients with this disease (Table 1-1). Novel approaches targeting mesothelioma have been characterised according to Hanahan and Weinberg's "Hallmarks of Cancer" by Kondola *et al.* [81, 82]. The two most significant classes pertaining to this PhD will be described in more detail:

1.1.7.4.1 Receptor tyrosine kinase inhibitors

The capacity of tumour cells to release growth factors that facilitate and accelerate tumour cell growth has resulted in the development of drugs to antagonise the action of these growth factors. To date however, the majority of these trials have yielded disappointing results, with no meaningful increase in progression-free survival (PFS) for patients.

The epidermal growth factor receptor (EGFR) is expressed by a variety of epithelial malignancies. The dysregulation of EGFR activation results in reduced apoptosis, uncontrolled cell proliferation and increased angiogenesis [83]. Over-expression of EGFR is found in the majority of mesothelioma tumours [84-86]. A number of clinical trials have been conducted using EGFR inhibitors (Table 1-1), although disappointing results have been observed thus far. The results from recent studies assessing the tyrosine kinase inhibitor (TKI) gefitinib, in malignant mesothelioma are yet to be published (NCT00787410; NCT00025207). A further study is evaluating the use of cetuximab (a monoclonal antibody targeted against EGFR) combined with either cisplatin or carboplatin and pemetrexed (MesoMab - NCT00996567). Targeting of the insulin-like growth factor (IGF)-1 receptor is also under evaluation in MPM, using the inhibitor cixutumumab (IMC-A12 - NCT01160458). Tivantinib, a TKI targeting the c-Met receptor is further detailed in section 1.4.6, however a study was recently terminated in malignant mesothelioma (NCT01861301). A second study evaluating the combination of tivantinib plus the chemotherapy agents' pemetrexed and carboplatin is currently recruiting patients with both MPM and non-squamous cell lung cancer (NSCLC) (NCT02049060).

Table 1-1. Summary of published clinical trials evaluating EGFR inhibitors in malignant mesothelioma. Adapted from [87]

Agent	Study design	N	Median survival (months)	Overall 1-year survival	Response
Gefitinib [88]	Phase II No prior chemo	43	6.8	32%	1 CR 1 PR
Erlotinib [89]	Phase II No prior chemo	63	10	43%	No response
Erlotinib + Bevacizumab [90]	Phase II Prior chemo	24	5.8	24%	No response 12 SD
EGFR, epidermal growth factor receptor; N, number of patients; CR, complete response; PR, partial response.					

Vascular endothelial growth factor (VEGF) stimulates neovascularisation in a plethora of tumours, including MPM. Higher expression levels are associated with more-advanced disease and poorer prognosis [91]. Numerous clinical trials evaluating the effect of VEGF inhibitors either alone or in combination with chemotherapy in MPM have been conducted. Results to date have been largely disappointing and our summarised in a review by Kotova et al. [87].

1.1.7.4.2 Immunotherapy of mesothelioma using immune checkpoint blockade

Clinical evidence to date suggests that the immune system plays a critical role in protection against MPM [92-94]. Tumour infiltrating lymphocytes (TILs) play a significant role in anti-tumour responses, with the recognition of tumour-specific antigens. T-cell infiltration is strongly correlated with improved prognosis in several cancer types. In MPM, a high number of $CD8^+$ TILs has been reported to indicate improved prognosis [95-97]. The findings are subject to variance between studies however as investigators have also intimated there is no clear association [98]. Nonetheless, it is clear T lymphocytes are vital for anti-tumour activity however there are several mechanisms at play to evade immune destruction. Importantly, the host immune system retains potent mechanisms known as checkpoint molecules to stem potentially auto-reactive T-cells, preventing tissue damage in normal states.

The first checkpoint molecule to be successfully blocked for anti-cancer therapy was cytotoxic T lymphocyte antigen-4 (CTLA-4). Following normal T-cell activation, CTLA-4 is normally upregulated as a negative regulator, competing with the costimulatory molecule CD28 to bind to B7 ligands. This switches the positive costimulatory signal into a negative signal for activated T-cells. Although necessary under normal conditions to protect against autoimmunity, this mechanism is also manipulated by tumour cells to restrain antitumor immunity. By blocking checkpoint molecules, a strategy known as 'checkpoint blockade', the anti-tumour immune response can be restored. These agents have been established as a new drug class with meaningful therapeutic efficacy in many cancers, particularly melanoma [99].

Examples of monoclonal antibodies against CTLA-4 receptor include ipilumumab and tremelimumab. Currently the latter CTLA-4 inhibitor, Tremelimumab, is undergoing clinical evaluation in malignant mesothelioma. Building on preclinical evidence of synergy between chemotherapy and CTLA-4 therapy [100, 101], CTLA-4 blocking therapy has shown promise in MPM patients [102]. Calabro *et al.*, reported encouraging results with tremelimumab in patients with chemotherapy-resistant MPM (MESOT-TREM-2008; NCT01649024). With no serious adverse toxicity, disease control was reported in 31% patients with a median overall survival of 10.7 months, in comparison to 8.7 months for patients receiving second line chemotherapy (retrospective review) [103]. A second trial with 29 patients investigating a higher frequency of doses at a lower concentration of tremelimumab (10mg/kg) reported immune-related partial responses in 14% of patients and a disease control rate of 52%, with median OS of 11.3 months and median immune-related PFS of 6.2 months (NCT01655888) [104, 105]. A large, randomised phase II double blind trial comparing tremelimumab to placebo in pleural or peritoneal mesothelioma is ongoing (although no longer recruiting) and the field is awaiting the results (NCT01843374 – last verified May, 2016).

A second related mechanism by which tumour cells evade immune destruction involves the expression of programmed death 1 ligand and programmed death 2 ligand (PD-L1 and PD-L2). Expression of PD-L1 by MPM tumours has been evaluated predominantly by immunohistochemistry on formalin-fixed paraffin embedded material. The expression data reported has ranged between 20% and 70% depending on the respective threshold distinguishing positive PD-L1 expression in MPM. This has varied from >1% to ≥50% of expression between studies [106-109]. Most studies reporting the expression data have also specific expression based upon histological subtype (Table 1-2). Notably, expression of PD-L1 was associated with significantly poorer outcome. The median survival for patients whose tumours expressed PD-L1 was 5 months compared to 14.5 months for tumours devoid of PD-L1 expression ($p < 0.0001$) [107].

Table 1-2. Summary of PD-L1 expression published in mesothelioma using immunohistochemistry. Adapted from [109].

Method	Antibody clone	Sample size	Cut off (%)	% PD-L1+	Refs.
IHC	5H1-A3	106	≥ 5	40% (E 21%, S 94%, B 57%)	[107]
IHC	E1L3N	119	> 1	20% (E 13%, NE 38%)	[108]
IHC	5H1-A3	45	≥ 50	27% (E 17%, B 7%)	[110]
IHC	5H1-A3	33	≥ 5	70%	[111]
IHC	22C3	80	> 1	45.2%	[112]

IHC, immunohistochemistry; E, epithelioid subtype; S, sarcomatoid subtype; B, biphasic subtype; NE, non-epithelioid subtype. Cut off (%) represents the % threshold determining positive expression; % PD-L1 represents the % of tumours that were deemed positive by the criteria established in 'cut off % column'.

The first results of clinical evaluation of inhibition of the PD-1/PD-L1 axis in mesothelioma were presented last year. The KEYNOTE-028 (NCT02054806) trial is a nonrandomised Phase 1b study that is investigating activity and safety of the PD-1 inhibitory antibody pembrolizumab in patients with locally advanced or metastatic MPM. An overall disease control rate of 76% was observed (n=25 patients), with partial response in 28% and stable disease in 48% of patients [112]. The prolonged responses to date are striking although the relatively short follow-up time must be taken into consideration [112]. Other monoclonal antibodies against PD-L1 and PD-1 are currently being tested in phase II trials for patients with MPM (ClinicalTrials.gov identifiers: NCT02399371, NCT02497508) (Table 1-3).

However, it remains controversial as to whether PD-L1/2 expression constitutes a reliable biomarker of activity of checkpoint blockers that target this axis - conflicting observations have been reported by different groups [113, 114]. Presently, a phase II study is underway assessing pembrolizumab in malignant mesothelioma (NCT02399371). The study will also explore whether PD-L1 expression could be a good predictive biomarker for response to PD-1 inhibitors. A further study evaluating chemotherapy and/or pembrolizumab is due to commence shortly (NCT02784171). MPM patients will either receive cisplatin and pemetrexed alone or in conjunction with pembrolizumab compared to pembrolizumab alone.

Table 1-3. Selection of novel agents undergoing or about to undergo clinical evaluation in patients with malignant pleural mesothelioma. Adapted from [81].

Therapeutic Class	Agent	Phase	ClinicalTrials.gov identifier
Chemotherapy	Maintenance pemetrexed	II	NCT01085630
Antibody against CTLA-4	Tremelimumab	IIb	NCT01843374
Antibody against PD-1	Pembrolizumab	II	NCT02399371
Antibody against PD-1	Nivolumab	II	NCT02497508
Met Tyrosine kinase inhibitor	Tivantinib	I	NCT02049060
Met Tyrosine kinase inhibitor	Tivantinib	II	NCT01861301
Monoclonal antibody against mesothelin	Amatuximab	II	NCT02357147
Anti-mesothelin antibody-drug conjugate	BAY94-9343	I	NCT01439152
Pan-VEGF receptor tyrosine kinase inhibitor	Cediranib	I/II	NCT01064648

CTLA-4, cytotoxic T lymphocyte antigen-4; PD-1, programmed death 1; PD-L1, programmed death 1 ligand; VEGF, vascular endothelial growth factor; Met, mesenchymal epidermal transition factor.

From **https://clinicaltrials.gov/**, accessed May 21st, 2016

1.2 The c-Met receptor tyrosine kinase

1.2.1 c-Met receptor Structure and function

The *MET* proto-oncogene was first identified following the characterisation of a translocation in which a portion of this gene was joined to the translocated promoter region (TPR) locus [115]. The name MET was originally derived from the chemical that induced the TPR-MET translocation (*N*-**met**hyl-*N*'-nitroso-guanidine) but has also been used to in reference to its role in **met**astasis or **m**esenchymal-**e**pithelial **t**ransition [116]. The c-Met receptor is synthesised as a single polypeptide precursor of 1436 amino acids, and like its unique ligand, hepatocyte growth factor (HGF), it undergoes post-translational processing in order to become functional. Furin-mediated cleavage occurs between amino acids 307 and 308, leading to the formation of the mature αβ c-Met heterodimer. The resultant product functions as a single mature 190kDa unit that undergoes ligand-induced homodimerisation via the formation of a 2:2 complex with HGF [117] (Figure 1-4).

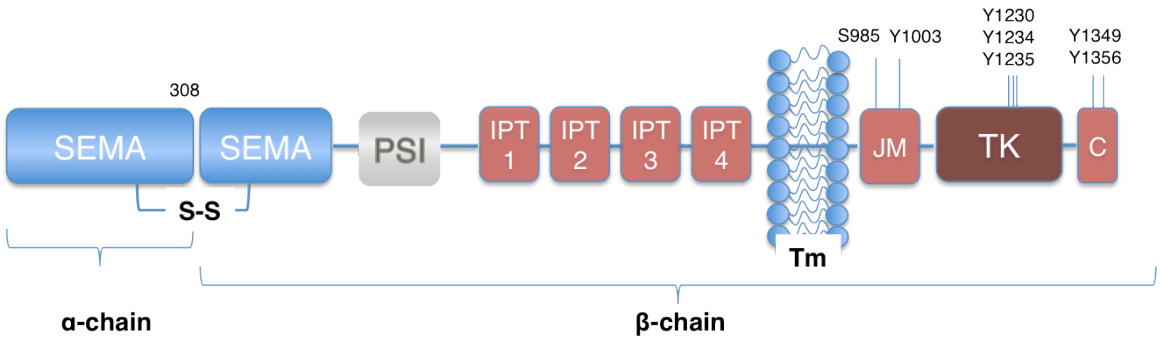

Figure 1-4. Structural domains present in the c-Met receptor tyrosine kinase. c-Met is produced as an inactive precursor that undergoes proteolytic cleavage and re-assembles as a disulphide-linked αβ heterodimer. The SEMA (semaphorin) domain comprises the α and part of the β chain and constitutes the main ligand-binding moiety. Next follows a cysteine rich PSI domain (found in plexins, semaphorins and integrin) and a sequence of four immunoglobulin-like IPT (immunoglobulin-plexin-transcription) domains, here numbered as IPT1-4. Following the transmembrane (Tm) region, the endodomain of the c-Met receptor contains a regulatory juxtamembrane (JM) region, catalytic tyrosine kinase (TK) domain and C-terminal motif (C). Key sites of tyrosine and serine phosphorylation within the receptor endodomain are indicated.

The extracellular region of c-Met comprises three distinct elements. The first of these is the N-terminal SEMA (semaphorin) domain, which shows homology to semaphorin and plexin family members and forms a seven bladed β-propeller fold [118]. The SEMA domain provides the HGF β-chain binding unit [119] and consists of the Met α subunit and proximal portion of the β chain. Following next is the cysteine-rich or PSI domain (found in plexins, semaphorins and integrin) and finally a sequence of four IPT (immunoglobulin-plexin-transcription) domains. The endodomain of the c-Met receptor is also divided into three modular components. The juxtamembrane region plays a key regulatory role and contains two elements that inhibit receptor function when phosphorylated. The first of these, S985, serves to inhibit receptor kinase activity [120]. Located closely downstream, Y1003 provides a c-Cbl ubiquitin protein ligase-binding motif that promotes the physiological down-regulation of receptor expression [121]. Immediately beyond the juxtamembrane region is the kinase/ catalytic element of the c-Met receptor. Upon binding of HGF, three closely located tyrosine residues (Y1230, Y1234, Y1235) are phosphorylated within the activation loop of the kinase domain, leading to initiation of tyrosine kinase catalytic activity [116, 122, 123]. As a result, two additional tyrosines (Y1349 and Y1356) in the terminal endodomain region (the unstructured C-terminal motif) are phosphorylated. This serves to create a “bi-dentate” docking site for several adaptor and signalling proteins, focussed around the Gab1 (Grb2 associated binder 1) adaptor and including Grb2-SOS (growth factor receptor bound protein 2 complexed with Son of Sevenless), SHC, Crk and Crk-like, pp60c-src, PI3K and phospholipase Cγ [124, 125]. Phosphorylation of both Y1349 and Y1356 is sufficient to render the c-Met receptor transforming [126]. Several downstream signalling systems are activated as a result, including the canonical Ras-MAP kinase/Bcl-xl, Rac/CDC42, PI3K/Akt, PI3K/Erk5/Fra1, Rap1/FAK, protein kinase C, Pak4 and STAT3 pathways [116, 127-129]. Collectively, these account at least in part for the diversity of mitogenic, motogenic and morphogenetic outputs elicited by this receptor ligand axis (Figure 1-5).

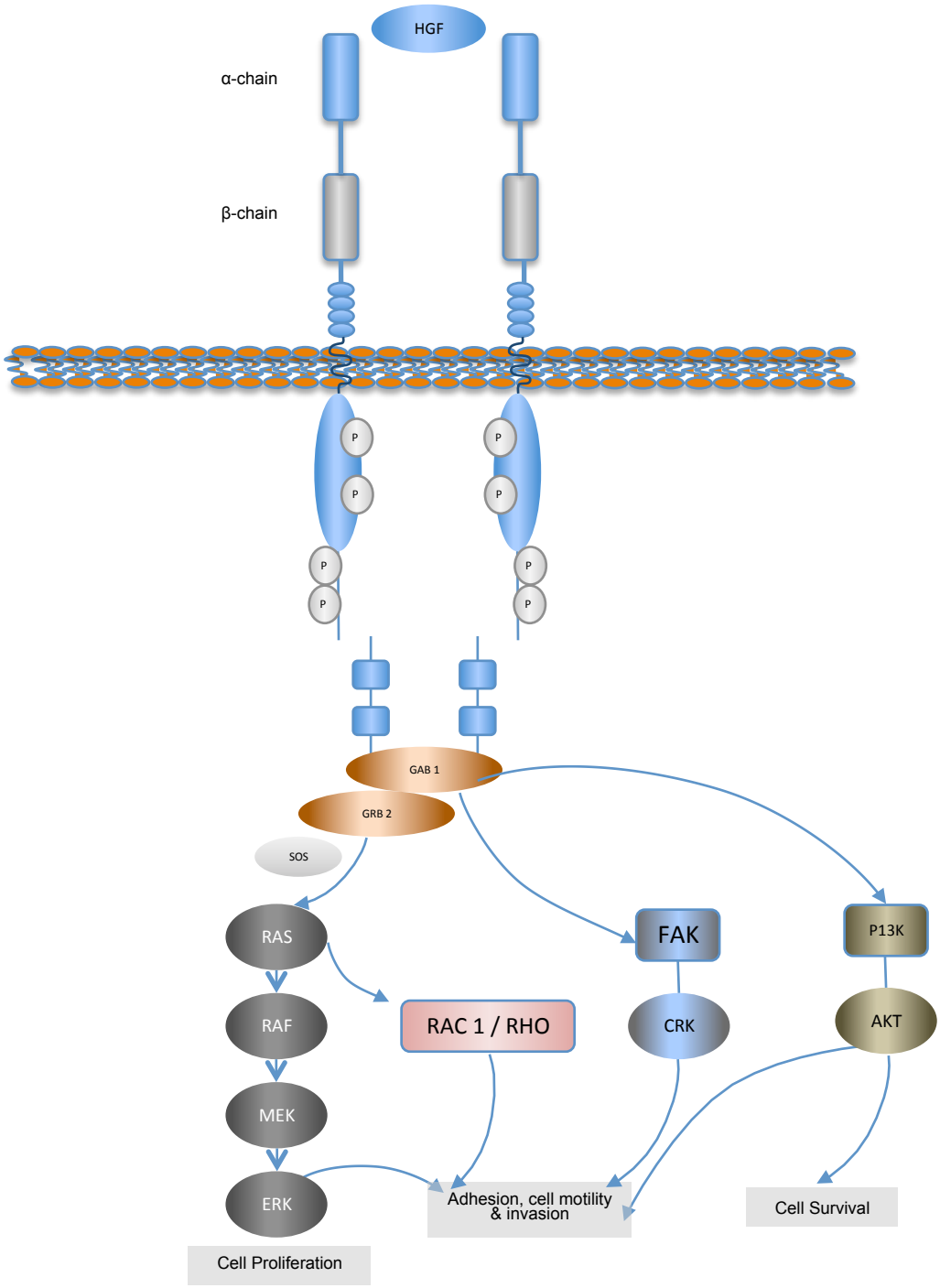

Figure 1-5. The HGF-c-Met Signalling Pathway
The main signalling pathways activated by the HGF-c-Met axis. HGF binding to c-Met stimulates receptor dimerisation, leading to the activation of different signalling pathways. Upon activation, c-Met kinase domain mediates signalling via adaptor proteins and other signalling proteins leading to (i) proliferation through MAPK activation, via Gab1-Grb2 resulting in Ras activation; (ii) cell survival via the PI3K and Gab1 mediated activation of AKT, resulting in an anti-apoptotic response; (iii) adhesion and cell motility mediated via Ras activation and direct interaction with the PI3K-FAK pathway which contributes to the invasive phenotype.

The c-Met receptor tyrosine kinase is activated upon binding by a single ligand species, named hepatocyte growth factor (HGF). Hepatocyte growth factor is principally secreted by a variety of mesenchymal cell types, including fibroblasts, vascular smooth muscle cells and other stromal cells, whereas c-Met is primarily expressed on the surface of epithelial cells. By this arrangement, the HGF/ c-Met axis establishes a mesenchymal–epithelial communication pathway that regulates a number of physiological processes, including embryogenesis, organ development, wound healing, angiogenesis and tissue homeostasis and regeneration [130]. In keeping with these fundamental activities, mice that are null for either *MET* or HGF are embryonically lethal [131-133]. Several functional consequences ensue after the binding of HGF to c-Met, including enhanced cell survival, proliferation, cell movement and branching morphogenesis.

1.3 Hepatocyte Growth Factor

Hepatocyte growth factor (HGF) is a 90 kiloDalton (kDa) cytokine that was independently identified as a stimulus to epithelial cell movement ("scatter factor" [134]) and as a potent stimulator of hepatocyte proliferation [135]. Cell scattering refers to the ability of HGF to disrupt E-cadherin-based cell-cell adhesion, followed by acquisition of a migratory and invasive fibroblast-like phenotype. Hepatocyte growth factor is a member of the plasminogen-related growth factor family and is elaborated as an inactive precursor polypeptide (pro-HGF) that binds c-Met, but does not activate receptor signalling. Pro-HGF protein contains a linear arrangement of six modular elements, namely an N-terminal hairpin (N), four Kringle domains (K1-K4) and a serine proteinase homology (SPH) region that lacks enzymatic activity (Figure 1-6). In response to tissue injury, this precursor undergoes proteolytic cleavage at the junction between R494 and V495 and re-assembles as a disulphide-linked active αβ heterodimeric unit [136]. While the α subunit alone can bind to c-Met with comparable affinity to HGF, it is biologically inactive [137]. A number of smaller splice variants of HGF have been described, including NK1, NK2 and NK4 (Figure 1-6). Several soluble and membrane anchored serine proteases have the capacity to activate pro-HGF, including HGF activator, urokinase-type plasminogen activator, matriptase, hepsin, plasma kallikrein and the coagulation Factors XIa and XIIa [116, 138]. Counterbalancing this, two inhibitors of pro-HGF activation have also been described [116].

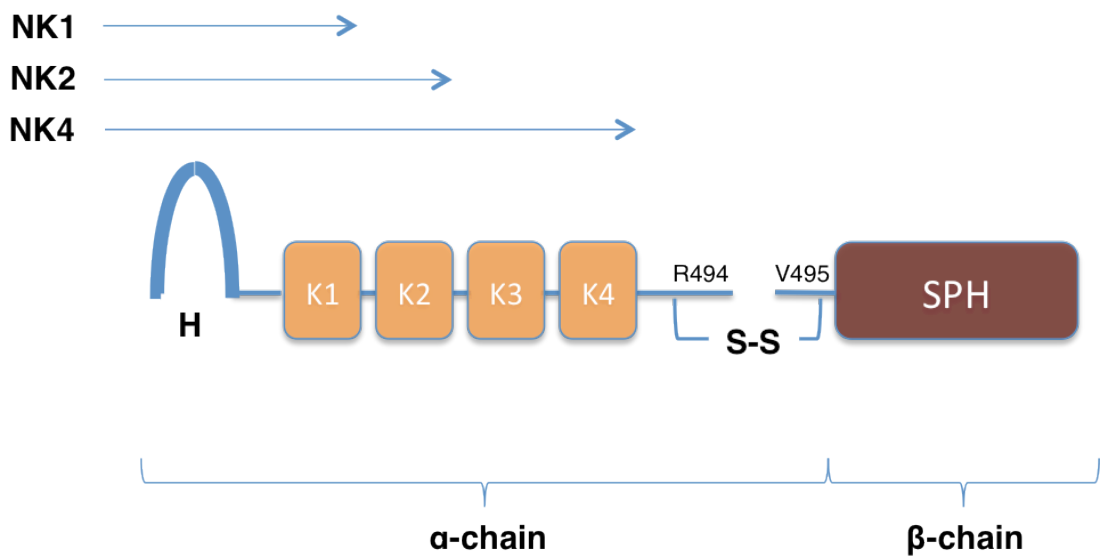

Figure 1-6. Structural domains present in hepatocyte growth factor
Hepatocyte growth factor is secreted as a single polypeptide precursor that undergoes proteolytic cleavage between R494 and V495. The resultant α and β chains form an interchain disulphide bond to yield the mature HGF heterodimer. The cartoon shows the structural domains present, namely the N-terminal hairpin (H), Kringle (K) domains 1-4 and the serine protease homology domain (SPH). A number of antagonistic or partial agonistic splice variants are also produced in which the N-terminal hairpin and 1 (NK1), 2 (NK2) and/ or 4 (NK4) Kringle domains are also present.

Following its secretion, much of HGF is tethered through binding to cell surface and matrix heparin sulphate proteoglycans [139]. Heparin sulphate proteoglycans play an important role in the presentation of HGF to the c-Met receptor [140]. Although heparin sulphate is not required for binding between HGF and c-Met, it potentiates ligand-induced c-Met dimerisation and subsequent functional outcome. The NK1 variant of HGF contains the high-affinity binding site for c-Met but it does not bind in the absence of heparin [141]. When basic amino acids responsible for heparin binding are substituted with glutamic acid, NK1 acquires the ability to bind c-Met in a heparin-independent manner. However, this mutein is functionally inactive and thus acts as a competitive c-Met antagonist [142].

1.4 The HGF/ c-Met axis and mesothelioma

Although activity of the HGF/ c-Met system is required for development, expression of these binding partners is generally found at low levels in healthy adult tissues. By contrast, dysregulation of the HGF/ c-Met system is prevalent in many lung and other cancers, including malignant mesothelioma, and may result from mutation, gene amplification or protein over-expression [143].

1.4.1 HGF expression in mesothelioma

Harvey and colleagues were first to investigate the expression of c-Met and HGF in malignant pleural mesothelioma (MPM) [144]. Using immunohistochemistry, they demonstrated that nine of nine MPM tumours (representing all three histological subtypes) were reactive for HGF. Eight of the tumours were graded as intensely positive, with uniform and diffuse cytoplasmic staining evident in tumour cells together with frequent stromal reactivity. In agreement with this finding, HGF was also detected in four of four tested MPM-associated pleural effusions [145].

Tolnay *et al.* subsequently assessed a larger number of MPMs and found that 33 of 39 stained positively with anti-HGF antibody. Once again, reactivity was evident in both in tumour cells and accompanying stroma [146]. While virtually all epithelioid and biphasic MPM were positive, the authors noted that biphasic tumours exhibited stronger staining in the epithelioid compared to the sarcomatoid portion. Furthermore, only 1 in 8 of the sarcomatoid tumours tested positive for HGF. Normal mesothelial cells were negative, a finding that contrasts with an earlier report of weak HGF expression in 4 of 8 cases [144]. Expression of HGF (but not c-Met) was correlated with tumour micro-vessel density, in keeping with the known role of HGF in promoting angiogenesis [146].

In keeping with these findings, serum levels of HGF (and epidermal growth factor (EGF)) are elevated in patients with mesothelioma, compared to healthy individuals of a similar age [147]. However, autocrine release of HGF is uncommon in immortalized MPM cell lines [148, 149], having primarily been described in cell types with a sarcomatoid or mixed phenotype [150]. By analogy with other tumour types [129], this raises the possibility that stroma is also an important source of HGF production in mesothelioma. In keeping with this, Li *et al.* have presented evidence that mesothelioma cells release platelet-derived growth factor and fibroblast growth factor, which in turn promote an influx of activated HGF-secreting fibroblasts into the tumour microenvironment [151]. This suggests that a paracrine relationship between stroma and tumour cells may also serve to reinforce disease progression in mesothelioma.

1.4.2 c-Met expression in mesothelioma

Using immunohistochemistry, Harvey *et al.* also demonstrated strong expression of the c-Met receptor in MPM tumour cells and associated stroma [144]. Once again, staining was diffuse and mainly cytoplasmic, with some membranous reactivity also apparent. Furthermore, in all six MPM-associated pleural effusions where tumour cells were identified, c-Met expression was detected [152]. These findings were subsequently extended in four larger series, which respectively demonstrated that 74% (n= 39) [146] 80% (n=35) [153], 82% (n=66) [147] and 76% (n=157) [154] of MPM tumours tested

positive for c-Met expression. Similar to HGF staining, expression was most common in epithelioid tumours, least frequent in sarcomatoid variants, whereas in biphasic MPMs, reactivity was most apparent in the epithelioid component [146]. Fluorescence *in situ* hybridisation confirmed a direct correlation between c-Met expression in tumours at the mRNA and protein levels [146]. In the majority of tumours tested, c-Met phosphorylation was detected [153, 154]. In mesotheliomas with high-level expression, c-Met was predominantly located on the plasma membrane, whereas cytoplasmic staining was predominantly seen in tumours where expression was lower [154]. Intriguingly however, high plasma membrane expression of c-Met was associated with improved outcome, although the authors note that this finding requires independent validation [154]. By contrast, normal mesothelial cells have generally been found to lack c-Met expression at the protein [146] or RNA level [152]. Nonetheless, polarised expression along the apical surface was demonstrated in normal mesothelium in one study [144].

In keeping with these findings, studies of both human and murine mesothelioma cell lines have confirmed that the majority of those tested express the c-Met receptor [152, 153]. Comparison with an immortalised cell line derived from healthy mesothelium indicates that *MET* is transcriptionally upregulated in 75% of cases [153].

1.4.3 MET mutation in mesothelioma

A number of *MET* mutations have been identified in primary MPM and derived cell lines [147]. Overall however, it has been estimated that somatic mutation of *MET* is only detectable in approximately 3% of such tumours [149]. Similarly, no activating *MET* mutations were identified in an assessment of 30 mesothelioma cell lines [148, 153]. A polymorphism (T1010I) that affects the juxtamembrane regulatory domain of MET has been identified in a small number of cases of MPM [149] and in derived cell lines [147]. While this polymorphism has the capacity to transform an IL-3-dependent cell line, it remains uncertain whether this finding has clinical relevance in mesothelioma [149].

1.4.4 Factors that dysregulate the HGF/ c-Met axis in mesothelioma

Several factors have been identified that have the capacity to dysregulate expression of HGF and/ or c-Met in mesothelial or other cell types and thus may have relevance to mesothelioma pathogenesis.

Exposure of murine mesothelial cells to crocidolite (the most pathogenic form of asbestos) promotes upregulation of the Fra-1 (fos-related antigen-1) proto-oncogene. This in turn leads to AP-1-dependent c-Met upregulation [155]. Furthermore, increasing evidence from a number of tumour systems suggests that hypoxia can drive the transcriptional upregulation of c-Met expression [116].

Related to this, Adamson *et al.* [156] performed an *in vivo* study in which rats were exposed to crocidolite asbestos, delivered by intratracheal instillation. As a result, a proliferative burst of bronchoalveolar epithelium and pleural mesothelial cells ensued. To dissect mechanisms, they demonstrated that HGF and keratinocyte growth factor levels increased in bronchoalveolar and pleural lavage fluid over the following days. Evidence that both cytokines contributed to mesothelial cell proliferation was supported by antibody blocking studies.

Genetic factors may conspire to upregulate the HGF/ c-Met axis. Studies using a murine model of asbestos-induced mesothelioma have indicated that haplo-insufficiency for both *CDKN2A* and *NF2* enhances tumour aggressiveness, associated with upregulated expression and activation of c-Met and expression of stem cell-associated attributes [157]. In addition, loss of function p53 mutation favours c-Met upregulation, perhaps via dysregulated microRNA expression [158].

Finally, the SV40 tumour virus has been linked in a number of studies to mesothelioma development, although this remains controversial [159]. Notably however, in mesothelioma cell lines that express the large T antigen (an SV40-derived oncoprotein), c-Met is constitutively phosphorylated as a result of the establishment of an HGF autocrine loop [14].

1.4.5 Consequences of aberrant activation of the HGF/ c-Met axis in mesothelioma

Addition of HGF (either recombinant or derived from tumour samples) to mesothelioma-derived cell lines results in increased phosphorylation of Akt [160], Erk1/2 and c-Met itself [147]. As a result, these cells exhibit an increase in non-directional motility, chemotactic migration, altered morphology, cell division and invasiveness *in vitro* [152, 161].

In vivo studies using cell lines have also shed light on possible effects of activation of the c-Met /HGF axis in malignant mesothelioma. When an autocrine c-Met / HGF loop is established in NIH3T3 fibroblasts, these cells acquire tumourigenic capacity when inoculated in nude mice [162]. Tumours aberrantly express a number of epithelial markers, suggesting that c-Met signalling can promote epithelial trans-differentiation of these mesenchymal cell types [163]. This finding is noteworthy since mesotheliomas commonly display both epithelial and mesenchymal/ sarcomatoid features and molecular markers [164].

1.4.6 Targeting the HGF/c-Met axis in cancer – clinical studies

Several clinical trials are currently evaluating therapeutic agents directed against the HGF/ c-Met axis, in solid and some haematological malignancies [165]. They can be grouped into three major categories, based upon their specific targets (HGF and c-Met) and mechanisms of actions (monoclonal antibodies and TKIs) – anti-HGF antibodies, anti-c-Met antibodies and c-Met TKIs. [166, 167].

1.4.6.1 Anti-HGF / c-Met Antibodies

Clinically, the best characterised anti-HGF antibody is Rilotumumab (AMG 102) - a fully humanised monoclonal antibody against HGF. In a phase II trial of advanced gastric or oesophago-gastric cancer, efficacy was demonstrated in patients with c-Met^{high} tumours (>50% of cells with intermediate or strong c-Met staining) [168]. A phase I/II trial of rilotumumab plus erlotinib in NSCLC patients (NCT01233687) is actively recruiting (however last verified in 2014; clinicaltrials.gov). The anti-c-Met antibody ornatuzumab (MetMab) has been studied predominantly in lung cancer [169]. MetMab is a humanised, monoclonal antibody that binds to the Sema domain of c-Met, inhibiting HGF binding; a phase II clinical study testing ornatuzumab in combination with erlotinib for advanced NSCLC showed significant PFS and OS in c-Met^{+} NSCLC [170, 171]. However, results from this phase II study were not replicated in a larger, phase III study of c-Met IHC-positive NSCLC patients (NCT02031744 –not verified >1 year) that has been halted due to lack of clinically meaningful efficacy [172].

1.4.6.2 c-Met Tyrosine Kinase Inhibitors

Several small molecule c-Met kinase inhibitors are currently undergoing evaluation in patients with advanced c-Met-expressing malignancy [165]. Multi-kinase inhibitors include amuvatinib (phase II), cabozantinib (phase II), crizotinib (phase I/II) and foretinib (phase I/II) whilst capmatinib (phase I/II) and Tivantinib (phase II) are selective c-Met inhibitors.

Cabozantinib strongly inhibits c-Met, VEGFR2 and RET. Approved by the US FDA for treatment of aggressive metastatic thyroid cancer [173], phase II studies evaluating this agent within a cohort of different solid tumours – melanoma, NSCLC, hepatocellular cancer (HCC) and breast cancer all respectively reached objective tumour regression [174]. Subsequent studies investigating cabozantinib in CRC and prostate cancer are also underway [167].

Clinical studies with tivantinib have been generally well tolerated, showing selected signs of clinical activity in patients with cancer [175-182] however interstitial lung disease was a serious adverse event resulting in the discontinuation of the ATTENTION trial [167]. In

a phase II study for the treatment of HCC, significant improvement was observed in patients with c-Met^{high} tumour expression [179]. However, a multicentre phase II clinical trial evaluating tivantinib in patients with mesothelioma who had failed prior therapies (NCT01861301) was terminated after recruitment of 18 patients owing to disappointing results.

It is evident more potent small molecule TKIs are under clinical evaluation than c-Met/HGF antibodies, with diverse responses documented. Importantly, results will need to be interpreted in the light of increasing evidence that kinase inhibitors engage multiple off-targets, typically amidst kinases of structural similarity, which is a significant limitation in their widespread use [183].

1.5 Caught in the crossfire: interactions between c-Met and other signalling networks

Increasing evidence indicates that aberrantly activated receptor/ ligand systems do not operate in isolation, but instead engage in cross-talk with other pathways in healthy and transformed cells. Many examples of such "cross-talk" have been described in relation to the HGF/ c-Met axis and may afford opportunities for the emergence of tumour cell resistance to the targeted inhibition of this pathway in isolation [158, 184].

Recent studies have shown complex interactions between HGF/c-Met with other membrane receptor tyrosine kinases (RTKs) such as Semaphorin-4D/Plexin B1 [185] and SDF1/CXCR4 [186], suggesting the importance of crosstalk between membrane receptors of various types [187, 188]

1.5.1 Cross-talk between c-Met and other receptor tyrosine kinases

The c-Met receptor engages in cross-talk with several other receptor tyrosine kinases, many of which are co-expressed in malignant mesothelioma. The best characterised of these interactions occurs between c-Met and EGFR. Amplification of *MET* is a well-recognised mechanism of mediating resistance of EGFR-mutant lung cancer cells to EGFR kinase inhibitors [189]. Stimulation of MPM cells with HGF causes the phosphorylation of EGFR while knock down of *MET* or inhibition of c-Met kinase activity can lead to reduced EGFR phosphorylation [149]. The converse relationship also applies in that EGF stimulation of MPM cells promotes the enhanced phosphorylation of c-Met. In mesothelioma, the EGFR is upregulated in the majority of tumours and is phosphorylated in virtually all cases [89]. Nonetheless, EGFR inhibitors have proven

ineffective to date when used in isolation to treat patients with mesothelioma [190]. Pre-clinical studies using a panel of mesothelioma cell lines have demonstrated that combined inhibition of both c-Met and EGF receptor achieved greater suppression of cell growth, migration and invasion, compared to selective targeting of either receptor alone [153]. Furthermore, the AKT inhibitor perifosine also reduced the ligand-induced phosphorylation of EGFR and c-Met receptors in mesothelioma cell lines, accompanied by inhibition of proliferation and enhanced sensitivity to platinum agents [191]. These data raise the possibility that c-Met signalling can buffer against the inhibitory effects of EGFR blockade in mesothelioma and raise the prospect that combined inhibition of both pathways may warrant clinical evaluation.

Studies of other model systems provide evidence of cross-talk between c-Met and other receptor tyrosine kinases. The HGF/ MET axis is closely related to a second ligand receptor pair, comprising macrophage stimulating protein (MSP) and the Ron receptor tyrosine kinase [130]. In gastric carcinoma models, heterodimerisation and cross-phosphorylation of the c-Met and RON receptors has been demonstrated upon binding of either HGF or MSP [192]. Such a mechanism may also operate in mesothelioma since recent preliminary data suggest that both MSP and RON are commonly expressed in this tumour [193]. Furthermore, the AXL receptor is also commonly expressed in mesothelioma [23] and signals co-operatively and in a bidirectional manner with HGF/ c-Met in some models [194]. There is also evidence that other RTKs such as IGF-1R, RET [195] and VEGF receptor [62] can elicit the ligand independent transactivation of the c-Met receptor. Co-operative signalling between c-Met and ErbB2/ ErbB3 has also been described [158]. Together, these findings place c-Met as an effector of signalling by several other receptor systems and warrants further investigation of the intermediates that relay such signals and which may provide important targets for therapeutic exploitation.

1.5.2 Cross-talk between c-Met and other receptor types

Emerging evidence also suggests that cross-talk between c-Met and other (non-tyrosine kinase) receptor types also occurs. In several cellular systems, CD44 receptor isoforms containing the variant 6 exon (CD44v6) are required in order that HGF can elicit c-Met activation, through ternary complex formation [196]. The CD44 variant exon 3 contains a heparin sulphate binding site, enabling isoforms that contain this exon to bind HGF, perhaps facilitating the more efficient capture and presentation of this ligand to c-Met [158]. HGF has also been reported to promote the association of c-Met with CD44 containing variant exon 10, leading to efficient phosphorylation of c-Met and recruitment into caveolin-enriched microdomains [197]. Although CD44 is commonly upregulated on

mesotheliomas [198], there has been relatively little study of which CD44 variants are expressed in this disease.

Transactivation of MET (and several other RTK) has also been reported upon stimulation of several G protein coupled receptors [158, 199]. Additionally, ligand-independent c-Met activation has been described following integrin engagement [200]. In keeping with this, c-Met can physically associate with a number of integrins [158]. Furthermore, full c-Met functioning in some models requires complex formation with the $\alpha_3\beta_1$ [201] or $\alpha_6\beta_4$ integrin [202].

Another example of this type of cross-talk is the ability of c-Met to associate with Semaphorin receptors, namely Plexins and Neuropilins [203]. For example, Sema4D (a Plexin B1 ligand) increases the phosphorylation of both its receptor and c-Met leading to enhanced tumour invasiveness [204], although the importance of this interaction in mesothelioma is unclear.

1.5.3 The role of co-factors in binding of HGF to c-Met

NK1 binds both to c-Met and heparin sulphate proteoglycans (HSPGs), which are widely co-expressed on the mammalian cell surface. Furthermore, a number of co-factors have been described that strengthen this interaction. In several cellular systems, CD44 receptor isoforms containing the variant 6 exon (CD44v6) are required in order that HGF can elicit c-Met activation, through ternary complex formation [196]. In keeping with this, antagonistic peptides derived from the variant exon 6-encoded 42 amino acid sequence can block the binding of HGF to c-Met and thereby abrogate its function [205].

The CD44 variant exon 3 contains a heparin sulphate binding site, enabling isoforms that contain this exon to bind HGF, perhaps facilitating the more efficient capture and presentation of this ligand to c-Met [158]. HGF has also been reported to promote the association of c-Met with CD44 containing variant exon 10, leading to efficient phosphorylation of c-Met and recruitment into caveolin-enriched microdomains [197].

Although CD44 is commonly upregulated on mesotheliomas [198], there has been relatively little study of which CD44 variants are expressed in this disease. One study has suggested that CD44v6 may be under-represented in mesothelioma compared to other lung tumours [206]. To add complexity, one recent study in CD44-deficient mice suggests that ICAM-1 may alternatively be recruited to provide this co-receptor function [207] and small studies within mesothelioma suggest that ICAM-1 is very commonly and highly expressed in this tumour [208].

The other characterised molecules promiscuous to the HGF/c-Met axis are heparin sulphate proteoglycans (HSPGs). Heparan sulfate proteoglycans are proteins that are covalently linked to sulphated GAG chains [209, 210]. Ubiquitously expressed within mammalian tissue, these molecules have been implicated in several important biological processes including cell adhesion and migration, tissue morphogenesis, angiogenesis, and regulation of blood coagulation [211].

Within the HSPG family, the most well characterised and abundant member is syndecan-1 [210]. It is highly expressed on many epithelial cells where it plays an active role in cell adhesion and epithelial morphogenesis [210, 212]. The interaction of HGF with syndecan-1 has been described by Derksen and colleagues, who have shown that syndecan-1 on multiple myeloma cells binds HGF. Importantly, syndecan-1 strongly promotes HGF-induced signalling through c-Met, resulting in enhanced activation of signalling pathways involved in the control of tumour cell proliferation and survival [211]. The relationship of expression suggests that HGF might not only interact with c-Met but also with syndecan-1, resulting in a ternary interaction between c-Met, HGF, and syndecan-1 promoting tumourigenesis [213, 214]. Their findings suggest cell surface syndecan-1 increases the effective concentration of HGF on the plasma membrane, where the binding of several HGF molecules to syndecan-1 may promote dimerisation and oligomerisation of the c-Met receptor, leading to enhanced receptor activation [211]. An alternative hypothesis put forward was the induction of a conformational change, whereby syndecan-1 may influence the affinity of HGF for c-Met. Sakata and colleagues have also previously demonstrated this with respect to HSPG binding of the NK1 splice variant of HGF [215].

1.6 Cancer immunotherapy using chimeric antigen receptor-engineered T-cells

Immunotherapy uses the immune system's cytotoxic mechanisms for targeted tumour cell destruction. The existence of sophisticated immune surveillance mechanisms for cancer has been well characterised [216]. These immunological mechanisms are overcome however once cancer is clinically detectable – a disease that will affect one in two individuals born after the year 1960 [217].

A key challenge in overcoming the poorly immunogenic nature of transformed, malignant cells is the fact that most tumour-associated antigens are derived from self, or subtly modified variations. Numerous mechanisms by which tumour cells evade the

immune system have been detailed below – in addition to the impairment of antigen–presenting machinery, down-regulated expression of both HLA molecules and reduced expression of tumour antigens themselves. As tumours progress, they acquire stromal support, creating a local and systemic environment that significantly impairs the development and maintenance of immune responses [218].

1.6.1 Immune surveillance of cancer and immune evasion by tumour cells

Immunotherapy was designated breakthrough of the year in 2013, with the dawn of immune checkpoint blockers, described in section 1.1.7.4.2. This novel class of therapeutic agents represents a paradigm shift in the clinical management of cancer - with emphasis on pharmacological manipulation of the host, rather than of the disease.

Immune suppression within the tumour microenvironment is predominantly mediated by $CD4^+$ $CD25^+$ $FoxP3^+$ regulatory T-cells (Tregs) [219], in addition to other types of suppressor cells. It has previously been reported that tumour-derived Tregs possess higher suppressive activity over naturally occurring Tregs [220, 221]. Tumour cell-mediated chemokine production [222, 223] recruiting Tregs to the tumour microenvironment, with evidence suggesting transforming growth factor (TGF)-β (also produced by tumour cells), aids the conversion of $CD4^+$ T-cells into suppressive Tregs in situ [224]. Myeloid-derived suppressor cells (MDSCs), modulated dendritic cells (DCs) and M2 macrophages facilitate in creating an inflammatory microenvironment, mediating tumour initiation, angiogenesis and metastasis [225, 226]. Moreover, myeloid suppressor cells further inhibit antitumour T-cell function via the production of nitric oxide (NO) via the enzyme arginase [219].

Another mediator of T-cell suppression is the immunosuppressive enzyme indoleamine 2,3-dioxygenase (IDO) [227]. Predominantly produced by plasmacytoid dendritic cells (PDC) within tumours and draining lymph nodes (LN), induction is mediated via the B7-1/2 / CTLA-4 axis [228, 229]. Indoleamine dioxygenase inhibits T-cell responses via tryptophan catabolism. Since activated T-cells are highly sensitive to tryptophan deprivation, IDO upregulation induces metabolic apoptosis [227].

1.6.2 Introduction to Chimeric Antigen Receptors

Under the far-reaching umbrella of cancer immunotherapy, the genetic engineering of peripheral blood T-cells using chimeric antigen receptor technology represents an exciting platform-technology. Chimeric antigen receptors (CARs) are HLA-independent fusion molecules that couple the target-specific binding of a cell surface antigen to the delivery of a potent cytotoxic T-cell activating signal (Figure 1-7). These molecules are delivered to peripheral blood T-cells or natural killer cells by gene transfer, generally using retroviral or lentiviral vector systems.

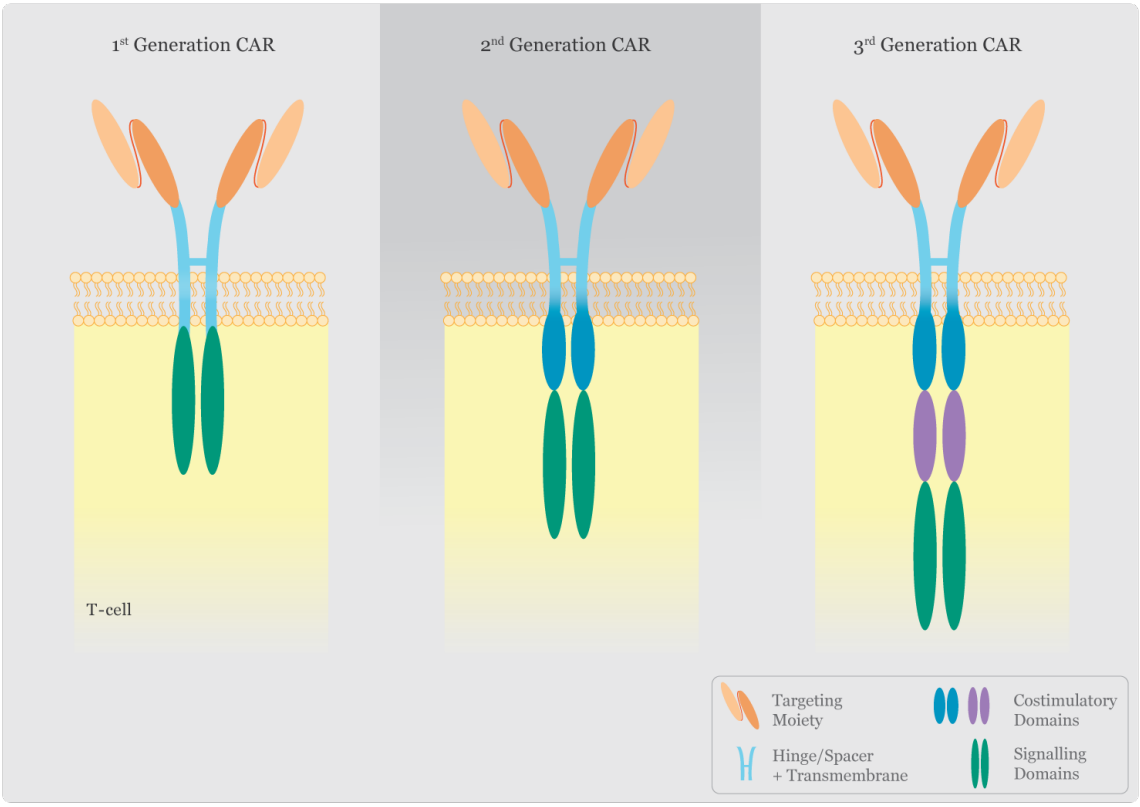

Figure 1-7. The structural features of chimeric antigen receptors.
An antigen-binding targeting moiety is typically comprised of antibody variable heavy and light chains from a monoclonal antibody that are able to self-assemble through the inclusion of a linker sequence to form a single chain variable fragment (scFv). In a 1st generation CAR, the targeting moiety is coupled via a hinge and transmembrane domain to an intracellular T-cell signalling domain, typically the CD3ζ chain of the TCR complex. The 2nd and 3rd generation CARs contain an additional one or two co-stimulatory endodomains, respectively. Co-stimulatory molecules CD28 and 4-1BB are most commonly used, although alternative designs may include motifs from ICOS, OX40, CD27 or GITR for example.

The ability to generate large numbers of target specific CAR T-cells that can be directed against native cell surface antigens circumvents a number of the immune evasion mechanisms discussed above.

Immunotherapy using CAR T-cells has been under development for almost three decades, but has witnessed a substantial increase in interest over the past 5 years. This development has been largely driven by the unprecedented success of the CAR T-cells in Phase I clinical trials targeted against a variety of B-cell malignancies, most notably acute lymphoblastic leukaemia (ALL) [230]. In that setting, several centres in the United States have reported that autologous CAR T-cell immunotherapy targeted against the ubiquitous B-cell antigen, CD19, yields complete remission (CR) rates of 80% or greater in patients with otherwise untreatable disease. While these clinical data are unprecedented for a new cancer medicine, efficacy of this approach has not been demonstrated in patients with solid tumours such as MPM.

1.6.3 Evolutionary design of Chimeric Antigen Receptors

The overall structure of a CAR consists of four domains joined in series, namely: (i) an antigen recognition ectodomain (targeting moiety) (ii) a hinge/space (iii) a transmembrane domain and (iv) a signalling endodomain (Figure 1-7). These features are described in further detail in the following sections.

1.6.3.1 Targeting domain

The specificity of the CAR is determined by the targeting moiety, which enables the CAR to recognise native cell-surface antigens, independent of HLA presentation (Figure 1-7). Chimeric antigen receptors have been developed against a multitude of targets [231]. As indicated earlier, greatest success has been achieved in patients with B-cell malignancy, using CARs targeted against CD19, which is a ubiquitous B-cell antigen. In the context of solid tumours, examples of commonly used targets include HER2 [232, 233], the variant III mutation of epidermal growth factor receptor (EGFRvIII) [234] and mesothelin [235].

Development of targeting moieties used in CAR constructs has proceeded over thirty years. In the late 1980's Kuwana *et al.* studied T-cell and B-cell antigen recognition differences by replacing the structural variable (V)-regions of T-cell receptors (TCRs) with those of Immunoglobulin (Ig)-derived V-regions. This initial CAR design required that T-cells expressed antibody variable heavy (V_H) and light chains (V_L) in two separate polypeptide chains [236, 237]. To transfer this specificity upon a single chimeric receptor molecule, Eshhar *et al.* pioneered the use of the single chain antibody fragment (scFv). In an scFv, the V_H and V_L chains from a single antibody are joined together using a short

linker sequence [238]. In modern CAR designs, antibody-derived single-chain variable fragments (scFvs) are most commonly used for target antigen recognition and binding. Alternatively, targeting may be achieved using peptides [239], single domain antibodies [240] or ligands such as the T1E peptide, which binds several ErbB hetero- and homodimers [241-243].

The ability of CARs to mediate HLA-independent antigen recognition confers two advantages over other adoptive cell therapies such as TCR-engineered T-cell protocols. First, antigen recognition is not compromised by the frequent occurrence of HLA down regulation on tumour cells [244]. Second, this also makes CAR therapy available to all patients, regardless of their HLA-haplotype.

The choice of binding moiety is influenced by several factors. The binding of the CAR to target antigen usually involves a relatively high-affinity interaction, although this is somewhat a "double-edged sword" - if the affinity is too high, healthy tissue that may also be expressing the target antigen at low levels may also be targeting, resulting in on-target off-tumour toxicity [245]. The use of murine hybridoma-derived scFvs is disadvantaged by their ability to induce host immunogenicity. The production of human anti-mouse antibodies (HAMAs) within the host can also block CAR T-cell function and may contribute to the accelerated clearance of these cells *in vivo* [246]. Furthermore, these blocking antibodies may occasionally lead to life-threatening complications such as anaphylaxis, as reported recently in a patient treated with repeated doses of mesothelin-specific CAR T-cells in whom IgE HAMA developed [247]. Using a humanised or fully human scFv sequence for targeting can reduce the risk of such an occurrence.

1.6.3.2 Hinge/ spacer domain

The hinge and spacer domains play a predominantly structural role in the CAR, however they are thought to elicit a functional role in certain cases. The spacer physically separates the targeting moiety from the T-cell membrane (Figure 1-7). However, the optimum distance required is likely to be different for various antigens. Guest *et al.*, evaluated the effects of a spacer/hinge in four different CARs, targeting the pan-B-cell antigen CD19, the onco-foetal antigen 5T4, carcinoembryonic antigen (CEA) or neutral cell adhesion molecule (NCAM). Enhanced cytokine release and cytotoxicity was observed when a spacer was included in 5T4- and NCAM-targeted CARs. However the opposing effect was observed with CD19- and CEA-targeted CARs [248].

In a more recent study, both long and short versions of the same spacer region were tested in a CD19-targeted CAR. It was shown that only CAR T-cells incorporating the short spacer were able to eradicate xenograft tumours. By contrast, CAR T-cells

containing the longer spacer regions displayed poor efficacy, nor could they be potentiated through increased dosing or combining dual co-stimulatory domains CD28 and 4-1BB. This same study also noted an increased rate of activation induced cell death with cells expressing the longer spacer [249].

The conclusion from these studies is that there is likely to be an optimal length of the CAR ectodomain. Membrane distal epitopes do not require a hinge, whereas when targeting membrane-proximal epitopes, a spacer region is required for optimal activation [250]. However, use of an unnecessarily long spacer increases the distance between the surface of the CAR T-cell and tumour cell surface, reducing target cell lysis. This is because phosphatases with large ectodomains (e.g. CD45, CD148) may gain access to the formed immune synapse between the CAR T-cell and its target, dephosphorylating activated molecules of the signalling cascade [250].

Human IgG-derived spacers are commonly used due to their stabilising effect on CAR expression. However, interactions between the Fc domain of the spacer and Fc gamma receptors (FcγRs) on myeloid cells can lead to activation-induced cell death of T-cells and limited persistence *in vivo* [251, 252]. This can be overcome by deleting or modifying regions of the constant heavy (CH)2 domain that are essential for FcγR binding, thereby improving the CAR T-cell persistence and anti-tumour activity *in vivo* in pre-clinical models [252, 253].

1.6.3.3 Transmembrane domain

Similarly, the transmembrane domain may have a combined functional and structural role (Figure 1-7). For example, the CD3ζ transmembrane domain has been used in some CAR configurations, in which it has been shown to play a vital role in the recruitment of endogenous elements of the TCR/CD3 complex to the CAR structure [254]. Other transmembrane domains commonly used include those derived from T-cell molecules such as CD28 or CD8.

1.6.3.4 Intracellular signalling domain

Chimeric antigen receptor T-cell activation in response to target antigen is dictated by the intracellular signalling domain. This element of CAR engineering has been the subject of considerable innovative modifications, in an effort to optimise function and therapeutic efficacy. Generically, the evolution of CARs can be characterised within three generations depending on the structure of the endodomain (Figure 1-7).

When physiological T-cell activation occurs, the TCR/CD3 complex delivers an activating signal known as ‘signal 1’. The CD3 complex is an arrangement of homo- and

heterodimers consisting of four subunits – ζ, δ, ε and γ [255-257]. First generation CAR T-cells contain a single T-cell activating domain, most commonly derived from the ζ chain of the TCR/CD3 complex. Crucially, studies revealed CD3ζ alone provides a sufficiently potent 'signal 1' from its three immunoreceptor tyrosine-based activation motifs (ITAMs) which is capable of substituting for the comprehensive signal provided by the entire CD3 complex [258, 259].

Aside from the downregulation of HLA molecules, the poor immunogenicity of tumours results from a lack of expression of costimulatory molecules, which are required to provide T-cells with activation 'signal 2'. This second signal is essential for activated T-cells to undergo optimal proliferation, accompanied by the release of cytokines, such as IL-2. To provide this signal using a CAR-based system, second and third generation fusion receptors have been developed, incorporating one or two co-stimulatory domains respectively that are placed upstream of CD3ζ (Figure 1–7).

The costimulatory molecule CD28 has typically been used to provide an early second signal, leading to high-level IL-2 secretion [260, 261]. A multitude of alternative second generation CAR T-cells have also been described, incorporating co-stimulatory elements as diverse as 4-1BB [262-265], CD27 [266, 267], OX40 [262, 263], ICOS [263] and DAP10 [262, 267].

Second generation CAR T-cells have consistently been shown to improve T-cell function compared to first generation counterparts [262, 266, 268]. Highest levels of IL-2 production have been observed with the incorporation of CD28 [262], although depending on the certain disease states, this may be counter productive with enhanced intra-tumoural infiltration by regulatory T-cells [269]. Chimeric antigen receptors containing 4-1BB have been shown to promote the highest multi-functionality of cytokine production [270] and constitutive signalling resulting in sustained T-cell survival [268]. Comparatively, co-stimulation by ICOS induced the greatest cytotoxicity [263], promoting the persistence of Th_{17}-type CAR^+ T-cells [271].

Second generation CARs used in clinical trials most often incorporate CD28 or 4-1BB signalling domains, both of which demonstrated prolonged persistence when expressed in CD19-targeted CARs [272, 273]. Emerging clinical experience with these two second generation configurations suggests that CD28-containing constructs undergo more rapid *in vivo* expansion and decline whereby 4-1BB-contianing fusions may persist for longer periods [274].

Third generation CARs incorporate two co-stimulatory modules placed in series within the CAR endodomain [275, 276]. Since CD28 and TNF receptor family members each initiate different signalling pathways (PI3K for CD28 compared to tumour necrosis family receptor-associated factor (TRAF) adaptor proteins for 4-1BB), this approach may enhance overall T-cell activity [233, 277]. Third generation CAR T-cells have recently commenced clinical evaluations [278], although it remains too soon to comment as to whether these represent a significant therapeutic advance over second generation configurations.

Co-stimulatory signals to CAR T-cells may also be provided *in trans*. Functionality of *trans* co-stimulatory fusion molecules were first demonstrated in human T-cells a number of years ago [279]. Building upon this foundation, groups from a number of institutions have co-expressed a first generation CD3ζ-based CAR with a co-stimulatory fusion receptor that engages a second target molecule. This "dual targeting" CAR approach has been tested pre-clinically targeting MUC-1 and HER-2 [280], prostate-specific membrane antigen (PSMA) and prostate stem cell antigen (PSCA) [281], and the combination of folate receptor α and mesothelin [282]. The main advantage of separating the co-stimulatory molecule from the CD3ζ endodomain is to provide a greater level of tumour specificity, diminishing the risk of "on target – off tumour" toxicity.

1.6.4 Clinical studies of CAR T-cell immunotherapy

The past decade has seen an unprecedented rise in the number of clinical studies undertaken to evaluate CAR T-cell based immunotherapy. Presently, there are over 120 clinical trials investigating CAR T-cell therapies listed on clinicaltrials.gov.uk (search date 19/05/16), involving a multitude of malignant diseases. CD19-targeted CAR T-cell immunotherapy of B-cell malignancy account for the majority of studies, although several trials are evaluating CAR T-cell therapy of various solid tumour types.

1.6.4.1 CAR T-cell immunotherapy for haematological malignancy

Unquestionably, the greatest success with CAR T-cell therapy to date involves CD19-targeted treatment of B-cell malignancies. CD19 is arguably one of the most ideal antigens targeted to date – it is expressed by the majority of B-cell malignancies and at all stages of B-cell lineage differentiation. Importantly however, it is not found on haematopoietic stem cells or other tissues [283]. Effective targeting of CD19-expressing cells by engineered CAR T-cells is generally accompanied by B-cell depletion and impaired antibody-generating capabilities, which can be effectively mitigated by immunoglobulin replacement therapy [284].

Striking complete response (CR) rates have been achieved with second-generation CD19-targeted CAR T-cells in both adult and paediatric patients with B-cell ALL. Relatively large-scale studies conducted by groups at Memorial Sloan Kettering Cancer Centre (MSKCC), University of Pennsylvania (UPenn) and the National Cancer Institute (NCI) have all attained results with remarkable efficacy (average CR rate approaching 90%) [285-287]. The significance of near symmetrical results are particularly noteworthy when one considers the differences between centres in the selection of CAR scFv targeting moieties, co-stimulatory molecules (MSKCC, Seattle and NCI - CD28; UPenn – 4-1BB) and conditioning regimens [230].

First reported in 2011, Sadelain and colleagues from MSKCC have now treated 45 ALL patients with CD19-targeted CAR T-cells [272, 288] [285]. An 82% CR rate was observed without any difference in survival of patients who subsequently did or did not receive an allogeneic haematopoietic stem cell transplant (HSCT; John Maher, personal communication May 2015).

Maude *et al.*, have reported a 90% CR rate (27/30) in ALL patients treated at UPenn, some of whom had failed previous HSCT [287]. Sustained remission (24 months) was achieved in 19 patients. A notable difference emerging between these results and those from MSKCC was the sustained, long-term persistence of 4-1BB containing CD19-targeted CAR T-cells, which regularly persisted in high numbers for up to four years post infusion. Contrastingly, CD19 re-targeted T-cells containing CD28 co-stimulatory domains appear to persist at significant levels for a considerably shorter duration (1-3 months) [285]. At the NCI, a 70% CR rate was reported from an intent-to-treat analysis of 20 children and young adults with ALL [286].

The method to induce sufficient co-stimulation has evolved to a more refined system with the use of second generation CARs. In patients with relapsed or refractory non-Hodgkin's lymphoma Savoldo *et al.*, directly compared the expansion and persistence *in vivo* of T-cells transduced with a first generation (CD3z) or second (CD28/ CD3z) generation CD19-targeted CAR [289]. Only second generation, CD19-28z T-cells were able to expand *in vivo*, resulting in trafficking and infiltration within tumour lesions [289].

1.6.4.2 CAR T-cell immunotherapy of solid tumours

Refractory or metastatic solid tumours continue to represent the greatest unmet need within cancer medicine. Thus, initial clinical studies of CAR T-cell immunotherapy were conducted in patients with solid malignancies [246, 290]. However, results were disappointing with no detectable efficacy observed. Building upon this foundation, the

field of CAR T-cell immunotherapy has evolved to combat this extremely challenging setting.

Kershaw *et al.* undertook the first Phase I CAR T-cell study in patients with metastatic epithelial ovarian cancer in 2006 [246]. Patients were treated with a first-generation scFv-based CAR targeted against folate receptor-α. Administered intravenously (IV), no toxicity was observed; however there was also no evidence of efficacy. The lack of an anti-tumour response was linked to poor T-cell homing to the tumour and failure of transduced T-cell persistence [246]. Park and colleagues observed a similar result in neuroblastoma patients treated with CAR-engineered T-cells redirected against the L1-cell adhesion module CD171 [291]. Although a single partial response (PR) was recorded, limited T-cell persistence *in vivo* was also cited as an explanation for poor anti-tumour activity.

The absence of sufficient co-stimulatory signals within first-generation CAR T-cells has been cited as the probable reason for the limited persistence and poor efficacy. One strategy to improve the persistence of T-cells *in vivo* has resulted in the greatest success to date in patients with solid tumours. Epstein-Barr virus (EBV) specific cytotoxic T-cells were transduced with a GD2-specific CAR to treat patients with neuroblastoma. The underlying rationale was that native T-cell receptors would be engaged on CAR^+ T-cells by EBV infected B-cells or latent viral antigens, thereby providing co-stimulation *in vivo* [292]. Long-term persistence (up to 192 weeks) was associated with clinical benefit observed in eleven patients with active disease resulting in three complete remissions [293].

An interesting observation was the positive correlation between T-cell persistence and $CD4^+$ and central memory $CD8^+$ T-cells in the adoptive cell product [293]. A number of studies have subsequently studied the expression of CARs within defined populations of T-cell subsets [294], or potentially long-lived subsets such a memory stem cells (T_{scm}) [295, 296].

1.6.5 Toxicity associated with CAR T-cell immunotherapy

Toxicity induced by CAR T-cell immunotherapy in clinical studies has broadly been characterised within three major categories – tumour lysis syndrome, cytokine release syndrome and on-target off-tumour toxicity.

1.6.5.1 Tumour lysis syndrome

Tumour lysis syndrome encompasses a combination of metabolic disturbances - including elevated serum levels of potassium, uric acid and phosphate. Furthermore,

hypocalcaemia may develop, possibly progressing to renal failure. It has been reported following the rapid elimination of large numbers of tumour cells, most notably within the context of haematological malignancy. It has also presented surprisingly late in some patients following delivery of CAR T-cells [273, 297], presumably due to expansion of CAR^+ T-cells following adoptive transfer resulting in delayed tumour destruction.

1.6.5.2 Cytokine release syndrome

Cytokine release syndrome (CRS) is the most frequent life-threatening event induced by CAR T-cell immunotherapy [287]. This process involves the release of a cascade of cytokines from CAR T-cells themselves and cells of the mononuclear phagocyte lineage. High concentrations of pro-inflammatory cytokines, including tumour necrosis factor (TNF-α), interferon-γ (IFN-γ) and IL-6 [298] have been registered. In certain cases, the macrophage activation syndrome accompanies CRS – a notable observation following pre-clinical models in which CAR T-cell induced CRS implicate macrophage activation as a key component of disease pathogenesis [299].

Recent clinical evidence suggests the severity of CRS depends upon the disease burden [272, 287]. Due to the often rapid (but unpredictable) onset of CRS, close monitoring of patients is required - particularly within 24-48 hours following the infusion of CAR T-cells. However, there have also been reports of delayed onset of CRS, particularly when a small dose of CAR T-cells are administered and undergo substantial expansion *in vivo*. A fine balance exists between the management of CRS relative to T-cell activation and effector function. Since a degree of cytokine release is expected, the potential dilemma in therapeutically blocking this process may entail the use of immunosuppressive agents diminishing any potential anti-tumour efficacy. However, severe CRS may be be rapidly lethal, as exemplified in one patient treated with HER2 directed CAR T-cells [300]. Recently, further understanding has led to both diagnostic and grading systems being developed for this syndrome [285, 301]. A potential biomarker for CRS is the serum C-reactive protein (CRP). Furthermore, the IL-6 receptor α-blocker, tocilizumab, has also been widely incorporated in clinical study protocols as an immunosuppressive agent that diminishes the manifestations of CRS.

1.6.5.3 On-target off-tumour toxicity

On-target off tumour toxicity results from CAR T-cells recognising antigens that are not only overexpressed in tumours but also present in healthy tissues at lower levels. Although an 'acceptable' adverse event in the context of CD19-targeted CAR T-cell therapy for otherwise untreatable B-cell malignancy, the challenges with on-target off

tumour toxicity within the context of solid tumours has been highlighted by two major serious adverse events reported in CAR T-cell Phase I trials.

The first reported case in solid malignancy was a patient with metastatic colon cancer treated with an IV infusion of HER-2 re-targeted T-cells [300]. The third generation CAR incorporated an scFv derived from the trastuzumab antibody coupled to CD28 + 4-1BB + CD3ζ signalling domains. Following lymphodepletion chemotherapy, a total of 1 x 10^{10} T-cells (79% CAR^{+}) were infused systemically resulting in recognition of low levels of HER-2 within lung endothelium, leading to rapid onset of respiratory distress, multi-organ failure, cytokine release syndrome (CRS) and unfortunately, death [300, 302]. As a consequence, subsequent protocols were amended and HER-2 has been safely targeted in sarcoma patients following systemic infusion of second generation (CD28/ CD3ζ) CAR T-cells at lower doses and without prior lymphodepletion [303].

The second reported example of on-target off-tumour toxicity occurred in patients with metastatic renal cell carcinoma. Carbonic anhydrase-IX (CAIX) is frequently overexpressed in the clear cell subtype of this tumour, justifying a clinical trial using first-generation CAR T-cells that were targeted against this molecule [290, 304, 305]. Significantly however, hepatotoxicity was observed in a number of patients owing to recognition of CAIX on biliary epithelial cells. Toxicity was circumvented in subsequent studies using a low dose of CAIX blocking antibody, administered prior to CAR T-cells [304].

Whilst solid tumours have largely proven refractory to CAR T-cell therapy to date, the encouraging data presented in patients with B-cell malignancy fuels further clinical development (recent published CAR T-cell trials in solid tumours [306]. Nonetheless, there remain a large number of obstacles to the effective treatment of solid malignancies with CAR-engineered T-cells. These include the need to refining T-cell trafficking to tumour sites and to enhance their persistence, intra-tumoural penetration and effector function within hostile tumour microenvironments. Overcoming these challenges will require greater innovation in CAR engineering in addition to potential combinatorial therapy with existing or emerging treatment modalities [231].

1.7 Aims of this Thesis

This thesis details the work that I have undertaken to investigate the feasibility of using c-Met re-targeted CAR T-cells for the treatment of MPM.

The specific aims of this PhD study are:

1. Engineering a panel of c-Met-specific CARs.
2. To determine the target specificity and co-factor dependency of these CARs using an NIH 3T3-derived aAPC system.
3. To evaluate and compare *in vitro* cytotoxic activity of c-Met re-targeted CAR T-cells using a panel of four mesothelioma cell lines.
4. To investigate combinatorial therapy approaches to potentiate c-Met re-targeted CAR T-cell immunotherapy of mesothelioma.
5. Development of a c-Met-expressing MPM tumour xenograft model that is amenable to serial monitoring using bioluminescence imaging.
6. Evaluation of *in vivo* anti-tumour activity of c-Met re-targeted CAR T-cells against an established MPM tumour xenograft.

CHAPTER 2 Materials and Methods

2.1 Molecular Biology Techniques

Generic molecular biology methods are described first before the description of how these were used in the construction of novel plasmids used in this project.

2.1.1 Restriction enzyme digestion of plasmid DNA

The production of the novel CAR constructs required DNA digestion with restriction enzymes. Additionally, restriction patterns were used to accurately verify plasmid inserts. Digestion was performed in the presence of relevant buffers designed to optimise enzyme efficiency.

2.1.1.1 Materials, Reagents and Equipment

- Restriction enzymes — New England Biolabs (NEB)
- 10x Enzyme buffer — NEB
- 100x Bovine Surum Albumin (BSA)* — NEB
- Nuclease Free H_2O — BioLine
- DNA template
- Eppendorf Mastercycler Gradient PCR Machine — Eppendorf
- 37°C Water bath
- Ice

* only when required with certain restriction enzymes

2.1.1.2 Protocol

1. A 20µl reaction mixture, as detailed below for a double digest, was produced. All components were kept at 4°C throughout

a) 0.5-1.0µg DNA template

c) 2µl NEB buffer

d) 10-20U Enzyme 1

e) 10-20U Enzyme 2

f) 1µl 1:10 diluted BSA

g) made to a final volume of 20µl with nuclease free H_2O

N.B. in reactions requiring a single enzyme, the 20µl reaction volume was achieved using additional ultrapure water. For sequential digests, a 20µl reaction containing the first

enzyme only was produced. The second enzyme (1.2µl) and respective buffer (3µl) were added after the completion of the first incubation. When performing these sequential digest, the enzyme requiring the buffer containing a lower salt concentration was used in the first reaction.

2. Reaction mixtures were incubated for one hour in a PCR machine or water bath at the temperature required for optimal enzyme activity.

3. Once completed, 20µl aliquot reactions were mixed with 4µl DNA loading buffer and separated by electrophoresis on an agarose gel.

2.1.2 Isolation of DNA fragments using Agarose Gel Electrophoresis

Separation of DNA fragments was achieved using agarose gel electrophoresis. The constant mass to charge ratio of DNA molecules means that separation is determined by fragment size. Migration rates are therefore influences by the pore size of the gel, which in turn is determined by the agarose concentration (Table 2-1). Consequently, careful selection of the percentage of agarose used ensured optimal resolution of the fragments of interest.

Table 2-1. Agarose concentrations to achieve specific DNA fragments.

Agarose (% w.v)	**Range of separation (kb)**
0.5	0.7-2.5
0.8	0.5-15
1.0	0.25-12
1.2	0.15-6
1.5	0.08-4

(Adapted from [307])

2.1.2.1 Materials, Reagents and Equipment

- Electrophoresis grade agarose — MP Biomedicals
- TBE buffer*
- Ethidium bromide — Sigma
- DNA loading buffer — NEB
- 1kb DNA ladder — Invitrogen
- Gel mould — Biorad
- Gel comb — Biorad
- Gel tank — Life Technologies
- Power pack — Kingshill
- Microwave oven — Proline

- UV Transilluminator — UVI Tech
- TV Zoom lens — Avenir
- P90 Thermal Monochrome Printer — Mitsubishi

Buffers and solutions:
*10x TBE = 108g Tris-base, 55g boric acid, 9.3g EDTA in 1L deionised water;

2.1.2.2 Protocol

N.B. The protocol detailed below is for the production of a 1% 100ml agarose gel. The weight of agarose used and the volume of TBE into which it was dissolved differed depending upon the size and percentage of the gel required.

1. 1g of agarose was mixed with 100ml 1xTBE and heated in a microwave oven (with regular agitation) until completely dissolved.
2. After cooling under cold running water to 37°C, 0.30µg/ml ethidium bromide was added and the mixture swirled vigorously to ensure even distribution without the introduction of air bubbles.
3. The gel was poured into a pre-cast mould, a comb inserted and left to set at room temperature.
4. Prior to loading, samples were mixed 5:1 with 6x DNA loading buffer. In addition to the samples, a 1kb DNA ladder was loaded to allow the size of migrating DNA fragments to be estimated.
5. Once loaded, the gel was run at 5-8V/cm until sufficient migration (as visualised by the loading dye) had occurred.
6. The DNA was visualised with UV light at 154nm using a UV transilluminator. Images were taken using a TV zoom lens and thermal monochrome printer.

N.B. In instances when DNA was required for further manipulation, the level of UV exposure was minimised to reduce the risk of mutagenesis.

2.1.3 Retrieval of DNA from Agarose Gel

DNA fragments were isolated from agarose gel to enable their insertion into a viral vector. Isolation of the DNA relies its ability to bind the silica membrane of a purification column in the presence of chaotropic salt. The DNA is subsequently eluted following the replenishment of the hydration gel upon the addition of water.

2.1.3.1 Materials, Reagents and Equipment

- Wizard SV Gel and PCR CleanUp System — Promega
- Water bath

- Eppendorf 5415R Microcentrifuge	Eppendorf
- 1.5mL Eppendorfs	Greiner Bio-One
- Vortex	Rotormixer
- Scalpel	Swann Morton Ltd
- Balance	Mettler Toledo
- UV Transilluminator	UVI Tech

Buffers and solutions:

Membrane Binding Solution (MBS) = 4.5M guanidine isothiocyanate, 0.5M potassium acetate (pH 5.0);

Membrane Wash Solution (MWS) = 10mM potassium acetate (pH 5.0), 80% ethanol, 16.7µM EDTA.

2.1.3.2 Protocol

1. The location of the required DNA fragment was visualised with UV light at 254nm using a UV transilluminator.
2. The required DNA band was excised from the gel using a sterile scalpel and placed into a nuclease-free 1.5ml Eppendorf tube.
3. The gel fragment was weighed and submerged in the requires volume of membrane binding solution (MBS, v/w 1µl/1mg) and incubated at 54°C with frequent vortexing until the gel had completely melted.
4. The resulting mixture was added to the silica membrane within a purification column and centrifuged at 10,700g for one minute in a microcentrifuge.
5. The eluate was discarded, the column washed with 700µl membrane wash solution and subsequently centrifuged for one minute at 10,700g.
6. The eluate was discarded, the column washed with 500µl membrane wash solution and subsequently centrifuged for five minutes at 10,700g.
7. Following an additional dry centrifugation step, the DNA bound to the membrane was eluted by the addition of nuclease-free water and centrifugation at 10,700g. A one-minute incubation step at room temperature was performed prior to centrifugation to ensure complete dissociation of the DNA from the membrane.

2.1.4 Calf Intestinal Alkaline Phosphatase Treatment of DNA

Calf Intestinal Alkaline Phosphatase (CIP) catalyses the removal of 5' phosphate groups from DNA, RNA, ribo- and deoxyribonucleoside triphosphates. Since CIP-treated fragments lack the 5' phosphoryl termini required by ligases, they cannot self-ligate. This property can be used to decrease the vector background in cloning strategies [307].

2.1.4.1 Materials, Reagents and Equipment

- CIP (10,000U/ml) NEB
- DNA template NEB
- Nuclease free H_2O BioLine
- Ice

2.1.4.2 Protocol

N.B. All steps of the protocol (except for incubations) were performed on ice.

1. The CIP was diluted 1/30 in nuclease free H_2O to a final concentration of 0.3U/µl.
2. For each 1µg of DNA template (from a previously performed restriction digest), 0.5U CIP was added.
3. The mixture was incubated at 37°C for 45 minutes.
4. Optional: CIP was incompletely inactivated by incubating the samples for 30 minutes at 65°C. Because CIP cannot be completely heat inactivated, further processing of the sample was required immediately.
5. The appropriate amount of 6x loading buffer was added and the sample was run on an agarose gel.

2.1.5 Fragment Insertion using DNA Ligation

New DNA fragments were inserted into a linearised vector backbone using a ligation reaction.

2.1.5.1 Materials, Reagents and Equipment

- T4 DNA Ligase NEB
- 10x T4 DNA Ligase Buffer NEB
- Nuclease-Free water Promega
- Eppendorf mastercycler Gradient PCR Machine Eppendorf
- 0.5ml Eppendorfs Greiner Bio-One

2.1.5.2 Protocol

1. A 20µl ligation mixture, as detailed below, was produced. The example given is representative of a three-piece ligation.
    a) Xµg DNA Backbone
    b) Xµg Fragment 1
    c) Xµg Fragment 2
    d) 2µl 10x DNA Ligase Buffer
    e) 2µl (4000 cohesive end units) DNA Ligase
    f) Xµl Nuclease-free water

N.B. For reactions requiring ligation of fewer or more fragments, the volume of nuclease-free water was altered to ensure a final reaction volume of 20µl.

2. The reaction was incubated overnight at 15°C in the Eppendorf mastercycler Gradient PCR Machine.

2.1.6 Analysis of DNA Concentration

The concentration of DNA was measured using the Nanodrop ND-1000 system. The Nanodrop is a full-spectrum (220-750nm) spectrophotometer that can assay 1uL samples. The sample is pipetted onto the end of a fibre optic cable (the receiving fibre). A second fibre optic cable (the source fibre) is then brought into contact with the liquid sample causing the liquid to bridge the gap between the fibre optic eds. The gap is controlled to both 1mm and 0.2mm paths. A pulsed xenon flash lamp provides the light source and a spectrometer utilising a linear CCD array is used to analyse the light after passing through the sample.

2.1.6.1 Materials, Reagents and Equipment

- Nuclease Free H_2O	BioLine
- Elution Buffer	Qiagen
- Nanodrop ND-1000	Thermo Scientific

2.1.6.2 Protocol

1. The Nanodrop is equilibrated using 1µl nuclease-free H_2O.
2. Blank measurement is made using 1µl of elution buffer.
3. 1µl of DNA is added to the Nanodrop
4. The DNA concentration is directly calculated by the Nanodrop software and given in ng/µl, using the measured absorbance and the Beer-Lambert equation.
    a) Absorbance = $-\log(\text{intensity}_{\text{sample}}/\text{intensity}_{\text{blank}})$

b) The Beer-Lambert equation is used to correlate the calculated absorbance with concentration:

A = E * b * c

A = the absorbance represented in absorbance units

E = the wavelength-dependent molar absorptivity coefficient with units of litre/mol-cm

b = path length in cm

c = analyte concentration in moles/litre or molarity

2.1.7 Transformation of *Escherichia (E.) Coli* TOP10F' Strain

Replenishment of plasmid stocks and selection of newly produced vectors was achieved by introducing the plasmid onto chemically competent *E. Coli*. All steps followed common microbiological practise, using a Bunsen burner to provide the sterile vacuum.

2.1.7.1 Materials, Reagents and Equipment

- TOP10F' *E. Coli* — Invitrogen, UK
- Plasmid DNA
- Agar plates
- Ampicillin
- Super Optimal broth with Catabolite repression (SOC) media
- Glucose — BDH
- Water Bath
- Ice
- Oven set at 37°C — Genlab Ltd
- Bunsen Burner
- Excella E-25 shake incubator
- Eppendorf 5415R refrigerated Microcentrifuge — Eppendorf
- Glass spreaders
- 100% Ethanol — Fisher Scientific
- L broth

Buffers and solutions:

Membrane Binding Solution (MBS) = 4.5M guanidine isothiocyanate, 0.5M potassium acetate (pH 5.0);

Membrane Wash Solution (MWS) = 10mM potassium acetate (pH 5.0), 80% ethanol, 16.7µM EDTA.

2.1.7.2 Protocol

1. 25µl aliquot of competent *E. Coli* was thawed on ice.
2. 1µg Plasmid DNA was added to the *E. Coli* and incubated for 30 minutes on ice.
3. Bacteria were heat shocked at 42°C for 90 seconds and subsequently incubated on ice for 5 minutes.
4. Following addition of 300µl SOC media, samples were shaken at 160rpm for one hour at 37°C.
5. Simultaneously, agar plates (see 2.1.13) containing the required antibiotic (ampicillin) were warmed in an oven at 37°C.
6. 150µl SOC media, bacteria were spread onto the pre-dried agar plate and incubated either at 37°C overnight, or at room temperature for 72 hours.

2.1.8 Production of Agar Plates

2.1.8.1 Materials, Reagents and Equipment

- LB-Agar — Novagen
- Ampicillin — Sigma
- Microwave Oven
- Non-tissue culture treated 10cm petri-dishes — Falcon
- Bunsen burner

Buffers and solutions:

Agar = 5g yeast extract, 10g peptone from casein, 10g NaCl in 1L deionised water

2.1.8.2 Protocol

1. 500ml agar was melted in a microwave oven for 20 minutes at 40% maximum power to obtain a molten solution.
2. After cooling down, 50mg ampicillin was added and mixed thoroughly.
3. The solution was distributed evenly over 20 petri dishes and left to solidify at room temperature.
4. Petri dishes were stored at 4°C (upside down).

2.1.9 Selection of Bacterial Clones

2.1.9.1 Materials, Reagents and Equipment

- L-Broth
- Ampicillin
- 14ml Polystyrene round-bottom tubes
- 20µl pipette tips — Star Lab
- Excella E-25 Shake Incubator

Buffers and solutions:

L-broth: 10g tryptone, 5g yeast extract, 0.5g NaCl

2.1.9.2 Protocol

1. 3ml of L-broth, containing 150ng of ampicillin was aliquoted into the 14ml round-bottom tubes.
2. Single bacterial colonies were selected using a pipette tip and submerged in the L-broth.

3. The tubes were shaken at 160rpm for 16 hours at 37°C prior to being centrifuged at 1500g for 10 minutes to pellet the bacteria. The supernatant was discarded and the pellet subjected to plasmid isolation.

2.1.10 Isolation of Plasmid DNA - Miniprep

Retrieval of plasmid DNA was achieved using a QIAprep Spin Miniprep kit. Approach is based on the rapid alkaline procedure reported by Birnboim and Doly [308], in which bacterial lysis was achieved using sodium dodecyl sulphate (SDS) in the presence of 200mM sodium hydroxide (NaOH). The resulting denaturing of proteins and chromosomal DNA caused by the strongly alkaline environment ensured their co-precipitation with SDS upon neutralisation of the solution and the conversion to high salt conditions by the addition of potassium acetate. The supercoiled conformation of the plasmid DNA prevented separation of the DNA strands, thereby ensuring that it remained in solution. Contaminating RNA was removed by both the addition of RNAse A to the initial resuspension buffer and precipitation in the high salt environment of the neutralisation buffer. Removal of any remaining impurities was achieved by running the aqueous phase through a column containing a silica membrane. The presence of the chaotropic salt, guanidine hydrochloride, in the neutralisation buffer induced dehydration of the plasmid DNA, allowing it to bind strongly to the silica membrane [309], whilst other contaminating factors were removed in the flow-through. Following wash steps with chaotropic salt and ethanol-containing buffers, the purified plasmid DNA was eluted from the column using a low salt buffer.

2.1.10.1 Materials, Reagents and Equipment

- QIAprep spin Miniprep kit — Qiagen
- Transformed TOP10F' *E. Coli*
- 1.5ml Eppendorfs
- Eppendorf 5415R refrigerated Microcentrifuge — Eppendorf

Buffers and solutions:

Buffer P1 = 50mM Tris-Cl, 1mM EDTA, 100µg/ml RNAse

Buffer P2 = 200mM NaOH, 1% SDS

Buffer EB = 10mM Tris-Cl (pH 8.5)

N.B. Qiagen does not publish the full composition of the neutralising N3 buffer, buffer PB or buffer PE. Buffer N3 is known to contain guanidine hydrochloride (as the source of chaotropic salt) and acetic acid (possibly potassium acetate) to neutralise the alkaline environment caused by the NaOH in buffer P2. The composition of buffer PE is not publically available.

2.1.10.2 Protocol

1. Pelleted bacteria were resuspended in 250µl buffer P1.
2. An equal volume of buffer P2 was added and the sample was gently inverted approximately 10 times to ensure complete mixing.
3. After a five-minute incubation at room temperature, 350µl buffer N3 was added to each sample. Complete mixing was achieved thorough gentle inversion.
4. Configuration at 15,700g pelleted the white precipitate in each sample.
5. The aqueous phase was carefully transferred to a QIAprep spin column and the white precipitate discarded.
6. Each column was washed with 750µl buffer PE and centrifuged at 15,700g and the eluate was again discarded.
7. After an additional centrifugation at 15,700 x g to remove any residual ethanol, the DNA was eluted in 50µl buffer EB through centrifugation at 15,700g.
8. The concentration of the isolated DNA was determined and stored at -20°C.

2.1.11 Isolation of plasmid DNA - maxiprep

Maxi-preps were used for the isolation of highly concentrated plasmid DNA. As with mini-preps, the process relies on bacterial lysis under strong alkaline conditions, with proteins and chromosomal DNA removed by precipitation upon neutralisation and conversion to a high salt environment. RNA impurities were removed through the addition of RNase A in the initial re-suspension buffer. Once insoluble contaminants had been removed by centrifugation, the supernatant (containing the plasmid DNA) was subjected to anion-exchange chromatography. The negatively charged plasmid DNA binds strongly to the positively charged diethylaminoethyl (DEAE) resin beads and is then eluted using a high-salt containing buffer. Intermediate washes with buffers of increasing salt concentrations ensured the removal of remaining contaminants. Once eluted, the DNA was precipitated and desalted using a series of alcohol washes before being dissolved in TE buffer.

2.1.11.1 Materials, Reagents and Equipment

- 100mL TOP10F' *E. coli* containing plasmid of interest
- QIAGEN Plasmid Maxi Kit
- 1.5mL Eppendorf tubes
- Oak Ridge polycarbonate centrifuge tubes
- Oak Ridge polypropylene copolymer centrifuge tubes
- Sorvall RC 5B Centrifuge

- 70% Ethanol
- Isopropanol

Buffers and Solutions:

Buffer P1 = 50mM Tris.HCl (pH 8.0), 10mM EDTA, 100μg/mL RNase A

Buffer P2 = 200mM NaOH, 1% (w/v) SDS

Buffer P3 = 3M Potassium Acetate

Buffer QBT = 750mM NaCl, 50mM 3-(N-Morpholino)-propanesulfonic acid (MOPS), 15% (v/v) isopropanol, 0.15% (v/v) Triton X-100

Buffer QC = 1M NaCl, 50mM MOPS, 15% (v/v) isopropanol

Buffer QF = 1.25M NaCl, 50mM Tris.HCl (pH 8.5), 15% (v/v) isopropanol

TE Buffer = 10mM Tris.HCl (pH 8), 1mM EDTA.

2.1.11.2 Protocol

1. Once pelleted, the bacteria were re-suspended in 10 mL buffer P1 and bacterial lysis was induced by addition of an equal volume of buffer P2. Mixing ensured complete lysis.
2. Pre-chilled buffer P3 (10 mL) was added after a maximum of five minutes of lysis and the solution was well mixed to ensure complete neutralisation.
3. The solution was incubated on ice for approximately 15 minutes before being centrifuged at 20,200g for 30 minutes at 4°C.
4. The supernatant was decanted into a fresh polycarbonate centrifuge tube and centrifuged at 20,200g for 15 minutes at 4°C to ensure complete removal of all insoluble contaminants.
5. The resulting supernatant was added to a pre-equilibrated QIAGEN-tip 500 and left to filter by gravity flow.
6. The tip was washed twice using 30 mL buffer QC before the plasmid DNA was eluted into a polypropylene copolymer centrifuge tube using 15 mL buffer QF.
7. The DNA was precipitated by adding 10.5 mL isopropanol and pelleted by centrifugation for 30 minutes at 17,700g and 4°C.
8. The pellet was washed with 5 mL 70% ethanol to remove the salt and the DNA pelleted by centrifugation at 20,000g for 10 minutes.
9. After removal of the supernatant and air-drying of the DNA pellet at 37°C for approximately five minutes, the DNA was re-suspended in 200 μL of TE buffer.
10. Once the concentration of DNA had been calculated it was stored at -20°C until required.

2.1.12 Generation of Chimeric antigen receptor-encoding retroviral constructs

2.1.12.1 Targeting moieties for candidate c-Met re-targeted CARs

To engineer candidate c-Met re-targeted CARs, three peptide sequences derived from the N and K1 domains of HGF were engineered to create targeting moieties:

(i) IK1 – in which the NK1 polypeptide was stabilised with two mutations, at K132E and R134E [141].
(ii) The M2.2 D127N peptide contains several stabilising mutations within NK1.
(iii) The cdM2.2 D127N peptide is identical to (ii) except that it contains an N-terminal cysteine.

Amino acid sequences of all three peptides are shown in Figure 2-1A. Codon optimised cDNAs encoding for these sequences were generated using Gene Designer software (version 2.0, Newark California) and were flanked by 5' NcoI and 3' NotI restriction sites. Synthetic cDNAs were provided in pUC57 for subcloning into retroviral plasmid vectors.

2.1.12.2 Cloning of CAR-encoding retroviral vectors

To engineer candidate CARs, The SFG V28z retroviral vector (a gift of Dr Lynsey Whilding) was used to provide the vector backbone. This vector was cleaved with NcoI and NotI and the large 6.3kB fragment was eluted as described in section 2.1.2. pUC57 plasmids containing the IK1, M2.2D127N and cdM2.2D127N cDNA sequences were digested with NcoI and NotI and the small (640bp approximately) fragments were extracted (section 2.1.2) and purified (section 2.1.3). After phosphatase treatment of the vector (section 2.1.4), DNA fragments were ligated (section 2.1.5) and *E. coli* transformed (section 2.1.7) after which clones were amplified (section 2.1.9). Miniprep DNA samples were prepared (section 2.1.10) and were screened by diagnostic restriction digestion enzyme analysis (section 2.1.1) in order to select one clone that contained the desired insert. This plasmid was expanded via mini/maxiprep (section 2.1.10, 2.1.11) and used to transfect retroviral packaging cells, as later described in section 2.2.4.

The schematic structure of the encoded CARs together with control CARs used in this project is shown in Figure 2-1B. The SFG T28z CAR vector was provided by Dr DM Davies (King's College London). The encoded CAR targets 8 of 9 possible homo- and heterodimers formed by the extended ErbB network [241]. The SFG V28z CAR vector was provided by Dr LM Whilding. It contains a 20mer targeting moiety derived from the foot and mouth disease virus which binds the αvβ6 integrin, but in which a critical RGDL amino acid sequence was mutated to AAAA, thereby abrogating all integrin binding

activity. Note that in all CARs, the CD28 hinge sequence contained a myc epitope tag (recognised by the 9e10 antibody) which had been inserted in SFG V28z in place of the MYPPPY motif (involved in the binding of CD28 to B7-1 and B7-2) [310]. Inclusion of the myc epitope tag allowed for detection of cell surface CAR expression by flow cytometry, as described in section 2.5.

2.1.12.3 Cloning of 4αβ-containing retroviral vectors

The chimeric cytokine receptor 4αβ comprises of the IL-4Rα ectodomain coupled to the IL-2/15Rβ endodomain. The construct was engineered by Dr SE Papa and Dr S Wilkie prior to the commencement of this PhD and allows the selective expansion of CAR-engineered T-cells using IL-4 [311]. The 4αβ sequence was followed by an optimised furin cleavage site (RRKR), a serine glycine linker, and a T2A sequence. This cDNA was flanked by NcoI restriction sites, allowing for cloning upstream of individual CAR cDNAs (Figure 2-2).

A

```
                1*                                                                  70
NK1             MWVTKLLPAL LLQHVLLHLL LLPIAIP YAE GQRKRRNTIH EFKKSAKTTL IKIDPALKIK TKKVNTADQC
1K1             ---------- ---------- ------- --- ---------- ---------- ---------- ----------
M2.2 D127N      ---------- ---------- ------- --- ---------- ---------- ---------- -E--------
cdM2.2 D127N    ---------- ---------- -------C--- ---------- ---------- ---------- -E--------


               71                                                                  140
NK1              ANRCTRNKGL PFTCKAFVFD KARKQCLWFP FNSMSSGVKK EFGHEFDLYE NKDYIRNCII GKGRSYKGTV
1K1              ---------- ---------- ---------- ---------- ---------- ---------- -E-E------
M2.2 D127N       ---------- ---------- ----R----- ---------- ---------- ------D--- -N----R---
cdM2.2 D127N     ---------- ---------- ----R----- ---------- ---------- ---------- -N----R---


              141                                                                  210
NK1              SITKSGIKCQ PWSSMIPHEH SFLPSSYRGK DLQENYCRNP RGEEGGPWCF TSNPEVRYEV CDIPQCSEVE
1K1              ---------- ---------- ---------- ---------- ---------- ---------- ----------
M2.2 D127N       ---------- ---------- ---------E --R------- ---------- --D------- ----------
cdM2.2 D127N     ---------- ---------- ---------E --R------- ---------- --D------- ----------


* A inserted between M and W to create NcoI cloning site
```

B

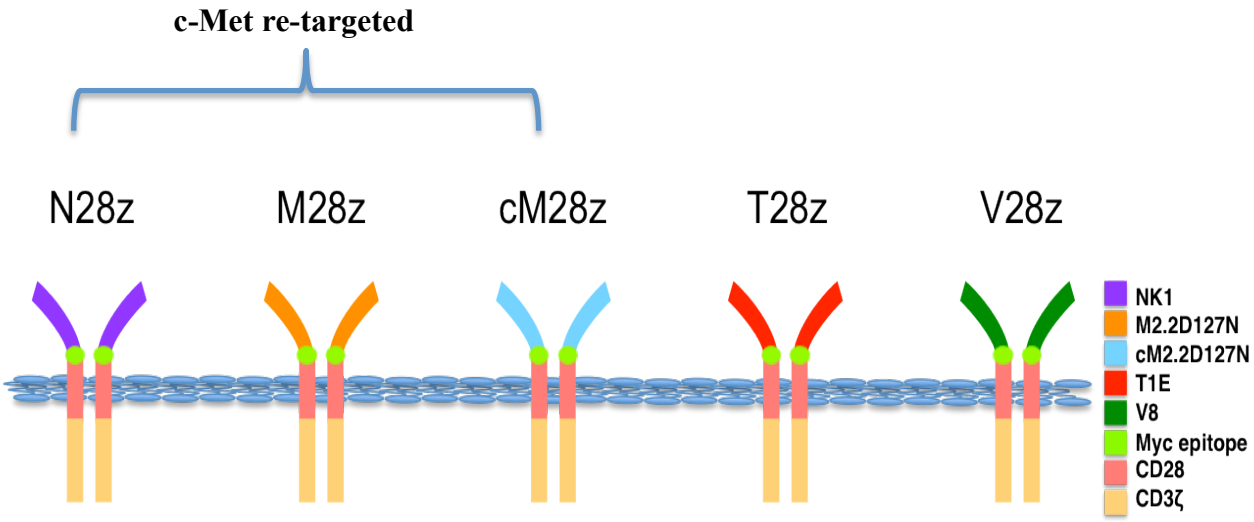

Figure 2-1. Schematic overview of candidate CARs generated to target c-Met
(A) Aligned amino acid sequences of c-Met targeting moieties (1K1, M2.2 D127N or cdM2.2 D127N), containing the N-terminal and first Kringle domains. The NK-1-derived signal peptide sequence is shown in blue. **(B)** Diagrams show structural features of candidate CARs engineered to target c-Met. The resulting CARs are referred to as N28z, M28z and cM28z respectively. Targeting moieties are housed within second-generation frameworks containing CD3ζ (signal 1) and CD28 (signal 2) modules within a fused CAR endodomain. The Myc epitope was added between the CD28 extracellular spacer and the c-Met targeting peptide to enable cell surface detection of the CAR by flow cytometry. The targeting moiety, T1E, within the T28z CAR$^+$ T-cells is a promiscuous ErbB ligand which has been fused to a CD28 + CD3ζ endodomain, serving as a useful positive control when targets expressed ErbB receptors. The V28z CAR contains a 20mer peptide that serves as a negative-control targeting moiety. This sequence was derived from the foot and mouth disease virus A20mer peptide that binds with high affinity to the integrin αvβ6, but in which a key RGDL sequence was replaced by AAAA to abrogate all integrin binding activity (Whilding & Maher, unpublished data).

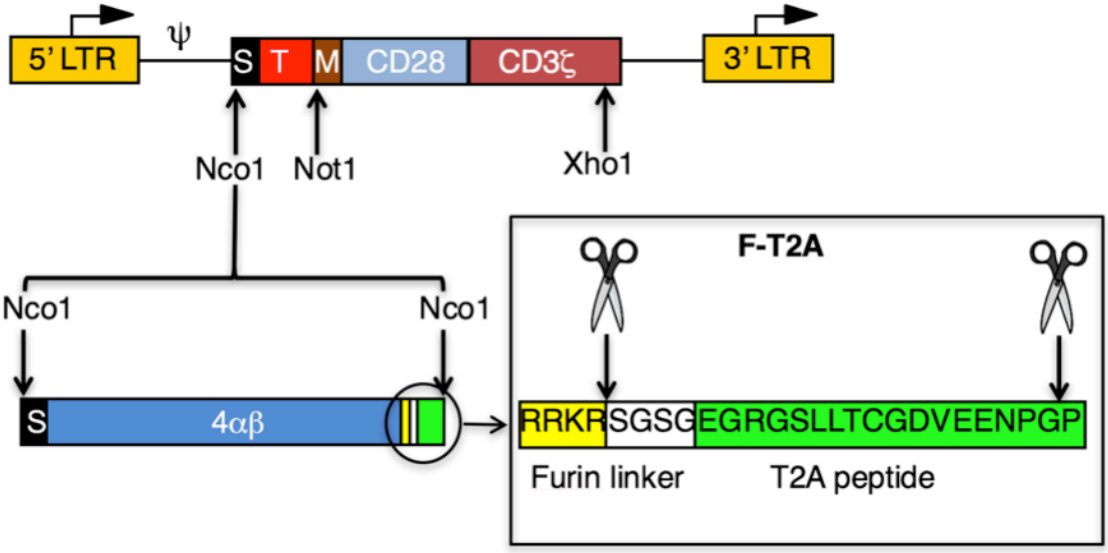

Figure 2-2. Schematic overview of bi-cistronic retroviral constructs
To co-express 4αβ with individual CAR constructs, SFG retroviral constructs were engineered to contain an intervening ribosomal skip 2A peptide from the insect virus, *Thosea Asigna* (T2A). A cassette was generated in which 4αβ was fused to a furin cleavage site (RRKR), SGSG linker and T2A peptide. This cassette was flanked by NcoI restriction sites, meaning that it could be conveniently inserted upstream of CAR cDNAs within SFG retroviral constructs. In these constructs, the NcoI restriction site is unique and coincides with the start codon (ATG) of each CAR construct. Abbreviations: LTR – log terminal repeat; S – signal peptide; T – chimeric receptor (in this case T28z); M – myc epitope tag, recognised by 9e10 antibody. It is predicted that the furin T2A peptide causes the ribosome to skip during translation between the terminal PG and P sequence within the 2A peptide, meaning that a peptide overhang is appended to the C-terminus of the upstream protein (here 4αβ). By inclusion of the furin cleavage site, it is hope that this overhang will be removed by furin as the protein passes through the Golgi.

2.1.13 Generation of Retroviral constructs encoding for c-Met and HGF co-factor molecules

SFG retroviral vectors were engineered to express human c-Met, human CD44v6 and human Syndecan-1. In each case the coding sequence for each molecule were were codon optimised for human expression using Gene Designer software (version 2.0, Newark California). Sequences were flanked by 5'NcoI and 3'XhoI restriction sites and were synthesised by Genscript (Hong Kong, China). These sequences were cloned into the unique NcoI and XhoI restriction sites of the SFG retroviral vector, as described in section 2.1.12.

2.1.14 Generation of Retroviral constructs encoding for Red fluorescent protein and firefly luciferase

The SFG retroviral vector was engineered to stoichiometrically co-express firefly luciferase (ffLuc) and tdTomato (tdTom). This was achieved through the use of T2A ribosomal skip sequence. The construct was engineered using a multi-step cloning protocol, as described in section 2.1. Sequences were flanked by 5'NcoI and 3'XhoI restriction sites. Firefly luciferase was isolated from the PUC57 LUC construct via NcoI/BamHI restriction enzyme digestion, yielding a fragment 1.7kB. TdTom was isolated from SFG Myc TOM using BamHI/XhoI restriction digest yielding a fragment 1.6kb. The SFG backbone (6.3kB size) was isolated using an NcoI/XhoI digest of the CAR vector SFG T4, which was kindly provided by Dr DM Davies (King's College London). These sequences were cloned, via 3-step ligation protocol, into the unique NcoI and XhoI restriction sites of the SFG retroviral vector, as described in section 2.1.12.

2.2 Cell Culture

All cells were incubated at 37°C, 95% O_2 / 5% CO_2

2.2.1 Media and Common Solutions

2.2.1.1 Media

D10	=	500ml Dulbecco's Modified Eagle Medium	
		(DMEM) + 4.5g/L glucose	Lonza
		50ml Foetal Bovine Serum	Sigma
		200mM GlutaMAX	Gibco
		50,000U Penicillin	Lonza
		50mg Streptomycin	Lonza

D10	=	500ml Dulbecco's Modified Eagle Medium	
(NIH 3T3)		(DMEM) + 4.5g/L glucose	Lonza
		50ml Calf Serum	
		200mM GlutaMAX	Gibco
		50,000U Penicillin	Lonza
		50mg Streptomycin	Lonza

R10	=	500ml Roswell Park Memorial Institute	
		(RPMI) 1640 Medium without L-Glutamine	
		50ml Human Serum	Sigma
		200mM GlutaMAX	
		50,000U Penicillin	
		50mg Streptomycin	

2.2.1.2 Common Solutions

Trypsin	=	0.25% Trypsin-EDTA	Gibco
CDB	=	Cell Dissociation Buffer	Invitrogen Life Tech
PBS	=	Phosphate Buffered Saline	Biochrom AG

2.2.2 MPM tumour cell lines

H28 – Human mesothelioma cell line derived from the pleural effusion of a patient with malignant mesothelioma – metastatic site. Epithelioid subtype (Disease stage 4).

REN – Human mesothelioma cell line. Epithelioid subtype.

JU77 - Human mesothelioma cell line derived from fluid of a male patient with malignant mesothelioma. The patient had known exposure to crocidolite asbestos. Cell line is not tumourigenic in nude mice. Cells of sarcomatoid subtype (no unanimous consensus). Cell are spindle shaped with few vacuoles.

LO68 – Human mesothelioma cell line derived from fluid of a male patient with malignant mesothelioma. The patient had known exposure to crocidolite asbestos. Cell line is non tumourigenic in nude mice. Epithelial-like subtype. Cells are spindle shaped with few vacuoles.

2.2.2.1 Retroviral Packaging Cell Lines

Gene transfer undertaken during this PhD was achieved using engineered retroviral vectors. The genome of each retrovirus (comprising two RNA copies) encodes at least four specific genes, named *gag*, *pol, env* and *pro* [312]. The binding of a mature retroviral particle to a target cell is mediated by a specific receptor or molecule on the surface of the host cell (Figure 2-3). These glycoproteins that bind this receptor are encoded by the retroviral *env* gene and thus responsible for the tropism of the viruses (i.e. the target cells with which it can interact) [312]. Following fusion of the retroviral envelope with the host cell membrane, the RNA genome is extruded into the host cell cytoplasm, upon when it is converted to a double stranded DNA copy via reverse transcriptase. This is subsequently integrated within the host cell genome by an integrase enzyme, resulting in a 'provirus' [312, 313]. Both of these enzymes are encoded by the *pol* gene in the retroviral genome and are contained within the packaged virus, prior to being released into the host cell cytoplasm after viral fusion. The transcription and translation of the viral genome by the host cell RNA polymerase results in the production of the proteins encoded by the *gag* gene, in addition to the production of new reverse transcriptase and integrase enzymes (Figure 2-3).

Although expressed as a single polypeptide until the later stages of viral budding, the *gag* gene encodes for a number of distinct proteins. One example is the Moloney murine leukaemia virus (MoMLV), the matrix (MA, p15), p12, capsid (CA, p30) and nucleocapsid

(NC, p10) structural proteins are all present within the *gag* polypeptide [312]. The N-terminal end of the polypeptide (the N-terminus of the MA protein) is myristoylated, thus anchoring it to the host cell membrane and providing a focal point for which new viral particles may be formed. Indeed, inhibition of myristoylation interferes with viral assembly [314]. At the C-terminal end of the *gag*-encoded polypeptide, the NC protein interacts with the viral genome and is responsible for ensuring its packaging into the new retroviral particle [315]. The reverse transcriptase and integrase enzymes are incorporated within the new viral particle, alongside a viral protease - the product of the pro gene found between the *gag* and the *pol* genes. Throughout and after budding, this protease is responsible for cleaving the gag-encoded polypeptide into its four constituent proteins. The significance of this polypeptide processing is highlighted by the fact mutations within the cleavage site between the p12 and CA proteins are sufficient to inhibit the formation of infectious MoMLV viral particles [316]. This cleavage event is part of the maturation process, during which retroviruses gain the ability to infect target cells prior to subsequent rounds of replication.

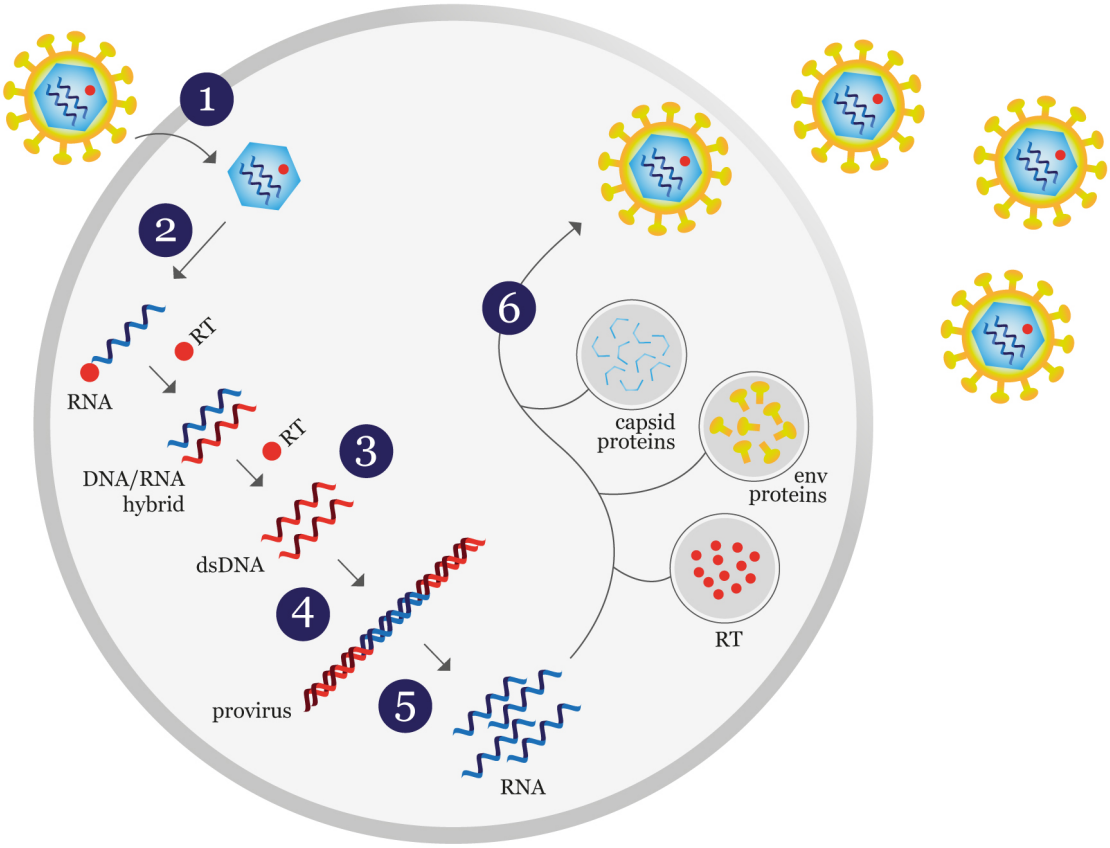

Figure 2-3. Retroviral Life Cycle. Adapted from **[317]**
Upon target cell infection (**1**), the viral particle envelope and capsid are disassembled, releasing the viral genome and proteins into the cytoplasm. The reverse transcriptase (RT) from the disassembled viral particle binds to a transfer RNA (tRNA) in the 5' LTR position of the viral genome, synthesising a complementary DNA strand (**2**). The template viral RNA is then degraded by the RNAse H subunit of the RT enzyme enabling synthesis of a second DNA strand (**3**). The double stranded DNA (dsDNA) is integrated as a provirus within the host genome by the viral integrase enzyme (**4**). Host RNA polymerase transcribes multiple viral RNA copies (**5**), which are then exported from the nucleus and transcribed to give the *gag*, *pol* and *env* proteins (**6**). These proteins, along with two copies of untranslated viral RNA are integrated within a new viral particle, which subsequently buds from the target cell.

The ability of retroviruses to integrate their genome into that of a host cell provides an appealing way of achieving stable expression of a transgene within a specific target cell population. However, an undesirable property is the continued virus replication following infection of the target cell population. One way of preventing the production of replication-competent retrovirus (RCR) within the target cells is to replace the *gag, pro, pol* and *env* genes with that of the transgene of interest. However, as detailed above, the proteins encoded by these four genes are essential for the production and function of viable virions. The use of retroviral packaging cell lines offers a way of producing viral particles that are unable to replicate following infection of the target cell.

The retroviral genomic sequence (containing the desired gene) is subsequently packaged within viruses, which are thenceforth capable of infecting the target cell of choice. However, as these viruses do not contain the necessary genes for the formulation of fresh viral particles, further replication is prevented. In order to minimise the risk of producing RCR, the *gag-pol* and *env* genes are expressed on separate plasmids within the packaging cells. Consequently, three separate recombination events are required before all genes are expressed in *cis*. The *pol* gene is always expressed on the same plasmid as *gag* due to the fact the gag-pro-pol genes are transcribed as a single mRNA transcript. The presence of a stop codon at the end of the *gag* coding sequence means that, in 95% of cases, translational read-through (caused by the misreading of the stop codon) results in the production of a *gag-pro-pol* polypeptide [318].

Retroviral packaging cells used during this PhD:

2.2.2.2 H29D

The H29D retroviral packaging cell line is based on the human embryonic kidney adenoviral 5-transformed cell lines (HEK293, [319]). H29D expresses the MoMLV *gag-pol* genes, regulated by the cytomegalovirus (CMV) immediately early (IE) [320]. Expression of the vesicular stomatitis virus-G (VSV-G) env proteins results in the production of viral particles exhibiting a broad tropism "pantropic". Constitutive expression of the VSV-G envelope protein is toxic, thus controlled expression was achieved via placing the VSV-G coding sequence under the control of a tetracycline-repressed promoter [320]. Activation of transcription from the promoter is dependent upon the binding of a tetracycline-transactivator (tTa) molecule [321]. However, in the presence of tetracycline, binding of the tTa molecule to promoter is inhibited, preventing subsequent gene expression. Consequently, to prevent constitutive expression of the VSV-G protein, cells were maintained in D10 media supplemented with 2µg/mL tetracycline. Fresh D10 and tetracycline were added every 72 hours and cells were passaged upon confluency. Tetracycline was removed to allow for the production of VSV-pseudotyped virus.

2.2.2.3 PG13

The PG13 retroviral packaging cell line is derived from the NIH 3T3 murine fibroblast cell line [322]. Akin to H29D cells, PG13 cells express the MoMLV gag-pol genes. Contrastingly, PG13 viral particles are pseudotyped with the gibbon-ape leukaemia virus (GaLV) envelope protein. As with the VSV-G pseudotyped virus, the PG13 GaLV pseudotyped viral particles are capable of infecting human cells.

2.2.3 Retroviral Vectors

Retroviral vectors constitute the backbone of the virus and include necessary elements, such as the promoter regions required for transcription of the inserted gene(s) and the packaging signal (ψ) required for packaging of the mRNA transcript into new viral particles.

2.2.3.1 SFG (based on MFG)

The SFG retroviral vector is based on the MFG vector [323], in which gene expression is driven by the MoMLV long terminal repeats (LTRs). The presence of the MoMLV ψ packaging signal ensures efficient packaging of the RNA within the virus. The presence of the splice donor and splice acceptor sites enables the production of the sub-genomic RNA transcripts, typically required for translation of the *env* gene [318]. The gene of interest is inserted from a naturally occurring NcoI site, ensuring that its start codon is in the precise location previously occupied by the deleted *env* gene. This vector does not contain a eukaryotic cell-compatible selectable marker gene. It does contain an ampicillin resistant gene for selection following transformation of competent bacteria.

2.2.4 Production of retroviral packaging cell lines

For the transduction of human T-cells stable PG13-retroviral packaging cell lines were produced using H29D viral supernatant as an intermediate for PG13 transduction. Two methods of transfection were used, involving calcium phosphate or polyethyleneimine. Both methods are described below.

2.2.4.1 Materials, Reagents and Equipment

- CalPhos mammalian transfection kit — CloneTech
- Vortex
- Polyethylenimine (PEI) — Sigma
- Plasmid DNA
- H29D cells
- PG13 cells
- H29D retroviral supernatant

Components of the CalPhos Calcium Phosphate transfection kit:

- 2M Calcium Solution ($CaCL_2$)
- 2x HEPES-buffered saline (HBS)
- Sterile H_20

2.2.4.2 Calcium-Phosphate transfection (H29D)

Preparation of H29D cells

1. H29D cells were transduced in 6-well culture plates.

2. Cells were split at least 2 days prior to transfection in 3mL D10 media supplemented with tetracycline.
3. The tetracycline was removed from the H29D cells, a minimum of 2 hours prior to transfection by replacing the tetracycline-containing D10 with fresh D10 media only.

Preparation of Transfection Mixture

1. Solution A was prepared and left to incubate at room temperature for 5 minutes;

Solution A:

- 12.4µl 2M Calcium Solution ($CaCL_2$)
- 1-3µg retroviral vector
- Sterile H_2O to a final volume of 100µL

2. Solution A was added to dropwise to 100µL 2x HBS whilst vortexing.
3. The mixture was incubated at room temperature for 20 minutes to ensure the formation of precipitate, before being added dropwise to the target cells.
4. After gentle rocking ensured complete mixing of the transfection mixture, the cells were incubated for 24 hours after which the media was replaced.
5. Supernatants were harvested daily from day 3-7 post transfection and directly used for infection of target cells (PG13).

2.2.4.3 PEI-mediated transfection (H29D)

1. H29D packaging cell lines were prepared as described in paragraph 2.2.4.2.
2. Transfection mixture was prepared and left to incubate at room temperature for 20 minutes.

- 400µl serum free DMEM
- 5µg plasmid DNA
- 1µl 1mM PEI

3. Transfection mixture was added dropwise to the target cells.
4. The cells were incubated for 3-4 hours after which the media was replaced with fresh D10 media.
5. Media was again refreshed 24 hours prior to the (first) harvest of retroviral supernatant.
6. Supernatants were harvested daily from day 3-7 post transfection and directly used for target cell infection (PG13).

2.2.4.4 PG13 Transduction

1. The media was removed from empty PG13 packaging cells and replaced with 3ml H29D supernatant containing the VSV-pseudotyped virions.

2. The PG13 were then incubated for 72 hours prior to analysis for transgene expression using flow cytometry.
3. PG13 cells expressing the virus of interest were subsequently used as stable packaging cell lines.

2.2.5 Generation of NIH 3T3 artificial antigen presenting cells

1. PG13 cells were engineered to express human c-Met or CD44v6 (plasmids described in section 2.1.13) as detailed in section 2.2.4).
2. Phoenix-eco packaging cells (purchased from the European Tissue Culture Collection) were seeded sparsely in 6-well plates and allowed to adhere overnight.
3. Supernatant was removed from PG13 packaging cells and was gently filtered onto phoenix-eco cells. Fresh viral supernatant was added every 48 hours.
4. After 7-9 days, phoenix-eco packaging cells were FACS analysed for confirmation of positive expression of the designated receptor.
5. NIH 3T3 cells were sparsely seeded in 6-well plates and allowed to adhere overnight.
6. Fresh viral supernatant from transduced phoenix eco cells was gently filtered onto NIH 3T3 cells and replaced with fresh virus-containing medium every 24-48 hours.
7. After 7-9 days culture, NIH 3T3 packaging cells were FACS analysed for confirmation of transduction for c-Met, CD44v6, or dual positive c-Met+CD44v6 expression.

2.2.6 PBMC isolation and activation

Peripheral blood mononuclear cells (PBMCs) were isolated from healthy donors using Ficoll-Paque gradient. Recruitment of healthy volunteer donors for this purpose was approved by the Guy's Hospital research Ethics Committee (09/H0804/92; Use of Donor Blood Samples for Pre-Clinical Development of Active and Passive Immunotherapy for Cancer and 09/H0707/086; Generation of clinical grade T-cells for adoptive cell therapy).

2.2.6.1 Materials, Reagents and Equipment

- Fresh Blood	
- Citrate-Dextrose Solution (ACD)	Sigma
- 50ml Syringe	BD Biosciences
- 21G Butterfly Needle	Greiner Bio-One
- 50ml Falcon tubes	SLS
- Ficoll-Paque Plus	GE Healthcare
- Eppendorf 5804 Centrifuge	Eppendorf

- Pasteur Pipettes — SLS
- Anti-CD3/Anti-CD28 Dynabeads — Invitrogen
- R10 Medium — Section 2.2.1

2.2.6.2 Protocol

N.B. All steps of the procedure and all reagents used are at room temperature for optimal cell recovery.

1. 15ml Ficoll-Paque was aliquoted into two separate 50ml Falcon tubes.
2. Fresh Blood (25ml) (anticoagulated with 1x citrate-dextrose solution) was slowly layered onto the Ficoll-Paque and then centrifuged at 1150g for 25 minutes (acceleration = 0, deceleration = 0).
3. The PBMC layer, present at the interface between the Ficoll-Paque and the plasma was transferred into fresh 50ml Falcon tubes using a Pasteur pipette and diluted to a final volume of 50ml in pre-warmed PBS and centrifuged for 10 minutes at 550g.
4. The cell pellet was re-suspended in 50ml PBS and centrifuged for 10 minutes at 550g.
5. Following aspiration of the supernatant, the cell pellet was re-suspended in 10ml R10 media and cells were counted.
6. Cells were re-suspended in R10 media at a concentration of 3 x 10^6 cells/m and activated with anti-CD3/CD28 paramagnetic Dynabeads at a 3:1 cell: bead ratio.

2.2.7 Production of RetroNectin coated 6-well plates

In order to improve T-cell transduction efficiency, non-tissue culture treated plates were pre-treated with RetroNectin (RN). Retronectin is a fragment of the extracellular matrix protein fibronectin that binds the target T-cell through a CS-1 domain and a cell-binding domain (CBD), which interacts with the VLA-4 and VLA-5 integrin receptors respectively. Attachment of the virus to the heparin binding domain present in RN between the CS-1 and CBD causes co-localisation of the target cell and the virus, thus greatly improving gene transfer efficiency [324, 325].

2.2.7.1 Materials, Reagents and Equipment

- RetroNectin — TaKaRa
- Non-tissue culture treated 6-well plates — Falcon
- PBS
- Pasteur pipettes
- 50ml syringe

2.2.7.2 Protocol

1. 200µg of RN was re-suspended in 12mL PBS/plate.
2. 2ml of the resulting solution was transferred using a Pasteur pipette into each well of a non-tissue culture treated 6-well plate, thereby giving coverage approximately 3.5µg/cm^2.
3. Plates were incubated for a minimum of 2 hours at room temperature or 24 hours at 4°C prior to use.
4. When the plate was ready to be used, unbound RN was transferred to a new plate using a Pasteur pipette. RN was used for a maximum of two transduction plates.

2.2.8 Retroviral-mediated Human T-cell Transduction

To introduce the CAR constructs into T-cells, they were subjected to retroviral-mediated transduction. This ensured integration of the inserted coding DNA into the host T-cell genome, thereby permitting stable CAR expression.

2.2.8.1 Materials, Reagents and Equipment

- Activated T-cells
- Retroviral packaging cell lines
- Centrifuge
- Retronectin-coated plate
- Pasteur pipettes
- Interleukin-2 (IL-2) (Proleukin) Novartis

2.2.8.2 Protocol

1. After the unbound RN had been transferred to a fresh plate using a Pasteur pipette, each well was coated with 3ml of retrovirus-containing supernatant from the desired packaging cell line.
2. Activated T-cells were counted using trypan-blue exclusion and 1 x 10^6 viable cells added to each well.
3. Each well was supplemented with 100U/ml of IL-2.
4. Plates were centrifuged for one hour at 50g, at room temperature.
5. Cells were subsequently cultured for 4-6 days, after which the transduction efficiency was determined using flow cytometry.

2.2.9 Determination of the anti-tumour potential of CAR$^+$ T-cells

In order to demonstrate the ability of CAR T-cells to recognise and destroy c-Met expressing targets, they were co-cultured with a variety of murine fibroblast cell lines and human tumour cell lines. Target recognition and activation of CAR T-cells monitored by measuring cytokine release using ELISA. Anti-tumour activity was quantified using an

MTT (3-[4,5-dimethylthiazol-2-yl]- 2,5I- diphenyltetrazolium bromide; thiazolyl blue) assay, which quantifies residual viable tumour cells.

2.2.9.1 Materials, Reagents and Equipment

- Transduced T-cells
- NIH 3T3 aAPCs
- Tumour cells
- D10 media
- R10 media
- IL-2
- IL-4
- 96-well cell culture plate
- 24-well cell culture plate

2.2.9.2 Protocol – 24 well plates

1. 2 x 10^5 Tumour or NIH 3T3 cells were seeded into a 24-well cell culture plate and allowed to adhere overnight.
2. T-cells were counted and re-suspended in R10 media at determined concentrations for respective effector to target ratios, and gently pipetted onto the surface of the tumour monolayer.
3. After 48 hours of incubation, 400µl supernatant was removed for analysis of cytokine (IL-2 and IFN-γ) secretion.

2.2.9.3 Protocol – 96 well plates

1. 2 x 10^4 Tumour or NIH 3T3 cells were seeded into a 96-well cell culture plate and allowed to adhere overnight.
2. T-cells were counted and re-suspended in R10 media at determined concentrations for respective effector to target ratios, and gently pipetted onto the surface of the tumour monolayer.
3. After 24/48 hours of incubation, 100µl supernatant was removed for analysis of cytokine (IL-2 and IFN-γ) secretion (section 2.3.1).

2.2.10 Quantification of tumour-cell destruction – MTT assay

In vitro anti-tumour activity of CAR^+ T-cells was quantified using an MTT (3-[4,5-dimethylthiazol-2-yl]- 2,5- diphenyltetrazolium bromide; thiazolyl blue) assay. MTT is a water soluble tetrazolium salt yielding a yellow solution when prepared in media or salt solution lacking phenol red. Mitochondrial dehydogenases of viable cells cleave the tetrazolium ring in dissolved MTT, yielding purple formazan crystals, which are insoluble in aqueous solutions. The crystals are dissolved in acidified isopropanol. The resulting

purple solution is detected optimally at a wavelength of 570nm using a spectrophotometer. Dead cells do not cause this change. An increase or decrease in viable cell number results in a concomitant change in the amount of formazan formed, enabling the level of target cell cytotoxicity to be extrapolated [326].

2.2.10.1 Materials, Reagents and Equipment

- MTT — Sigma
- PBS
- DMSO — VWR
- FLUOstar Omega — BMT Labtech
- Omega Software (version 1.20) — BMT Labtech
- MARS data analysis software (version 1.20 R2) — BMT Labtech

2.2.10.2 Protocol – 24-well plates

1. MTT assays were performed in 24-well cell culture treated plates.
2. MTT stock solution was reconstituted at a concentration of 5mg/ml in PBS. Stock solution is stored at -20°C.
3. MTT stock solution was diluted 1/10 (to a concentration of 500µg/ml) in D10 media. Medium was aspirated from the co-culture and 500µl MTT (250µg) was added to each well.
4. Cell cultures were incubated for 2 hours at 37°C and 5% CO_2.
5. The supernatant was aspirated and the formed formazan crystals were resuspended in 300uL DMSO.
6. Absorbance was measured spectrophotometrically at 570nm.
7. Relative cell viability was calculated using the following equation:

Viability = (absorbance of test well/average absorbance of untreated tumour monolayer)x100

2.2.10.3 Protocol – 96-well plates

8. MTT assays were performed in 96-well cell culture treated plates.
9. MTT stock solution was reconstituted at a concentration of 5mg/ml in PBS. Stock solution is stored at -20°C.
10. MTT stock solution was diluted 1/10 (to a concentration of 500µg/ml) in D10 media. Medium was aspirated from the co-culture and 50µl MTT (25µg) was added to each well.
11. Cell cultures were incubated for 1-2 hours at 37°C and 5% CO_2.
12. The supernatant was aspirated and the formed formazan crystals were resuspended in 50µl DMSO.
13. Absorbance was measured spectrophotometrically at 570nm.

14. Relative cell viability was calculated using the following equation:

Viability = (absorbance of test well/average absorbance of untreated tumour monolayer) x 100

2.3 Detection of cytokine release

2.3.1 Enzyme-Linked Immunosorbent Assay (ELISA)

2.3.1.1 Materials, Reagents and Equipment

- High-binding flat-bottom 96-well ELISA plates — Iwaki
- IFN-γ Ready-Set-Go ELISA Kit — eBioscience
- IL-2 Ready-Set-Go ELISA Kit — eBioscience
- HGF ELISA Kit
- FLOstar Omega plate reader — BMT Labtech
- Omega Software (vrsion 1.20) — BMT Labtech
- MARS data analysis software (version 1.20R2) — BMT Labtech

Contents of Ready-Set-Go ELISA Kits:

- Capture antibody
- Detection antibody
- Con. Standard
- 10x Coating buffer
- 5x Assay diluent
- Avidin-HRP
- Substrate solution
-

Buffers and solutions:

Wash buffer = PBS + 0.05% Tween-20

2.3.1.2 Protocol

1. The capture antibody was diluted 1/250 in 1x coating buffer. Subsequently, the 96-well ELISA plate was coated with 100µl/well of capture antibody. The plates were sealed and incubated overnight at 4°C.
2. All the wells were aspirated and washed 3 times with >250µl/well wash buffer. The wash buffer was allowed to soak for 1 minute during each step for increased effectiveness of the washes.

3. One part 5x concentrated assay diluent was diluted in 4 parts distilled water.
4. All wells were blocked with 200µl/well of 1x assay diluent for 1 hour at room temperature.
5. Plates were washed as described in step 3.
6. Standard curve samples were serially diluted two-fold in assay diluent to give a seven point standard curve ranging from an original concentration of 500pg/ml to 3.9pg/ml and were plated in duplicate. Background absorbance was measured by plating assay diluent alone. Supernatant samples from co-cultivation were diluted 1:20 to 1:100 to assay diluent prior to plating in triplicate. The plates were sealed and incubated overnight at 4°C.
7. The plates were washed as described in step 3.
8. Detection antibody was diluted 1/250 in assay diluent, and 100µl/well added. Plates were sealed and incubated for 1 hour at room temperature.
9. Plates were washed as described in step 3.
10. Avidin-HRP was diluted 1/250 in assay diluent, and 100µl/well added. Plates were sealed and incubated for 30 minutes at rom temperature.
11. Plates were washed as described in step 3. On this occasion, plates were washed a total of 5 times, allowing 1-2 minutes of soaking between washes.
12. 100µl/well of TMB substrate solution was added to each well and plates were incubated for 15 minutes at room temperature.
13. The reaction was stopped by adding 50µl/well of stop solution (2M H_2SO_4).
14. Absorbance was read at 450nm using the FLUOStar Omega plate reader.
15. Standard curves and cytokine concentration were calculated using the MARS data analysis software.

2.3.2 Determination of the combined anti-tumour potential of chemotherapy plus CAR$^+$ T-cells

In order to assess whether chemotherapy agents could sensitise MPM tumour cells to c-Met re-targeted CAR T-cells, MPM cells were co-cultured with increasing dose concentrations of both cisplatin ± pemetrexed to generate dose response curves. Designated concentration of each drug was added to MPM tumour cells for 24-hours. Culture medium was removed and replaced with medium containing designated number of CAR T-cells. Target recognition and activation of CAR T-cells monitored by measuring cytokine release (IL-2 and IFN-γ). Anti-tumour activity was quantified using an MTT (3-[4,5-dimethylthiazol-2-yl]- 2,5I- diphenyltetrazolium bromide; thiazolyl blue).

2.3.2.1 Materials, Reagents and Equipment

- Cisplatin — Guy's Hospital Chemotherapy Unit
- Pemetrexed — Guy's Hospital Chemotherapy Unit
- Transduced T-cells
- MPM tumour cells
- D10 media
- R10 media
- IL-2
- 96-well cell culture plate

2.3.2.2 Protocol – Dose response

1. 2 x 10^4 Tumour cells were seeded into 96-well cell culture plate and allowed to adhere overnight.
2. Chemotherapy agents (cisplatin ± pemetrexed) were added in decreasing 5-fold serial dilutions and incubated overnight at 37°C and 5% CO_2.
3. Tumour cell viability was determined by MTT – detailed in section 2.2.10.

2.3.2.3 Protocol – combination protocol

1. 2 x 10^4 Tumour cells were seeded into 96-well cell culture plate and allowed to adhere overnight.
2. Chemotherapy agents (cisplatin ± pemetrexed) were added in decreasing 5-fold serial dilutions and incubated overnight at 37°C and 5% CO_2.
3. Medium containing chemotherapy agents was removed and replaced with 100ul fresh D10 medium.
4. 2 x 10^4 T-cells (100ul) were gently seeded onto monolayers - co-cultures were incubated overnight at 37°C and 5% CO_2.
5. Tumour cell viability at 24/48 hours was determined by MTT – detailed in section 2.2.10.
6. 100µl supernatant was removed for analysis of cytokine (IL-2 and IFN-γ) secretion after 48-hour co-culture (section 2.3.1).

2.3.3 Determination of anti-tumour activity against MPM cell lines using combined immunotherapy with pembrolizumab and c-Met re-targeted CAR$^+$ T-cells

The PD-1 inhibitor, pembrolizumab, was tested for its ability to potentiate anti-tumour activity mediated by c-Met re-targeted CAR T-cells. Target recognition and activation of CAR T-cells monitored by measuring cytokine release (IL-2 and IFN-γ). Anti-tumour activity was quantified using an MTT (3-[4,5-dimethylthiazol-2-yl]- 2,5I-diphenyltetrazolium bromide; thiazolyl blue).

2.3.3.1 Materials, Reagents and Equipment

- Pembrolizumab (Keytruda – Merck) Guy's Hospital Pharmacy
- Transduced T-cells
- MPM tumour cells
- D10 media
- R10 media
- IL-2
- 96-well cell culture plate

2.3.3.2 Protocol – combination protocol

1. 2 x 10^4 MPM tumour cells were seeded into 96-well cell culture plate and allowed to adhere overnight.
2. T-cells were counted and re-suspended in R10 media ± 10μg or 100μg pembrolizumab at respective effector to target ratios (1 T-cell: 1 tumour cell), and gently pipetted onto the surface of the tumour monolayer. Co-cultures were incubated at 37°C and 5% CO_2.
3. After 24/48 hours of incubation, 100μl supernatant was removed for analysis of cytokine (IL-2 and IFN-γ) secretion.
4. Tumour cell viability at 24/48 hours was determined by MTT – detailed in section 2.2.10.

2.4 *In vivo* Models

All *in vivo* experiments were performed in accordance with the UK Home Office guidelines as stated in the project license (license number 70/6847) and personal license (PIL 70/23830) that governed this work. All animal models were conducted in NOD.Cg-Prkdc^{scid} Il2rg^{tm1wjl}/SzJ. This mice strain is immune-deficient, lacking mature T-cells, B-cells, functional NK-cells, and is also deficient in signalling by cytokines that employ the common γ receptor.

2.4.1 Development of an *in vivo* Mesothelioma Model

In order to test the anti-tumour potential of c-Met re-targeted CAR T-cells *in vivo*, a suitable xenograft model was established. Luciferase-expressing tumour cells were administered by either subcutaneous (s.c.) or intraperitoneal (i.p.) routes and monitored for engraftment and growth.

2.4.1.1 Materials, Reagents and Equipment

- D-Luciferin
- IVIS Lumina II Bioluminescent Imaging Platform — Caliper Life Science, UK
- Isoflourane anaesthetic — Baxter, UK
- 1ml syringe — BD Plastipak
- 25G Needle — BD Biosciences
- BD Matrigel Basement Membrane Matrix
- PBS

2.4.1.2 Protocol

The numbers of tumour cells and injection volumes used have been detailed within the individual experiments.

Intra-peritoneal (i.p.) tumour inoculation

1. Mice were randomised into the required number of groups.
2. The specified number of tumour cells were re-suspended in 200µl PBS and injected into the intra-peritoneal cavity using a 25G needle connected to a 1mL syringe.
3. Tumour growth was monitored using BLI (please refer to section 2.4.2).

Subcutaneous (s.c.) tumour inoculation

1. Mice were randomised into the required number of groups.

2. The specified number of tumour cells were re-suspended in 200µl PBS or Matrigel injected subcutaneously into the right flank using a 25G needle connected to a 1ml syringe.
3. Tumour growth was monitored using BLI (please refer to section 2.4.2).

2.4.2 Bioluminescence Imaging

Bioluminescence Imaging (BLI) is a sensitive, non-invasive technique for monitoring tumour growth *in vivo*. After delivery of the D-luciferin substrate, the luciferase-expressing tumours are visualised in situ whilst the mice are under general anaesthesia.

2.4.2.1 Materials, Reagents and Equipment

- D-Luciferin
- IVIS Lumina II Imaging Platform
- Isoflourane
- 1mL syringe
- 25G Needle
- PBS

2.4.2.2 Protocol

1. Mice were injected i.p. with 200µl (3mg) D-luciferin and placed back in their cages for seven minutes.
2. Mice were anesthetised with 3-4% gaseous isofluorane and transferred to IVIS Lumina platform.
3. Nine images of increasing duration (1s, 2s, 5s, 10s, 30s, 45s, 60s, 120s, 180s) were taken using small binning. Throughout imaging, mice were maintained under anaesthesia with 1.5% isofluorane.
4. The mice were returned to their cages once the imaging was completed and monitored until they had regained consciousness.

2.4.3 Therapeutic Study

To determine *in vivo* efficacy of T-cell immunotherapy, mice were treated with different doses of CAR^+ or control T-cells, administered using the i.p. route of administration.

2.4.3.1 Materials, Reagents and Equipment

- D-Luciferin
- IVIS Lumina II Imaging Platform
- Isoflourane
- 1ml syringe
- 25G Needle

- PBS

2.4.3.2 Protocol

1. On Day 0, 55 male NSG mice were inoculated i.p. with 5 x 10^4 firefly luciferase-expressing REN tumour cells.
2. Five days later, the mice underwent BLI in order to confirm successful tumour cell engraftment. Mice were subsequently used in the proceeding study.
3. On Day seven, mice were re-imaged to confirm tumour engraftment prior to treatment with T-cells the following day.
4. Day eight, the groups were treated as follows (N.B. CAR^+ T-cells were not corrected for transduction efficiency):
    a. 10 x 10^6 or 2.5 x 10^6 $N4^+$ T-cells i.p. (n=5)
    b. 10 x 10^6 or 2.5 x 10^6 $M4^+$ T-cells i.p. (n=5)
    c. 10 x 10^6 or 2.5 x 10^6 $cM4^+$ T-cells i.p. (n=5)
    d. 10 x 10^6 or 2.5 x 10^6 $V4^+$ T-cells i.p. (n=5)
    e. 10 x 10^6 untransduced UT T-cells i.p. (n=5)
    f. PBS i.p. (n=8)
5. Mice were imaged regularly over the duration of the study.

2.5 Flow Cytometry

2.5.1 Cell surface staining

2.5.1.1 Materials, Reagents and Equipment

- Antibodies (see below)
- Fortessa Flow Cytometer (BD biosciences)
- Cell Dissociation Buffer (Gibco)
- Trypsin/EDTA (Gibco)
- Ice box
- FlowJo software

2.5.1.2 Antibodies:

Staining for N28z, M28z, cM28z + T28z, V28z

9e10 hybridoma D10 supernatant (In house)

Goat anti-mouse IgG PE-conjugated (DAKO)

Staining for 4αβ
Mouse IgG_1 anti-human CD124 PE-conjugate (BD Pharmigen)
Goat anti-Mouse IgG1 isotype PE-conjugate (BD Pharmigen)

Staining for c-MET
Rat IgG1k anti-human c-Met (HGFR) FITC-conjugated (eBioscience)
Anti-Rat IgG1k isotype FITC-conjugated (eBioscience)

Staining for CD44v6
Mouse IgG1 anti-human CD44v6 FITC-conjugated (eBioscience)
IgG1 anti-mouse isotope FITC-conjugated (eBioscience)

Staining for Syndecan-1
Rat IgG1 anti-human CD138 APC-conjugated (BioLegend)
Anti-rat IgG2b isotype APC-conjugated (BioLegend)

Staining for checkpoint axis molecules
Mouse anti-Human CD279 (PD-1) PE-conjugated (BD Pharmingen)
Goat anti-Mouse IgG1k PE-conjugated (BD Pharmingen)

Mouse anti-human CD274 (PD-L1) APC-conjugated (BioLegend)
Mouse anti-human CD273 (PD-L2) PE-conjugated (BioLegend)

Staining for ErbB receptors
Rat anti-human ErbB1 (ICR62) (ICR)
Rat anti-human ErbB2 (ICR12) (ICR)
Goat anti-rat IgG PE-conjugated (Invitrogen)

Staining for αvβ6
Mouse anti-human αvβ6 (Biogen Idec)
Goat anti-mouse IgG PE-conjugated (DAKO)

2.5.1.3 Protocol – surface cell-staining

In order to determine the cell-surface expression, cells were regularly analysed. A universal FACS protocol has been detailed below.

1. A pre-determined number of cells were removed (adherent cells were removed with trypsin or cell dissociation buffer) and washed in PBS.

2. Cells were re-suspended in 200µl PBS in a flow cytometry tube and incubated with specified concentrations of primary or directly conjugated antibody/isotope on ice for 30 minutes.
3. *N.B.* Additional step for non-conjugated antibodies -Samples were washed in 2ml PBS, centrifuged and re-suspended in 200µl PBS.
4. *N.B.* Additional step for non-conjugated antibodies - Cells were then incubated with matched concentrations of secondary antibody for 30 minutes on ice in the dark.
5. Samples were again washed with PBS, centrifuged and resuspended in 350µl PBS prior to analysis. Sample FACS tubes were kept on ice and in the dark until analysis.
6. Results were compared to control using a matched staining protocol (or to cells stained with the secondary antibody alone where stated).

2.5.2 Flow sorting

To enable *in vivo* assessment of c-Met re-targeted CAR T-cells as detailed in section 2.4, MPM tumour cells were genetically engineered to stoichiometrically co-express firefly luciferase (ffLuc) and tdTomato (tdTom) (denoted LT - detailed in section). To ensure high LT positive expression minimising negative outgrowth, LT^+ MPM tumour cells (H28 and REN) were prepared as detailed in section 2.5.1 (5-10 x 10^6 tumour cells/ml; total number of cells >20 x 10^6. Cells were transported on ice and flow sorted for LT expression (>95% positive) using BD FACSAria™ II Cell Sorters (ARIA 1) within the Biomedical Research Centre Flow Core Unit, Guy's and St Thomas' NHS Foundation Trust and King's College London, located at Guy's Hospital, London. Cell acquisition and analysis on BD FACSAria™ II Cell Sorters via FACSDIVA software.

2.6 Experimental Design

Experiments were conducted with biological and process repeats. Where stated, the number of repeats (n=x) represents biological repeats – independent experiments with different healthy blood donors. Within each biological repeat, process repeats were conducted in duplicate or triplicate.

2.7 *In vivo* BLI image analysis

In vivo BLI images were analysed in accordance with the following protocol. The luciferase enzyme present within the tumour cells allowed tumour growth to be monitored over the indicated timeframe by bioluminescent imaging (BLI). The images gained for each time point were analysed using Living Image 3.1 software. The level of luminescent signal released by each mouse was calculated by drawing a region of interest (ROI). The software automatically calculated the level of photon release within the ROI and this was standardised to account for the size of ROI and scan duration. The values plotted represent the average luminescent signal ± the standard error of the mean. Images detailing the luminescent signal for an individual mouse within each group are provided in the appendix.

2.8 Statistical analysis

To investigate statistical significance, values were subjected to a Student's *t*-test, two-tailed and *p*-values <0.05 were taken as significant. Alternatively, for the therapeutic *in vivo* study, values were subjected to a two-way ANOVA, followed by a Bonferroni post-hoc test and *p*-values <0.05 were taken as significant (* p <0.05, ** p <0.005 and *** p <0.0005). Data was analysed using Graphpad Prism software (version 5).

CHAPTER 3 Engineering and characterisation of specificity of c-Met-targeted chimeric antigen receptors using NIH 3T3 artificial antigen-presenting cells.

3.1 Introduction

3.1.1 Design of chimeric antigen receptors that target c-Met

The important role of the c-Met receptor in malignant mesothelioma is detailed within section 1.4. Since high-level expression of this receptor is found in over 80% of mesothelioma tumours, I set out to engineer CARs that target this tyrosine kinase receptor.

Engineering of a c-Met-targeted CAR requires a targeting moiety capable of specific c-Met receptor binding. Traditionally, a single chain antibody fragment is used for this purpose, as was recently described by Frigault *et al.* [327]. Alternatively, targeting may be achieved using a peptide, natural ligand or derivative thereof [328]. Hepatocyte growth factor (HGF) is the only naturally occurring ligand that binds to c-Met. However, it is unsuitable as a CAR targeting moiety since it cannot bind to the c-Met receptor until cleaved to yield an αβ heterodimer (section 1.3). In addition, a number of splice variants of the HGF α chain also bind c-Met. The smallest of these comprises the **N**-terminal and **1st K**ringle domain and is consequently known as **NK1** [329].

The NK1 splice variant of HGF occurs naturally and binds to the c-Met receptor with low nanomolar affinity [329, 330]. The binding of NK1 to c-Met is enhanced by heparin sulphate proteoglycans, most likely due to their ability to promote NK1 homo-dimerisation and the formation of a NK1/ Met/ heparin sulphate ternary complex [141]. Nonetheless, NK1 is a weak agonist of c-Met and is a highly unstable polypeptide. The NK1 polypeptide may be stabilised with potentiation of its activity by incorporating two mutations, at K132E and R134E [141]. This derivative peptide has been termed IK1 (Table 3-1).

To provide an additional targeting approach, CARs were also engineered using two alternative NK1-derived peptide moieties that bind to c-Met. Cochran and colleagues

undertook a directed evolution approach in which NK1 was expressed on the surface of yeast and mutated using error-prone PCR in order to select for variants that had higher stability and/ or affinity in binding assays with recombinant c-Met [331]. Using this approach, they isolated the M2.2 peptide in which eight mutations are present, as summarised in Table 3-1. Some of these mutations were located close to the known heparin-binding site of NK1 (e.g.K62E, Q95R, K132N, and K170E) but still permitted strong heparin binding by the peptide [331]. However, the M2.2 peptide had virtually no agonistic activity owing to the mutation at position 127 (N127D), which is located within the NK1 homo-dimerisation domain. Consequently, this position was mutated back to wild type (M2.2 D127N), resulting in restoration of functional HGF-like activity in scatter assays [331]. To test the importance of dimerisation in this activity, Cochran *et al.* created the cdM2.2 D127N peptide, which is identical except that it contains an N-terminal cysteine. The latter peptide demonstrated enhanced functional activity and has also been used within this study to create a third candidate c-Met-targeted CAR.

To create candidate CARs, the IK1, M2.2D127N and cdM2.2D127N peptides (Table 3-1) were fused to a second generation CAR framework in which the CD28 hinge, transmembrane and endodomains were placed upstream of the CD3ζ endodomain [261]. The CD28 hinge sequence was modified to remove the MYPPPY motif (involved in the binding of CD28 to B7-1 and B7-2) [310], which was substituted with a myc-derived epitope tag to enable detection of the CAR at the cell surface. A structural overview of the derived CARs was shown in Figure 2-1B (page 85) together with control CARs that have been used in this and subsequent chapters.

Table 3-1. Properties of NK1-derived peptides used to engineer candidate c-Met-specific chimeric antigen receptors (adapted from [331]).

	Sites of mutations	Affinity	Stability	Agonistic activity	Ref
NK1	None	Low nanomolar	Unstable (high salt and low temperature only)	+*	[329]
IK1	K132E; R134E	Not reported	Stable	++**	[141]
M2.2	K62E; Q95R; N127D; K132N; K137R, K170E; Q173R; N193D)	Low nanomolar	Stable in low salt and at higher temperature	No	[331]
M2.2 D127N	Revert codon 127 to wild type N	Not tested	Stable in low salt and at higher temperature	+* –	[331]
cdM2.2 D127N	N-terminal cysteine added to promote homo-dimerisation	Not tested	Increased stability	++*	[331]

* potentiated by heparin; ** effect of exogenous heparin not reported

3.1.2 The role of co-factors in binding of HGF to c-Met

NK1 binds both to c-Met and heparin sulphate proteoglycans (HSPGs), which are widely co-expressed on the surface of mammalian cells. Furthermore, as detailed in section 1.5.3, a number of co-factors have been described that strengthen this interaction. The best characterised of these is an isoform of CD44 containing the variant 6 exon (CD44v6). In several model systems, the ability of HGF to induce c-Met activation is dependent upon through ternary complex formation with CD44v6 [196]. In keeping with this, antagonistic peptides derived from the variant exon 6-encoded 42 amino acid sequence can block the binding of HGF to c-Met and thereby abrogate its function [205].

Although CD44 is commonly upregulated on mesotheliomas [198], there has been relatively little study of which CD44 variants are expressed in this disease. One study has suggested that CD44v6 may be under-represented in mesothelioma compared to other lung tumours [206]. To add complexity, one recent study in CD44-deficient mice suggests that ICAM-1 may alternatively be recruited to provide this co-receptor function [207] and small studies within mesothelioma suggest that ICAM-1 is very commonly and highly expressed in this tumour [208]. In light of this background, it was important to investigate the dependence and influence of CD44v6 upon recognition of c-Met by CARs containing NK1-derivative targeting peptides.

3.1.3 Use of NIH 3T3 fibroblast-derived artificial antigen presenting cells to examine target specificity of CAR T-cells

The use of NIH 3T3 based artificial antigen-presenting cells (aAPC) to examine the antigenic specificity of T-cell populations was pioneered by Sadelain *et al.* [332]. Murine NIH 3T3 fibroblast cells were initially transduced to express MHC and co-stimulatory molecules to facilitate the study of T cell-APC interactions in mice and humans [332, 333]. In comparative studies NIH 3T3 aAPC cells proved more efficient than *Drosophila* aAPC and were as efficient as autologous adherent PBMC and EBV-transformed B cells for $CD8^+$ T-cell expansion, without the additional requirement of feeder cells [333]. Unlike *Drosophila* aAPC, NIH 3T3 cells express endogenously processed antigens, which can stimulate $CD8^+$ T-cell responses to both exogenously loaded and transfected antigen [332, 334]

To broaden applicability, NIH 3T3 cells have been transduced to express a number of human HLA molecules to provide a panel of aAPC that can be used to derive T-cell lines for immunotherapeutic use, depending on the HLA type of the patient. Illustrating this, transfection with human HLA-A2, CD80, ICAM-1, and LFA-3 enabled the successful stimulation of $CD8^+$ T-cells specific for influenza, cytomegalovirus and the hTERT and WT1 tumour associated antigens (TAA) respectively [333, 334]

In parallel, Sadelain *et al.*, adapted the NIH 3T3 aAPC system to evaluate the specificity of CAR T-cells. In this setting, antigen recognition is direct and thus NIH 3T3 cells were engineered to express membrane-anchored target antigen, either alone or together with one or more co-stimulatory receptors [335]. For example, when CAR T-cells with specificity for prostate-specific membrane antigen (PSMA) were stimulated on NIH 3T3 cells transduced to co-express CD80, 4-1BBL and cell surface PSMA, CAR T-cells expanded efficiently *in vitro*. Notably, the resulting T-cells were also effective in treating PSMA-positive tumours in a humanised mouse model [336]. In this chapter, the NIH

3T3 aAPC model has been adapted to examine the specificity of three candidate CARs for human c-Met, either when expressed alone or in combination with CD44v6.

3.1.4 Aims

1. To engineer a panel of c-Met-specific CARs
2. To determine the target specificity and co-factor dependency of these CARs using an NIH 3T3-derived aAPC system

3.2 Results

3.2.1 Cloning of the SFG retroviral vectors expressing candidate c-Met re-targeted CARs

Expression of all constructs in human T-cells was achieved by means of transduction using the SFG retroviral vector, which is derived from the MFG vector [337]. Gene expression is driven by the Moloney murine leukaemia virus (MoMLV) long terminal repeat (LTR). The presence of the MoMLV ψ packaging signal ensures efficient packaging of the RNA into the virus. The presence of the splice donor and splice acceptor sites enables the production of the sub-genomic RNA transcripts usually required for the translation of the *env* gene [338]. The gene of interest is inserted at a naturally occurring *NcoI* site, ensuring that its start codon coincides with that previously occupied by the deleted *env* gene. This vector does not contain a eukaryotic cell-compatible selectable marker gene but does contain an ampicillin resistance gene for selection following transformation of competent bacteria.

Schematic structure of test and control CARs was shown in Figure 2-1B. The structures of recombinant retroviral SFG vectors are shown in (Figure 3-1).

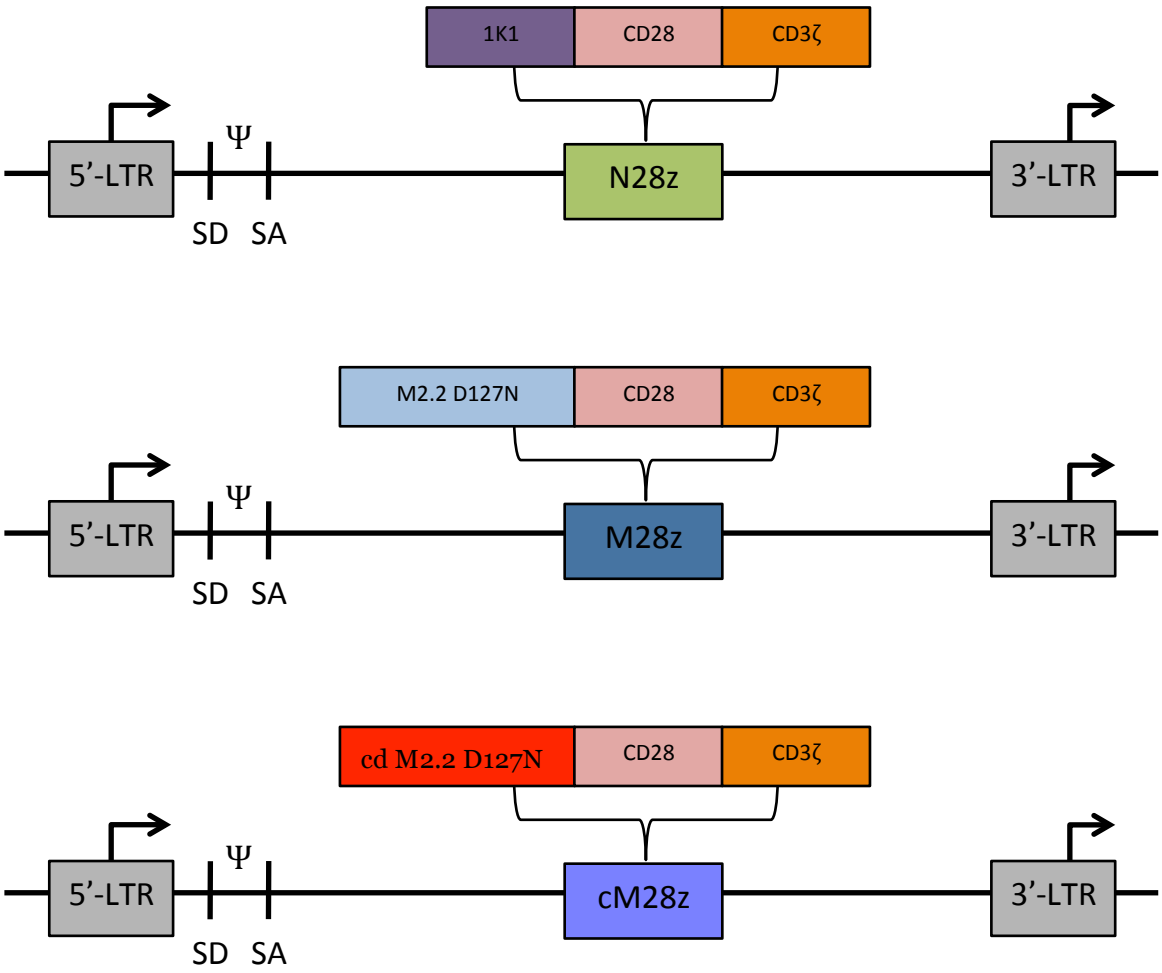

Figure 3-1. SFG Retroviral vectors encoding for candidate c-Met-specific chimeric antigen receptors.
All CARs were expressed in human T-cells using the SFG retroviral vector. Constructs were cloned as NcoI - NotI fragments into the SFG V8 vector (Whilding and Maher, unpublished), replacing the targeting peptide in that construct with 1K1-derivative of NK-1 or the mutated M2.2 D127N or cdM2.2 D127N versions. The resultant constructs are referred to as SFG N28z, SFG M28z and SFG cM28z respectively. Gene expression is driven by the promoter activity of the Moloney murine leukaemia virus (MoMLV) long-term repeat (LTR). The efficient packaging of SFG-based viral particles is enabled via the presence of the MoMLV packaging signal. SD = splice donor site; ψ = packaging signal; SA = splice acceptor site.

3.2.2 Expression of candidate c-Met re-targeted CARs in primary human T-cells

Prior to commencing investigations to test anti-tumour activity of candidate c-Met specific CARs, it was important to demonstrate efficient and stable expression of these chimeric receptors in primary human T-cells, along with appropriate control CARs. Following gammaretroviral-mediated gene transfer from PG13 retroviral packaging cell lines (Figure 3-2A), T-cells were investigated for cell surface expression of the CARs using flow cytometry. All CARs contain the same myc epitope tag within the CAR spacer domain, enabling their detection using the 9e10 monoclonal antibody. As shown in Figure 3-2B, expression of all three c-Met-targeted CAR candidates could be detected at the cell surface following retroviral gene transfer into activated human T-cells. These data indicate that all chimeric constructs were expressed and trafficked correctly to the cell surface. Cell surface expression of ErbB-targeted CAR, T28z and the scrambled peptide-targeted negative control, V28z was also established using the same protocol. As detailed in Figure 3-2C, the mean expression of the three c-Met-targeted candidate CARs in human T-cells was similar across five independent experiments.

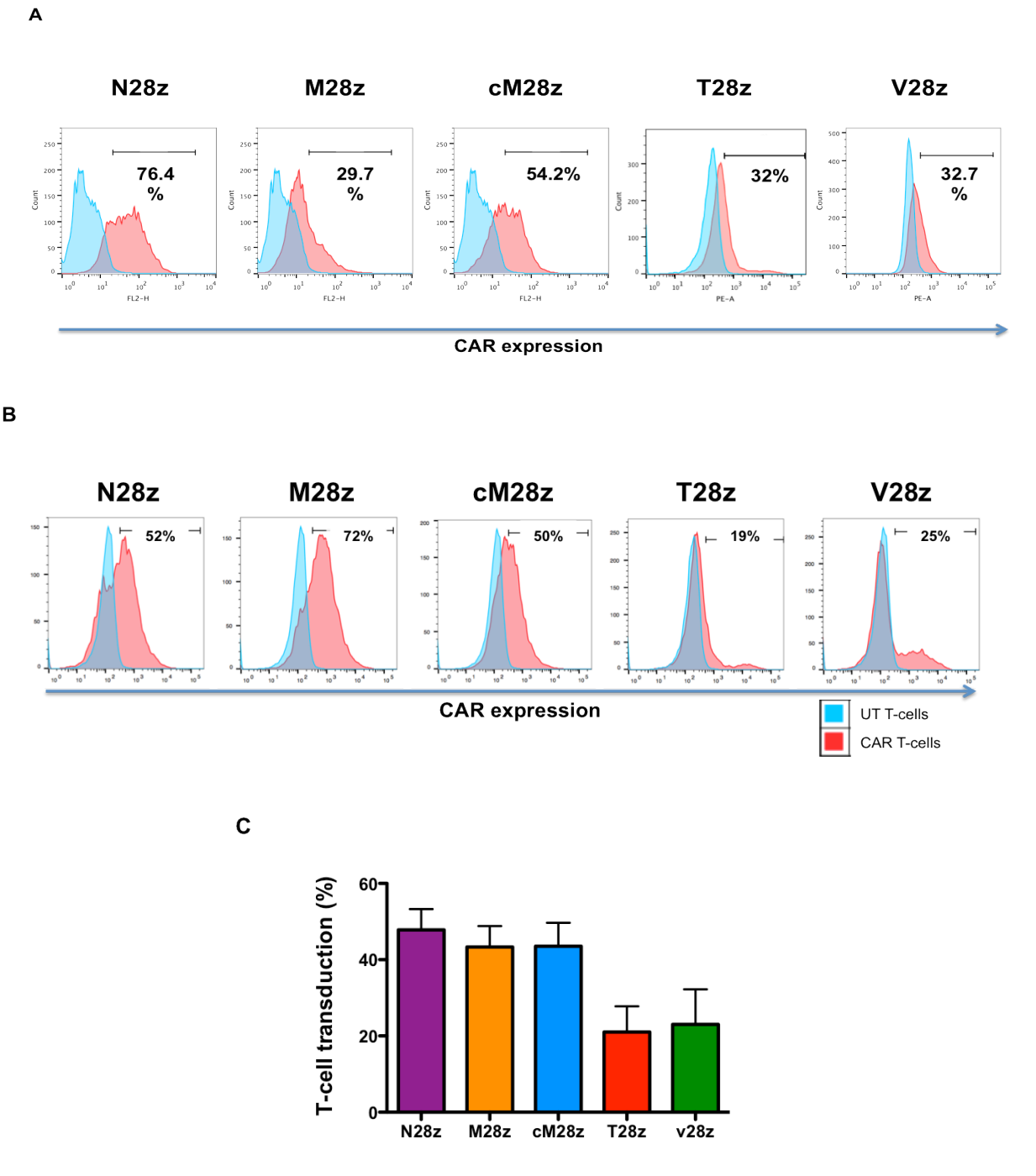

Figure 3-2. Expression of CARs in PG13 retroviral packaging cells and transduced human T-cells.

(A) Expression of N28z, M28z, cM28z, T28z and V28z was detected on the surface of PG13 retroviral packaging cells by flow cytometry, following incubation with the 9e10 antibody which detects a shared myc epitope tag present in all CAR ectodomains (filled pink histogram). Filled blue histograms show parental PG13 packaging cells stained with the same protocol. Percentage CAR positive cells is indicated. **(B)** Expression of N28z, M28z, cM28z, T28z and V28z (filled pink histograms) detected on the surface of transduced primary human T-cells by flow cytometry, as described in A. Filled blue histograms show untransduced T-cells stained with the same protocol. Black number indicates percentage of CAR positive cells. Data shown in panels A and B are representative FACS plots. **(C)** Pooled data in which human T-cells were transduced using the indicated SFG CAR retroviral constructs (mean $\pm$ SEM, n = 5 independent donors).

3.2.3 Production and validation of a matched panel of c-Met and CD44v6 expressing NIH 3T3 artificial antigen presenting cells (aAPC)

Hepatocyte growth factor and the derived NK1 splice variant can bind to human c-Met [141, 215, 331, 339]. This binding interaction is augmented by a number of co-factors, the best characterised of which is CD44v6 [196]. Consequently, I next set out to investigate the target specificity of the three candidate c-Met-targeted CARs described above. The NIH 3T3 fibroblast cell line provides a useful model system to investigate this. Since they are of murine origin, they do not express either human c-Met or CD44v6. Consequently, the introduction of the human c-Met receptor, CD44v6 receptor or the combination of both c-Met and CD44v6 receptors into these cells allows the controlled evaluation of the targeting specificity of the CAR T-cells. Expression of both transgenes was achieved in NIH 3T3 cells by retroviral gene transfer (section 2.2.5). Expression of human c-Met and/ or human CD44v6 was demonstrated in the appropriate engineered NIH 3T3 cells by flow cytometry (Figure 3-3).

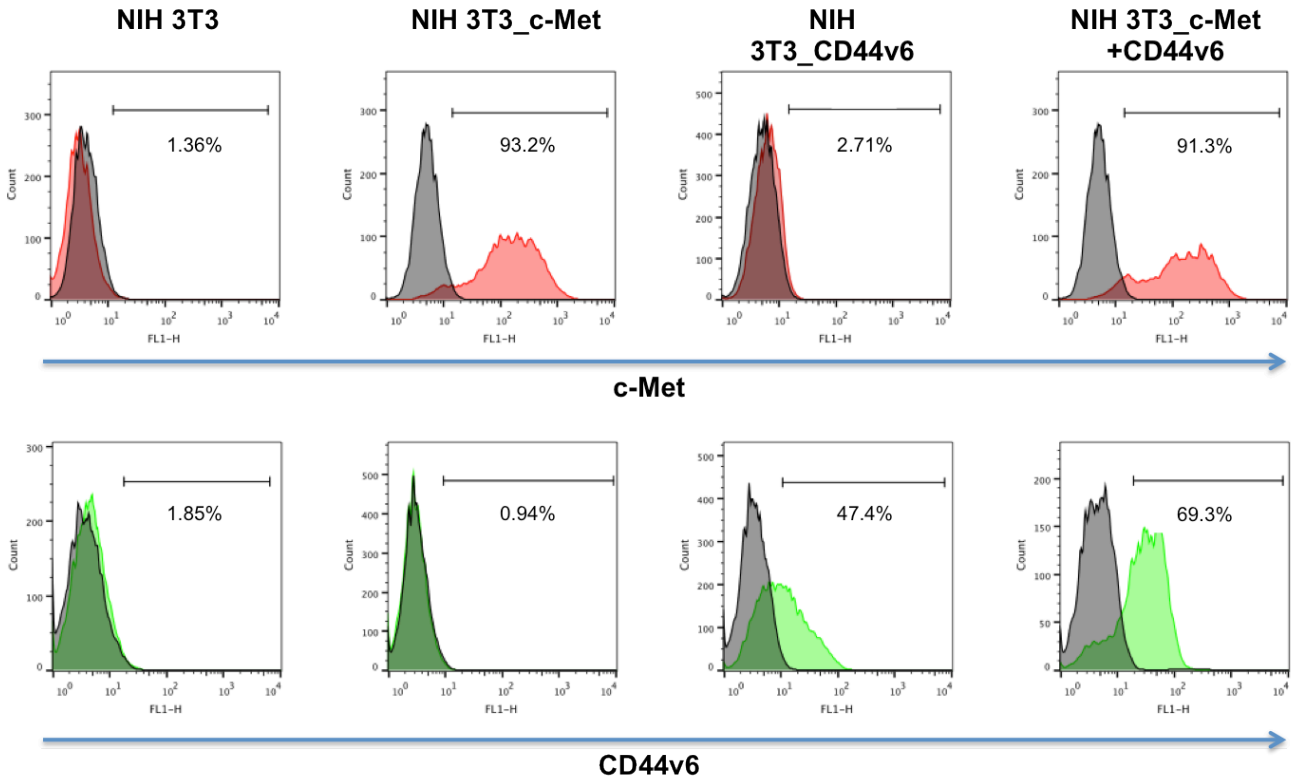

Figure 3-3. Expression of human c-Met and/or human CD44v6 in retroviral-engineered NIH 3T3 cells.
NIH 3T3 fibroblasts were transduced with retroviral vectors that encode for human c-Met and/ or human CD44v6 as labelled. Expression of the indicated transgene is shown by the pink histogram (c-Met) and green histogram (CD44v6). Staining of the same cells with a matched isotype control antibody is shown by the filled grey histograms. The percentages depicted within plots represent total percentage of cells that are transgene positive (corrected for isotype). Data are representative of similar findings in three independent replicate experiments.

3.2.4 Comparison of target-dependent cytotoxicity mediated by candidate c-Met re-targeted CARs using NIH 3T3 aAPC cells

Next, I established T-cell/ NIH 3T3 monolayer co-cultivation experiments in order to investigate the ability of the candidate c-Met-specific CARs to deliver a target-dependent cytotoxic signal. CAR^+ T-cells (effector) were co-cultivated with the aAPC panel of NIH 3T3 cells (target) at effector to target ratios of 1:1, 2:1 and 4:1 (1:1 = 2 x 10^4 NIH 3T3 and 2 x 10^4 T-cells – not corrected for transduction efficiencies). Parental NIH 3T3 cells were used as the negative control aAPC. To provide negative CAR T-cell control populations, NIH 3T3 aAPC cells were also co-cultivated with $T28z^+$, $V28z^+$ or untransduced T-cells, none of which would be expected to cause target cell destruction or undergo T-cell activation in this co-cultivation system.

Destruction of NIH 3T3 cells was quantified after 24 and 48 hours of co-cultivation using an MTT assay (Figure 3-4 to 3-6). These data indicate that NIH 3T3 cells engineered to express c-Met were highly susceptible to cytotoxic destruction by N28z, M28z and cM28z CAR^+ T-cells. There was no significant difference in target cell killing by the three candidate c-Met re-targeted CARs under evaluation. By contrast, c-Met re-targeted CAR^+ T-cells did not mediate killing of NIH 3T3 cells that expressed CD44v6 alone. In addition, co-expression of CD44v6 and c-Met did not enhance the sensitivity of NIH 3T3 cells to destruction by c-Met re-targeted CAR^+ T-cells. Control CAR^+ T-cells did not induce specific cytotoxicity against c-Met-expressing or other NIH 3T3 target cells. Furthermore, none of the three candidate c-Met re-targeted CARs (N28z, M28z and cM28z) or control CARs (T28z and V28z) induced significant destruction of parental NIH 3T3 cells, when compared to untransduced (UT) T-cells.

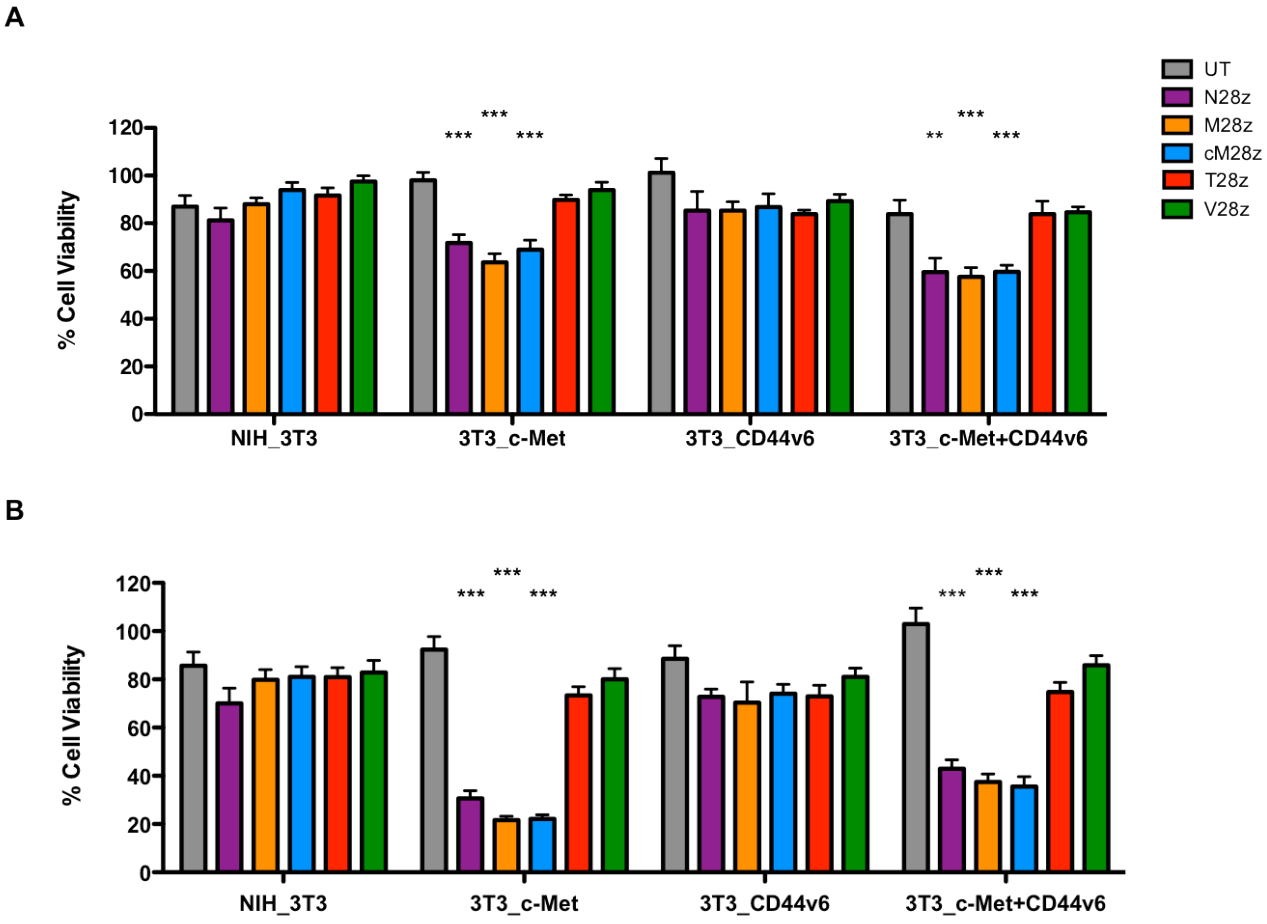

Figure 3-4. Target cell destruction following T-cell co-culture with a panel of NIH 3T3-derived aAPC (effector to target ratio 1:1).
Percentage viability of the indicated NIH 3T3 cell lines was determined following **(A)** 24 hour or **(B)** 48 hour incubation at an effector to target ratio of 1:1. Artificial antigen presenting cells (2 x 10^4 cells) were seeded, followed 24 hours later by addition of 2 x 10^4 N28z, M28z, cM28z, T28z, V28z or untransduced (UT) T-cells. Effector T-cells were not corrected for transduction efficiencies (shown in Figure 3-2). Following completion of the co-cultivation, T-cells were removed by decanting and residual aAPC cell viability was measured using an MTT assay. Data shown are mean ± SEM from five independent experiments. Statistical significance was determined using the unpaired Student's *t*-test, comparing cytotoxic activity of UT T-cells with CAR^+ T-cells against each aAPC line. * p <0.05, ** p <0.005 and *** p <0.0005.

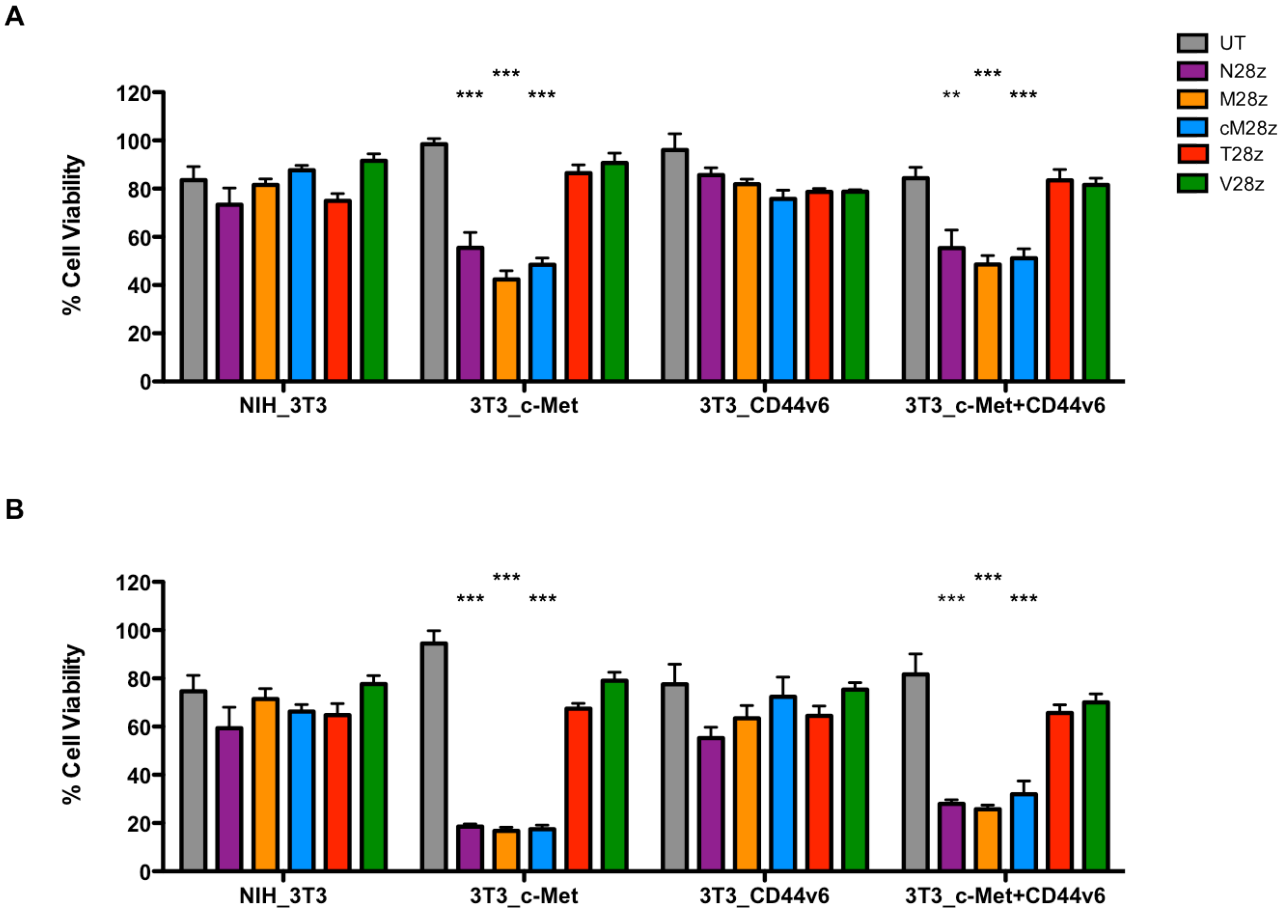

Figure 3-5. Target cell destruction following T-cell co-culture with a panel of NIH 3T3-derived aAPC (effector to target ratio 2:1).
Percentage viability of the indicated NIH 3T3 cell lines was determined following **(A)** 24 hour or **(B)** 48 hour incubation at an effector to target ratio of 2:1. Artificial antigen presenting cells (2 x 10^4 cells) were seeded, followed 24 hours later by addition of 4 x 10^4 N28z, M28z, cM28z, T28z, V28z or untransduced (UT) T-cells. Effector T-cells were not corrected for transduction efficiencies (shown in Figure 3-2). Following completion of the co-cultivation, T-cells were removed by decanting and residual aAPC cell viability was measured using an MTT assay. Data shown are mean ± SEM from five independent experiments. Statistical significance was determined using the unpaired Student's *t*-test, comparing cytotoxic activity of UT T-cells with CAR^+ T-cells against each aAPC line: * p <0.05, ** p <0.005 and *** p <0.0005.

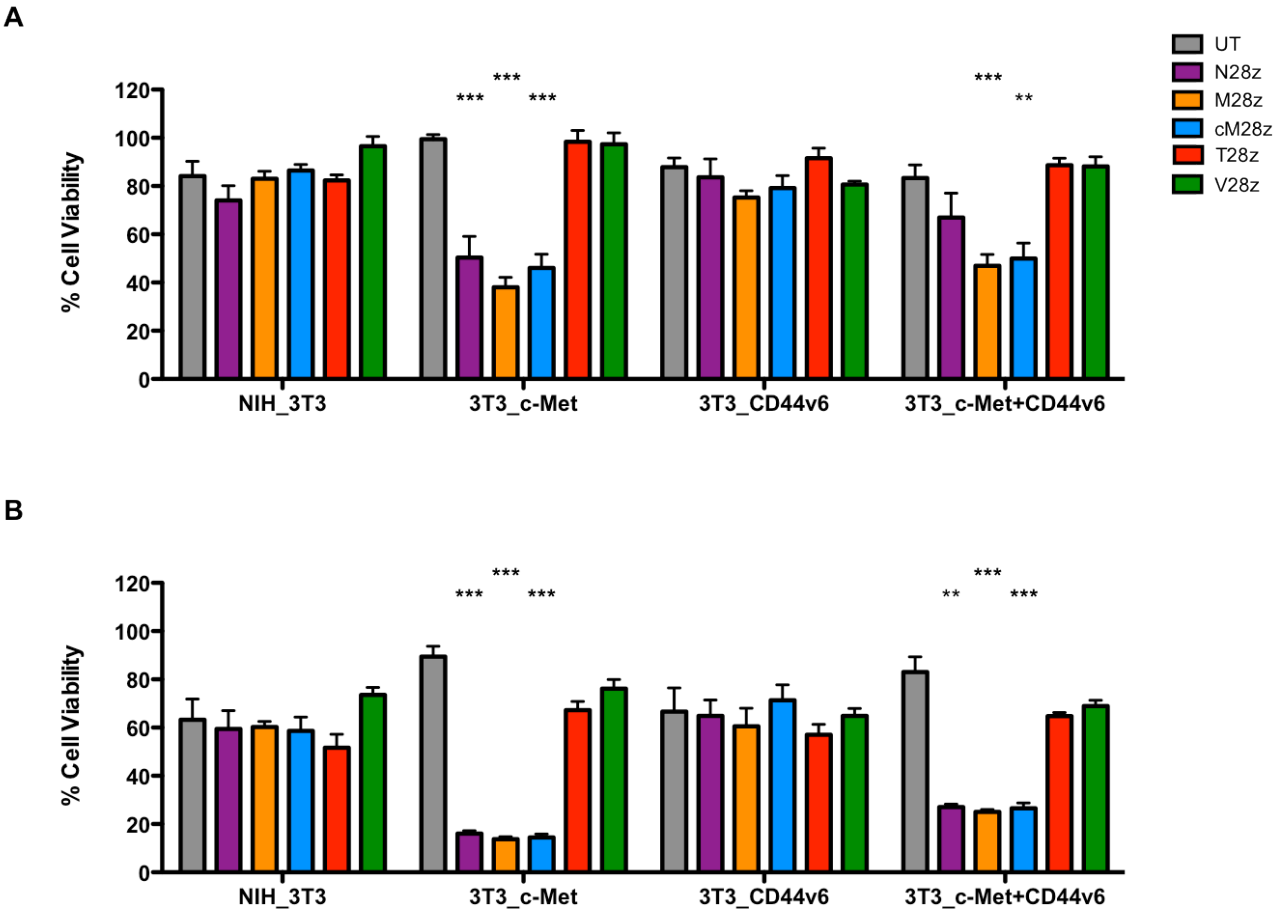

Figure 3-6. Target cell destruction following T-cell co-culture with a panel of NIH 3T3-derived aAPC (effector to target ratio 4:1).
Percentage viability of the indicated NIH 3T3 cell lines was determined following **(A)** 24 hour or **(B)** 48 hour incubation at an effector to target ratio of 4:1. Artificial antigen presenting cells (2 x 10^4 cells) were seeded, followed 24 hours later by addition of 8 x 10^4 N28z, M28z, cM28z, T28z, V28z or untransduced (UT) T-cells. Effector T-cells were not corrected for transduction efficiencies (shown in Figure 3-2). Following completion of the co-cultivation, T-cells were removed by decanting and residual aAPC cell viability was measured using an MTT assay. Data shown are mean ± SEM from five independent experiments. Statistical significance was determined using the unpaired Student's *t*-test, comparing cytotoxic activity of UT T-cells with CAR^+ T-cells against each aAPC line: * p <0.05, ** p <0.005 and *** p <0.0005.

3.2.5 Comparison of target-dependent cytokine release mediated by candidate c-Met re-targeted CARs using NIH 3T3 aAPC cells

Supernatants harvested from three co-cultivation experiments described in the previous section were analysed for interferon (IFN)-γ (Figure 3-7) and interleukin (IL)-2 (Figure 3-8) concentration by ELISA. This analysis demonstrated a modest but nonetheless significant increase in release of IFN-γ from candidate c-Met-targeted CAR$^+$ T-cells upon co-culture with c-Met-expressing NIH 3T3 cells. Similar findings were not observed in matched control cultures containing T28z$^+$, V28z$^+$ or UT T-cells. Furthermore, release of IFN-γ by c-Met re-targeted CAR$^+$ T-cells was increased during co-cultivation with c-Met-expressing NIH 3T3 in comparison to parental NIH 3T3 cells. However, the differences observed did not reach statistical significance at the 4:1 effector: target ratio. These findings are consistent with the cytotoxicity data presented earlier (Figure 3-4 to 3-6) and add to the evidence that N28z, M28z and cM28z CAR$^+$ T-cells undergo activation in a c-Met-dependent manner.

Importantly, release of IFN-γ was not seen when c-Met re-targeted CAR$^+$ T-cells were co-cultivated with NIH 3T3 cells engineered to express CD44v6 alone. These results indicate that c-Met re-targeted CAR$^+$ T-cells do not recognise the CD44v6 receptor alone. However, when both c-Met and CD44v6 receptors were co-expressed, N28z, M28z and cM28z CAR$^+$ T-cells released larger quantities of IFN-γ, compared to that by c-Met-expressing NIH 3T3 cells. These differences reached statistical significance in the case of N28z (at a 4:1 ratio) and cM28z (at both 1:1 and 2:1 ratios). These findings raise the possibility that target cells that co-express c-Met and its co-factor CD44v6 provides a more potent activation signal. Levels of IL-2 present in these supernatants are presented in Figure 3-8. Although some statistically significant differences were noted, levels were generally low and did not reveal any consistent pattern.

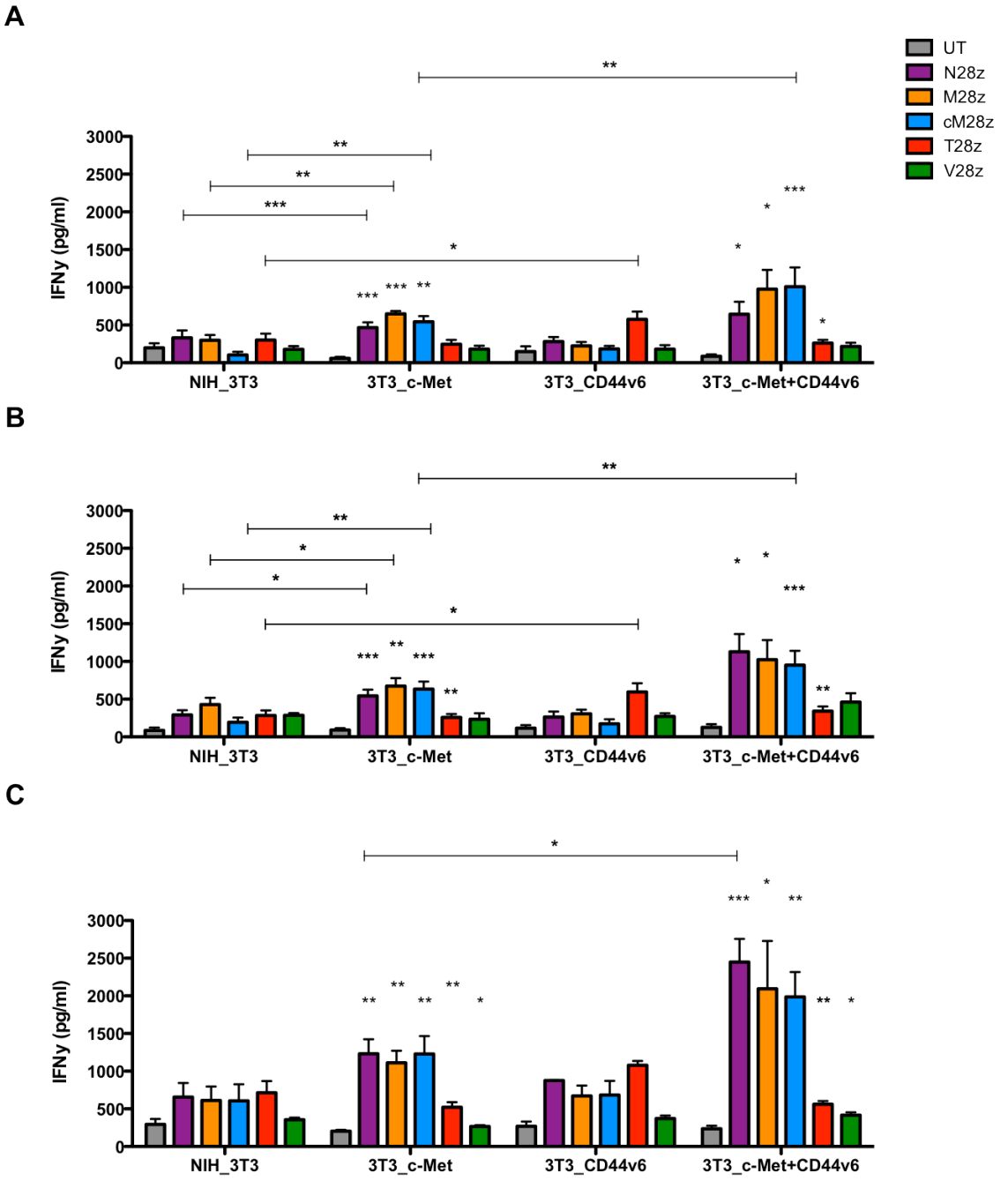

Figure 3-7. Determining the concentration of IFN-γ released following CAR T-cell co-culture with panel of target expressing NIH 3T3 cell lines

IFN-γ release by T-cells during co-culture with panel of NIH 3T3 cells expressing c-Met ± CD44v6. Untransduced T-cells or those expressing the N28z, M28z and cM28z, T28z or V28z CAR were co-cultured with the indicated NIH 3T3 monolayers for 48 hour at **(A)** 1:1, **(B)** 2:1 or **(C)** 4:1 effector to target ratios. Supernatants were collected and the concentration of IFN-γ was measured by ELISA. Data were obtained in three independent experiments and are presented as mean ± SEM. Statistical significance was determined using the unpaired Student's *t*-test, comparing UT T-cells with CAR$^+$ T-cells cultured on the same NIH 3T3 target cell line. Other statistical comparisons are indicated by the presence of an overhead line that extends over the relevant comparator groups. * p <0.05, ** p <0.005 and *** p <0.0005.

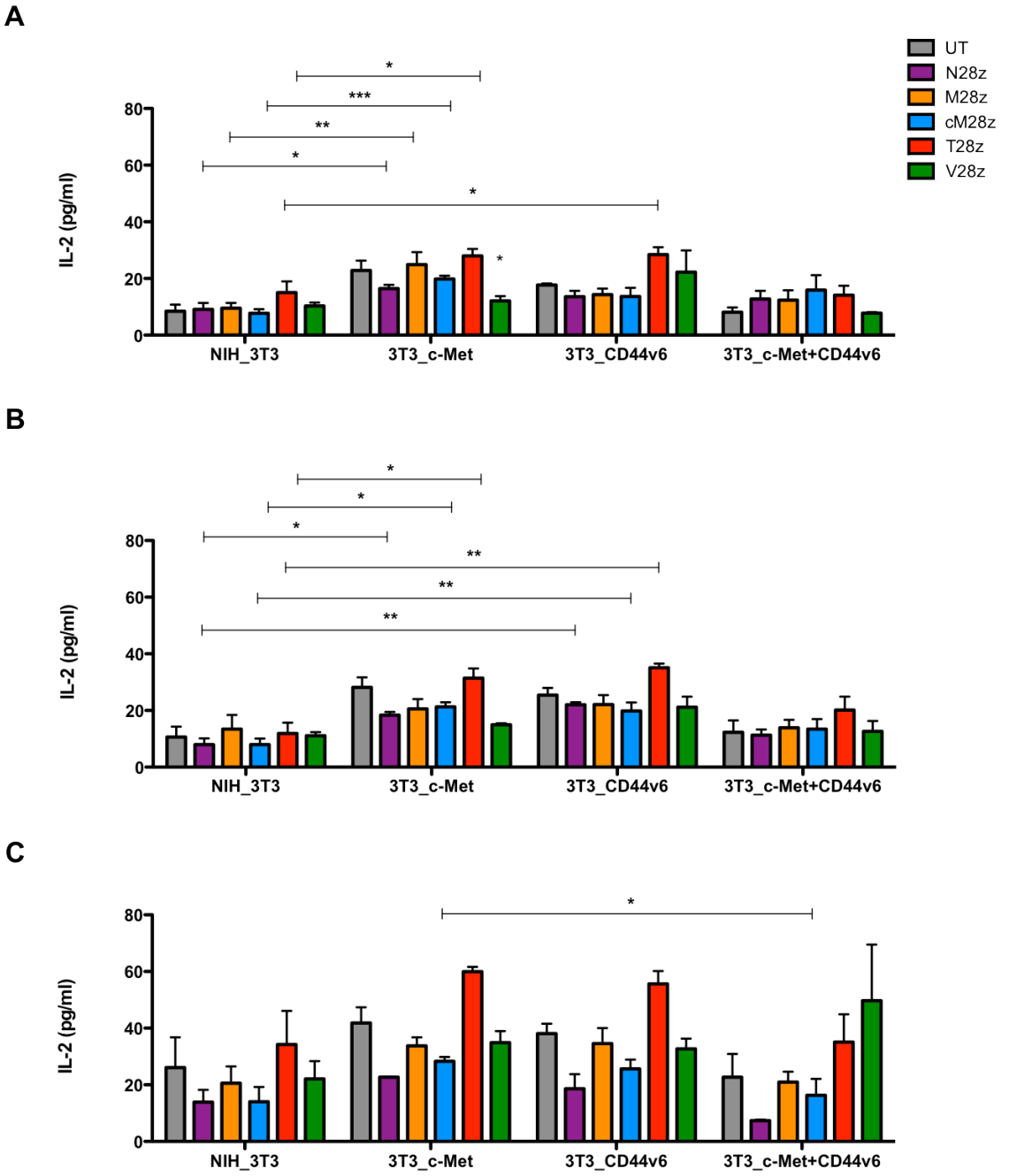

Figure 3-8. Determining the concentration of IL-2 released following T-cell co-culture with panel of target expressing NIH 3T3 cell lines

IL-2 release by T-cells during co-culture with panel of NIH 3T3 cells expressing c-Met and/or CD44v6. Untransduced T-cells or those engineered to express the N28z, M28z and cM28z, T28z or V28z CAR were co-cultured with the indicated NIH 3T3 monolayers for 24 hours at **(A)** 1:1, **(B)** 2:1 or **(C)** 4:1 effector to target ratios. Supernatants were removed and the concentration of IL-2 was measured by ELISA. Data were obtained in three independent experiments and are presented as mean ± SEM. Statistical significance was determined using the unpaired Student's *t*-test, comparing UT T-cells with CAR^+ T-cells cultured on the same NIH 3T3 target cell line. Other statistical comparisons are indicated by the presence of an overhead line that extends over the relevant comparator groups. * p <0.05, ** p <0.005 and *** p <0.0005.

3.3 Discussion

The growth and motility factor hepatocyte growth factor (HGF) and its receptor tyrosine kinase c-Met, which is the product of the MET proto-oncogene, are known to provide essential signals for both survival and long-distance migration of epithelial and myogenic precursor cells during embryogenesis. This HGF/c-Met axis for invasion and metastasis is utilised by a number of cancer types including mesothelioma, rendering these molecules attractive candidate targets for treatment of this tumour [340] [140].

This chapter has detailed the engineering and initial testing of three candidate CARs to target c-Met. The targeting strategy employed in this PhD involved the selection of targeting moieties that bind specifically to c-Met and are derived from NK1, which is the smallest splice variant of HGF. NK1 is capable of binding c-Met with low nanomolar affinity, but is naturally unstable and thus from a CAR engineering perspective it was considered desirable to utilise stabilised versions of this peptide. Stabilisation of NK1 had previously been achieved with the incorporation of two mutations (K132E and R134E), an approach that retained full affinity and activity of this ligand. In addition, two mutant NK1 peptides (M2.2 D127N and cdM2.2 D127N) have also been described that incorporate several mutations that considerably improved binding affinity and stability for the HGF-Met interaction [331]. Consequently, it was hypothesised that by utilising the NK1 or mutant NK1 peptides as the targeting moiety of a chimeric antigen receptor (CAR), it would be possible to re-direct primary human T-cells against target cells expressing the c-Met receptor. In order to achieve full T-cell activation upon the binding of target antigen, the sequence for each of the NK1 peptides Ik1, M2.2 D127N and cdM2.2 D127N were joined immediately upstream of the hinge, transmembrane and endodomains of CD28, followed by the signalling domain of CD3ζ chain to give three candidate second generation c-Met re-targeted CARs: N28z, M28z and cM28z respectively. The HGF (isoform 6) signal peptide was incorporated as the leader sequence at the 5' site of the cDNA to ensure cell surface expression of the CAR upon translation.

The main aim of the research described within this chapter was to determine whether the three c-Met re-targeted CARs were able to recognize the human c-Met receptor, leading to T-cell activation. Prior to investigating this, it was important to show expression and correct folding of the N28z, M28z and cM28z CARs at the T-cell surface. This was consistently confirmed by flow cytometry during independent studies. The level of T-cell transduction varied between the three c-Met re-targeted CAR constructs and across independent experiments. This variation may be attributed to a number of reasons. One

of the main variables across the experiments was the intrinsic difference associated with using T-cells from a variety of donors. Differences in surface expression levels of the GALV receptor, Pit1, between donors may account for some of the variation in CAR expression observed, since levels of expression of this receptor have previously been correlated with transduction efficiency [341]. Furthermore, differences in the level of response by donor cells to the CD3/CD28 beads may also play a decisive role in determining variations in T-cell transduction efficiencies, given the requirement of the recipient cells to enter the cell cycle in order that retroviral-mediated gene transfer can be achieved. Furthermore, since viral titre was not determined prior to gene transfer, the quantity of vector to which the T-cells were exposed would have varied between experiments. In addition, inherent experimental variation is also likely to cause small differences. Taken together, it can be concluded that the N28z, M28z and cM28z CAR were successfully and stably expressed in primary human T-cells.

The use of engineered NIH 3T3 cells as aAPCs enabled the assessment of c-Met specificity of the candidate N28z, M28z and cM28z CARs. This approach also allowed me to test the dependence of this interaction upon expression of a key co-factor that enables the binding of HGF to c-Met, namely CD44v6. The significant c-Met-dependent cytotoxic activity and release of IFN-γ mediated by all three candidate CARs provided initial evidence for their functionality. No discernable difference was observed in the c-Met-dependent re-targeting activity of N28z, M28z and cM28z in these experiments. With respect to cytotoxicity observed over time, greater c-Met re-targeted CAR^+ T-cell killing was observed at longer time points (48 hours). In addition, an increase in effector T-cell function was seen when the ratio of effector to target cells was increased.

Notably, cytokine release appeared to be enhanced when candidate c-Met re-targeted CAR T-cells encountered NIH 3T3 targets that co-expressed c-Met with the CD44v6 co-factor. These findings are in keeping with the reported ability of CD44v6 to form ternary complexes with c-Met and HGF, thereby enhancing activation of the c-Met receptor and signalling [196] (section 1.5.3). Since this would be expected to increase affinity of binding of HGF (or the NK1 derivative) to target cells in which c-Met and CD44v6 are co-expressed, this may account for the increased activation observed. Importantly however, no evidence of CAR T-cell activation was observed when NIH 3T3 aAPC expressed CD44v6 alone. It has also been reported that CD44v6 is required by some cell systems and cancers in order to facilitate the binding of HGF to c-Met [342]. However, data presented in this chapter demonstrate that the presence of CD44v6 is not absolutely essential for the ability of NK1-based candidate CARs to engage c-Met, since NIH 3T3 cells that express this receptor alone also promote the activation of these engineered T-cells.

In conclusion, the data presented in this chapter demonstrate that T-cells expressing the N28z, M28z and cM28z CARs undergo activation by NIH 3T3 aAPCs in a c-Met-dependent manner, manifested by cytotoxicity and release of IFN-γ. Furthermore, activation is enhanced if NIH 3T3 cells co-express CD44v6, suggesting that co-receptor expression may enhance activity of these CAR T-cells. Importantly however, CD44v6 alone does not provide a sufficient stimulus to activate any of the candidate CARs under evaluation. These findings set the scene for assessment of anti-tumour activity of these candidate CARs in models of MPM.

CHAPTER 4 Assessment of the *in vitro* cytotoxic activity of c-Met re-targeted chimeric antigen receptor T-cells against human mesothelioma cell lines

4.1 Introduction

It has been reported by a number of investigators that c-Met is expressed in 74 to 100% of MPM tumours [146, 147, 154, 343]. This suggests that these tumours may be susceptible to targeting by c-Met re-targeted CAR$^+$ T-cells [344]. In Chapter 3, I demonstrated that all three c-Met re-targeted CARs could recognise c-Met when ectopically expressed in NIH 3T3-based artificial antigen presenting cells. Next, I tested the anti-tumour activity of these CAR T-cells against a panel of human malignant pleural mesothelioma (MPM) cell lines.

4.1.1 Assessment of the *in vitro* functionality of CAR T-cells against a panel of mesothelioma cell lines.

Whilst I have shown that the candidate c-Met-targeted CARs under study can recognise this target when ectopically expressed in NIH 3T3 cells, this does not necessarily mean that they will exert cytotoxic activity against human mesothelioma tumour cells that over-express c-Met. To test this, I selected four pleural effusion-derived MPM cell lines named H28 (epithelioid), REN (epithelioid), JU77 (sarcomatoid) and LO68 (epithelioid) [345]. All cell lines were provided by Dr Sara Busacca, Department of Cancer Studies and Molecular Medicine, University of Leicester, Leicester, United Kingdom. These cells were characterised for expression of c-Met by flow cytometry prior to undertaking functional studies using CAR engineered T-cells.

To evaluate cytotoxic activity *in vitro,* c-Met re-targeted CAR$^+$ T-cells generated from healthy donors were co-cultivated with monolayer cultures of the indicated tumour cell lines. Tumour cell viability and cytokine release was assessed across the different cell lines.

4.1.2 Release of HGF in mesothelioma

Chapter 1 (section 1.4.1) summarises the evidence that HGF over-production occurs in mesothelioma. This could provide a source of competition for the NK1 targeted CARs

developed in this project, thereby inhibiting their function. Consequently, all four MPM cell lines were also evaluated by ELISA for their ability to secrete HGF.

4.1.3 Expansion of CAR T-cells that express the 4αβ chimeric cytokine receptor using IL-4

Many patients with advanced malignancy are lymphopenic and immune compromised, meaning that T-cell gene transfer efficiency and expansion of cell products is frequently compromised. In general, patients need to undergo leukapheresis in order to harvest sufficient quantities of T-cells to circumvent this issue. A second challenge to successful adoptive cell therapy, specifically CAR T-cell immunotherapy, is the survival and expansion of CAR^+ T-cells following infusion *in vivo*. Successful redirected T-cell therapy is dependent upon cytokine stimulation, with IL-2 and IL-15 potent stimulators. Traditionally, adoptive cell therapy is often combined with preceding lympodepletion followed by high dose IL-2 administered post T-cell infusion. However, use of IL-2 in this manner results in the total lymphoid population being stimulated in addition to being severely toxic [346].

Addressing both of these concerns, Wilkie *et al.*, developed a chimeric cytokine receptor (4αβ) to enable selective stimulation of CAR^+ T-cells without associated toxicity [311]. The 4αβ chimeric cytokine receptor couples the ectodomain of the IL-4Rα to the endodomain of the IL-2/IL-15-Rβ [311]. By co-expressing 4αβ with a particular CAR of interest, the selective expansion and enrichment of re-directed CAR^+ T-cells can generally be ensured via exogenous IL-4 stimulation. Co-expressing both receptors was achieved through the use of an intervening *Thosea asigna* virus 2A (T2A) peptide downstream of a furin cleavage site (Figure 2-2, page 86) [311].

Additionally, a number of tumours including mesothelioma [347] secrete IL-4 in the immediate microenvironment, thus potentially inducing 4αβ-CAR^+ T-cell trafficking towards the site of the tumour followed by local expansion and survival of the gene modified T-cells. The 4αβ system is currently in use in a clinical trial involving CAR T-cell immunotherapy of head and neck cancer [348]. Patients donate 130mL blood rather than undergoing leukapheresis and in all cases, cells products have expanded exponentially while undergoing enrichment during *ex vivo* culture (n=7 patients; Maher, unpublished data).

4.1.4 Aims

1. To investigate expression of c-Met and release of HGF by established MPM cell lines.

2. To evaluate and compare *in vitro* cytotoxic activity of c-Met re-targeted CAR^+ T-cells using a panel of 4 mesothelioma cell lines.

3. To investigate the anti-tumour activity of c-Met re-targeted CAR^+ T-cells that have been expanded using the IL-4/ 4αβ chimeric cytokine receptor system.

4.2 Results

4.2.1 c-Met expression in MPM cell lines

In order to determine the suitability of the c-Met re-targeted CAR$^+$ T-cells as a therapy for MPM, the c-Met expression profile of a panel of human MPM cell lines was assessed. All four cell lines were positive for c-Met expression in the order: H28 > JU77 > LO68 > REN (Figure 4-1A). Data presented in Chapter 3 suggested that co-expression of CD44v6 may enhance the activation of c-Met re-targeted CAR T-cells, as indicated by increased cytokine release. Therefore, I also assessed the expression of CD44v6 in these cell lines by flow cytometry and found that all lacked expression of this isoform of CD44 (Figure 4-1B). In addition, the cell lines were assessed for expression of three other co-factors that facilitate HGF binding to c-Met, namely ICAM-1 (Figure 4-1C), heparan sulphate proteoglycan (HSPG; Figure 4-2A) and Syndecan-1 (Figure 4-2B). This analysis demonstrated that other co-factors were expressed by all four MPM cell lines. All expressed high levels of HSPG, while high levels of ICAM-1 were found on Ju77, LO68 and REN cells and high levels of Syndecan-1 were found on H28, JU77 and LO68 cells.

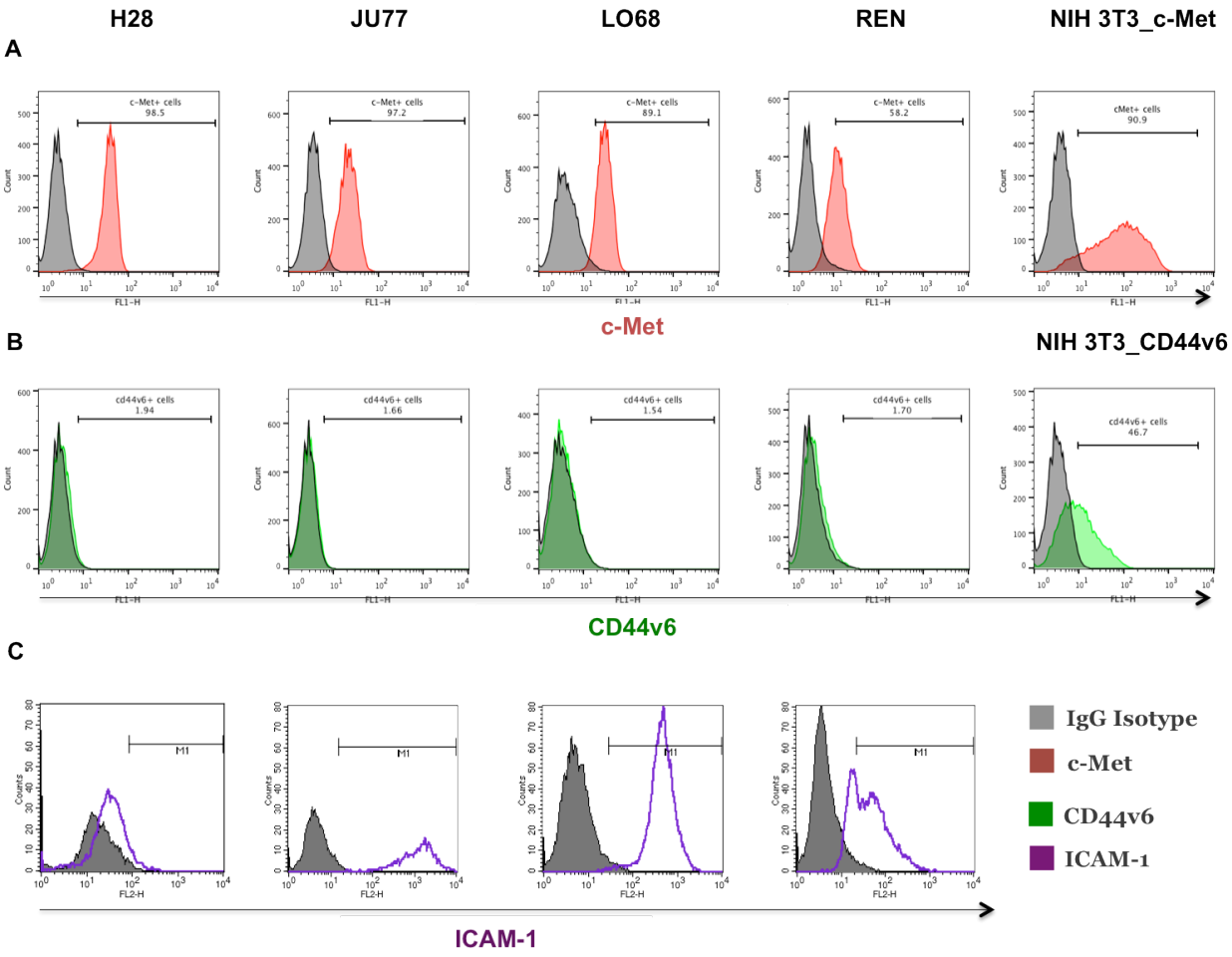

Figure 4-1. Expression of human c-Met, CD44v6 and ICAM-1 on malignant pleural mesothelioma cell lines.
(A) Expression of c-Met was detected on the mesothelioma cell lines by flow cytometry (red filled histogram). Staining with a matched isotype control antibody is also shown (grey filled histogram). The positive control used to validate binding of the anti-c-Met-FITC conjugated antibody was NIH 3T3 cells transfected to express human c-Met (NIH 3T3_c-Met). **(B)** Expression of CD44v6 was detected on the mesothelioma cell lines by flow cytometry (green filled histogram). Staining with a matched isotype control antibody is also shown (grey filled histogram). The positive control used to validate binding of the anti-CD44v6-FITC conjugated antibody was NIH 3T3 cells transfected to express human CD44v6. Above data are representative of findings in at least five independent experiments. **(C)** Expression of ICAM-1 was detected on the mesothelioma cell lines by flow cytometry (open purple histogram). Control staining with a matched isotype control antibody is shown in grey filled histogram (staining representative of two independent repeats).

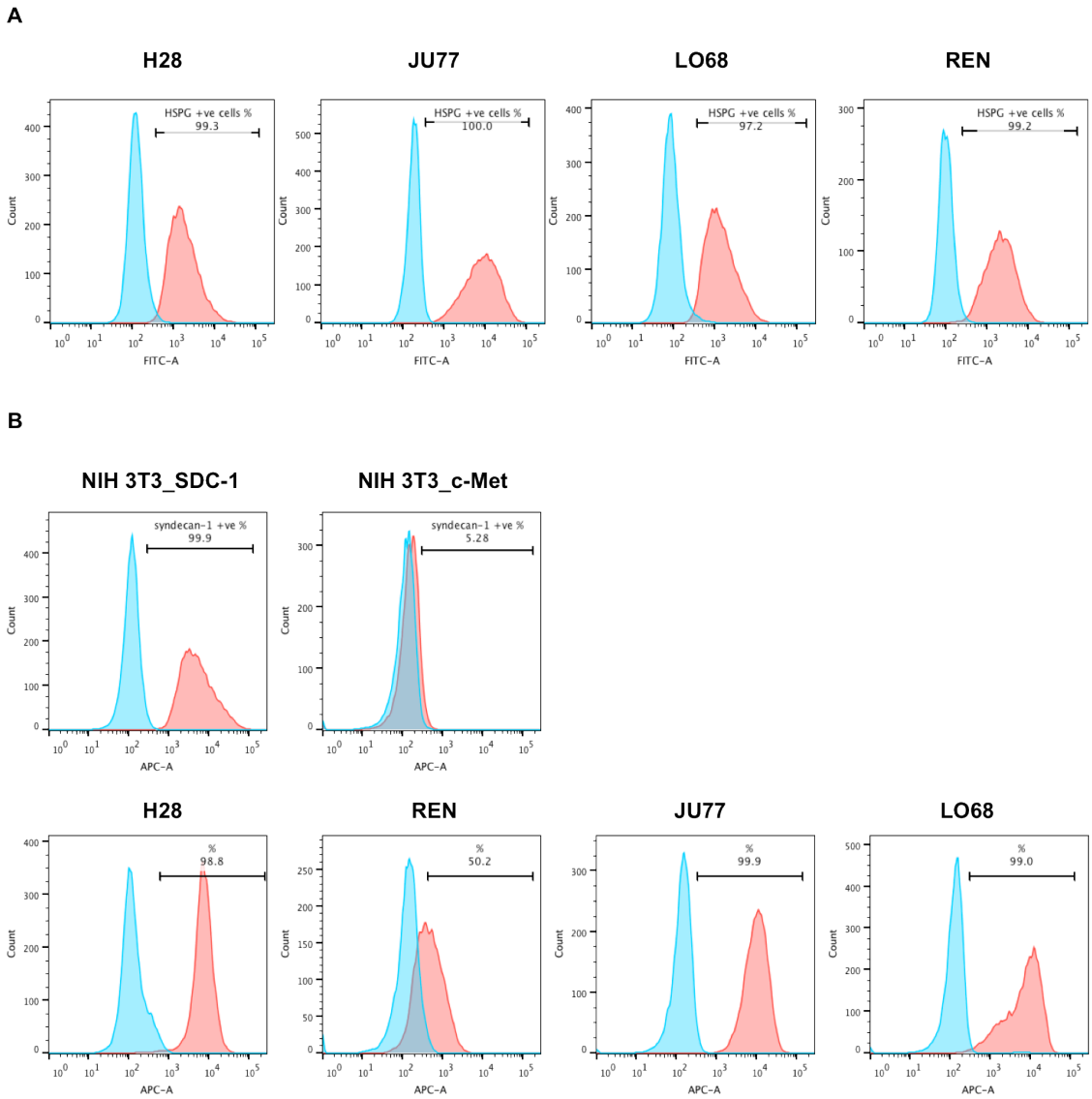

Figure 4-2. Heparan Sulphate Proteoglycan (HSPG) and Syndecan-1 expression on a panel of malignant pleural mesothelioma cell lines.
(A) Expression of HSPG was detected on the mesothelioma cell lines by flow cytometry (red filled histogram). Staining with a matched isotype control antibody is also shown (blue filled histogram). Percentage HSPG positive cells is annotated on individual plots. Data are representative of two independent repeats. **(B)** Expression of Syndecan-1 was detected on the mesothelioma cell lines by flow cytometry (red filled histogram). Staining with a matched isotype control antibody is also shown (blue filled histogram). The positive control used to validate binding of the anti-Syndecan-1-APC conjugated antibody was NIH 3T3 cells transfected to express human Syndecan-1. Staining of NIH 3T3_c-Met cells is also shown acting as a negative control. The percentage of Syndecan-1 positive cells is annotated on individual plots. Data are representative of three independent experiments.

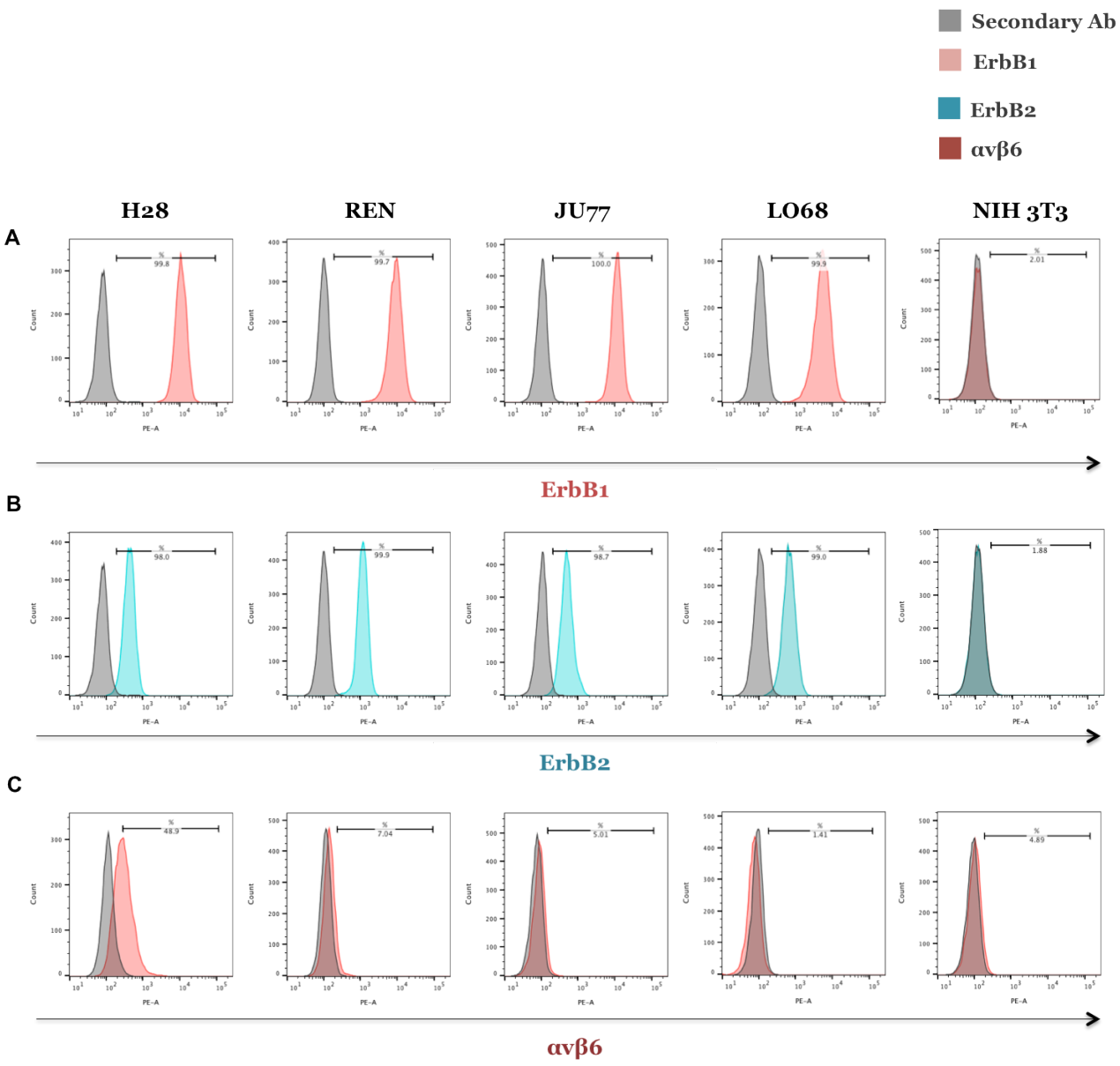

Figure 4-3. Expression of human ErbB1, ErbB2 and αvβ6 on malignant pleural mesothelioma cell lines.
(A) Expression of ErbB1 was detected on the mesothelioma cell lines by flow cytometry (red filled histogram). Staining with secondary antibody (Ab) is also shown (grey filled histogram). **(B)** Expression of ErbB2 was detected on the mesothelioma cell lines by flow cytometry (blue filled histogram). Staining with a matched isotype control antibody is also shown (grey filled histogram). The negative control used to validate antibody binding was NIH 3T3 cells. Above data are representative of findings in at least two independent experiments. **(C)** Expression of αvβ6 was investigated on the mesothelioma cell lines by flow cytometry (red histogram). Control staining with a secondary antibody alone is shown in grey filled histogram.

4.2.2 Cytokine release by N28z, M28z and cM28z T-cells following co-culture with MPM cell lines

Next, I investigated whether expression of the N28z, M28z or cM28z CARs could re-target human T-cell specificity against the panel of four c-Met-expressing mesothelioma cell lines shown in Figures 4-1 and 4-2. Activation of c-Met re-targeted CAR$^+$ T-cells was compared to that of T-cells expressing control CARs or untransduced (UT) T-cells. Since all of these tumour cells express ErbB receptors (Figure 4-3), T-cells expressing T28z (a pan ErbB specific CAR [241]) were used as a positive control. T-cells expressing V28z (containing an inactive targeting moiety derived from a scrambled 20mer peptide sequence) were used as a negative control. Chimeric antigen receptors were expressed in activated human T-cells by retroviral transduction at an efficiency indicated in Figure 4-4. To test CAR T-cell functionality, co-cultivation experiments were performed with all four MPM cell lines. T-cell activation was monitored by measurement of the release of IFN-γ at 48 hours (Figure 4-5) and IL-2 at 24 hours (Figure 4-6).

In three independent experiments, a significant increase in IFN-γ was observed when c-Met-targeted CAR$^+$ T-cells were co-cultivated with all four MPM cell lines (Figure 4-5). Most notable difference between c-Met re-targeted CAR$^+$ T-cells and control populations were observed in the co-cultures involving H28 or REN tumour cells. Despite variability in the concentrations of IFN-γ detected, the pattern of T-cell activation was reproducible across independent experiments.

It should be noted nonetheless that the amount of IFN-γ released by the c-Met re-targeted CAR$^+$ T-cells were considerably lower than that produced by T-cells expressing T28z, which is a potent CAR targeted against the extended ErbB network [241]. A similar observation was noted upon analysis of IL-2 release by MPM-stimulated c-Met re-targeted CAR$^+$ T-cells. All three c-Met re-targeted CAR$^+$ T-cell populations produced significantly greater levels of IL-2 when co-cultured with H28 or REN cells, when compared to UT or V28z$^+$ T-cells (Figure 4-6). Once more, T28z$^+$ T-cells produced far greater levels of IL-2 when activated by all four MPM cells.

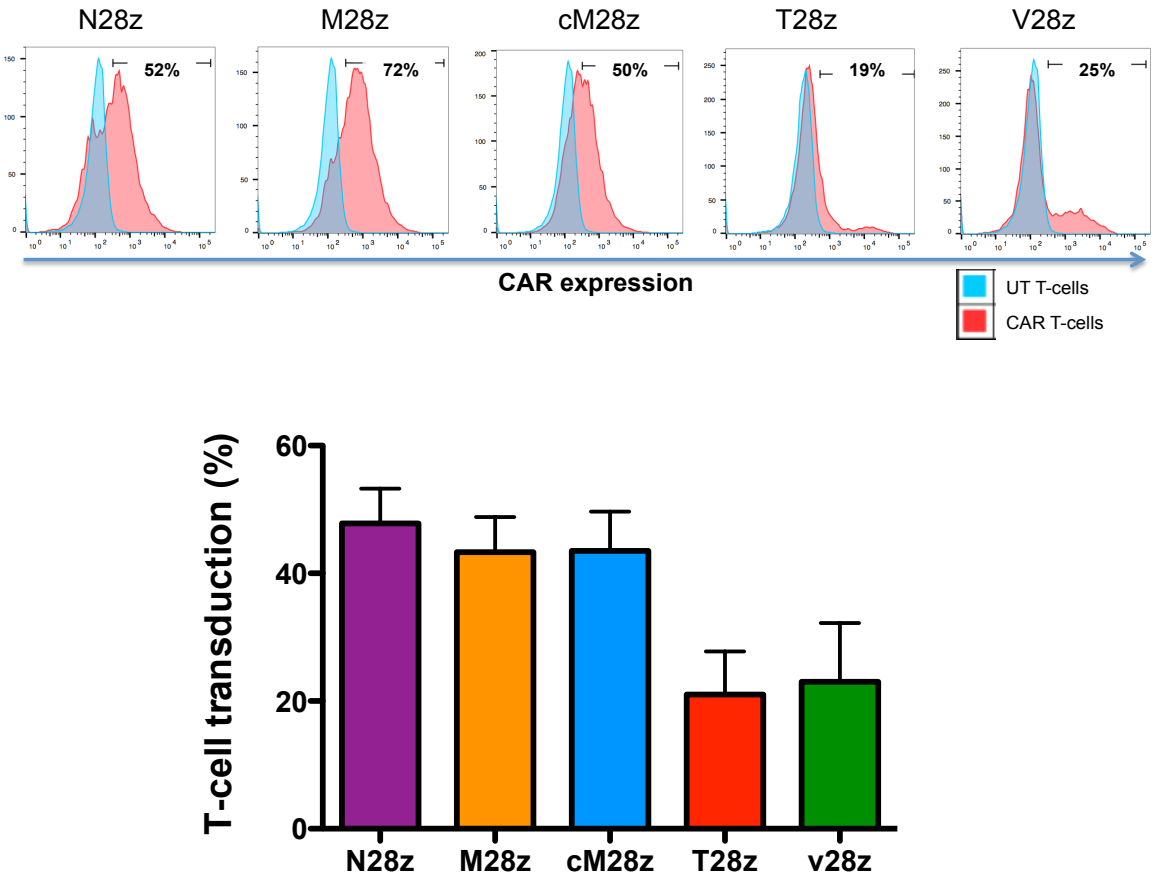

Figure 4-4. Expression of c-Met re-targeted and control CAR by retrovirus-transduced human T-cells.
(**A**) Expression of N28z$^+$, M28z$^+$, cM28z$^+$, T28z$^+$ (positive control CAR targeted against the ErbB family) and V28z$^+$ (negative control CAR with irrelevant targeting moiety) was detected on the surface of transduced primary human T-cells by flow cytometry. Staining was performed using the 9e10 antibody that binds to a c-Myc epitope tag present in the hinge of all five CARs, followed by PE-conjugated goat anti-mouse IgG (filled red histograms). Filled blue histograms show untransduced (UT) T-cells stained with the same protocol. Percentage of CAR positive cells is annotated on each flow cytometry data plot. Data are representative of four independent experiments. (**B**) Pooled data in which human T-cells were transduced using the indicated SFG CAR retroviral constructs (mean $\pm$ SD, n = 5 independent donors).

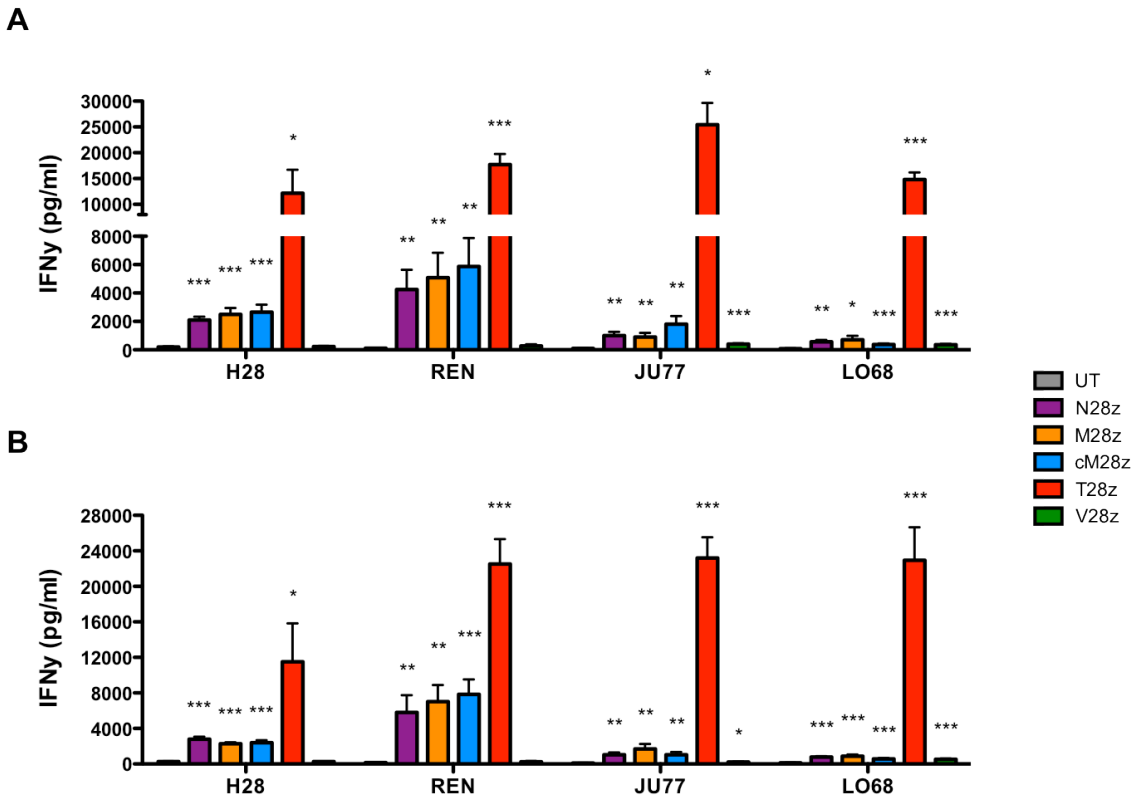

Figure 4-5. Quantification of IFN-γ release following 48hr co-culture of c-Met re-targeted and control CAR T-cells with a panel of MPM cell lines.
N28z$^+$, M28z$^+$, cM28z$^+$, T28z$^+$ (positive control), V28z$^+$ (negative control) or untransduced (UT) T-cells were co-cultivated with the indicated MPM cell lines at an effector to target ratio of 1:1 (**A**) or 2:1 (**B**). After 48 hours, supernatants were collected and the concentration of IFN-γ was determined using ELISA. The data presented have been compiled from results achieved in three independent experiments and presented as mean ± SEM. Significance was determined using the unpaired Student's *t*-test, comparing UT T-cells with CAR$^+$ T-cells for each target cell line: * p <0.05, ** p <0.005 and *** p <0.0005.

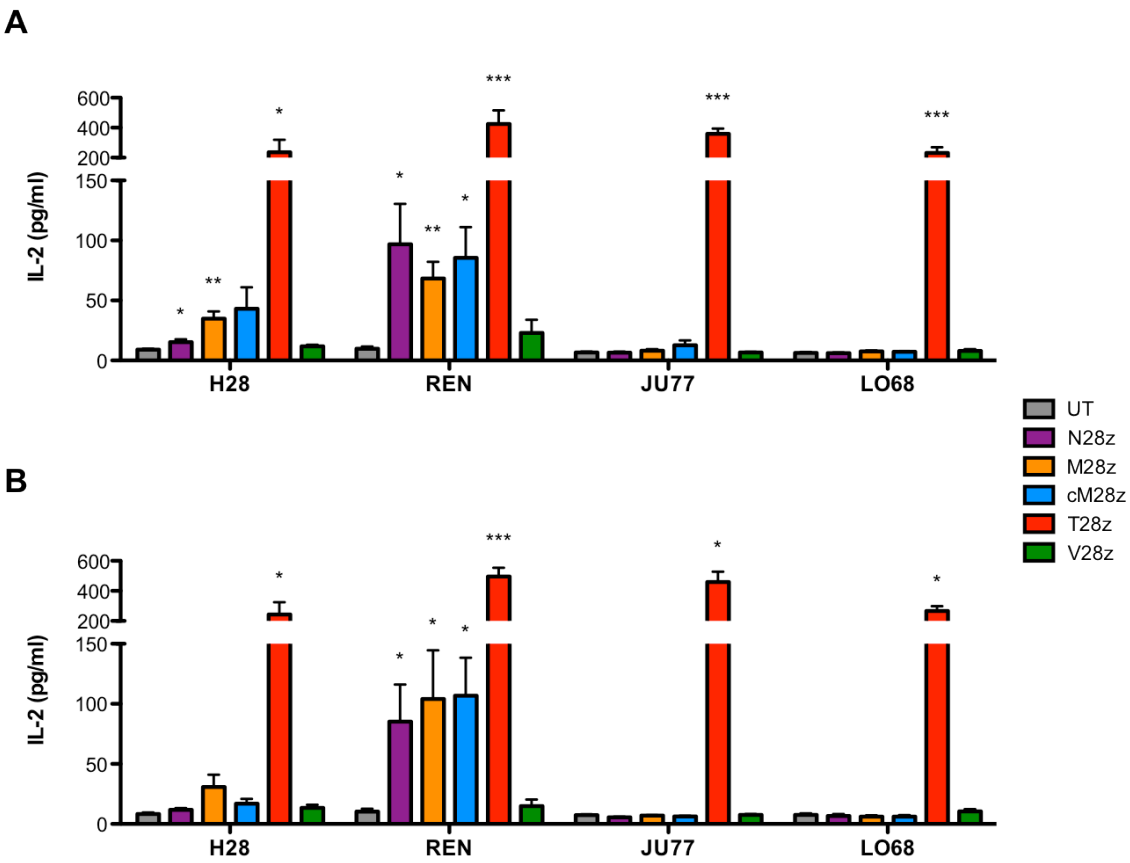

Figure 4-6. Quantification of IL-2 release following 24hr co-culture of c-Met re-targeted and control T-cells with a panel of target-expressing MPM cell lines.

N28z$^+$, M28z$^+$, cM28z$^+$, T28z$^+$, V28z$^+$ or untransduced (UT) T-cells were co-cultivated with the indicated MPM cell lines at an effector to target ratio of 1:1 (**A**) or 2:1 (**B**). After 24 hours, supernatants were collected and the concentration of IL-2 was determined using ELISA. The data presented have been compiled from results achieved in three independent experiments and presented as mean ± SEM. Significance was determined using the unpaired Student's *t*-test, comparing UT T-cells with CAR$^+$ T-cells for each target cell line: * p <0.05, ** p <0.005 and *** p <0.0005.

4.2.3 *In vitro* cytolytic activity of N28z, M28z and cM28z T-cells against MPM cell lines.

A key aim of this project was to determine whether c-Met re-targeted CAR$^+$ T-cells could represent a potential therapy for mesothelioma. Consequently, it was important to determine their ability to destroy MPM cell lines. This was assessed using MTT assays to quantify residual tumour cell survival following co-cultivation with CAR-engineered T-cells. N28z$^+$, M28z$^+$, cM28z$^+$, T28z$^+$, V28z$^+$ T-cells (Figure 4-4) and UT T-cells were co-cultured for either 24, 48 or 72 hours with a panel of MPM cell lines at an effector to target ratio of 1:1, 2:1 or 4:1 (Figure 4-7 to 4-9 respectively). Comparison was made with untreated tumour cells grown under the same conditions, but in the absence of T-cells, providing a measure of maximal tumour cell viability (quantified by formazan dye production).

As shown in Figure 4-7, co-culture of H28 tumour cells with N28z$^+$, M28z$^+$, cM28z$^+$ and T28z$^+$ T-cells for 24 hours resulted in substantial tumour cell lysis (60%) when compared to all control (UT or V28z$^+$ T-cells) cultures. This was further increased when the co-cultures were continued for 48 hours. As expected, there was only a small (20%) reduction in the level of H28 cell viability following incubation with either UT or V28z$^+$ control T-cells when compared to target cells grown in the absence of T-cells. In contrast, no difference could be discerned between the cytolytic activity of the c-Met re-targeted CAR$^+$ T-cells and control T-cells on the remaining three MPM cell lines after 24 hours, irrespective of the effector to target ratio. At 48 hours, a small increase in tumour cell lysis (significant with cM28z$^+$) could be observed on the REN cells and LO68 cells (15-20%) when compared to control UT or V28z$^+$ T-cells. When comparing the c-Met re-targeted CAR$^+$ T-cells against the T28z$^+$ T-cells at an effector to target ratio of 1:1, the difference in killing of REN, JU77 and LO68 MPM cells appears to be marginal. However, the average transduction of T28z$^+$ CAR T-cells was over 2-fold lower than N28z$^+$, M28z$^+$, cM28z$^+$ T-cells. This difference is overcome by increasing the effector to target ratio whereby substantially increased tumour cell lysis is observed with T28z$^+$ T-cells when compared to either c-Met re-targeted CAR$^+$ T-cells or UT and V28z$^+$ T-cells (compare Figure 4-7, Figure 4-8 and Figure 4-9).

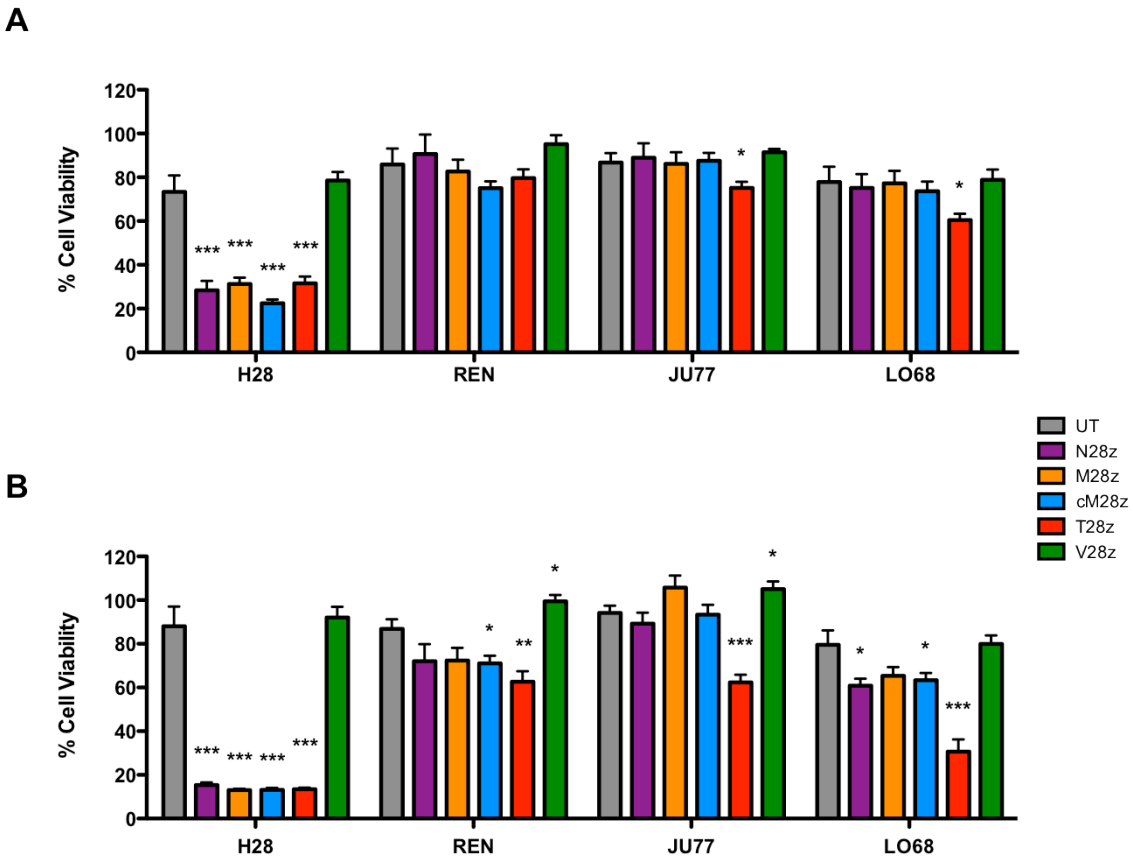

Figure 4-7. Cytotoxic destruction of MPM cell lines co-cultured with c-Met re-targeted and control CAR T-cells: effector to target ratio of 1:1.
The indicated MPM tumour cell lines (2 x 10^4 cells) were seeded in triplicate and allowed to adhere overnight. Percentage viability of the indicated MPM cell lines is shown following 24hr (**A**) and 48hr (**B**) incubation with an equal number (2 x 10^4 cells) of $N28z^+$, $M28z^+$, $cM28z^+$, $T28z^+$, $V28z^+$ or untransduced (UT) T-cells. Transduced cells were not corrected for transduction efficiency, which is shown in Figure 4-3. Tumour cell viability was measured using an MTT assay at the indicated time points. Data are presented as mean ± SEM from four independent experiments. Significance was determined using the unpaired Student's *t*-test, comparing UT T-cells with CAR^+ T-cells for each target cell line: * p <0.05, ** p <0.005 and *** p <0.0005.

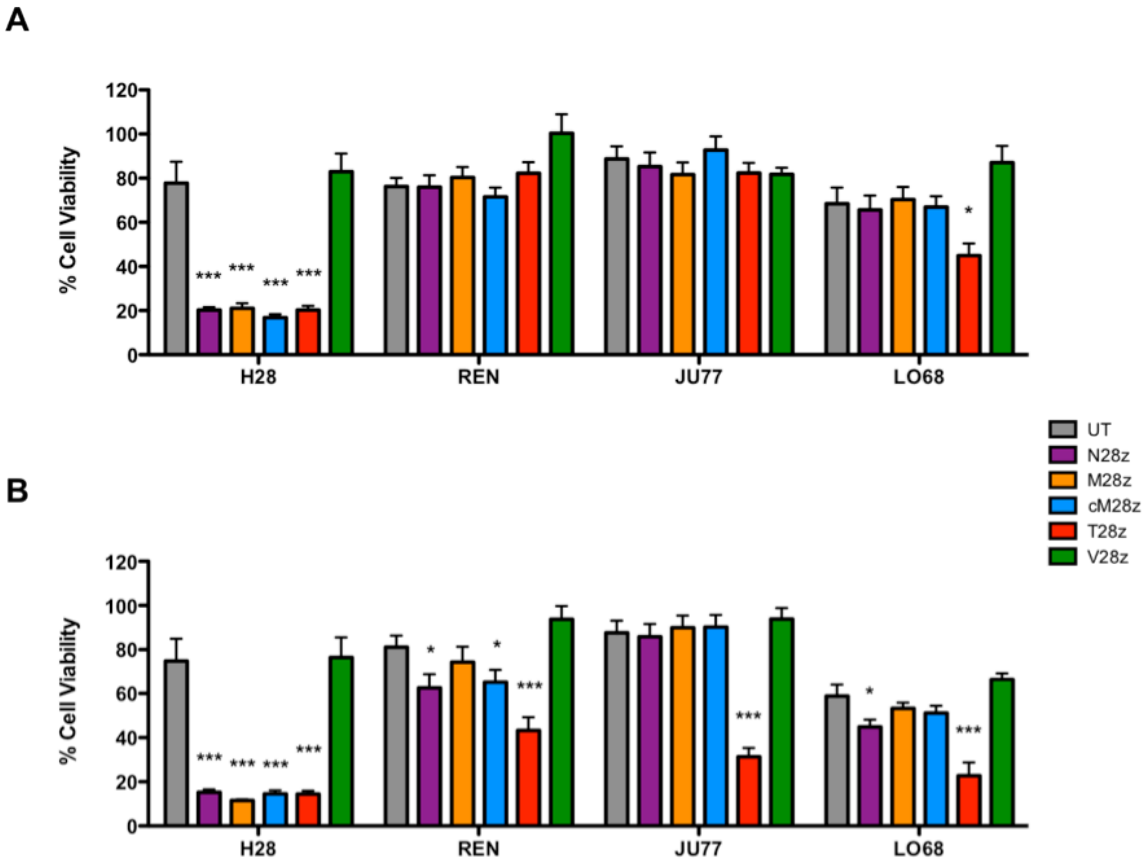

Figure 4-8. Cytotoxic destruction of MPM cell lines co-cultured with c-Met re-targeted and control CAR T-cells: effector to target ratio of 2:1.
The indicated MPM tumour cell lines (2 x 10^4 cells) were seeded in triplicate and allowed to adhere overnight. Percentage viability of the indicated MPM cell lines is shown following 24hr (**A**) and 48hr (**B**) incubation with a 2-fold excess (4 x 10^4 cells) of N28z$^+$, M28z$^+$, cM28z$^+$, T28z$^+$, V28z$^+$ or untransduced (UT) T-cells. Transduced cells were not corrected for transduction efficiency, which is shown in Figure 4-3. Tumour cell viability was measured using an MTT assay at the indicated time points. Data are presented as mean ± SEM from four independent experiments. Significance was determined using the unpaired Student's *t*-test, comparing UT T-cells with CAR$^+$ T-cells for each target cell line: * p <0.05, ** p <0.005 and *** p <0.0005.

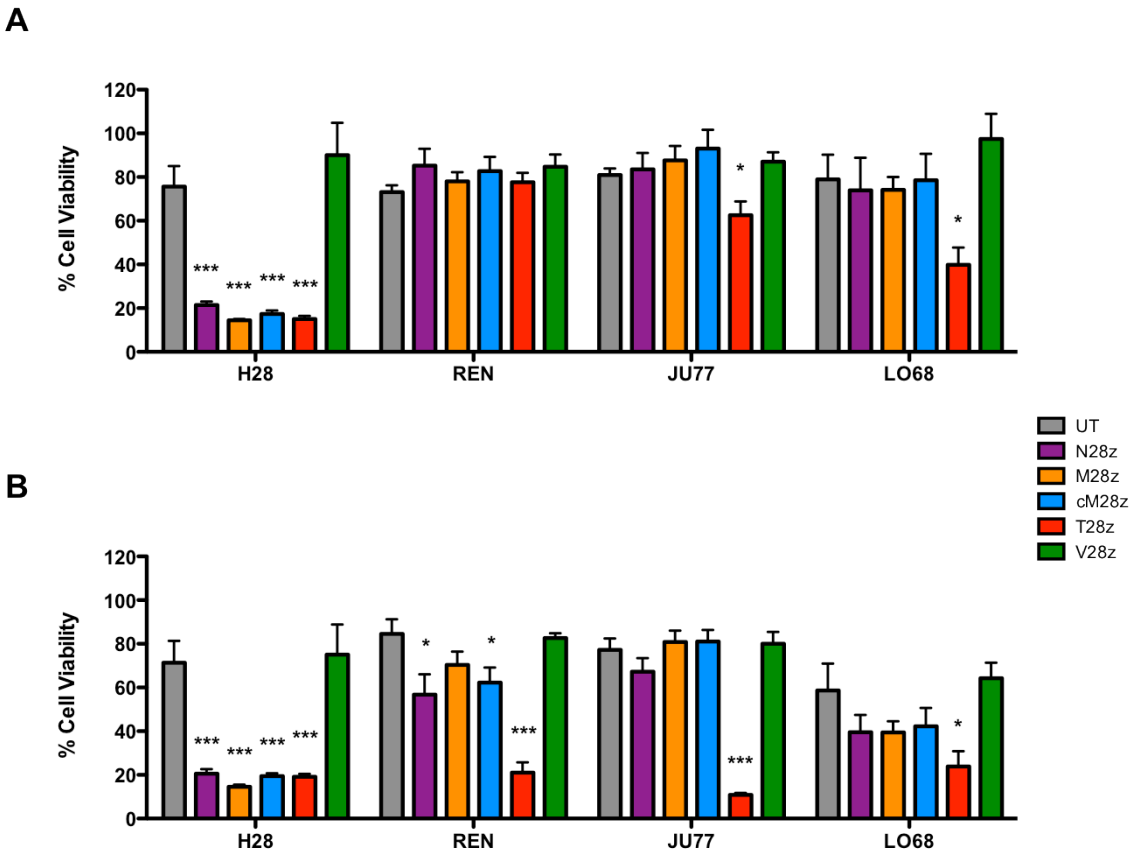

Figure 4-9. Cytotoxic destruction of MPM cell lines co-cultured with c-Met re-targeted and control CAR T-cells: effector to target ratio of 4:1.
The indicated MPM tumour cell lines (2 x 10^4 cells) were seeded in triplicate and allowed to adhere overnight. Percentage viability of the indicated MPM cell lines is shown following 24hr (**A**) and 48hr (**B**) incubation with a 4-fold excess (8 x 10^4 cells) of N28z$^+$, M28z$^+$, cM28z$^+$, T28z$^+$, V28z$^+$ or untransduced (UT) T-cells. Transduced cells were not corrected for transduction efficiency, which is shown in Figure 4-3. Tumour cell viability was measured using an MTT assay at the indicated time points. Data are presented as mean ± SEM from four independent experiments. Significance was determined using the unpaired Student's *t*-test, comparing UT T-cells with CAR$^+$ T-cells for each target cell line: * p <0.05, ** p <0.005 and *** p <0.0005.

4.2.4 Competitive ligand inhibition does not affect c-Met re-targeted CAR$^+$ T-cell function

I hypothesised that the discrepancy observed between high c-Met expression and reduced c-Met re-targeted CAR$^+$ T-cell mediated killing of REN, JU77 and LO68 cells might be due to HGF secretion by MPM cells, thus competitively inhibiting CAR T-cell function. To investigate this possibility, a HGF ELISA was performed on conditioned medium derived from all four MPM cell lines (Figure 4-10). Conditioned medium from NIH 3T3 fibroblast cells which are known not to release HGF were used as a negative control. It has previously been reported that HGF must be introduced via gene transfer to NIH 3T3 cells to establish an HGF/c-Met autocrine loop to make them tumourigenic [349].

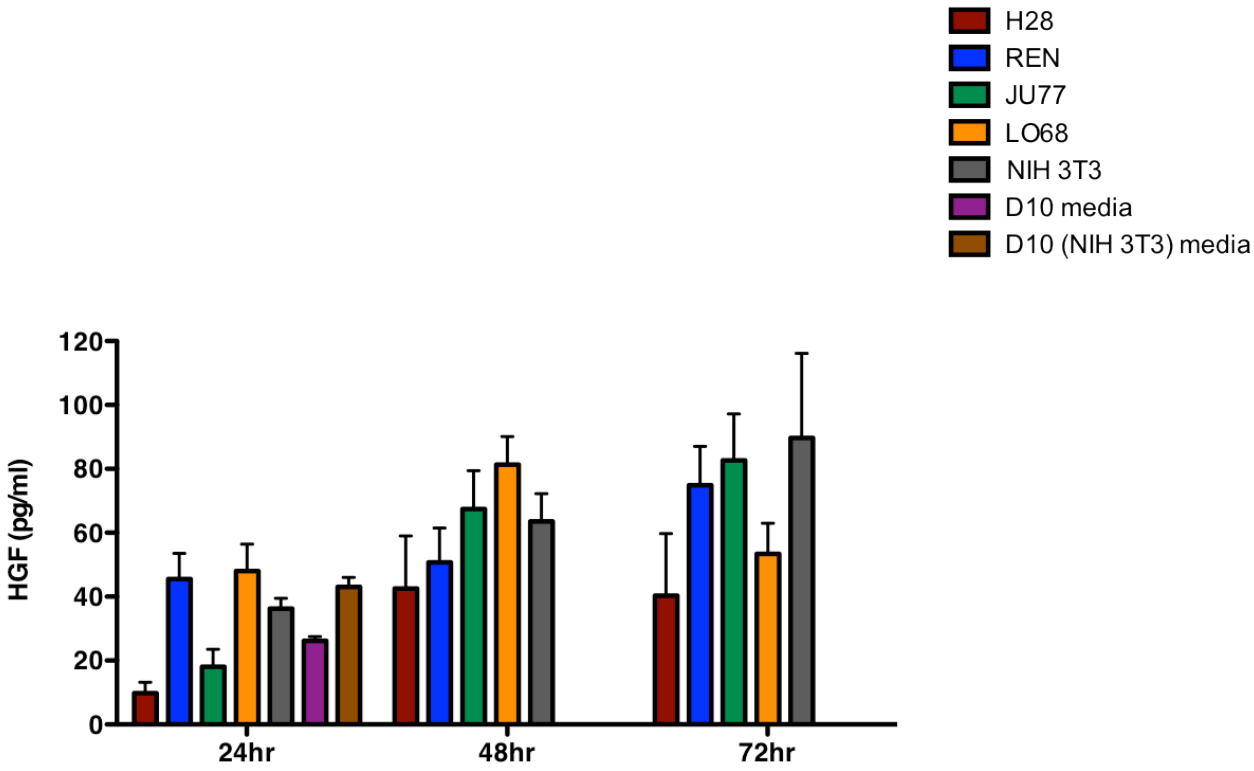

Figure 4-10. Quantification of human HGF released following time course from a panel of MPM tumour cell lines.
The indicated MPM tumour cell lines and NIH 3T3 cells (negative control) were seeded in triplicate at 2 x 10^4 cells per well and were allowed to adhere overnight. Thereafter, at 24hr, 48hr and 72-hour intervals, medium was collected and the concentration of human HGF was determined using ELISA. Data are from two independent experiments and are presented as mean ± SEM. An unpaired Student *t*-test was undertaken which demonstrated no significant increase in any sample, when compared to D10 medium. Abbreviations: D10, DMEM culture media supplemented with FBS. D10 NIH 3T3 media; conditioned medium obtained from NIH 3T3 cells cultured in D10 for 24 hours. The sensitivity of the ELISA was 5.5pg/ml.

The data presented suggests HGF levels in supernatant collected from all MPM cell lines is not significantly higher than in D10 medium (comprising DMEM + 10% FBS) or conditioned medium derived from NIH 3T3 cells, which are known not to release HGF (Figure 4-10) [349]. Taken together, the data presented suggests that ligand blocking is unlikely to account for poor function of the c-Met$^+$ CAR T-cells on REN, JU77 and LO68 MPM tumour cell lines. It should be noted however that no suitable positive sample was available for this analysis.

4.2.5 Engineering of MPM cells to over-express CD44v6

A variety of CD44 isoforms are commonly overexpressed in many tumours. The CD44 variant isoform v6 is a known co-factor that facilitates the binding of HGF to the c-Met receptor [196]. Although N28z$^+$, M28z$^+$ and cM28z$^+$ T-cells do not directly engage and kill NIH 3T3 cells expressing only CD44v6 (Figure 3-4 to 3-6), c-Met re-targeted CAR$^+$ T-cells release significantly higher levels of IFN-γ when co-cultivated with NIH 3T3 cells that co-express c-Met and CD44v6, compared to c-Met alone. This led me to hypothesise that the presence of this co-factor might enhance the cytotoxic activity of c-Met re-targeted CAR$^+$ T-cells against refractory MPM tumour cell lines such as REN, JU77 and LO68, which do not naturally express this isoform (Figure 4-1B).

To test this, human CD44v6 was over-expressed in REN, JU77 and LO68 cell lines by retroviral-mediated gene transfer. Figure 4-11C shows that transduced cells were strongly positive for CD44v6 expression with the exception of LO68, in which more modest expression was achieved.

Prior to testing these cell lines in MTT cytotoxicity assays, it was important to confirm that expression of CD44v6 had not altered the expression of c-Met by the MPM cell lines. When compared to c-Met expression on the parental MPM cell lines, the CD44v6 transduced MPM cell lines had near identical levels of c-Met expression, as detected by flow cytometry (Figure 4-12).

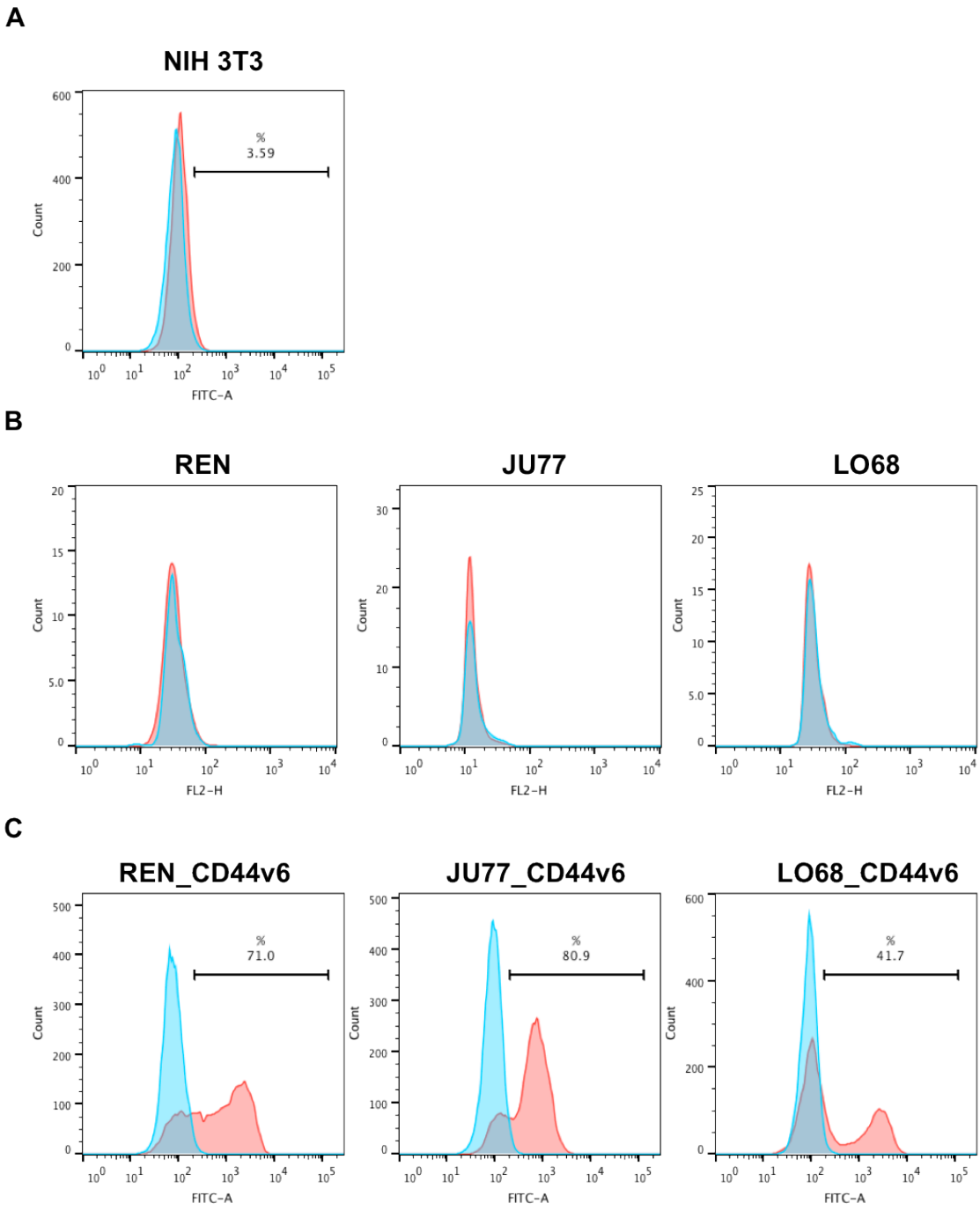

Figure 4-11. CD44v6 expression by retrovirus-transduced malignant pleural mesothelioma cell lines.
(**A**) NIH 3T3 cells used as a negative control for detection of the CD44v6 receptor using an anti-CD44v6-FITC antibody. In all cases, CD44v6 staining is shown as a filled red histogram while isotype control staining is shown as the blue histogram. (**B**) Cell surface expression of CD44v6 was not detected on the indicated parental MPM cell lines using an anti-CD44v6-FITC antibody (red histogram). Staining of the matched isotype control antibody is also shown (blue histogram). (**C**) Following retroviral-mediated gene transfer of CD44v6 into MPM cells, this analysis was repeated as above (CD44v6 - red histogram), making comparison with a matched isotype control (blue histogram). Data are representative of three independent experiments.

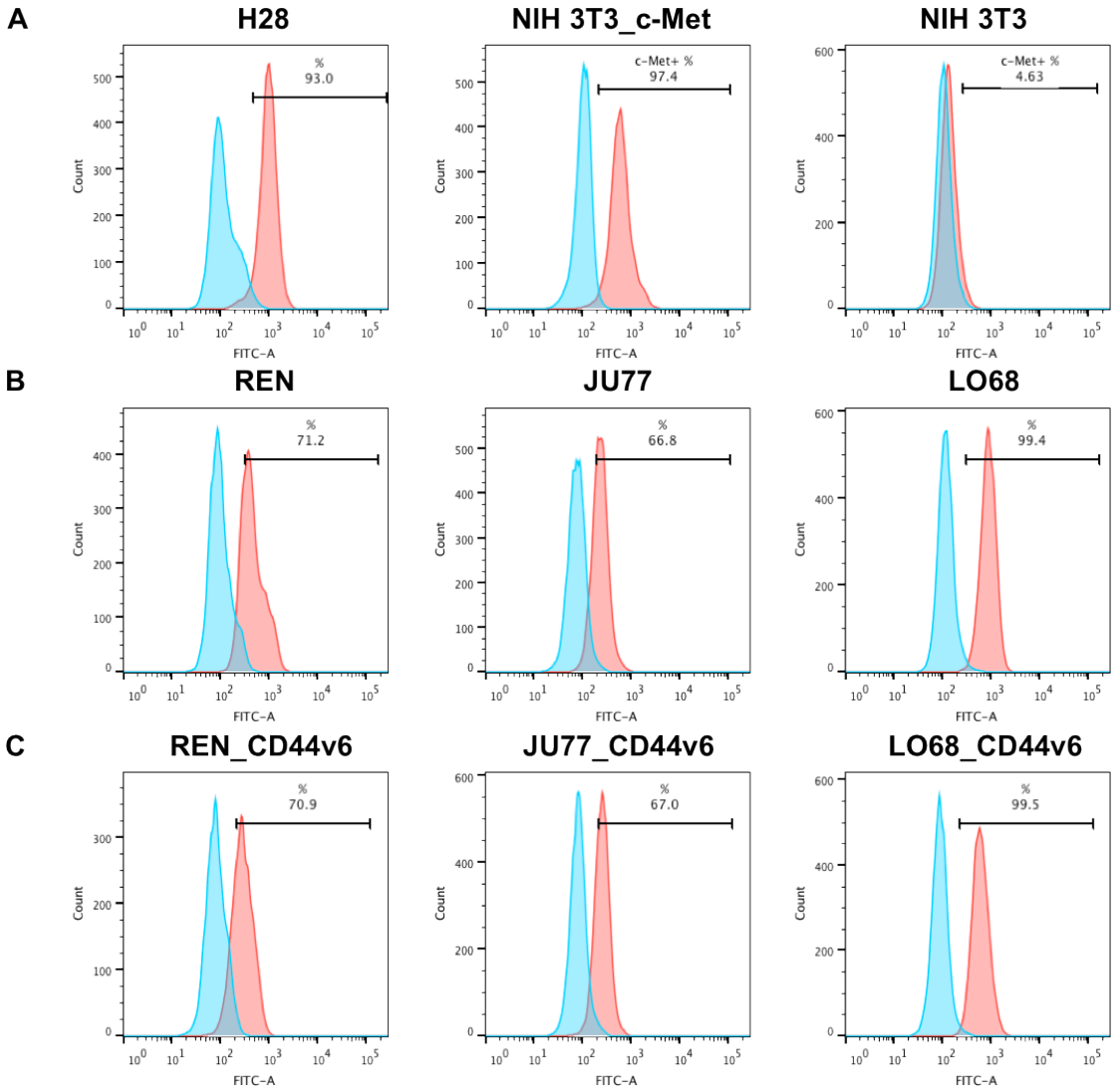

Figure 4-12. Retention of c-Met expression on malignant pleural mesothelioma cell lines engineered to overexpress human CD44v6.
(**A**) NIH 3T3 cells that over-express human c-Met were used as a positive control for detection of this receptor using an anti-c-Met-FITC antibody. Staining was also confirmed on H28 MPM cells, which have previously been shown to express high levels of cell surface c-Met expression. Parental NIH 3T3 cells served as negative control. In all cases, c-Met staining is shown as a filled red histogram while isotype control staining is shown as the blue histogram. (**B**) Expression of c-Met was detected in the indicated parental MPM cell line using an anti-c-Met-FITC antibody (red histogram). Staining of the matched isotype control antibody is also shown (blue histogram). (**C**) Following over-expression of CD44v6 in these cells, c-Met expression was determined by flow cytometry as above (red histogram), making comparison with a matched isotype control (blue histogram). Data are representative of three independent experiments.

4.2.6 Determination of N28z, M28z and cM28z T-cell activation by CD44v6 expressing MPM cell lines

Having validated both parental and CD44v6-over-expressing MPM cell lines, studies to test cytotoxic activity of c-Met re-targeted CAR$^+$ T-cells were conducted. Representative examples of transduction of N28z$^+$, M28z$^+$, cM28z$^+$, T28z$^+$ and V28z$^+$ T-cells are shown in Figure 4-13A while pooled transduction efficiency data from three independent donors are shown in Figure 4-13B.

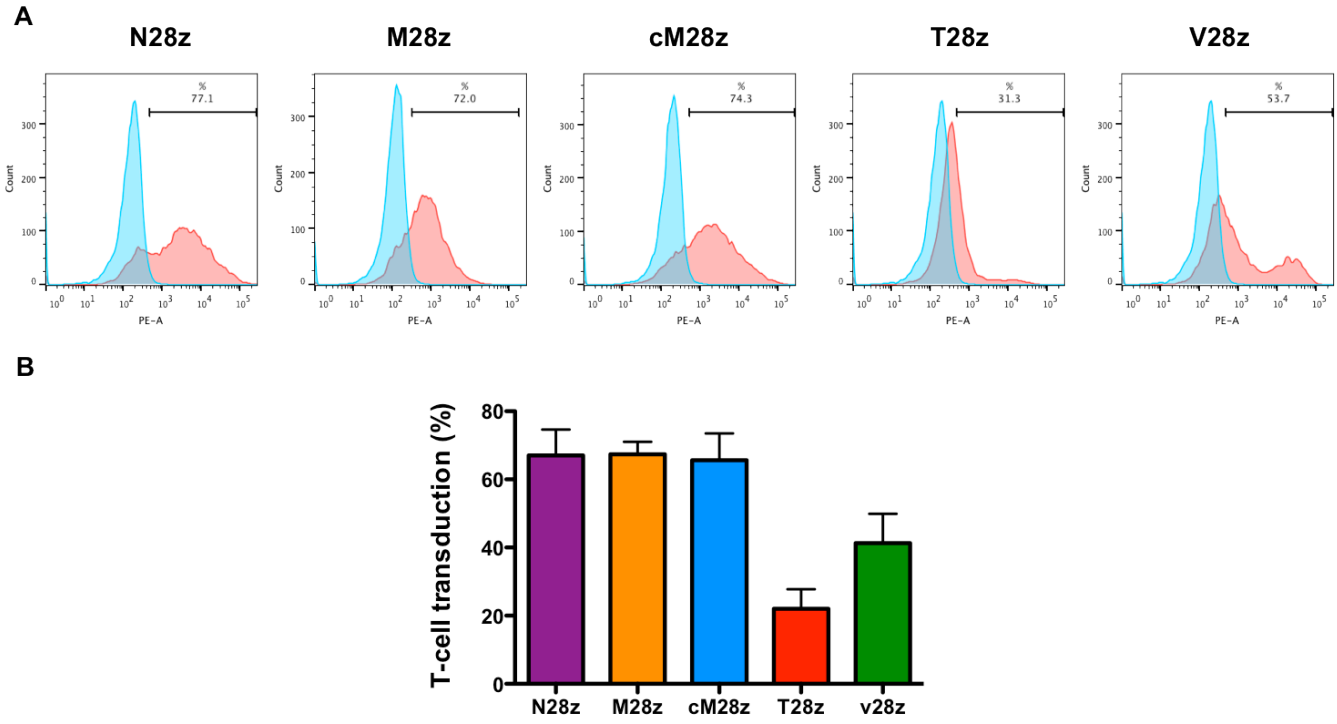

Figure 4-13. Transduction efficiency of CAR T-cells used in co-cultivation experiments with MPM cell lines engineered to express CD44v6.
(**A**) Expression of N28z, M28z, cM28z, T28z and V28z (filled red histogram) was detected on the surface of human T-cells using flow cytometry. Filled blue histograms show UT T-cells stained with the same protocol. Percentage CAR positive cells is annotated on each plot. (**B**) Pooled data in which human T-cells were transduced using the indicated SFG CAR retroviral constructs (mean $\pm$ SEM of three independent donors).

To investigate the effect of CD44v6 co-expression on anti-tumour activity of c-Met re-targeted T-cells, N28z$^+$, M28z$^+$ and cM28z$^+$ CAR T-cells were co-cultured with REN (Figure 4-14), JU77 (Figure 4-15) and LO68 MPM tumour cells (Figure 4-16). Release of IFN-γ in these co-cultures was compared on parental and CD44v6-engineered MPM tumour cell lines in each case. Activation of c-Met re-targeted CAR$^+$ T-cells was compared to that of T-cells expressing control CARs or untransduced (UT) T-cells.

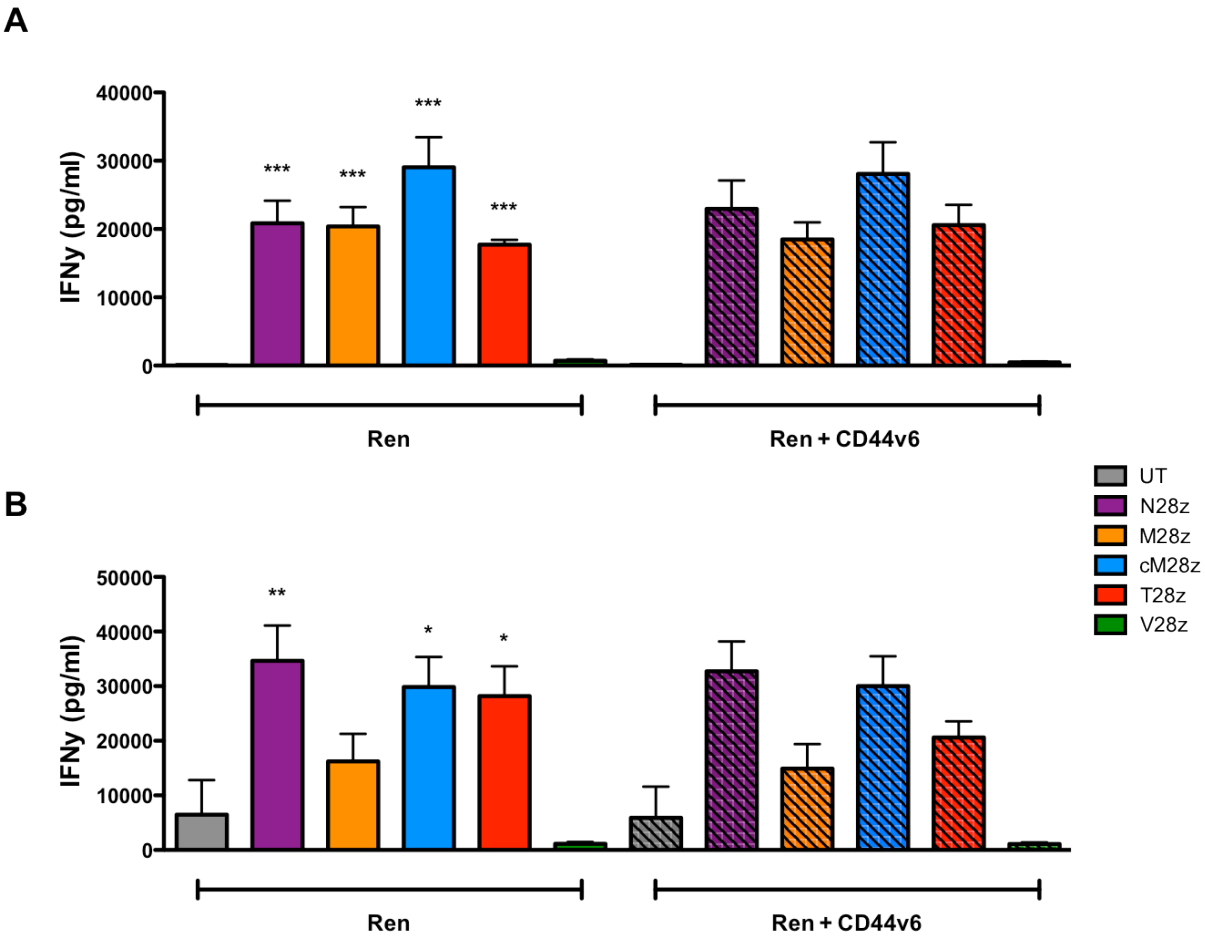

Figure 4-14. Quantification of IFN-γ release following 48hr co-culture of c-Met re-targeted and control CAR T-cells with matched REN and REN_CD44v6 expressing cells.

N28z$^+$, M28z$^+$, cM28z$^+$, T28z$^+$, V28z$^+$ or untransduced (UT) T-cells were co-cultivated with REN and CD44v6 expressing REN cells at an effector to target ratio of (**A**) 1:1 or (**B**) 2:1. After 48 hours, supernatants were collected and the concentration of IFN-γ was measured using ELISA. Data were compiled from three independent experiments and are presented as mean ± SEM. Symbols above individual bars represent significance determined using the unpaired Student's *t*-test, comparing UT T-cells with CAR$^+$ T-cells when co-cultivated on REN cells (this test was not conducted on REN+ CD44v6 cells). Unpaired Student's *t*-tests were also performed comparing CAR$^+$ T-cells co-cultivated on REN versus REN + CD44v6 tumour cells. However no significant differences were observed in any case: * p <0.05, ** p <0.005 and *** p <0.0005.

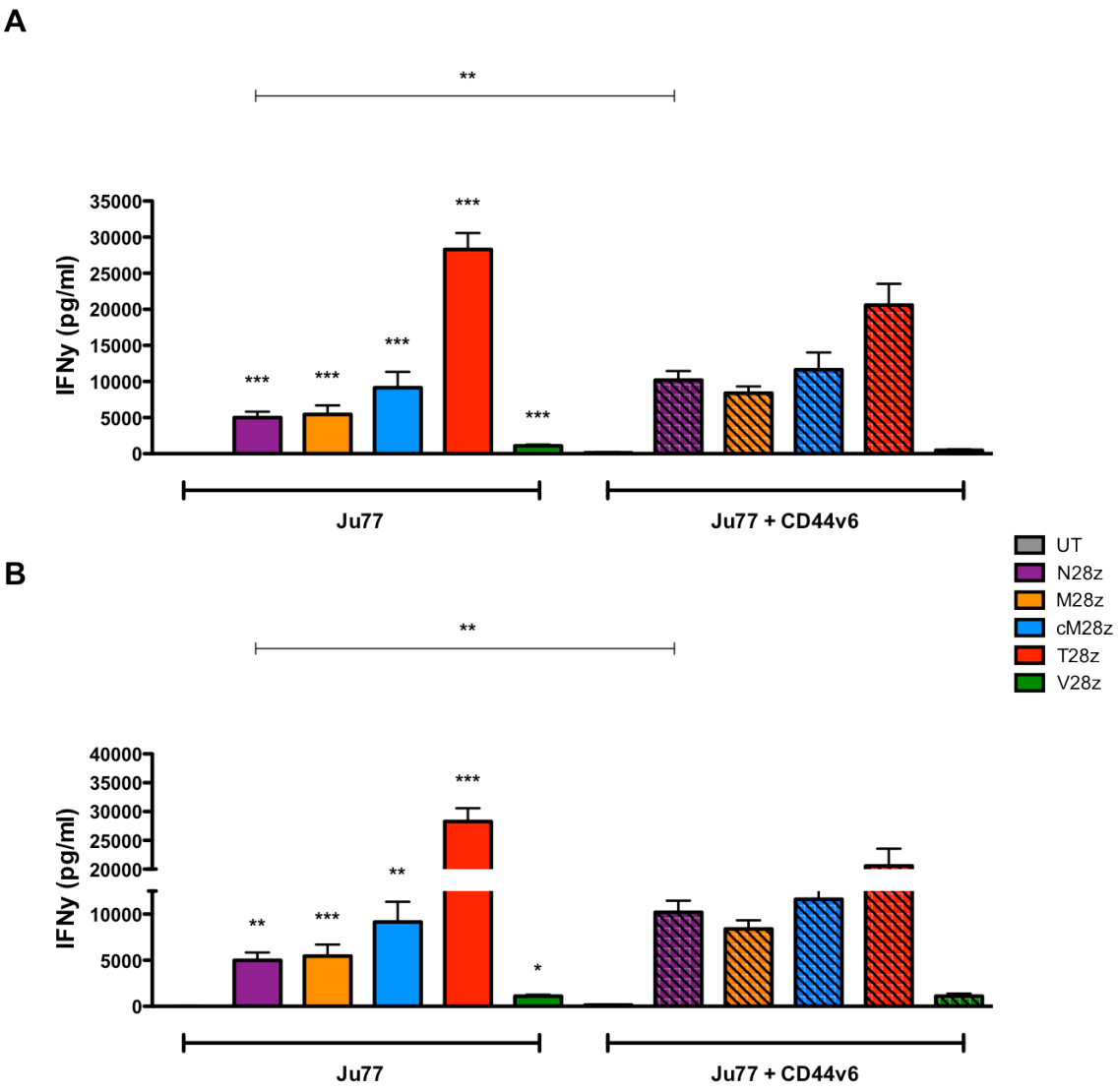

Figure 4-15. Quantification of IFN-γ release following 48hr co-culture of c-Met re-targeted and control CAR T-cells with matched JU77 and Ju77_CD44v6 expressing cells.
N28z$^+$, M28z$^+$, cM28z$^+$, T28z$^+$, V28z$^+$ or untransduced (UT) T-cells were co-cultivated with JU77 and CD44v6 expressing JU77 cells at an effector to target ratio of (**A**) 1:1 or (**B**) 2:1. After 48 hours, supernatants were removed and the concentration of IFN-γ was measured using ELISA. The data presented have been compiled from results achieved in three independent experiments and are presented as mean ± SEM. Symbols above individual bars represent significance determined using the unpaired Student's *t*-test, comparing UT T-cells with CAR$^+$ T-cells when co-cultivated on Ju77 cells (this test was not conducted on JU77 + CD44v6 cells). Where indicated by the overhead line, an unpaired Student's *t*-test has been performed comparing N28z$^+$ T-cells co-cultivated on Ju77 and Ju77 + CD44v6 tumour cells: * p <0.05, ** p <0.005 and *** p <0.0005.

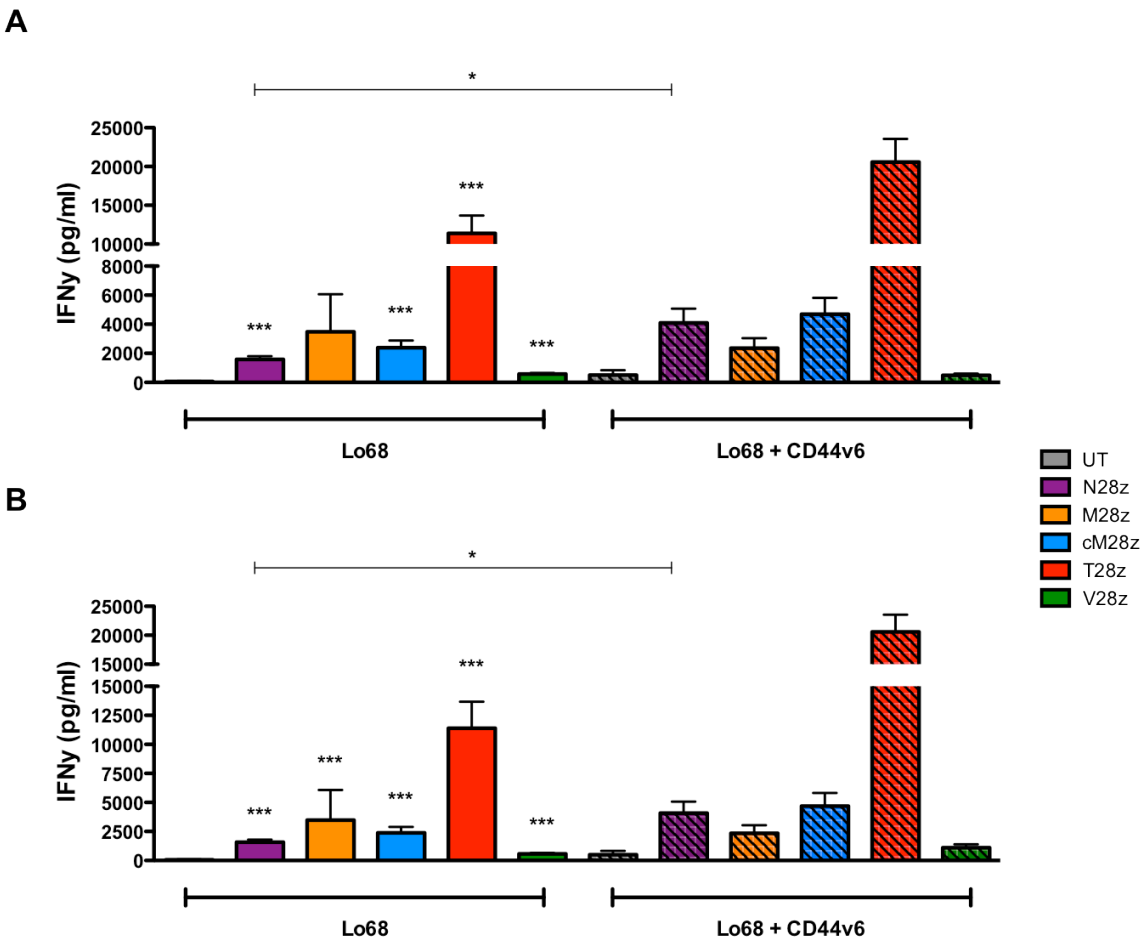

Figure 4-16. Quantification of IFN-γ release following 48hr co-culture of c-Met re-targeted and control CAR T-cells with matched LO68 and LO68_CD44v6 expressing cells.
N28z$^+$, M28z$^+$, cM28z$^+$, T28z$^+$, V28z$^+$ or untransduced (UT) T-cells were co-cultivated with LO68 and CD44v6 expressing LO68 cells at an effector to target ratio of (**A**) 1:1 or (**B**) 2:1. After 48 hours, supernatants were removed and the concentration of IFN-γ was measured using ELISA. The data presented have been compiled from results achieved in three independent experiments and are presented as mean ± SEM. Symbols above individual bars represent significance determined using the unpaired Student's *t*-test, comparing UT T-cells with CAR$^+$ T-cells when co-cultivated on LO68 cells (this test was not conducted on LO68 + CD44v6 cells). Where indicated by the overhead line, an unpaired Student's *t*-test has been performed comparing N28z$^+$ T-cells co-cultivated on LO68 and LO68 + CD44v6 tumour cells: * p <0.05, ** p <0.005 and *** p <0.0005.

In three independent experiments, comparing between parental and CD44v6 expressing tumour cells, no significant difference in IFN-γ release by N28z$^+$, M28z$^+$ or cM28z$^+$ T-cells was observed following their co-culture with REN MPM cells either effector to target ratio used (Figure 4-14). Following co-cultures with JU77 cells, only N28z$^+$ T-cells released significantly higher amounts of IFN-γ when co-cultured with JU77_CD44v6 cells compared to parental counterparts (Figure 4-15). A similar result was observed following co-culture with LO68 cells, with N28z$^+$ CAR T-cells releasing significantly

greater amounts of IFN-γ on LO68_CD44v6 compared to LO68 cells (Figure 4-16). Despite variability in the concentrations of IFN-γ detected, the pattern of T-cell activation was reproducible across independent experiments. Although statistical significance was reached with N28$^+$ T-cells on two of the three MPM cell lines, it is worth noting the level of IFN-γ released was still either below or comparable to levels produced by cM28z$^+$ T-cells. Reliably across independent donors, the concentrations of IFN-γ released by the c-Met re-targeted CAR$^+$ T-cells were considerably lower than that achieved by T-cells that express T28z when co-cultured with both JU77 and LO68 cells. However, this disparity was not observed during co-culture with REN MPM cells (Figure 4-14).

4.2.7 Comparison of susceptibility of parental and CD44v6 transduced MPM cells to cytotoxic destruction by N28z$^+$, M28z$^+$ and cM28z$^+$ CAR T-cells

Measurement of T-cell-mediated MPM cell destruction was achieved in three independent experiments performed using the same protocol described above (section 4.2.3). Following confirmation of CAR expression (Figure 4-13), N28z$^+$, M28z$^+$, cM28z$^+$, T28z$^+$, V28z$^+$ and UT T-cells were co-cultured with MPM cells for 24 - 72 hours at an effector to target ratio of 1:1, 2:1 or 4:1 (Figure 4-17 to 4-19 respectively). At 24 hours, c-Met re-targeted CAR$^+$ T-cells induced a similar level of lysis of parental MPM cells and those transduced to express CD44v6; with no significant difference between the c-Met re-targeted CAR$^+$ T-cells and control T-cells. At 48 hours, a statistically significant increase in tumour cell lysis could be observed on the REN cells of 40% (N28z & M28z) and LO68 cells with 20% increase in tumour cell lysis when comparing the c-Met re-targeted CAR$^+$ T-cells to UT or V28z$^+$ T-cells (Figure 4-18B). No difference was observed between the killing of parental and CD44v6-transduced MPM cells at 48 hours. At 72 hours (Figure 4-18C), the only cell line that suggested CD44v6 might enhance tumour cell lysis mediated by c-Met re-targeted CAR$^+$ T-cells was the JU77 cell line. However, this was not observed with increasing effector to target ratios, arguing that this difference does not have biological relevance. Overall, the data presented across the three effector to target ratios at the different time points suggest that the presence of CD44v6 did not enhance the efficacy of c-Met re-targeted CAR$^+$ T-cell mediated tumour cell lysis. Of note however is the increased anti-tumour activity observed with the c-Met re-targeted CAR$^+$ T-cells (especially at 48 and 72 hours) when co-cultured with parental MPM cells, when compared to the data shown in Figure 4-7 to Figure 4-9. This may in part be due to the increased transduction efficiency of the c-Met re-targeted CAR T-cells, which was almost 20% higher than previously achieved.

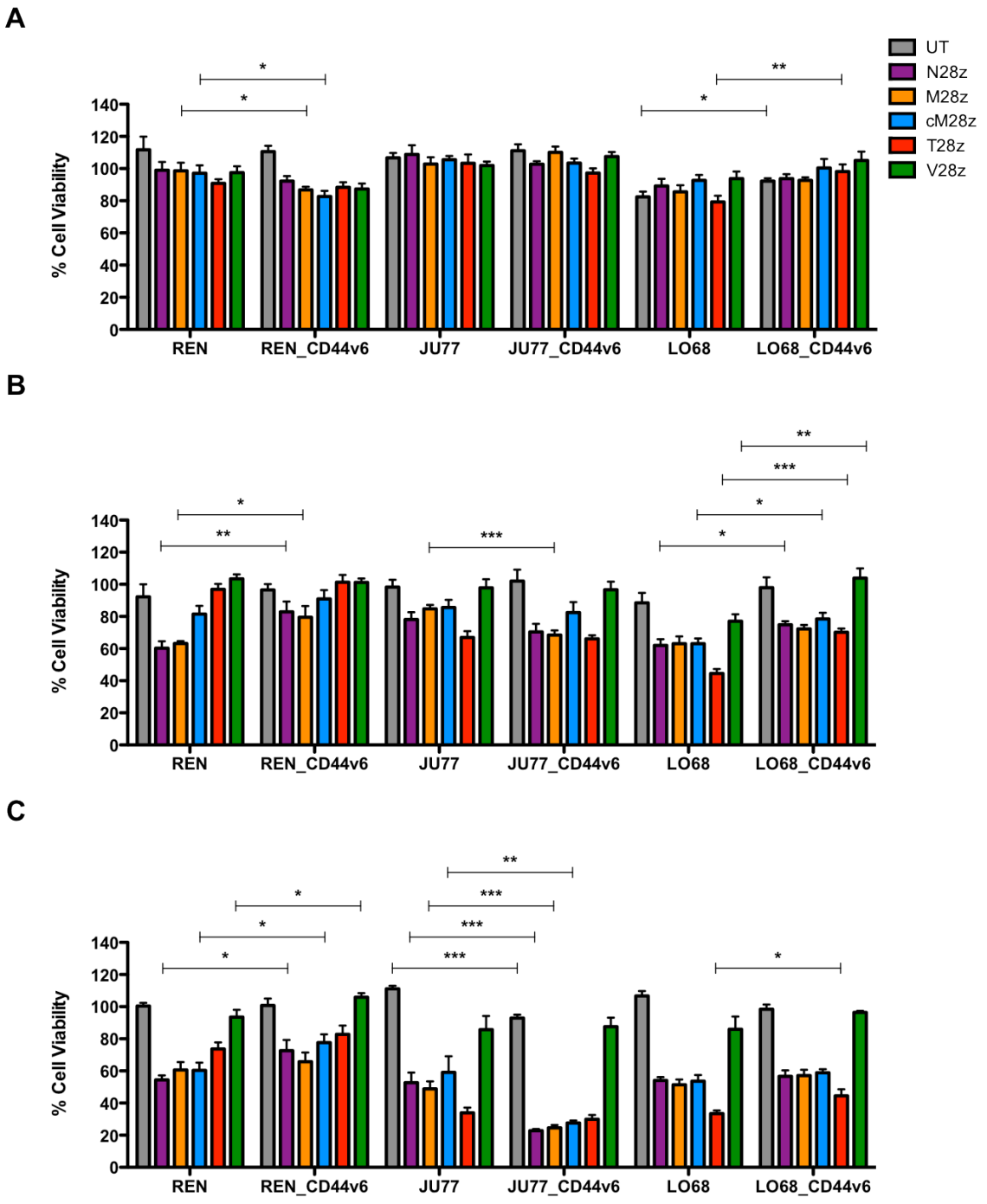

Figure 4-17. Cytotoxic destruction of matched parental and CD44v6 expressing MPM cell lines co-cultured with c-Met re-targeted and control CAR T-cells: effector to target ratio of 1:1.

A panel of MPM tumour cell lines (2 x 10^4 cells) were seeded in triplicate and allowed to adhere overnight. Percentage viability of MPM cell lines is shown following (**A**) 24hr, (**B**) 48hr or (**C**) 72hr incubation with an equal number (2 x 10^4 cells) of N28z$^+$, M28z$^+$, cM28z$^+$, T28z$^+$, V28z$^+$ or untransduced (UT) T-cells. Transduced cells were not corrected for transduction efficiency (shown in Figure 4-12B). Tumour cell viability was measured using an MTT assay at the indicated time points after removal of T-cells by gentle washing. Data presented as mean ± SEM from three independent experiments. Significance was determined using the unpaired Student's *t*-test, comparing T-cell populations between matched cell lines (comparing N28z on REN v REN_CD44v6) * $p<0.05$, ** $p<0.005$ and *** $p<0.0005$.

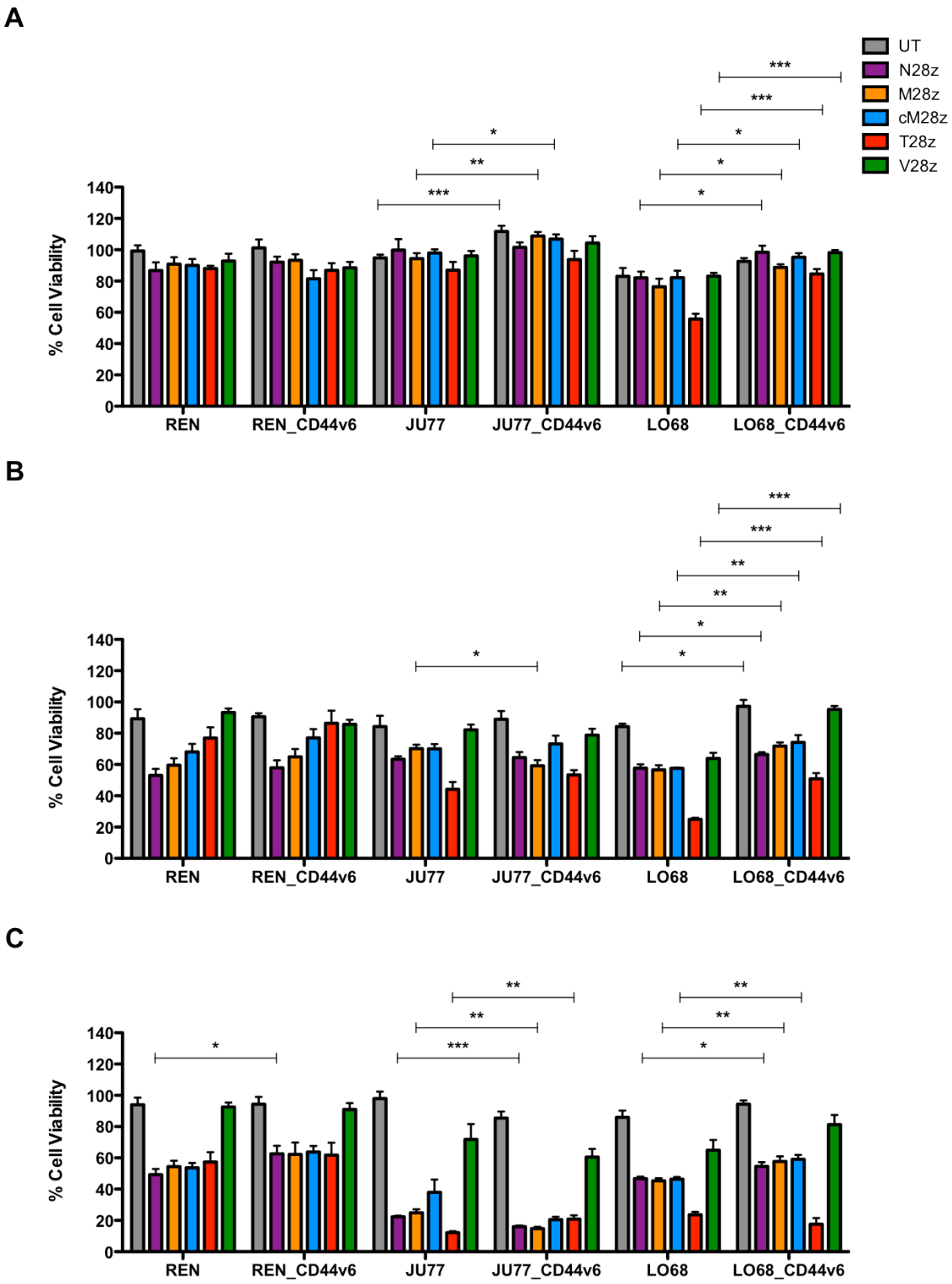

Figure 4-18. Cytotoxic destruction of matched parental and CD44v6 expressing MPM cell lines co-cultured with c-Met re-targeted and control CAR T-cells: effector to target ratio of 2:1.

A panel of MPM tumour cell lines (2 x 10^4 cells) were seeded in triplicate and allowed to adhere overnight. Percentage viability of MPM cell lines is shown following (**A**) 24hr, (**B**) 48hr or (**C**) 72hr incubation with 4 x 10^4 cells of N28z$^+$, M28z$^+$, cM28z$^+$, T28z$^+$, V28z$^+$ or untransduced (UT) T-cells. Transduced cells were not corrected for transduction efficiency (shown in Figure 4-12B). Tumour cell viability was measured using an MTT assay at the indicated time points after removal of T-cells by gentle washing. Data are presented as mean ± SEM from three independent experiments. Significance was determined using the unpaired Student's *t*-test, comparing T-cell populations between matched cell lines (comparing N28z on REN v REN_CD44v6) * $p<0.05$, ** $p<0.005$ and *** $p<0.0005$.

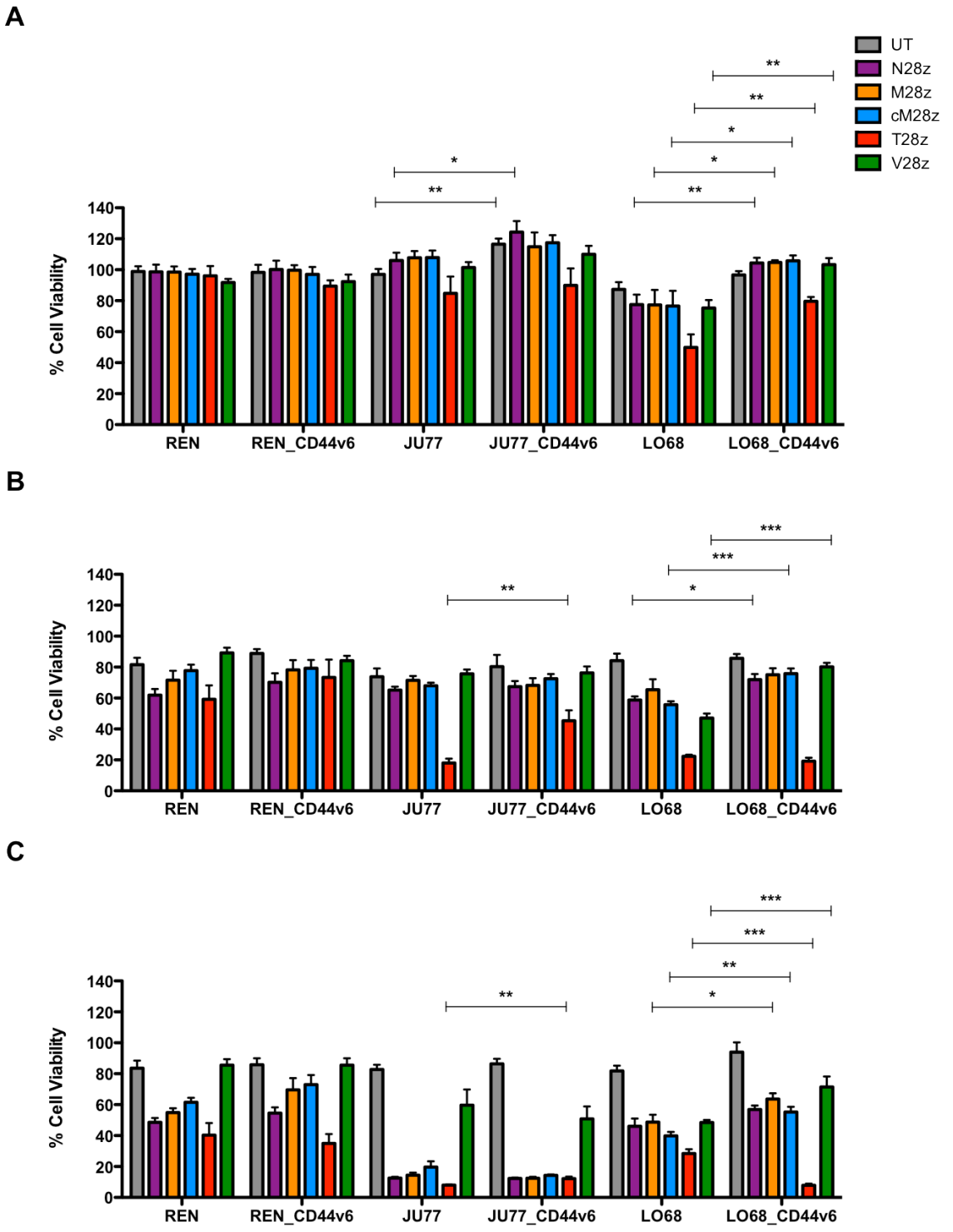

Figure 4-19. Cytotoxic destruction of matched parental and CD44v6 expressing MPM cell lines co-cultured with c-Met re-targeted and control CAR T-cells: effector to target ratio of 4:1.

A panel of MPM tumour cell lines (2 x 10^4 cells) were seeded in triplicate and allowed to adhere overnight. Percentage viability of MPM cell lines is shown following (**A**) 24hr, (**B**) 48hr or (**C**) 72hr incubation with 8 x 10^4 cells of N28z$^+$, M28z$^+$, cM28z$^+$, T28z$^+$, V28z$^+$ or untransduced (UT) T-cells. Transduced cells were not corrected for transduction efficiency (shown in Figure 4-12B). Tumour cell viability was measured using an MTT assay at the indicated time points after removal of T-cells by gentle washing. Data presented as mean ± SEM from three independent experiments. Significance was determined using the unpaired Student's *t*-test, comparing T-cell populations between matched cell lines (comparing N28z on REN v REN_CD44v6) * $p<0.05$, ** $p<0.005$ and *** $p<0.0005$.

4.2.8 Expansion of T-cells using the IL-4/ 4αβ chimeric cytokine receptor system

The 4αβ chimeric cytokine receptor couples the ectodomain of the IL-4Rα to the endodomain of the IL-2/IL-15-Rβ (Figure 4-20A) [311]. By co-expressing 4αβ with a particular CAR of interest, the selective expansion and enrichment of re-directed CAR^+ T-cells can be enhanced via exogenous IL-4 stimulation. Co-expression of both receptors was achieved through the use of an intervening *Thosea asigna* virus 2A (T2A) peptide downstream of a furin cleavage site (Figure 4-20B) [311].

The observation of increased c-Met re-targeted CAR^+ transduction efficiencies positively correlating with tumour cell cytolysis led me to co-express the 4αβ chimeric cytokine receptor with N28z, M28z and cM28z resulting in SFG N4, M4 and cM4 respectively (Figure 4-20C-D). By this means, I hoped to develop a reliable system to generate highly transduced cell products for further experiments.

4.2.9 Interferon-γ release by N4, M4 and cM4 T-cells following co-culture with MPM cell lines

To investigate whether expression of the $N4^+$, $M4^+$ and $cM4^+$ CARs enabled re-targeting of T-cell specificity against mesothelioma, engineered T-cells were co-cultured with four MPM tumour cell lines. Following expansion using IL-4 for 9 days, activation of $4\alpha\beta^+$ c-Met re-targeted CAR^+ T-cells was compared to that of T-cells expressing control CAR or untransduced (UT) T-cells. T-cells expressing V28z (containing an inactive targeting moiety derived from a scrambled peptide sequence) were used as a negative control. During the co-culture period, T-cell activation was monitored by measurement of the release of IFN-γ. Two effector-to-target ratios were assessed, namely 1:1 and 2:1 (T-cells: tumour cells).

In three independent experiments, $N4^+$, $M4^+$ and $cM4^+$ T-cells released a significantly greater concentration of IFN-γ during co-culture with all four of the MPM tumour cells when compared to UT T-cells (Figure 4-21). Reliably across independent donors, the concentrations of IFN-γ released by the c-Met re-targeted CAR^+ T-cells were considerably lower than that achieved by c-Met re-targeted CAR^+ T-cells previously cultured with REN (Figure 4-14) and JU77 cells (Figure 4-15). However, this disparity was not observed during co-culture with LO68 MPM cells (Figure 4-16). This result does however highlight the effect of the relatively poor transduction efficiencies observed in Figure 4-20D, following 9-days of IL-4 enriched culture.

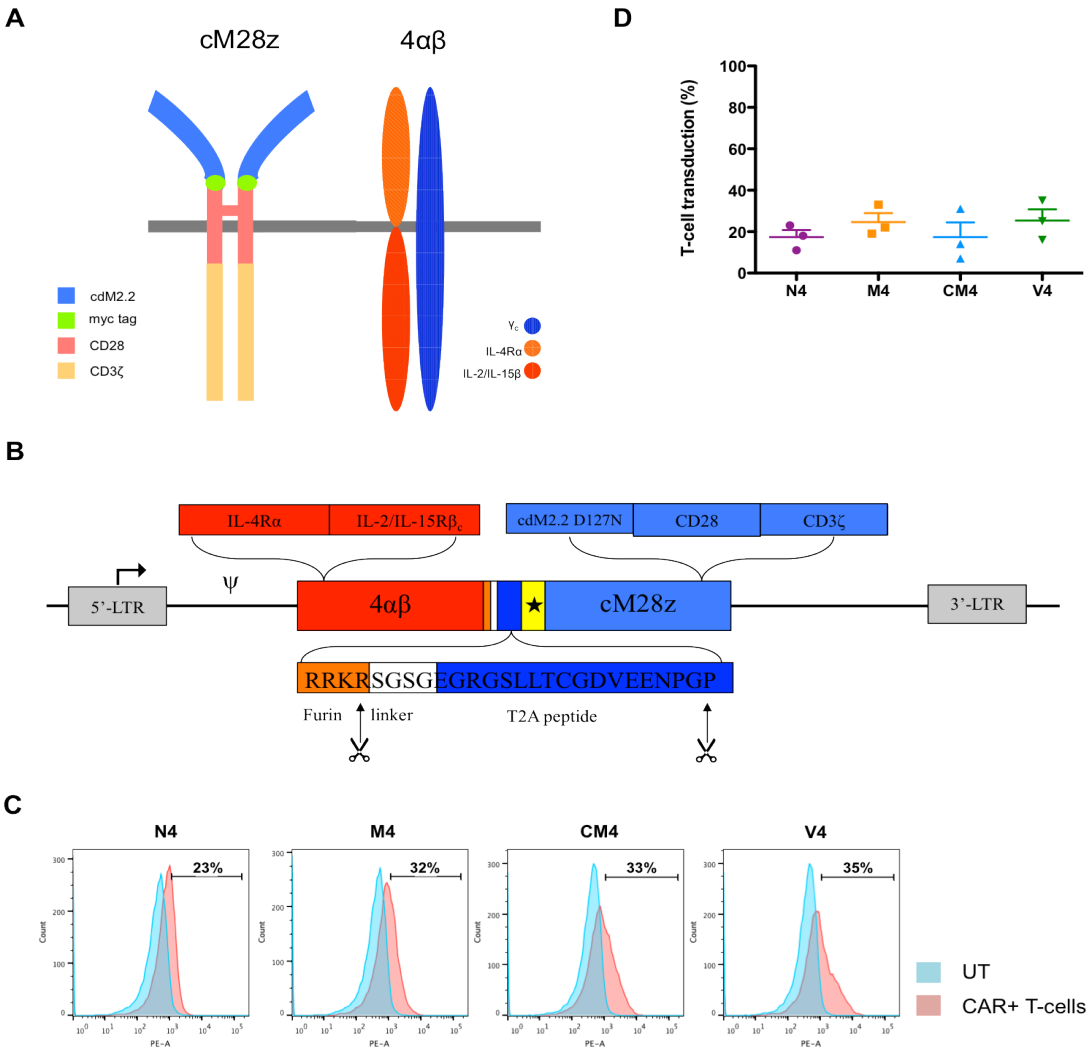

Figure 4-20. Co-expression of 4αβ chimeric cytokine receptor with Met-targeted CARs

(**A**) The combined expression of the c-Met$^+$ (e.g. cM28z) CAR and the 4αβ chimeric cytokine receptor is referred to cM4 (representative example shown), N4 (N28z), M4 (M28z) or V4 (V28z) respectively. In 4αβ, the IL-4Rα ectodomain has been coupled to the IL-2/15Rβ endodomain. Upon binding with IL-4, the receptor dimerises with the common γ-chain (γc) (shown in dark blue). (**B**) Within the N4, M4, CM4 (shown) and V4 combinations, the coding sequences are separated by the T2A peptide derived from the *Thosea asigna* plant virus, which induces a ribosomal 'skip' and therefore misses a peptide bond between the glycine and proline (as indicated by the right pair of scissors). Expression of the T2A peptide sequence at the C-terminus of the mature 4αβ protein is prevented by the presence of a furin cleavage site (as indicated by the left pair of scissors). The furin cleavage site is linked to the T2A peptide by a serine-glycine linker. LTR: long terminal repeats; Ψ: packaging signal; ⋆: HGF leader sequence. *Note: size of the blocks is not representative of the sizes of individual elements.* (**C**) Representative FACS plots detecting CAR expression on the cell surface of T-cells after 9 days of IL-4 culture. UT (blue) and respective CAR$^+$ T-cells (pink). (**D**) The average transduction efficiency of 4αβ$^+$ c-Met$^+$ T-cells (N4, M4 and CM4) alongside control T-cell population V4 – results averaged across three individual donors.

4.2.10 *In vitro* cytolytic activity of N4, M4 and cM4 T-cells against MPM cell lines

To test anti-tumour activity of 4αβ c-Met re-targeted CAR$^+$ re-targeted T-cells, their ability to destroy MPM tumour cell lines was determined. As detailed in Chapter 4, T-cell/ tumour cell co-cultivation experiments were performed and viable tumour cells were quantified thereafter using an MTT assay. Following confirmation of 4αβ and CAR expression (Figure 4-20), N4$^+$, M4$^+$, cM4$^+$, V4$^+$ and UT T-cells were co-cultured for 48 hours with an established panel of c-Met expressing MPM tumour cell lines at an effector to target ratio of 1:1 or 2:1. Supernatants were harvested and were analysed for IFN-γ content (Figure 4-21). Cytotoxicity was quantified by MTT assay (Figure 4-22).

In three independent experiments, co-culture of H28, REN and LO68 tumour cells with N4$^+$, M4$^+$ and cM4$^+$ T-cells all resulted in significantly increased release of IFN-γ (Figure 4-21) and tumour cell killing (Figure 4-22), when compared to all control (UT or V4$^+$ T-cells) cultures. As expected, this was further increased when the number of effector T-cells was increased (2:1). Once again, H28 tumour cells proved most susceptible to c-Met re-targeted CAR T-cell mediated killing. However, significant anti-tumour activity was also observed on both REN and LO68 cells. Co-cultures with the latter MPM cell line resulted in similar levels of cytolytic activity, with M4$^+$ and cM4$^+$ cells (E-T 2:1 in particular). By contrast, there was little tumour cell killing observed when c-Met re-targeted CAR$^+$ T-cells were co-cultured with JU77 tumour cells.

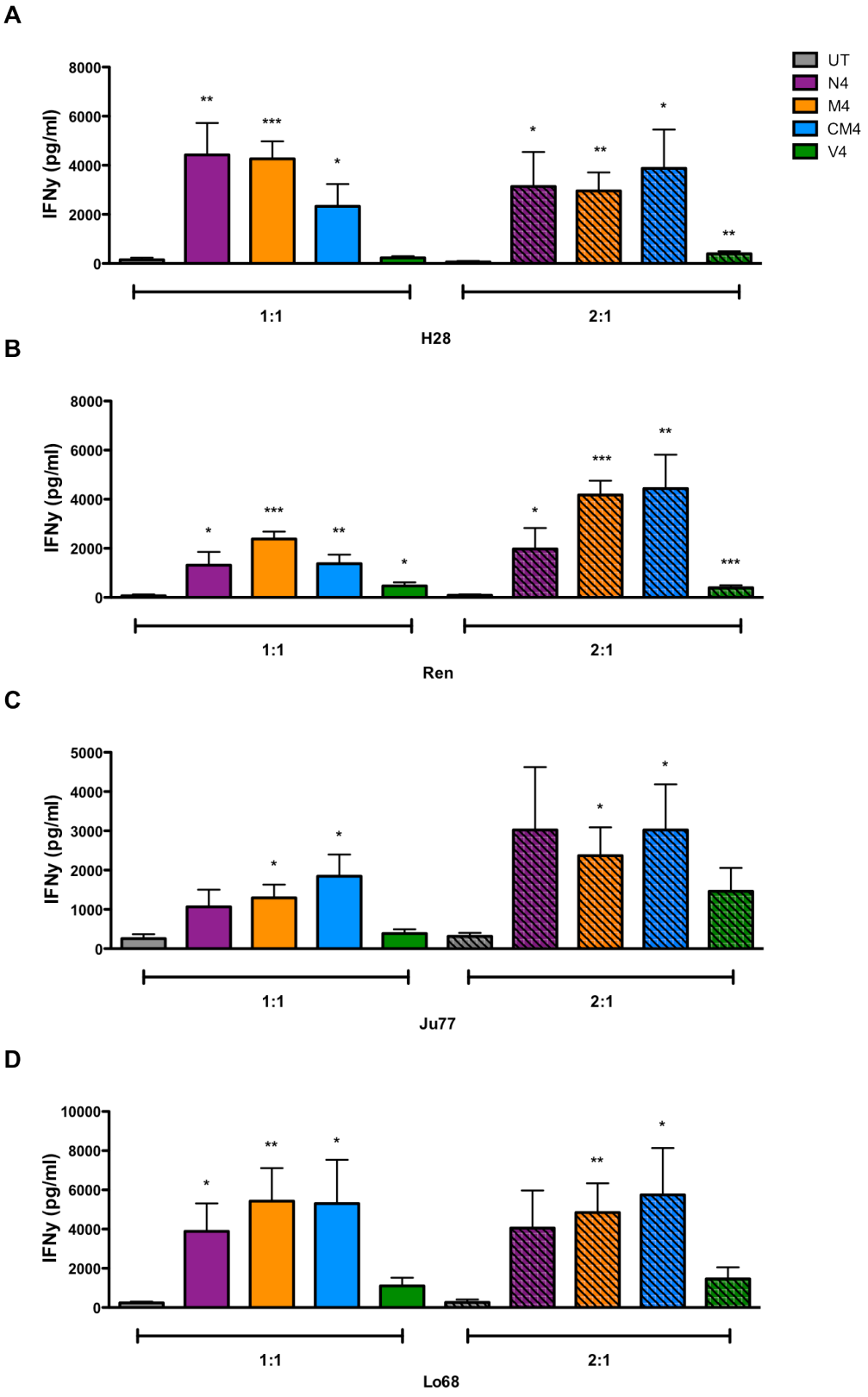

Figure 4-21. IFN-γ release during N4⁺, M4⁺ and CM4⁺ T-cell co-cultures with a panel of MPM cell lines

N4⁺, M4⁺, CM4⁺, V28z⁺ or untransduced (UT) T-cells were co-cultivated with panel of four MPM tumour cell lines. After 48 hours, supernatants from either effector to target ratio of (**A**) 1:1 or (**B**) 2:1 were removed and the concentration of IFN-γ measured using ELISA. The data presented was compiled from results achieved in three independent experiments and presented as mean ± SEM. Significance was determined using the unpaired Student's *t*-test, comparing UT T-cells with CAR⁺ T-cells: * p <0.05, ** p <0.005 and *** p <0.0005.

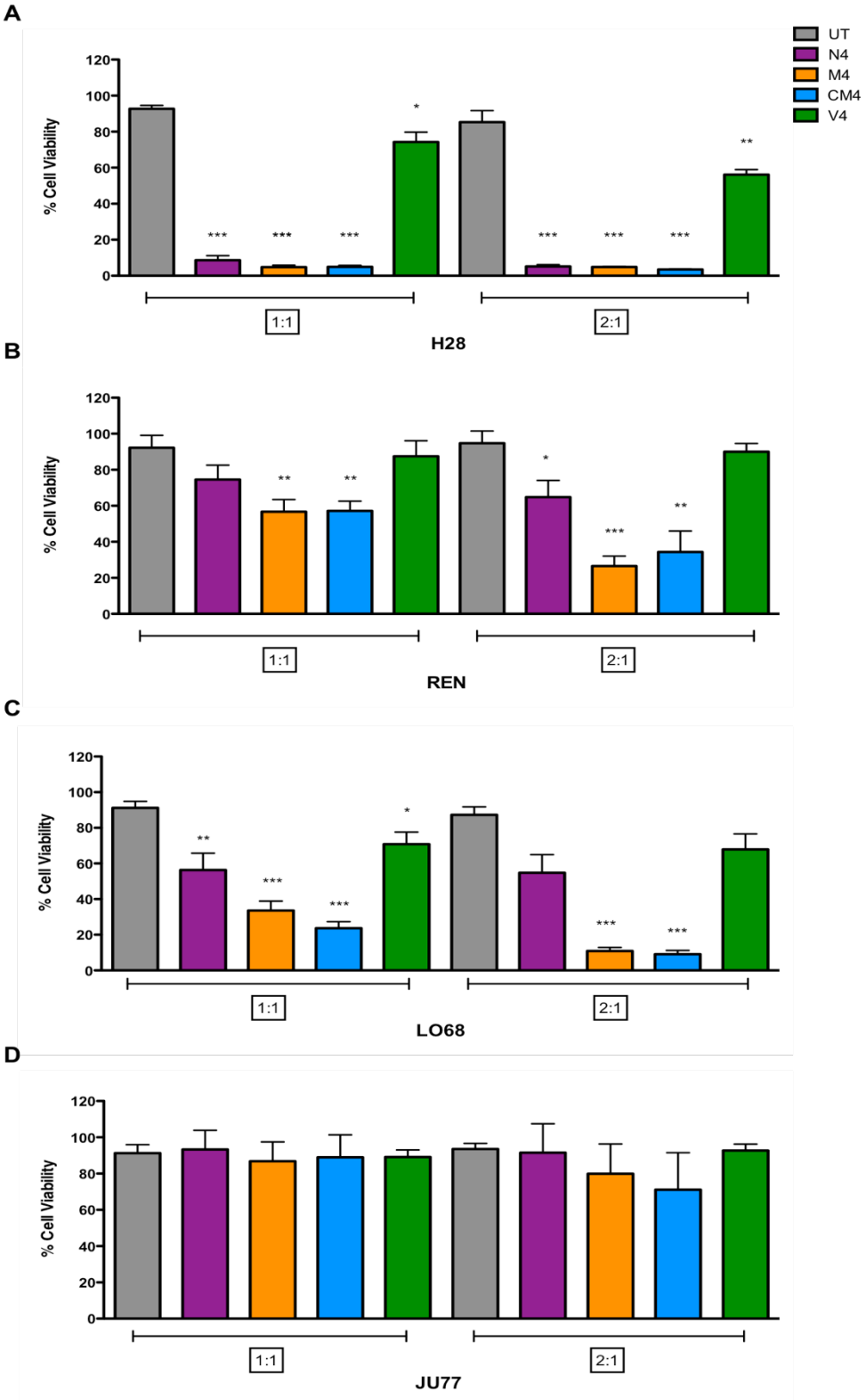

Figure 4-22. *in vitro* cytolytic activity of N4$^+$, M4$^+$ and CM4$^+$ T-cells against a panel of MPM tumour cell lines

MPM tumour cell lines (2 x 10^4 cells) were seeded in triplicate and allowed to adhere overnight. Percentage viability of (**A**) H28, (**B**) REN, (**C**) LO68 and (**D**) JU77 tumour cells is shown following 48hr incubation with either 2 x 10^4 or 4 x 10^4 cells of N4$^+$, M4$^+$, cM4$^+$, V4$^+$ or untransduced (UT) T-cells. Transduced cells were not corrected for transduction efficiency (shown in Figure 4-19D). Tumour cell viability was measured using an MTT assay (48hr). Data presented as mean ± SEM from three independent experiments. Significance was determined using the unpaired Student's *t*-test, comparing UT T-cells with CAR$^+$ T-cells: * p <0.05, ** p <0.005 and *** p <0.0005.

4.3 Discussion

The overall aim of the work undertaken in this chapter was to investigate the *in vitro* anti-tumour activity of a panel of three c-Met re-targeted CARs (named N28z, M28z and cM28z) engineered to target the c-Met receptor tyrosine kinase.

In Chapter 3, I showed that all three candidate CARs could re-target human T-cells against c-Met expressing NIH 3T3-based aAPCs. Consequently, I next investigated their anti-tumour activity using a panel of MPM tumour cell lines. I selected four commonly studied cell lines representative of epithelioid and sarcomatoid subtypes of MPM (LO68, H28, JU77 and REN) and found that all expressed c-Met at varying levels. Accordingly, I hypothesised that these MPM tumour cells would promote the activation of $N28z^+$, $M28z^+$ and $cM28z^+$ T-cells, facilitating a direct comparison of their *in vitro* anti-tumour activity.

Functionality of the CARs was investigated by measurement of IFN-γ and IL-2 production and tumour cell cytotoxicity. These experiments demonstrated that significantly greater quantities of IFN-γ were released by c-Met re-targeted CAR^+ T-cells in comparison to control T-cells, when stimulated by MPM tumour monolayers. A substantial increase in IL-2 production by c-Met re-targeted CAR^+ T-cells was also observed (significant for H28 and REN). However, in the initial experiments I undertook, significant tumour cell killing was only apparent when c-Met-targeted CAR T-cells were cultured with H28 tumour cells. This observation was made in multiple independent experiments analysing tumour cell viability by MTT. By contrast, no significant killing of REN, JU77 or LO68 MPM cells was observed. This was an unexpected result given the significant levels of c-Met expression seen on these tumour cells. Since $T28z^+$ T-cells caused destruction of these tumour cells despite poorer transduction efficiency, this shows that tumour cells are not inherently resistant to the cytotoxic machinery deployed by CAR T-cells. It should be noted however that both CARs are directed against two different targets - therefore any direct comparison of their functionality is subject to this limitation.

Initially, I hypothesised that the activation of $N28z^+$, $M28z^+$ and $cM28z^+$ T-cells requires c-Met expression to be above a certain threshold. In keeping with this, H28 cells expressed the highest level of cell surface c-Met among the panel of 4 MPM cell lines used and were efficiently killed using these CAR T-cells. Such a threshold effect might have been advantageous for clinical translation of $c\text{-}Met^+$ CAR T-cells since it could be speculated that low levels of c-Met expressed by healthy tissue (e.g. liver) would be

insufficient to promote activation, thus reducing potential for "on-target, off-tumour" toxicity. However, subsequent studies conducted using highly transduced T-cells revealed the ability of all three candidate c-Met-targeted CARs to mediate destruction of all four Met-expressing MPM tumour cell lines.

An alternative explanation for the lack of straightforward relationship between c-Met expression and activation of c-Met retargeted T-cells is the possibility that some mesothelioma cell lines produce HGF [150]. However, none of the MPM cell lines used in this study produced significant quantities of this cytokine, as detected by ELISA analysis. This argues that receptor blockade by natural ligand is not a significant hindering factor to the activity of the candidate c-Met re-targeted CARs under study here.

Data presented in Chapter 3 raised the possibility that co-expression of CD44v6 enhanced the activation of c-Met-targeted CAR T-cells, indicated by greater release of IFN-γ without enhancement of cytotoxicity against c-Met-engineered NIH 3T3 fibroblasts. CD44v6 is the best characterised co-factor that facilitates the binding of HGF to c-Met. Since all of my CARs retain key elements from HGF (derived from the N and K1 domains), I hypothesised the engagement between c-Met, CD44v6 and the CAR targeting moiety might promote enhanced target-dependent T-cell activation. However, a similar effect of CD44v6 was not observed in functional studies performed using MPM tumour cells that were engineered to over-express this co-factor. While tumour cells were not uniformly positive for CD44v6 following gene transfer, it would nonetheless have been expected that IFN-γ release would have been enhanced if CD44v6 promoted enhanced binding of these NK1-derived CARs to c-Met, leading to increased CAR T-cell activation. A possible explanation for the discrepant results obtained using both models relates to the fact that NIH 3T3 cells are derived from immortalised mouse fibroblasts, whereas all MPM tumour cells are of human origin. Consequently, NIH 3T3 cells may not express one or more molecules that are found on human tumour cells and which can substitute for the co-factor function of CD44v6. Examples include Syndecan-1 and ICAM-1, both of which were expressed by MPM tumour cells and which in some models can replace CD44v6 as a co-factor to promote the binding of HGF to c-Met [207]. Further investigation of this finding is clearly warranted.

In light of the variable efficiency of gene transfer encountered in this study, I also explored the use of the 4αβ/ IL-4 system to expand CAR T-cells. However, I did not achieve reproducible enrichment of CAR T-cells using this system for reasons that remain unclear. CAR T-cells expanded using this system demonstrated similar functionality to those expanded using IL-2, although the level of IFN-γ recorded was

notably lower than previously achieved with well-transduced c-Met re-targeted CAR T-cells.

The experiments described in this chapter permitted an initial comparison of the functionality of the three candidate c-Met-targeted CAR molecules developed in this project. However, no convincing or reproducible difference in cytotoxicity or cytokine release mediated by these CAR molecules was observed. These findings are in agreement with the data presented in Chapter 3 although it is acknowledged that *in vivo* comparison of functionality is still necessary before one can conclude that these molecules are equipotent.

In summary, the data presented in this chapter show that N28z$^+$, M28z$^+$ and cM28z$^+$ T-cells are effectively re-targeted against a panel of c-Met-expressing MPM tumour cell lines, providing that high transduction efficiency is achieved. Confirmation of successful targeting was achieved using a variety of experimental readouts, including target cell destruction and T-cell cytokine secretion. In light of the requirement for highly efficient gene transfer in order to elicit reproducible anti-tumour activity, I next elected to explore approaches in which c-Met re-targeted CAR T-cells are combined with alternative therapeutic approaches in use in MPM, such as chemotherapy and immune checkpoint blockade. These experiments are described in Chapter 5.

CHAPTER 5 Investigation of the use of chemotherapy or immune checkpoint blockade to potentiate immunotherapy of mesothelioma using c-Met-targeted chimeric antigen receptor-engineered T-cells

5.1 Introduction

Data presented in Chapter 4 demonstrate that all three candidate c-Met-targeted CARs exert anti-tumour activity against the H28 MPM cells. Anti-tumour activity was also demonstrated against the REN, LO68 and JU77 cell lines, albeit dependent upon high efficiency CAR T-cell gene transfer. In light of these findings, I next explored whether the therapeutic potency of this approach could be potentiated using two other therapeutic modalities that are commonly used to treat mesothelioma, namely combination chemotherapy and immune checkpoint blockade.

5.1.1 Use of chemotherapy in combination with CAR$^+$ T-cell immunotherapy

Combination chemotherapy regimens used to treat mesothelioma are described in detail in section 1.1.7. A commonly used regimen in current use employs a combination of cisplatin and pemetrexed [81]. It has previously been shown that chemotherapy can sensitise tumour cells to destruction by CAR T-cells, even when tumour cells are intrinsically chemotherapy resistant [350]. Here, I set out to see if cisplatin and/or pemetrexed could similarly be used to sensitise tumour cells to destruction by c-Met re-targeted CAR$^+$ T-cells.

5.1.2 Combined use of immune checkpoint blockade with CAR T-cell immunotherapy

A summary of the use of checkpoint blockade within MPM are described in detail within section 1.1.7. Both CAR T-cell therapy and checkpoint blockade have had striking success to date, however both treatment modalities are in their infancy, and requiring further investigation into untapped potential. Moreover, approaches to further optimise outcome are ongoing. One method stems from the strong rationale for the combination of checkpoint inhibition with CAR T-cell therapy – systemic immunotherapy in

combination with local, targeted immunotherapy. For maximal anti-tumour effect, adoptive T-cells require a permissive environment – checkpoint blocking antibodies remove T-cell inhibition; however, studies to date suggest their effectiveness is dependent upon functional tumour-specific T-cells. Thus, providing re-directed tumour-specific CAR T-cells in conjunction with checkpoint inhibitors has the potential for enhanced anti-tumour efficacy.

This combinatorial approach, using CAR T-cells and checkpoint inhibition (PD-1 blocking antibody), was first investigated by John *et al.* [351]. A transgenic Her-2 mouse model was used, treated with Her-2 CAR T-cells, PD-1 mAb or a combination of both agents. The authors demonstrated Her-2 CAR^+ (CD28) T-cell engagement with PD-$L1^+$ Her-2^+ tumour cells triggered PD-1 upregulation on CAR T-cells. Additionally, PD-1 blockade enhanced proliferation and anti-tumour function of Her-2 CAR T-cells – an enhanced regression of established Her-2 breast carcinoma-transplanted tumours was observed compared to control arms receiving Her-2 CAR^+ T-cells alone [351]. PD-1 blockade significantly enhanced intracellular expression of Ki-67, in addition to IFN-γ and granzyme B in CAR^+ T-cells. Notably, utilising the aforementioned Her-2 transgenic mouse model, the authors demonstrated the safety of this combinatorial approach, citing no pathology to Her-2^+ brain or mammary tissues [351].

An alternative novel approach to merging CAR T-cell therapy with checkpoint blockade is being explored preclinically, in which CAIX-targeted CAR T-cells have been engineered to secrete PD-L1 antibodies within the tumour milieu. Utilising a humanised murine model of clear cell renal cell carcinoma (ccRCC), the authors demonstrated significant delay in tumour growth and tumour weight decrease of 50-80% when compared with anti-CAIX CAR T-cells alone [352]. Similarly, expression of PD-L1 and Ki-67 within the tumours decreased and elevated granzyme B was observed CAR^+ T-cells.

Consequently, I set out to investigate whether the therapeutic potency of this approach could be potentiated for MPM using c-Met re-targeted CAR^+ T-cells in combination with a PD-1 blocking antibody.

5.1.3 Aims

1) To investigate whether standard of care chemotherapy can sensitise MPM tumour cells to c-Met re-targeted CAR^+ T-cell immunotherapy *in vitro*.
2) To evaluate and compare *in vitro* anti-tumour activity of c-Met re-targeted CAR T-cells in the presence or absence of the PD-1 inhibitor, pembrolizumab, using a panel of mesothelioma cell lines.

5.2 Results

5.2.1 Establishing the maximal dose of cisplatin / pemetrexed that elicits limited direct cytotoxic effect against MPM cell lines

The ultimate goal of these experiments was to investigate if chemotherapy could be used to sensitise MPM tumour cells to destruction by c-Met re-targeted CAR T-cells. Consequently, it was important to select doses of these drugs that had a modest cytotoxic effect against the tumour (set at ≤20%), thereby allowing me to evaluate whether tumour cell destruction could be potentiated by subsequent exposure to CAR T-cells. Cisplatin and/ or pemetrexed were added to MPM cells for 24 hours before being washed off. Viability of tumour cells was monitored over the ensuing 48 hours (experimental plan summarised in Figure 5-1). Dose-response curves for cisplatin alone (Figure 5-2), pemetrexed (Figure 5-3) or cisplatin plus pemetrexed (Figure 5-4) were performed, using the MTT assay to determine the cytotoxic effects of each dose level on MPM cells. Dose ranges assessed were in accordance with previous experience with previously published data and were as follows: cisplatin 0-200μM ± pemetrexed 0-500μM.

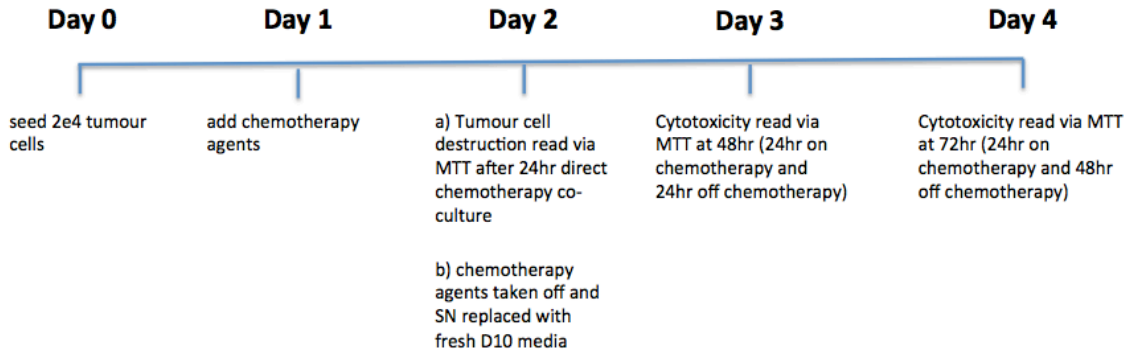

Figure 5-1. MPM tumour seeding and treatment protocol timeline for chemotherapy dose response studies – cisplatin and pemetrexed.
2 x 10^4 Tumour cells were seeded in three 96-well plates per cell line (Day 0) and were incubated overnight. Chemotherapy agents - cisplatin 0-200μM ± pemetrexed 0-500μM were added (Day 1) in decreasing 5-fold serial dilutions to enable dose response to be determined. After 24 hours, tumour cell viability was assessed using an MTT assay (Day 2). Medium from second and third plates for each respective cell line were replaced with fresh D10 (not containing chemotherapy agents). After 24 hours (Day 3) and 48 hours (Day 4), tumour cell viability was assessed using an MTT assay.

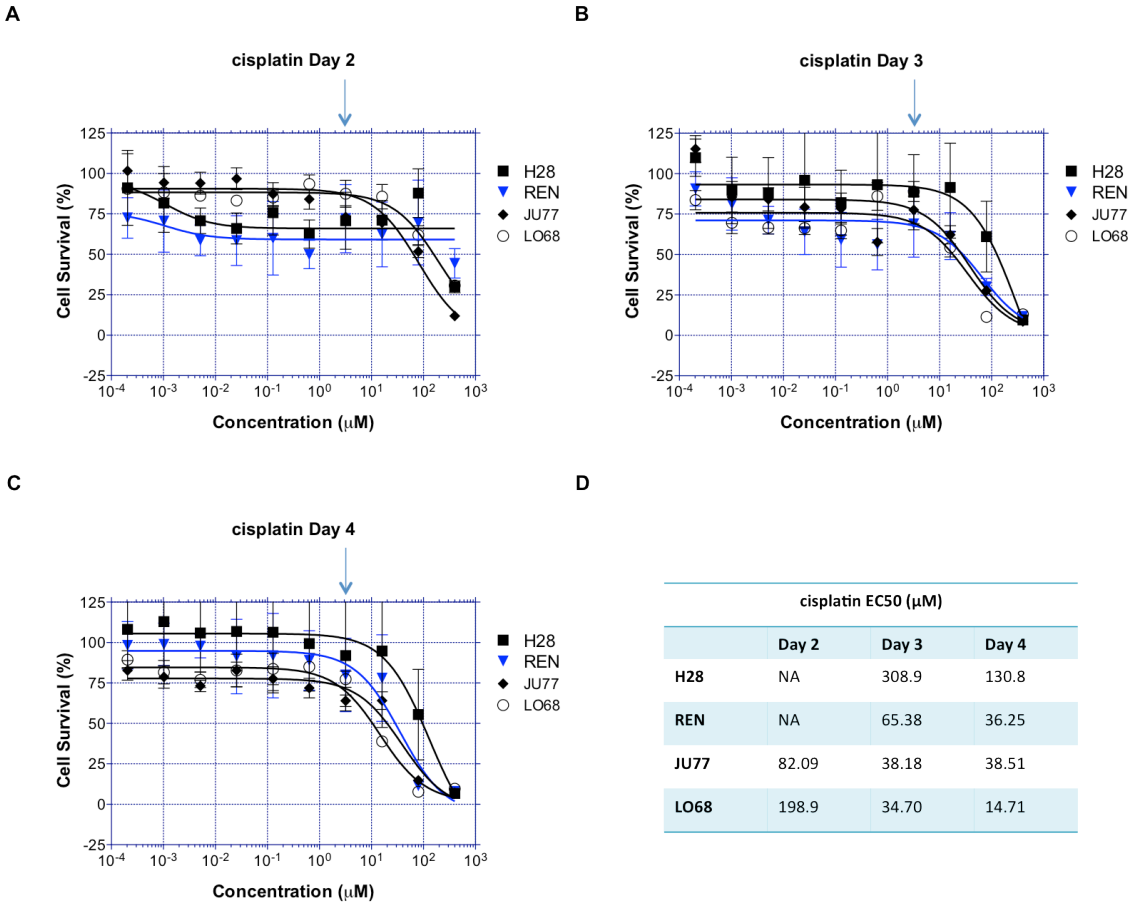

cisplatin EC50 (μM)

	Day 2	Day 3	Day 4
H28	NA	308.9	130.8
REN	NA	65.38	36.25
JU77	82.09	38.18	38.51
LO68	198.9	34.70	14.71

Figure 5-2. Dose response studies of cisplatin-mediated cytotoxicity of MPM tumour cell lines.

2 x 10^4 MPM tumour cells were seeded in 96-well plates incubated as detailed in Figure 5-1. Cells were cultured in the presence of cisplatin 0-200μM for 24 hours (**A**) "Day 2", followed by 24 hours (**B**) "Day 3" or 48 hours (**C**) "Day 4" after cisplatin removal. Cell viability was determined by MTT assay. (**D**) The EC50, calculated in μM is stated where applicable data presented are the mean ± SEM from two independent experiments. Calculations were evaluated using Graphpad Prism software. EC50, half maximal response – the concentration of drug required eliciting 50% cell death. The arrow depicts the 3.2μM concentration resulting in ≤20% cell death – note starting % viability of certain MPM cell lines are not 100%. NA, not applicable as EC50 concentration was not reached.

A

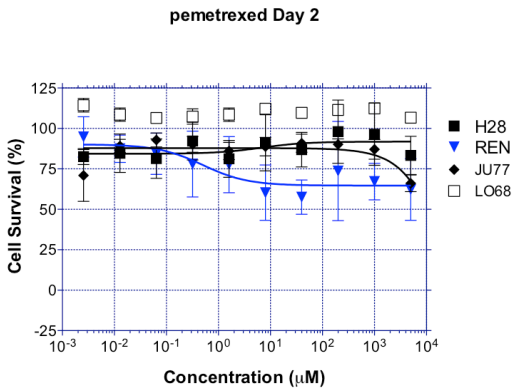

B

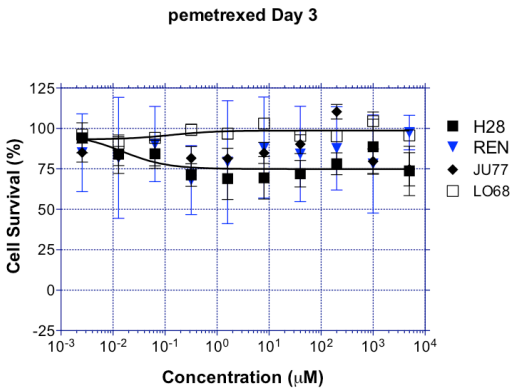

C

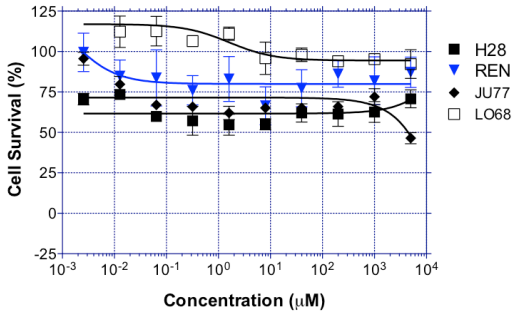

D

pemetrexed EC50 (μM)

	Day 2	Day 3	Day 4
H28	NA	NA	NA
REN	NA	NA	NA
JU77	NA	NA	NA
LO68	NA	NA	NA

Figure 5-3. Dose response studies of pemetrexed-mediated cytotoxicity of MPM tumour cell lines.

2 x 10^4 MPM tumour cells were seeded in 96-well plates incubated as detailed in Figure 5-1. Cells were cultured in the presence of pemetrexed 0-500μM for 24 hours (**A**) "Day 2", followed by 24 hours (**B**) "Day 3" or 48 hours (**C**) "Day 4" after cisplatin removal. Cell viability was determined by MTT assay. (**D**) The EC50, calculated in μM is stated where applicable data presented are the mean ± SEM from two independent experiments. Calculations were evaluated using Graphpad Prism software. EC50, half maximal response – the concentration of drug required eliciting 50% cell death. NA, not applicable as EC50 concentration was not reached.

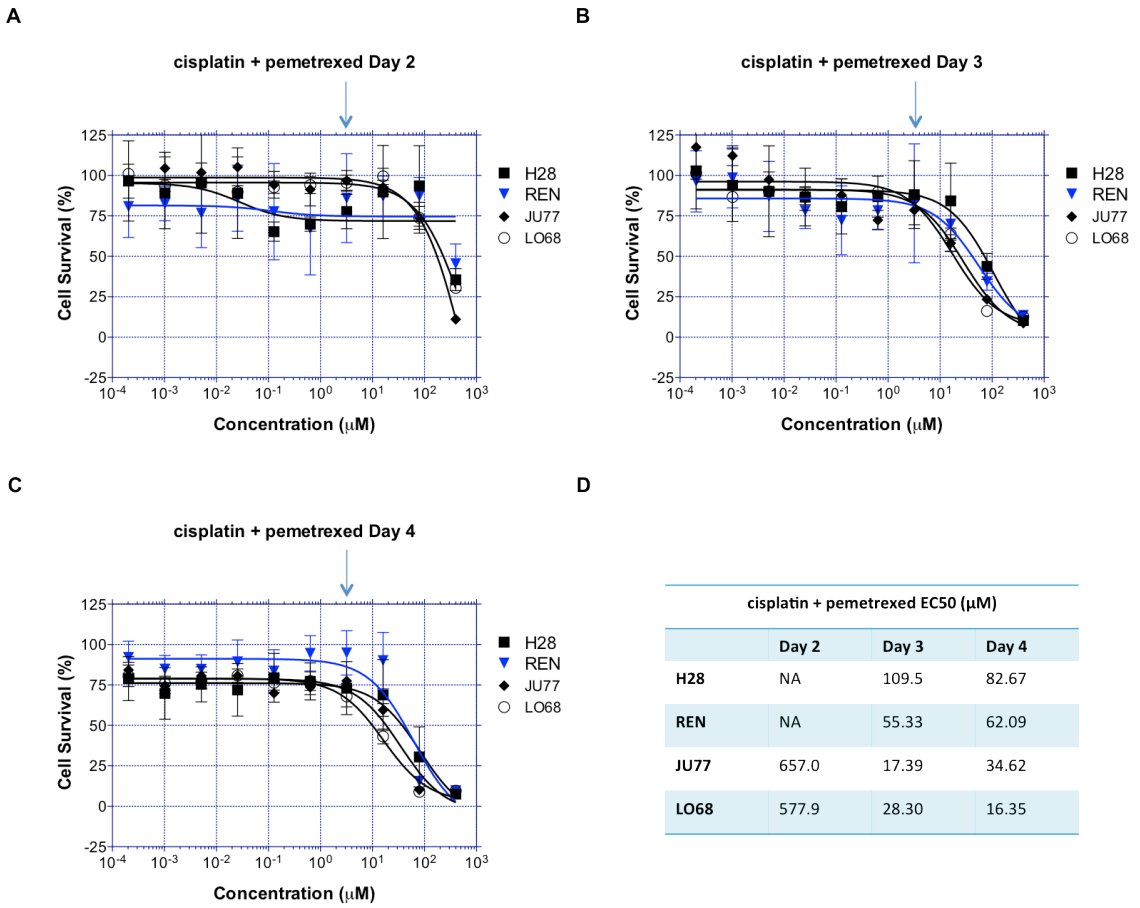

D

cisplatin + pemetrexed EC50 (μM)

	Day 2	Day 3	Day 4
H28	NA	109.5	82.67
REN	NA	55.33	62.09
JU77	657.0	17.39	34.62
LO68	577.9	28.30	16.35

Figure 5-4. Dose response studies of combined cisplatin + pemetrexed-mediated cytotoxicity of MPM tumour cell lines.
2 x 10^4 MPM tumour cells were seeded in 96-well plates incubated as detailed in Figure 5-1. Cells were cultured in the presence of both cisplatin 0-200μM + pemetrexed 0-500μM for 24 hours (**A**) "Day 2", followed by 24 hours (**B**) "Day 3" or 48 hours (**C**) "Day 4" after cisplatin removal. Cell viability was determined by MTT assay. (**D**) The EC50, calculated in μM is stated where applicable data presented are the mean ± SEM from two independent experiments. The arrow depicts the 3.2μM cisplatin concentration resulting in ≤20% cell death (as identified in Figure 5-2 – please note starting % viability of certain MPM cell lines are not 100%. Calculations were evaluated using Graphpad Prism software. EC50, half maximal response – the concentration of drug required eliciting 50% cell death. NA, not applicable as EC50 concentration was not reached.

Treatment of all four MPM cell lines with cisplatin alone or cisplatin ± pemetrexed resulted in complete dose-dependent killing from 24 hours onwards, with the exception of H28 and REN tumour cells in which complete dose-dependent killing was observed from 48 hours onwards. By contrast, pemetrexed alone did not elicit tumour cell death at doses of up to 500μM. The dose of cisplatin that resulted in ≤20% tumour cell death across all three time points evaluated was 3.2μM for all cell lines (as indicated by a blue arrow on Figure 5-2). It is important to note the starting tumour cell viability is not 100% for each cell line thus this threshold was calculated within each respective MPM cell line. Additionally, increased variability was observed thus to further validate this selection, I set up an independent experiment in which H28 (Figure 5-5), REN (Figure 5-6) and JU77 (Figure 5-7) cells were treated for 24 hours with cisplatin (3.2μM) in combination with either 300, 400 or 500μM pemetrexed. Although further variability was observed within this experiment, a combination of 3.2μM cisplatin with 500μM pemetrexed resulted in ≤20% cell death at 24 hours (with the exception of H28 cells). The concentration of either cisplatin ± pemetrexed required eliciting 50% cell death (EC50) has been noted in tables within Figure 5-2 to Figure 5-4.

The experimental scope of this particular study was to assess the sensitisation effect of chemotherapy on the more unresponsive MPM tumour cell lines for CAR T-cell mediated efficacy, thus this dose was chosen to continue assessment.

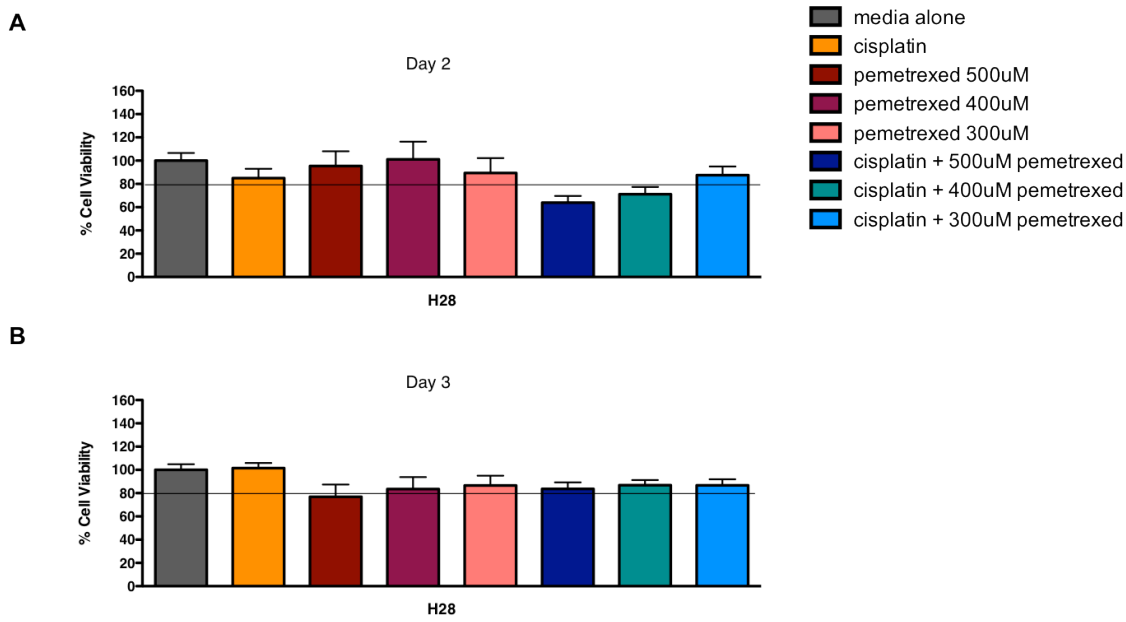

Figure 5-5. Validation of *in-vitro* sensitivity of H28 cell line to cisplatin + pemetrexed.
2 x 10^4 H28 tumour cells were seeded in 3x 96-well plates incubated as detailed in Figure 5-1. Cisplatin 3.2µM ± pemetrexed 300-500µM were added to the culture medium the following day. Three 96-well plates were set up as detailed in Figure 5-1. After 24 hours, cell viability was assessed via MTT assay (**A**-Day 2), followed by 24 hours (**B**-Day 3) with no cisplatin ± pemetrexed in the medium. Cell viability was determined by MTT assay. Data presented are the mean ± SEM from two independent experiments.

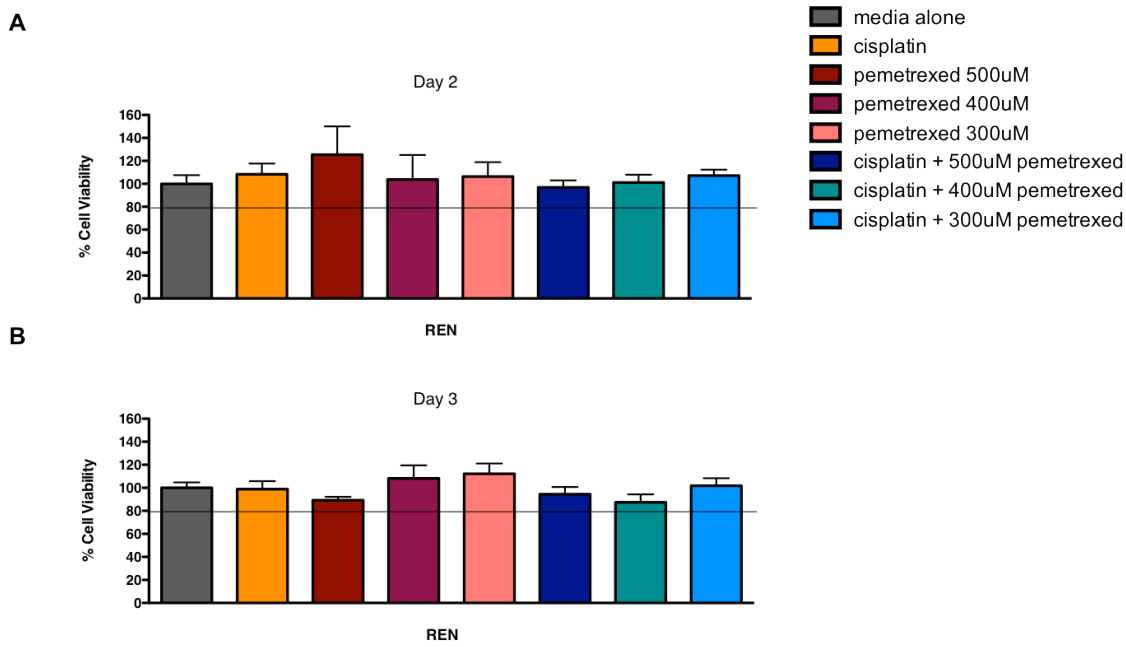

Figure 5-6. Validation of *in-vitro* sensitivity of REN cell line to cisplatin + pemetrexed.
2 x 10^4 REN tumour cells were seeded in 3x 96-well plates as detailed in Figure 5-1. Cisplatin 3.2µM ± pemetrexed 300-500µM were added to the culture medium the following day. After 24 hours, cell viability was assessed via MTT assay (**A**-Day 2), followed by 24 hours (**B**-Day 3) with no cisplatin + pemetrexed in the medium. Cell viability was determined by MTT assay. Data presented are the mean ± SEM from two independent experiments.

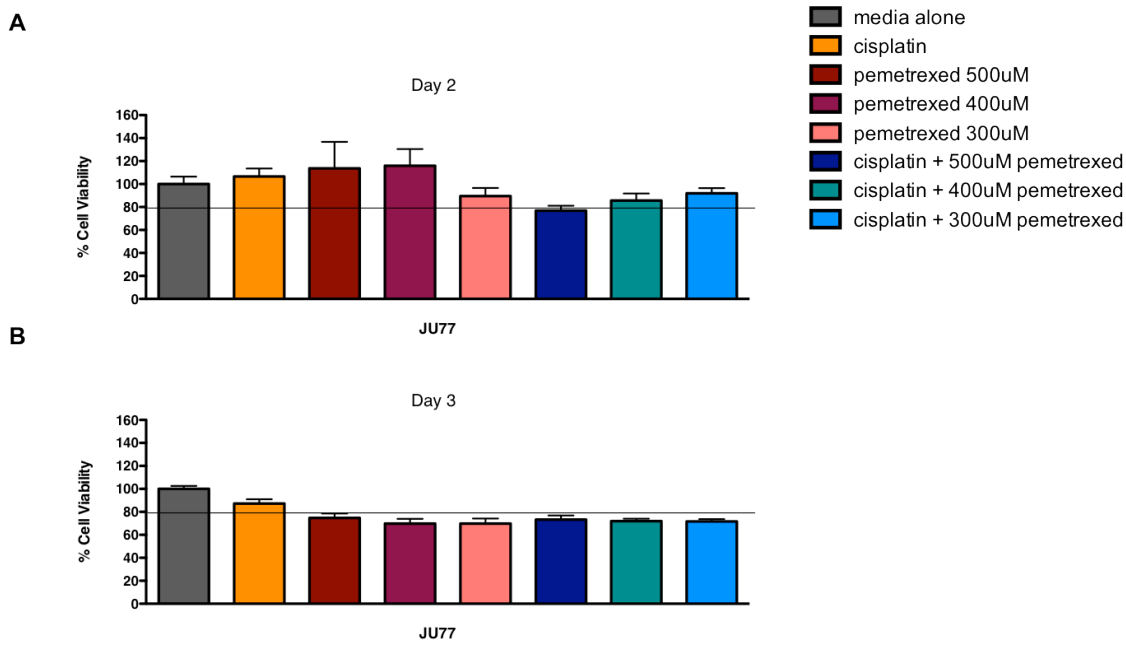

Figure 5-7. Validation of *in-vitro* sensitivity of JU77 cell line to cisplatin + pemetrexed.
2 x 10^4 JU77 tumour cells were seeded in 3x 96-well plates as detailed in Figure 5-1. Cisplatin 3.2µM ± pemetrexed 300-500µM were added to the culture medium the following day. After 24 hours, cell viability was assessed via MTT assay (**A**-Day 2), followed by 24 hours (**B**-Day 3) with no cisplatin + pemetrexed in the medium. Cell viability was determined by MTT assay. Data presented are the mean ± SEM from two independent experiments.

5.2.2 Interferon-γ release by N28z-, M28z- and cM28z-engineered T-cells when co-cultured with chemotherapy treated or untreated MPM cell lines

Next, I investigated whether 24 hours sensitisation of MPM tumour cells with cisplatin and pemetrexed enhances the release of IFN-γ by c-Met$^+$ CAR T-cells when co-cultivated with mesothelioma tumour cell lines. Experimental design in shown in Figure 5-8A and transduction efficiency of c-Met re-targeted and control CAR T-cells are shown in Figure 5-8B. In these experiments, T-cells expressing control V28z CAR or untransduced (UT) T-cells were used as negative controls. One effector-to-target ratio was assessed - 1:1 (T-cells: tumour cells).

In three independent experiments, c-Met$^+$ CAR T-cells did not release a significantly greater concentration of IFN-γ during co-culture with all four of the MPM tumour cells that had been pre-treated with cisplatin and pemetrexed (Figure 5-9). When comparing between T-cells with chemotherapy against chemotherapy alone (benchmark), a significantly greater concentration of IFN-γ during co-culture with all tumour cells was only observed with c-Met$^+$ CAR T-cells. As expected, chemotherapy did not elicit increased IFN-γ production by V28z$^+$ or UT T-cells (Figure 5-9). Despite variability in the concentrations of IFN-γ detected, the pattern of T-cell activation was reproducible across independent experiments, highlighting the consistency of this result.

A

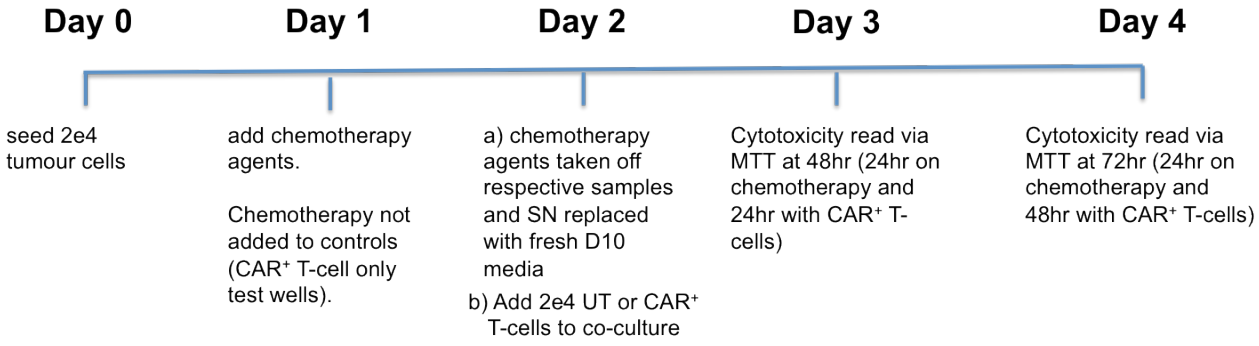

B

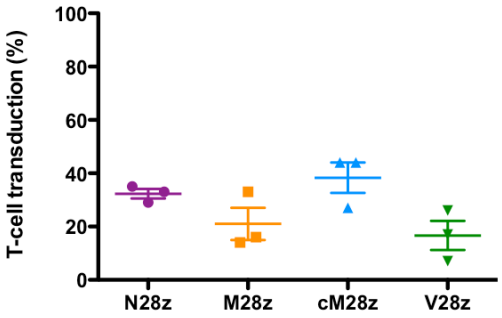

Figure 5-8. Investigation of the sensitising effect of chemotherapy exposure of MPM cells to subsequent addition of Met re-targeted CAR T-cells.
(**A**) Experimental design: 2 x 10^4 tumour cells were seeded in three 96-well plates per cell line (Day 0) and incubated overnight. Cisplatin (3.2μM) + pemetrexed (500μM) were added after 24 hours (Day 1). After a further 24 hours, medium containing chemotherapy agents was replaced with fresh D10 medium and 2 x 10^4 c-Met re-targeted or control ($V28z^+$ / UT) T-cells were added to co-cultures. After a further 24 or 48 hours, tumour cell viability was assessed using an MTT assay. Medium from 48-hour co-cultures was stored for subsequent cytokine analysis. (**B**) Transduction efficiency of c-Met re-targeted and control CAR T-cells (mean ± SEM, n=3).

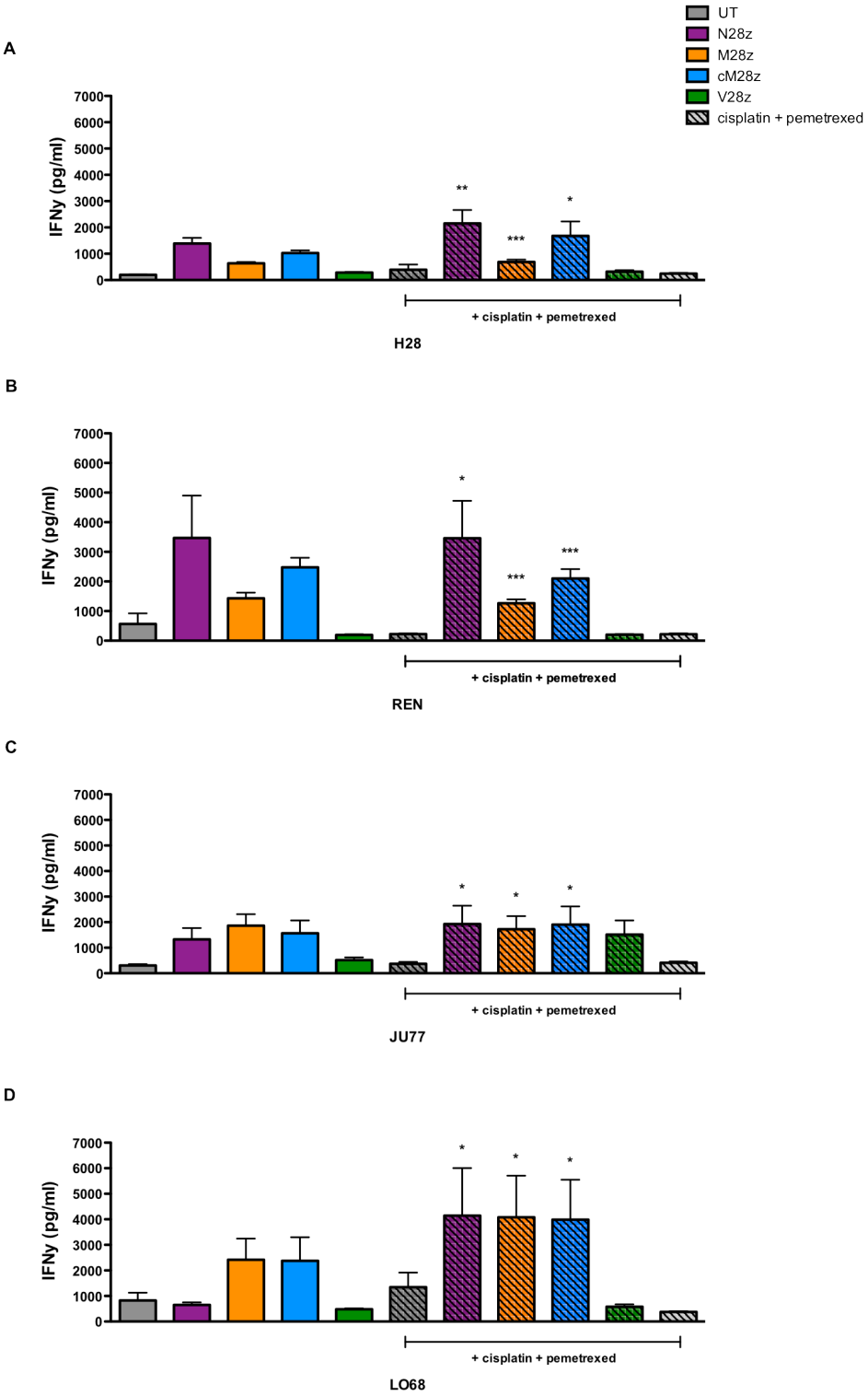

Figure 5-9. IFN-γ release by CAR T-cells when co-cultured with chemotherapy treated or untreated MPM cells.
N28z$^+$, M28z$^+$, cM28z$^+$, V28z$^+$ or untransduced (UT) T-cells were co-cultivated at a 1:1 ratio with panel of four MPM tumour cell lines that were untreated or had been pre-treated with cisplatin and pemetrexed as described in Figure 5-8A. After 48 hours, supernatants were removed from co-cultures with (**A**) H28, (**B**) REN, (**C**) JU77 or (**D**) LO68 tumour cells and the concentration of IFN-γ measured using ELISA (mean ± SEM; n=3 independent replicates). Symbols above individual bars represent significance determined using the unpaired Student's *t*-test, comparing chemotherapy alone with combined T-cell + chemotherapy. An unpaired Student's *t*-test has been performed comparing T-cells co-cultivated on MPM cells and MPM cells + chemotherapy, however no significant findings were observed: * p <0.05, ** p <0.005 and *** p <0.0005.

5.2.3 Cytotoxicity of N28z-, M28z- and cM28z-engineered T-cells when co-cultured with chemotherapy treated or untreated MPM cell lines

Next, I set out to test if cisplatin and/ or pemetrexed at the doses indicated above could sensitise MPM cell lines to enhanced destruction by c-Met re-targeted CAR$^+$ T-cells (experimental plan shown in Figure 5-8A). Following confirmation of CAR expression (Figure 5-8B), N28z$^+$, M28z$^+$, cM28z$^+$, V28z$^+$ and UT T-cells were co-cultured with H28, REN, LO68 or JU77 MPM tumour cells that had been pre-treated with chemotherapy, making comparison with untreated control tumour cells.

When c-Met re-targeted CAR$^+$ T-cells were cultured with H28 cells, tumour cell lysis was significantly increased when compared to UT or V28z$^+$ T-cells. After 24 hours, a slight increase in H28 cell death was observed in cM28z$^+$ T-cell cultures, comparing chemotherapy pre-treated and untreated cultures (Figure 5-10A). After 48 hours, no convincing difference was observed with tumour cells that had been pre-sensitised with chemotherapy drugs (Figure 5-10B). A statistical significance was observed with cM28z T-cells at 24-hours and N28z T-cells at 48-hours, although none of these differences were substantial in magnitude and thus are likely to be of questionable biological significance.

In the case of REN MPM cultures, c-Met re-targeted CAR$^+$ T-cells combined with chemotherapy resulted in a small but significant increase in tumour cell lysis after 24 hours when compared to c-Met re-targeted CAR$^+$ T-cells alone (Figure 5-11A). After 48 hours, this difference increased substantially in N28z$^+$, M28z$^+$ and cM28z$^+$ T-cells with a 50% average increase in tumour cell lysis with the combined therapy when compared to T-cells alone (Figure 5-11B). A similar pattern emerged in co-cultures of the JU77 cell line (Figure 5-12) and LO68 cell lines (Figure 5-13), which was maximal 48 hours after addition of CAR T-cells.

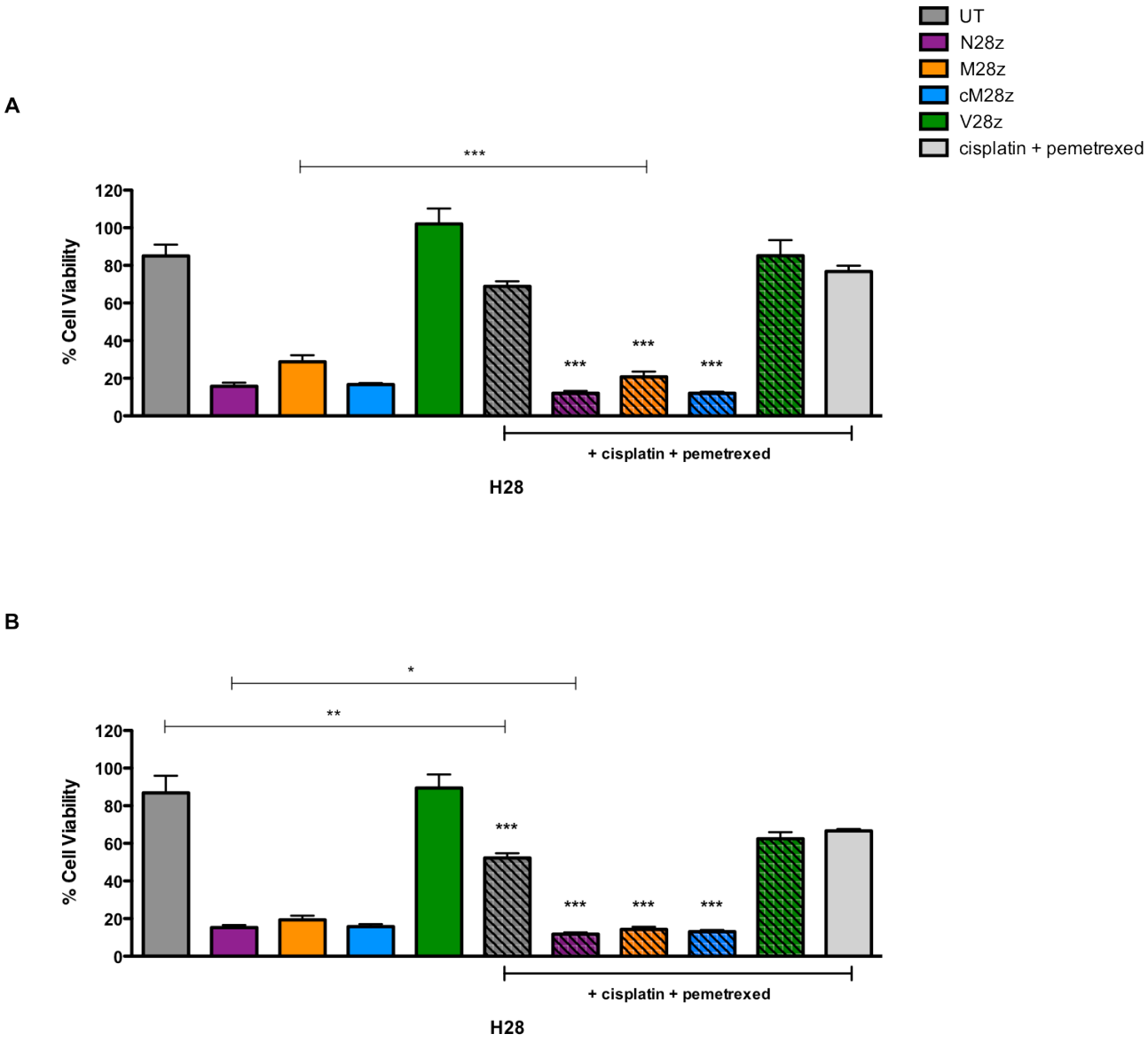

Figure 5-10. Cytotoxic effect of combining chemotherapy with CAR⁺ T-cells against MPM: H28 cell line.
H28 MPM cells were co-cultivated with an equal number (2 x 10^4 cells) of N28z⁺, M28z⁺, cM28z⁺, V28z⁺ or untransduced (UT) T-cells. Tumour cells had been pre-treated for the preceding 24 hours with cisplatin (3.2μM) and pemetrexed (500μM) or nil. Transduced cells were not corrected for transduction efficiency (shown in Figure 5-8B). Cell viability was measured using an MTT assay after 24 hours (**A**) or 48 hours (**B**). Data has been presented as mean ± SEM from three independent experiments. Significance was determined using the unpaired Student's *t*-test, either comparing UT T-cells with CAR⁺ T-cells for each target cell line or CAR⁺ T-cell plus chemotherapy against chemotherapy only: * $p < 0.05$, ** $p < 0.005$ and *** $p < 0.0005$.

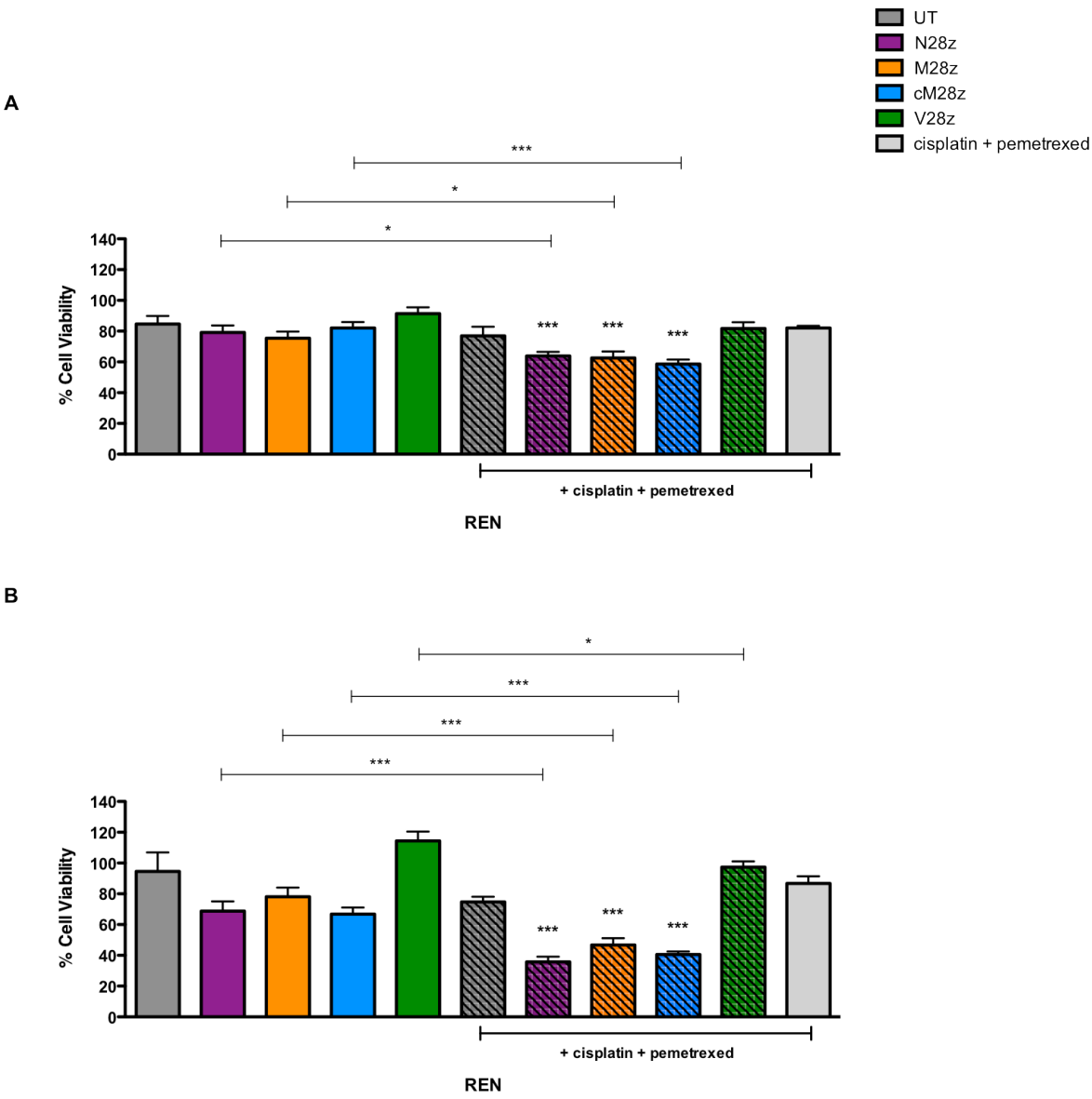

Figure 5-11. Cytotoxic effect of combining chemotherapy with CAR T-cells against MPM: REN cell line.

REN MPM cells were co-cultivated with an equal number (2 x 10^4 cells) of N28z$^+$, M28z$^+$, cM28z$^+$, V28z$^+$ or untransduced (UT) T-cells. Tumour cells had been pre-treated for the preceding 24 hours with cisplatin (3.2μM) and pemetrexed (500μM) or nil. Transduced cells were not corrected for transduction efficiency (shown in Figure 5-8B). Cell viability was measured using an MTT assay after 24 hours (**A**) or 48 hours (**B**). Data has been presented as mean ± SEM from three independent experiments. Significance was determined using the unpaired Student's *t*-test, either comparing UT T-cells with CAR$^+$ T-cells for each target cell line or CAR$^+$ T-cell plus chemotherapy against chemotherapy only: * p <0.05, ** p <0.005 and *** p <0.0005.

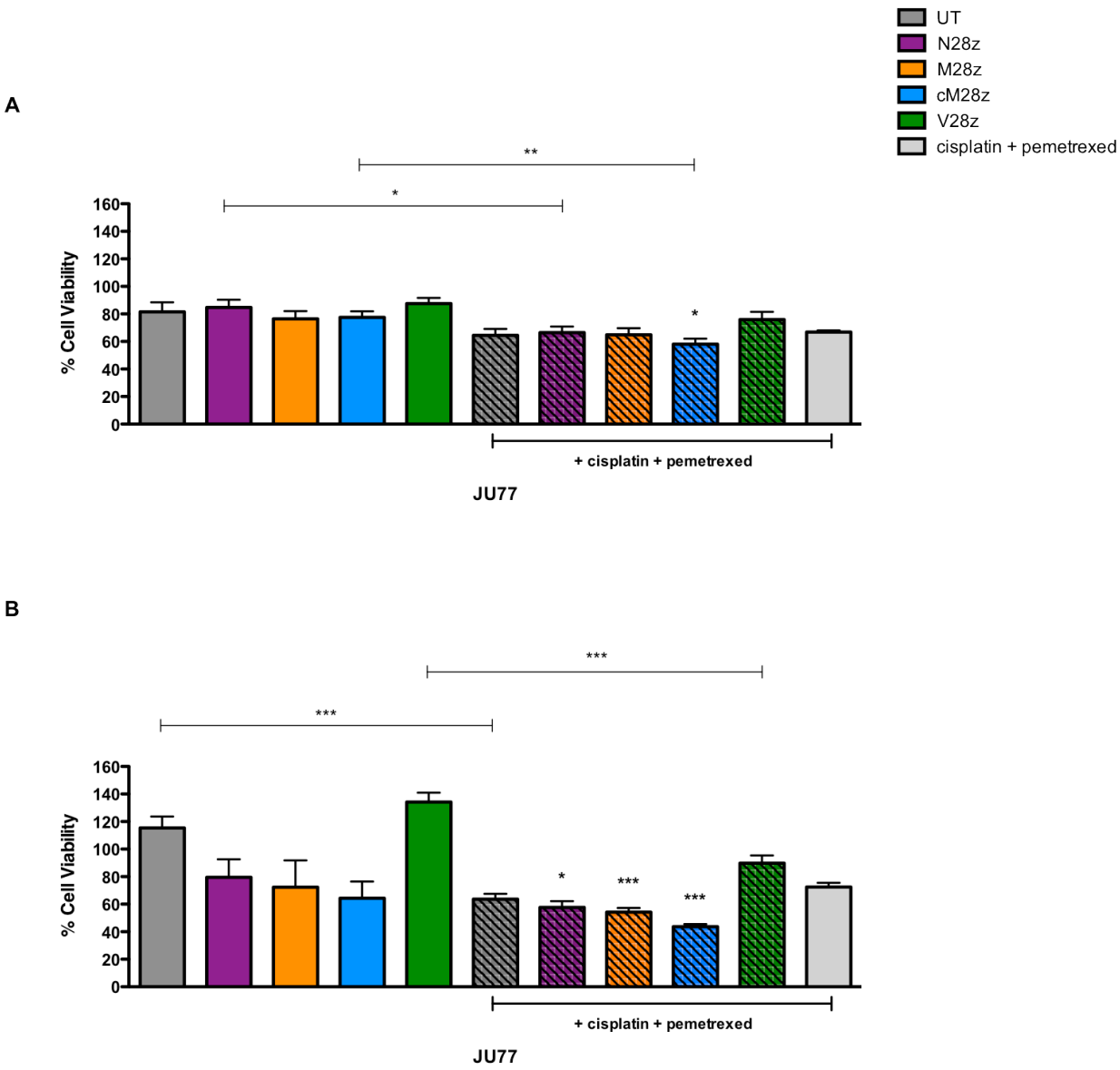

Figure 5-12. Cytotoxic effect of combining chemotherapy with CAR T-cells against MPM: JU77 cell line.
JU77 MPM cells were co-cultivated with an equal number (2 x 10^4 cells) of N28z$^+$, M28z$^+$, cM28z$^+$, V28z$^+$ or untransduced (UT) T-cells. Tumour cells had been pre-treated for the preceding 24 hours with cisplatin (3.2µM) and pemetrexed (500µM) or nil. Transduced cells were not corrected for transduction efficiency (shown in Figure 5-8B). Cell viability was measured using an MTT assay after 24 hours (**A**) or 48 hours (**B**). Data has been presented as mean ± SEM from three independent experiments. Significance was determined using the unpaired Student's *t*-test, either comparing UT T-cells with CAR$^+$ T-cells for each target cell line or CAR$^+$ T-cell plus chemotherapy against chemotherapy only: * p <0.05, ** p <0.005 and *** p <0.0005.

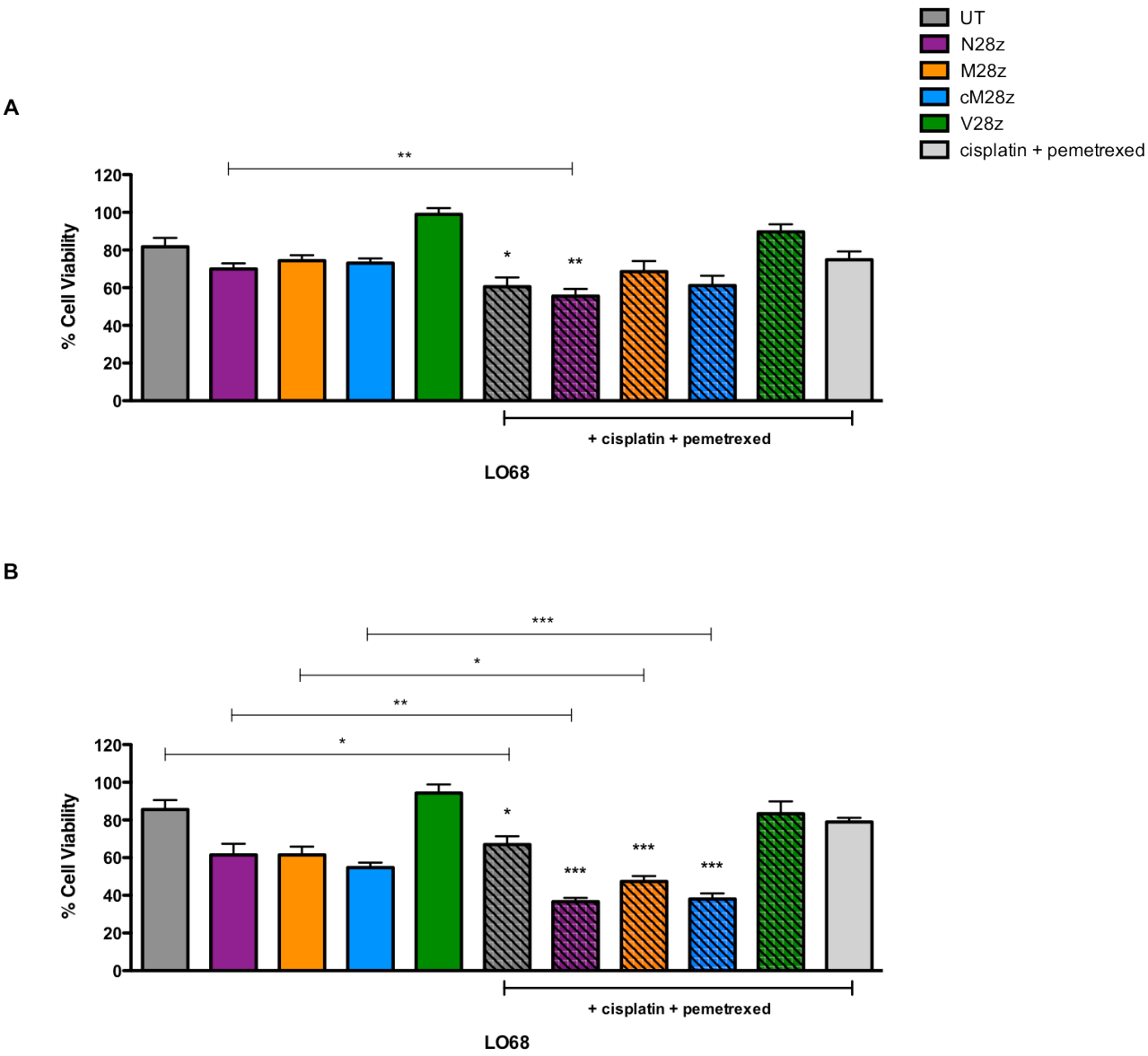

Figure 5-13. Cytotoxic effect of combining chemotherapy with CAR T-cells against MPM: LO68 cell line.

LO68 MPM cells were co-cultivated with an equal number (2 x 10^4 cells) of N28z$^+$, M28z$^+$, cM28z$^+$, V28z$^+$ or untransduced (UT) T-cells. Tumour cells had been pre-treated for the preceding 24 hours with cisplatin (3.2μM) and pemetrexed (500μM) or nil. Transduced cells were not corrected for transduction efficiency (shown in Figure 5-8B). Cell viability was measured using an MTT assay after 24 hours (**A**) or 48 hours (**B**). Data has been presented as mean ± SEM from three independent experiments. Significance was determined using the unpaired Student's *t*-test, either comparing UT T-cells with CAR$^+$ T-cells for each target cell line or CAR$^+$ T-cell plus chemotherapy against chemotherapy only: * p <0.05, ** p <0.005 and *** p <0.0005.

5.2.4 *In vitro* evaluation of combination treatment of MPM cell lines with PD-1 blockade and c-Met re-targeted CAR$^+$ T-cells

There is increasing interest in the use of PD-1 blockade as a therapeutic approach in MPM. Consequently, it was of interest to determine if this approach could be used to potentiate the anti-tumour activity of c-Met re-targeted CAR$^+$ T-cells against MPM. Firstly, the PD-L1 and PD-L2 expression profile of the MPM cell lines was assessed by flow cytometry. Figure 5-14 shows that all four MPM cells expressed PD-L1, ranging from low levels on H28 and LO68 cells to high levels on both REN and JU77 cells.

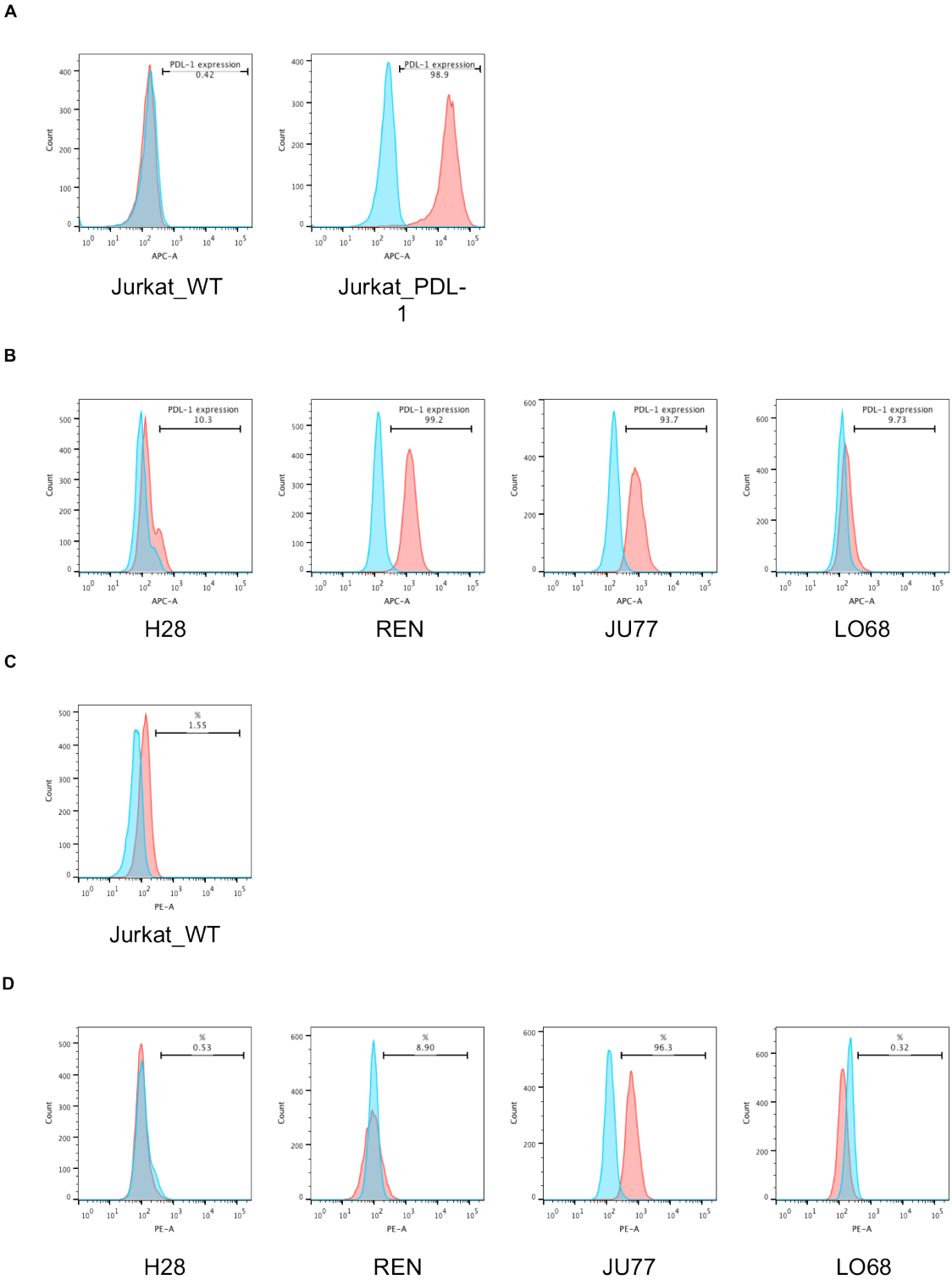

Figure 5-14. PD-L1 and PD-L2 expression profile of a panel of human MPM cell lines.

The PD-L1 and PD-L2 expression profile of the MPM cell lines was assessed by flow cytometry (filled red histograms). Filled blue histograms show staining with a matched isotype control antibody. (**A**) Jurkat cells that had been engineered to over-express PD-L1 served as positive control while parental Jurkat cells were a negative control in this analysis. (**B**) Expression of PD-L1 on the indicated MPM cells. (**C**) Parental Jurkat cells were used as control for PD-L2 expression profiling – however low expression of PD-L2 appear to be present and qRT-PCR would be required for further analysis. (**D**) Expression of PD-L2 on the indicated MPM cell lines. Data are representative of 2 independent experiments that yielded similar results.

Jurkat cells that had been engineered to over-express PD-L1 (gift of Dr Marc Davies, King's College London) served as positive control while parental Jurkat cells were a negative control in this analysis. Only JU77 cells expressed very high levels of PD-L2, although no suitable controls were available for this analysis.

Based on these expression profiles, I hypothesised that PD-1 blockade with the pembrolizumab monoclonal antibody would potentiate the anti-tumour activity of c-Met re-targeted CAR$^+$ T-cells, especially against the REN and JU77 cell lines. To test this, c-Met re-targeted CAR$^+$ T-cells (transduction efficiency shown in Figure 5-15) were combined with ± 10μg pembrolizumab during a 48-hour co-cultures with MPM cell lines (REN, JU77, LO68) at a 1:1 effector to target ratio. T-cells expressing V28z CAR or UT T-cells were used as negative controls. During the co-culture period, T-cell activation was monitored by measurement of the release of IFN-γ (Figure 5-16).

It is extremely difficult to calculate an *in vitro* dose based upon doses used *in vivo*, because *in vivo* doses take into account the pharmacokinetics that are absent in an *in vitro* setting. In clinical studies, the highest dose given to patients was 10mg/kg, which crudely translates to an in vitro calculation of 10μg/ml. This concentration was taken as the baseline. Additionally, to ensure complete saturation, an elevated dose of 100μg/ml was also evaluated. This study design was undertaken as a model to establish whether blocking PD-1 correlated with improved anti-tumour activity of c-Met re-targeted CAR T-cells. Moreover, the 100μg/ml dose is far greater than one would ever achieve *in vivo*, however was conducted to ensure complete saturation in the event a synergistic effect may be seen.

In three independent experiments, there was no significant increase in IFN-γ release by MPM-stimulated c-Met re-targeted CAR T-cells when cultured in the presence or absence of pembrolizumab. Although variability in the concentrations of IFN-γ was detected, the trend of T-cell activation was reproducible across independent experiments, highlighting the consistency of this result.

Next, I investigated if PD-1 blockade could potentiate tumour cell killing mediated by c-Met re-targeted CAR T-cells. Quantification of T-cell mediated tumour cell destruction was achieved using MTT assays. Following confirmation of CAR expression (Figure 5-15), N28z$^+$, M28z$^+$, cM28z$^+$, V28z$^+$ or UT T-cells were co-cultured for 48 hours with REN (Figure 5-17), JU77 (Figure 5-18) or LO68 (Figure 5-19). In these experiments, I also tested the addition of a supra-therapeutic dose of pembrolizumab (100μg/mL).

Forty eight hours after T-cell addition, similar levels of killing of REN or JU77 cells was observed when comparing CAR⁺ T-cells alone or in combination with pembrolizumab. This was noteworthy since both cell lines expressed the highest levels of PD-L1. By contrast, a modest but significant enhancement of killing of LO68 cells by c-Met re-targeted CAR⁺ T-cells was seen in the presence of pembrolizumab (Figure 5-19).

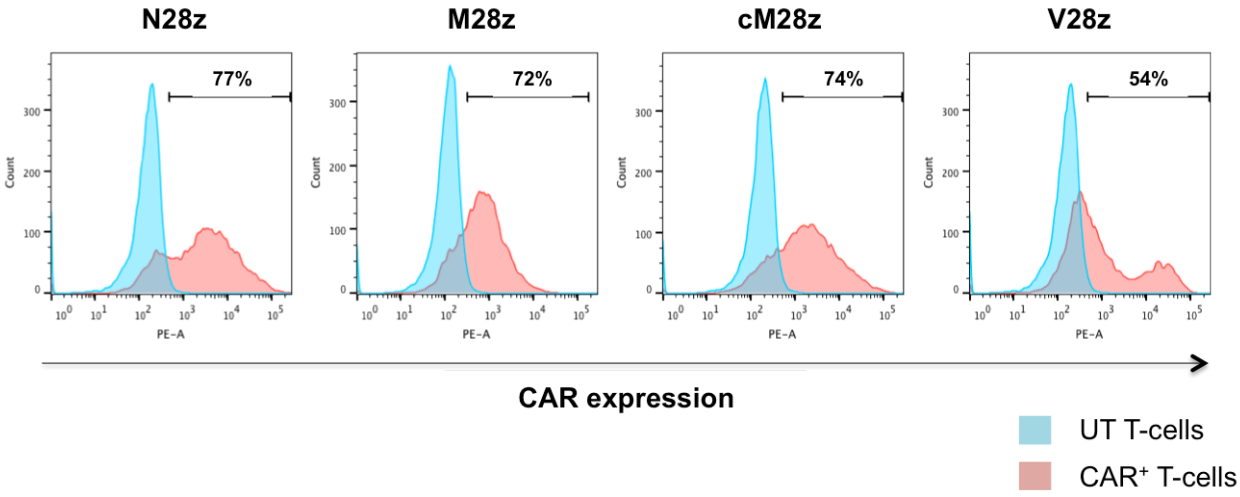

Figure 5-15. CAR T-cell transduction efficiencies.
Example of CAR T-cell transduction percentages obtained for use in experiments evaluating the combination of pembrolizumab with c-Met re-targeted CAR T-cells using a panel of MPM cell lines.

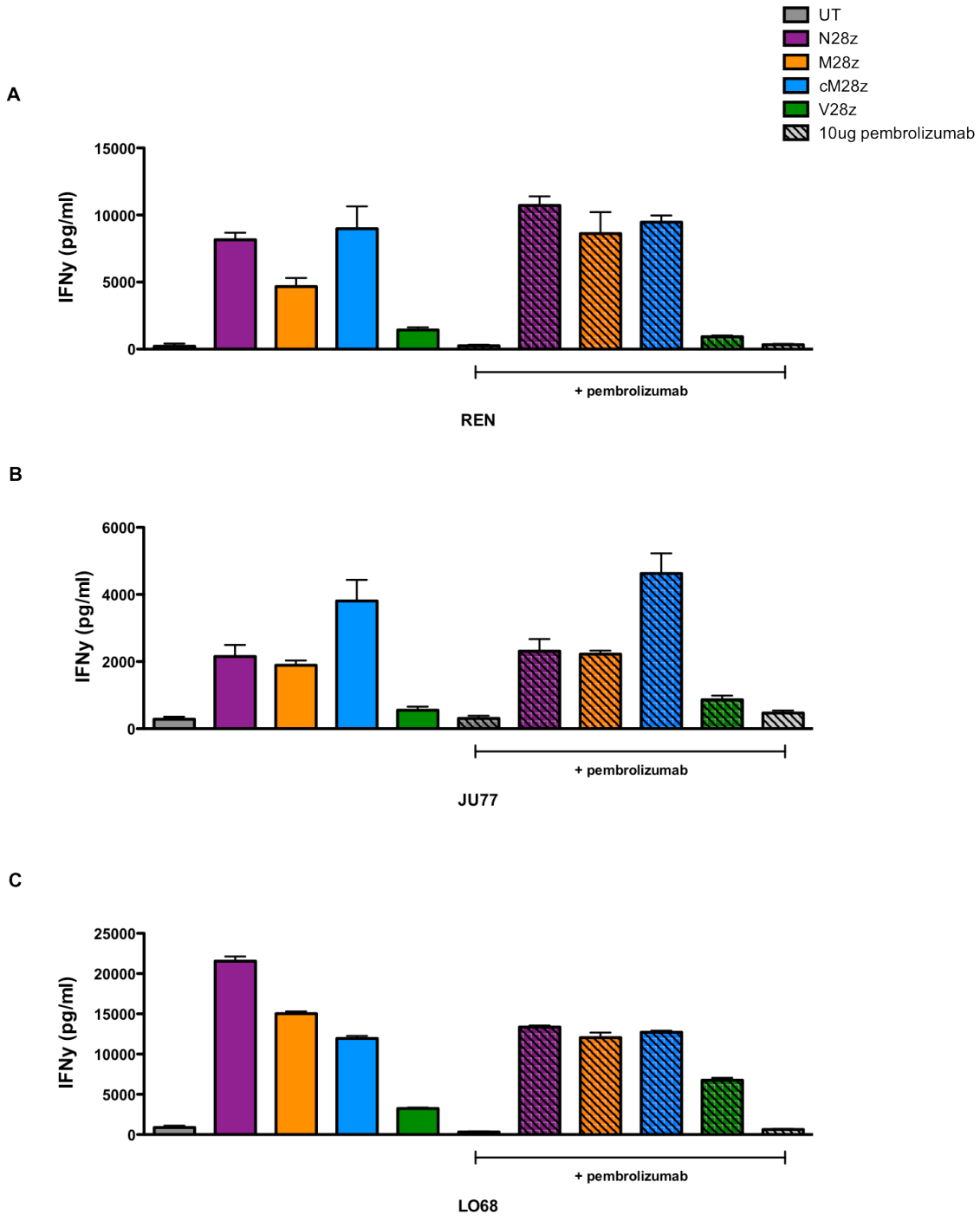

Figure 5-16. IFN-γ release during c-Met re-targeted CAR⁺ T-cell co-cultures with or without pembrolizumab on panel of MPM cell lines.
N28z⁺, M28z⁺, cM28z⁺, V28z⁺ or untransduced (UT) T-cells were co-cultivated at an effector to target ratio of 1:1 with a panel of four MPM tumour cell lines ± 10μg/ml PD-1 checkpoint inhibitor pembrolizumab. The bar shown on the extreme right shows tumour cell cultures in which pembrolizumab alone was added (e.g. no T-cells). After 48 hours, supernatants were removed from co-cultures with (**A**) REN, (**B**) JU77, (**C**) LO68 tumour cells and the concentration of IFN-γ measured using ELISA (mean ± SEM; n=3 independent experiments). Significance was determined using the unpaired Student's *t*-test, comparing UT T-cells with CAR⁺ T-cells: comparisons between pembrolizumab-treated and untreated cultures were not significant.

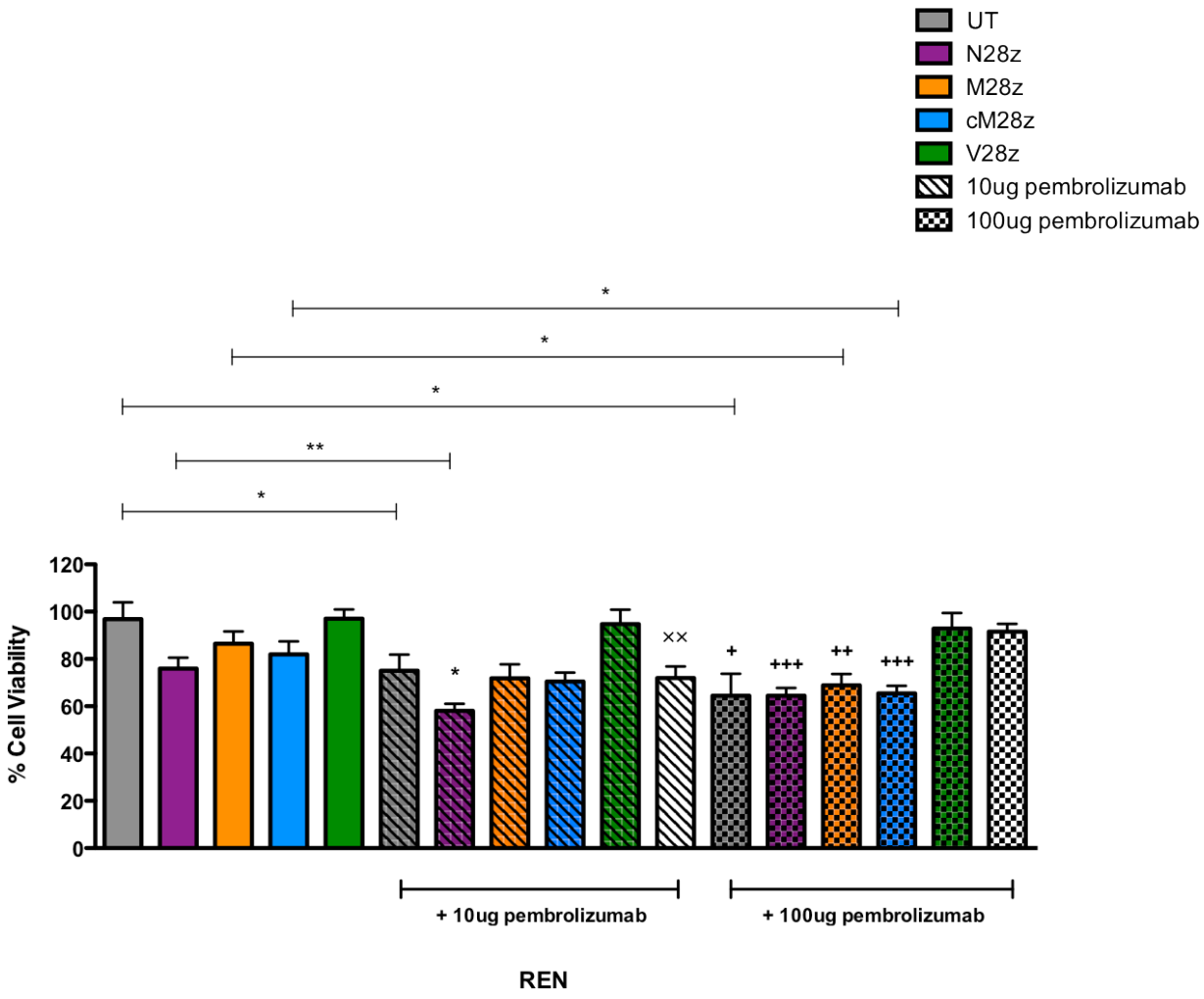

Figure 5-17. Cytotoxic effect of combining PD-1 blockade with CAR T-cells against MPM: REN cell line.
REN MPM cells were co-cultivated with an equal number (2 x 10^4 cells) of $N28z^+$, $M28z^+$, $cM28z^+$, $V28z^+$ or untransduced (UT) T-cells ± pembrolizumab at two indicated doses (10µg / 100µg). Pembrolizumab was added without T-cells to those cultures indicated by the black and white hatched bars. T-cells were not corrected for transduction efficiency (shown in Figure 5-15). Residual tumour cell viability was measured using an MTT assay after 48 hours. Data are presented as mean ± SEM from three independent experiments. Significance was investigated using the unpaired Student's *t*-test comparing only T-cells with pembrolizumab plus T-cells – as depicted by horizontal line. A test (above individual bars) was also conducted comparing T-cells supplemented with pembrolizumab against each respective dose of pembrolizumab (* denotes 10µg pembrolizumab comparisons) (+ denotes 100µg pembrolizumab comparisons); A further statistical test test was conducted between 10ug and 100ug of pembolizumab, denoted by (×) above bars. * p <0.05, ** p <0.005 and *** p <0.0005.

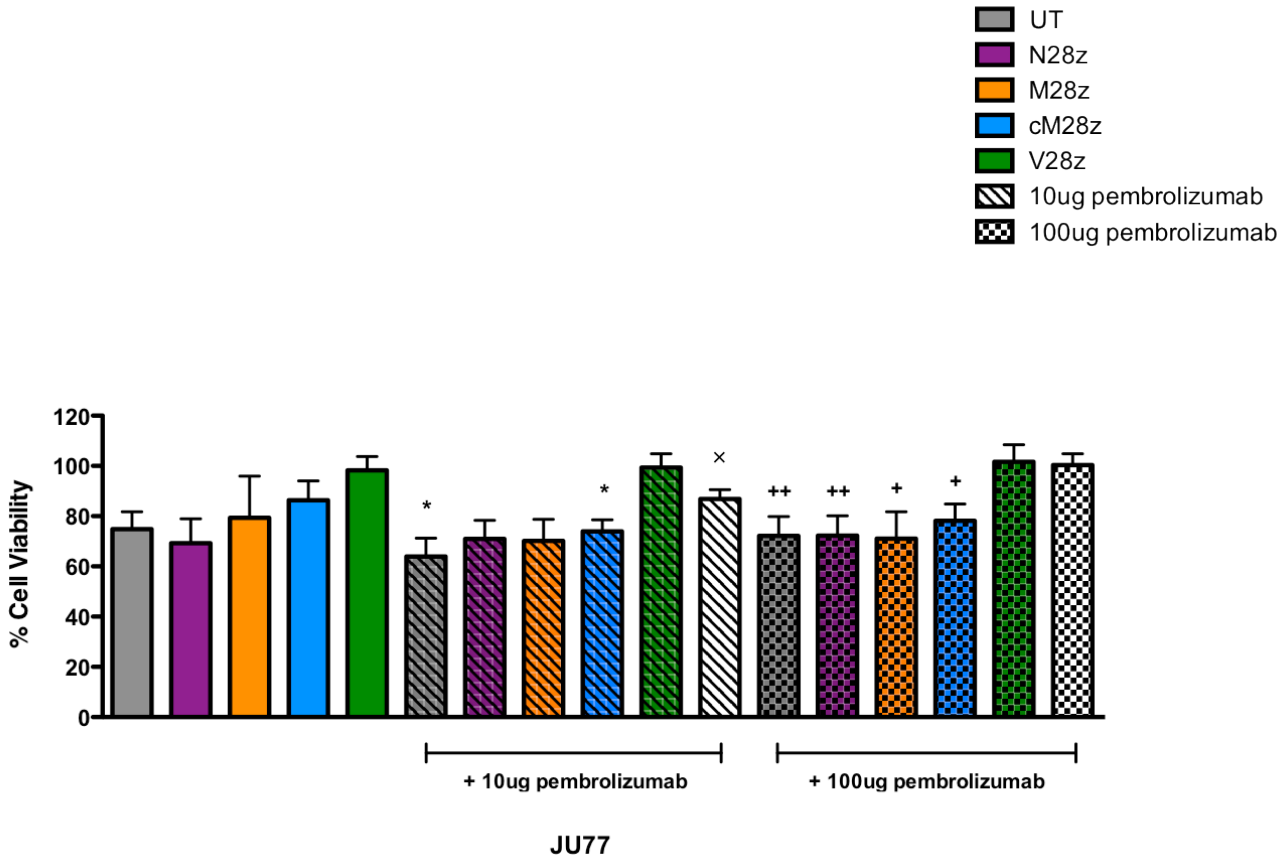

Figure 5-18. Cytotoxic effect of combining PD-1 blockade with CAR T-cells against MPM: JU77 cell line.
JU77 MPM cells were co-cultivated with an equal number (2 x 10^4 cells) of $N28z^+$, $M28z^+$, $cM28z^+$, $V28z^+$ or untransduced (UT) T-cells ± pembrolizumab at two indicated doses (10µg / 100µg). Pembrolizumab was added without T-cells to those cultures indicated by the black and white hatched bars. T-cells were not corrected for transduction efficiency (shown in Figure 5-15). Cell viability was measured using the MTT protocol after 48 hours. Data presented as mean ± SEM from three independent experiments. Significance was investigated using the unpaired Student's *t*-test comparing either T-cells against respective dose of pembrolizumab plus T-cells (* with line) or T-cells plus pembrolizumab against the respective dose of pembrolizumab alone (* denotes 10µg pembrolizumab comparisons) (+ denotes 100µg pembrolizumab comparisons); (×) denotes unpaired Student's *t*-test comparing pembrolizumab doses alone without T-cells: Representational * p <0.05, ** p <0.005 and *** p <0.0005.

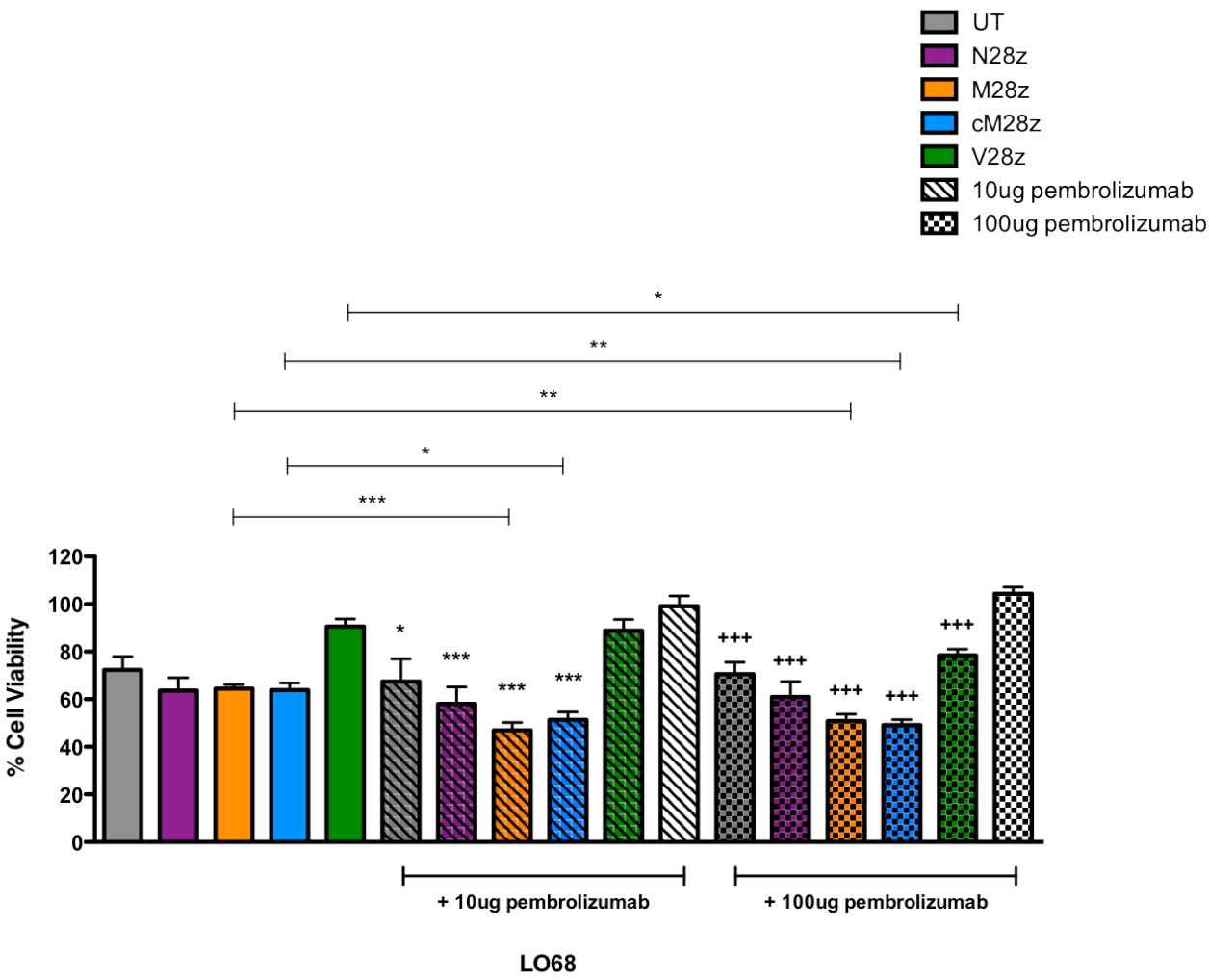

Figure 5-19. Cytotoxic effect of combining PD-1 blockade with CAR T-cells against MPM: LO68 cell line.

LO68 MPM cells were co-cultivated with an equal number (2 x 10^4 cells) of $N28z^+$, $M28z^+$, $cM28z^+$, $V28z^+$ or untransduced (UT) T-cells ± pembrolizumab at two indicated doses (10µg / 100µg). Pembrolizumab was added without T-cells to those cultures indicated by the black and white hatched bars. T-cells were not corrected for transduction efficiency (shown in Figure 5-15). Cell viability was measured using the MTT protocol after 48 hours. Data presented as mean ± SEM from three independent experiments. Significance was investigated using the unpaired Student's *t*-test comparing either T-cells against respective dose of pembrolizumab plus T-cells (* with line) or T-cells plus pembrolizumab against the respective dose of pembrolizumab alone (* denotes 10ug pembrolizumab comparisons) (+ denotes 100ug pembrolizumab comparisons); (×) denotes unpaired Student's *t*-test comparing pembrolizumab doses alone without T-cells: Representational * $p < 0.05$, ** $p < 0.005$ and *** $p < 0.0005$.

5.3 Discussion

The overall aim of the work undertaken in this chapter was to investigate whether the anti-tumour activity of a panel of c-Met re-targeted CARs (N28z, M28z and cM28z) could be further potentiated through combining chemotherapy or immune-checkpoint inhibitors with CAR T-cell therapy.

Initial experiments were conducted with a combination of cisplatin and pemetrexed, a doublet chemotherapy regimen that is commonly used in the treatment of patients with MPM. Doses were selected to have relatively low intrinsic cytotoxic activity, in order to investigate for a sensitising effect of these drugs to subsequent addition of c-Met re-targeted CAR^+ T-cells. These experiments revealed that a concentration of 3.2μM cisplatin alone or in combination with pemetrexed (500μM) caused low level killing of all four MPM tumour cell lines within 48 hours. Next, MPM tumour cells were pre-treated with this cocktail of drugs for 24 hours prior to their removal and addition of c-Met re-targeted CAR^+ T-cells. These experiments demonstrated no convincingly reproducible increase in CAR T-cell activation (indicated by release of IFN-γ). However, a statistically significant - albeit biologically modest - increase in killing of REN, JU77 and LO68 MPM cells was observed after addition of CAR T-cells.

Both of these findings are consistent with a previous report of the sensitising effect of chemotherapy in models of ovarian cancer. In that setting, pre-treatment of platinum-resistant SKOV-3 tumour cells or derived xenografts with carboplatin achieved significant sensitisation to cytotoxic destruction by ErbB re-targeted CAR T-cells, in the absence of enhanced T-cell activation [350].

The immune-potentiating effects of chemotherapy drugs is increasingly being appreciated [353]. A number of studies have evaluated the immunomodulatory effects of low-dose chemotherapy, such as the increased APC function of DC and depletion of Tregs [354, 355]. In MPM, immunomodulatory roles have previously been identified for agents cisplatin and pemetrexed. Studies have shown that patients treated with platinum-based chemotherapy have greater $CD8^+$ tumour infiltrating T-cells, correlating with improved survival [97]. A study by Su *et al.*, reported that pemetrexed is able to sensitise tumour cells to immune cell killing via the upregulation of the death receptor, DR5 [356]. Likewise, cisplatin has also been reported to increase the sensitivity of tumour cells to cell lysis induced by $CD8^+$ T-cells [357]. Although the mechanism underlying this effect was unclear, more recent reports have shown cisplatin can activate the Fas-ligand

(CD95) related apoptotic pathway in tumour cells [358]. Nonetheless, mechanisms underlying the sensitising effect remain to comprehensibly be determined.

Substantial further investigation would also be required to further optimise the therapeutic potential of this combinatorial approach. Such an analysis would require testing of a broader range of doses of cisplatin and pemetrexed (including dose levels that are more potently cytotoxic), employing a spectrum of CAR T-cell effector to target ratios and an extended panel of MPM cell lines that include tumour cells that are naturally sensitive or resistant to the cytotoxic effects of these agents. Once *in vitro* sensitisation was better characterised, it would then be appropriate to explore such regimens *in vivo* in mice bearing established MPM tumour xenografts.

In an alternative approach, I explored the combination of CAR T-cell immunotherapy in combination with a PD-1 inhibitor, pembrolizumab. Pembrolizumab is currently undergoing clinical development for the treatment of patients with this cancer. As detailed in chapter 1, numerous inhibitory immune-checkpoint pathways, such as PD-1, CTLA-4, FasL the anti-tumour ability of TILs in MPM and other tumour types. Furthermore, the PD-1/PD-L1 axis has been shown to suppress the activation of CAR T-cells within the tumour microenvironment [359, 360]. Moon et al. showed that CAR T-cells undergo rapid loss of function within tumours – a change that was correlated to the up-regulation of intrinsic T-cell inhibitory enzymes and cell surface expression of inhibitory receptors [361]. The use of checkpoint inhibitors targeting the PD-1/PD-L1/2 axis or CTLA4 pathway has previously been demonstrated to enhance clinical response in a number of cancers, such as melanoma and renal cancer [99, 113] and similar findings are now emerging in trials of these agents in MPM [112].

Elevated expression of PD-L1 in mesothelioma provides a strong rationale for investigation of the clinical use of PD-1 or PD-L1 inhibition in patients with MPM. It has been reported greatest expression of inhibitory markers were found in sarcomatoid subtypes, directly correlating to poorer prognosis. The panel of four mesothelioma cell lines were tested for the cell surface expression of both PD-L1 and PD-L2. Greatest expression of both ligands was identified in the JU77 (sarcomatoid) cell line, with REN cells also expressing high levels of PD-L1. Lower levels of PD-L1 expression were identified on LO68 cells, with H28 cells expressing the lowest levels. The REN, JU77 and LO68 cell lines were subsequently taken forward to evaluate whether the combination of c-Met re-targeted CAR$^+$ T-cells with an anti-PD-1 blocker, pembrolizumab, could further enhance the anti-tumour activity observed against the respective mesothelioma cell lines. Two concentrations, 10µg/mL and 100µg/mL were chosen to initially identify whether the combination yielded significant differences. The activation of c-Met re-targeted CAR$^+$

T-cells was assessed by measurement of release of IFN-γ following stimulation by MPM cell lines. This analysis revealed that pembrolizumab did not enhance the activation of c-Met re-targeted CAR$^+$ T-cells when stimulated on MPM cells that express cognate target.

Further assessment of whether functionality of c-Met re-targeted T-cells was potentiated by anti-PD-1 therapy involved an assessment of tumour cell viability in co-cultivation assays (Figure 5-17). Once again, these studies failed to unmask any convincing potentiating effect of pembrolizumab on CAR T-cell mediated anti-tumour activity, with the possible exception of LO68 tumour cells which express minimal levels of PD-1 ligands. Following the relatively insignificant differences observed with this combinational approach, further experimental designs should be considered. One alternative *in vitro* approach method that could unmask effects of PD-1 blockade entails re-stimulation of c-Met re-targeted CAR$^+$ T-cells on fresh tumour cell monolayers, every 72-96 hours. Significant differences may emerge with repeated stimulation of c-Met re-targeted CAR$^+$ T-cells upon the same tumour monolayer, particularly as exhaustion markers such as PD-1 are upregulated on T-cells.

Additionally, further assessment using *in vivo* studies would be required to truly understand whether the combination of anti-PD-1 therapy combined with c-Met re-targeted CAR$^+$ T-cell therapy may enhance c-Met directed anti–tumour activity. Such a finding would be consistent with a recently reported study involving Her2 transgenic mice [351]. As detailed in section 5.1.2, adoptively infused Her2-specific CAR$^+$ T-cells were combined with a mAb to PD-1, resulting in enhanced proliferation and functional capability of Her2-specifc T-cells. Potent regression of established Her2 positive sarcomas and breast cancers were induced [351]. Although checkpoint inhibitors such as anti-PD-1 antibodies are clinically available and generally well tolerated (over 7000 patients have received anti-PD-1 therapy [362]), a more refined method to merge CAR T-cell engineering with checkpoint blockade is also being explored in preclinical studies. “Chimeric switch-receptors” are chimeric proteins that fuse the extracellular/ transmembrane domains of CTLA-4 or PD-1 to traditional intracellular signalling domain such as CD28 or 4-1BB. Using this approach, a potentially inhibitory signal delivered by a PD-1 ligand is transformed into positive stimulatory signal, leading to potentiation of anti-tumour activity [363]. PD-1/CD28 chimeric molecules have been shown to enhance cytokine secretion with superior *in vivo* anti-tumour activity in two xenograft melanoma models [364]. A subsequent study using PD-1/CD28 CAR T-cells against aggressive models of human solid tumours resulted in significant regression of tumour volume due to enhanced CAR TIL infiltration and decreased susceptibility of tumour-induced hypofunction [365]. Building upon this novel emerging data, further

investigations would be required to fully understand the potential therapeutic value of this combinational approach in relation to mesothelioma specifically.

CHAPTER 6 Determining the anti-tumour efficacy of c-Met targeting CAR$^+$ T-cells *in vivo*

6.1 Introduction

Data presented in Chapters 3-5 of this thesis demonstrate that all three candidate CARs developed in this project can confer specificity for c-Met upon engineered T-cells, enabling them to destroy target cells in a c-Met-dependent manner. Clinical development of a strategy such as this requires the generation of a pre-clinical data package that demonstrates the efficacy and safety of this approach using the therapeutic agent itself (e.g. human CAR engineered T-cells). Consequently, I next set out to develop xenograft models in order to evaluate the anti-tumour activity of c-Met re-targeted CAR T-cells against an established MPM tumour xenograft burden.

6.1.1 Assessing the therapeutic efficacy of CAR$^+$ T-cells *in vivo*

A significant hurdle in the translation of novel cancer therapies into the clinic is reproducing results observed *in vitro* using more physiologically appropriate systems. In particular, the testing of anti-tumour activity of CAR re-directed T-cells *in vivo* is a vital step in this pre-clinical development process. To date, a variety of different CAR$^+$ T-cells targeting a diverse spectrum of tumour associated antigens have been evaluated in this manner [231, 366].

The need for assessing CAR T-cell functionality using animal models stems from the multitude of complex interactions that occur *in vivo* and which are not recapitulated by *in vitro* assay systems. Examples include the need to optimise T-cell homing and trans-endothelial migration within tumour deposits, attributes that cannot easily be monitored within current *in vitro* systems. Additionally, investigation of the inhibitory and regulatory influences of the tumour microenvironment on CAR engineered T-cells can be studied using some *in vivo* models, in particular those that involve the use of immune competent mice. While these do not allow the study of human CAR T-cells, an increasing number of humanised mouse models are under development, which may help to address this limitation.

6.1.2 Establishment of animal models of malignant mesothelioma

Mesothelioma can be recapitulated in murine models using the same defined carcinogen (e.g. asbestos exposure) as has been implicated in most human disease. Although these models have clear relevance to the human MPM, the long lag time (1.5 years) and poor (25%) success rate renders this option unsuitable for most investigations [367].

Subcutaneous models using murine mesothelioma cell lines were widely used to evaluate many of the chemotherapy agents used clinically today [368]. An advantage of these models is the fact that tumours grow reproducibly within a short time frame in immune competent hosts and are readily amenable to serial measurement without the need to kill the animal to quantify tumour burden. However, development of tumours at an anatomically irrelevant site may result in significant differences in response to therapy when compared to orthotopic models [369]. The microenvironment of subcutaneous tissue bears little resemblance to the tissue milieu within which human mesothelioma tumours are found.

To model MPM most precisely, it is logical to inject tumour cells into the pleural cavity. Previous literature has described a number of such intrapleural models [370, 371]. Additionally, consistent with human disease, tumour cells grow along the serosal surface, forming nodules [370, 371]. However, this imposes substantial technical challenges, considering in particular the difficulty in obtaining successful access to the pleural space in mice. In order to test CAR T-cell immunotherapy, such access would be required on two separate occasions, in order to engraft the tumour and subsequently to deliver T-cells to this site. The latter approach is justified (rather than intravenous administration of T-cells) in light of the propensity of MPM to spread locally. Furthermore, recent data published using a mesothelin-targeted CAR demonstrate that efficacy of this therapeutic approach is substantially enhanced if T-cells are delivered into the pleural cavity rather than into the bloodstream [235].

To establish an *in vivo* model that balances all of these requirements, I elected to establish an intraperitoneal xenograft model. Peritoneal mesothelioma accounts for almost 10% of all cases, demonstrating the clinical relevance of this approach. Like MPM, tumours tend to progress by loco-regional spread, providing a rationale for direct delivery of CAR T-cells to this body cavity. Intraperitoneal injection of tumour cells and T-cells is considerably less invasive that intrapleural injection in mice. Finally, the same biological features, in terms of pathology, histology and progression are reportedly conserved in intraperitoneal mesotheliomas [372, 373]. While xenograft models do not allow the study of interaction between the immunotherapy and the host immune system,

they do allow the investigation of the therapeutic agent (e.g. human CAR T-cells) for its efficacy and safety, as is required by regulatory bodies in clinical trial applications.

One of the hurdles with successfully implemented orthotopic models is the challenge of measuring tumour burden. However, this may been countered with the use of bioluminescence imaging techniques [374]. Such an approach enables the serial real time and non-invasive imaging of tumour status in immune compromised animals. Tumours are engineered to express luciferase enzymes, most commonly from the firefly (*Photinus pyralis*). Following the administration of a substrate (d-luciferin), tumours emit light in proportion to their size. This allows the assessment of tumour burden and therapeutic efficacy without the need to kill animals at each time point.

6.1.3 Aims

1. Development of a c-Met-expressing MPM tumour xenograft model that is amenable to serial monitoring using bioluminescence imaging.
2. Evaluation of *in vivo* anti-tumour activity of c-Met re-targeted CAR T-cells against an established MPM tumour xenograft.

6.2 Results

6.2.1 Generation of firefly luciferase-expressing MPM tumour cell lines

To enable the non-invasive *in vivo* monitoring of MPM xenograft growth using bioluminescence imaging (BLI), the REN and H28 tumour cell lines were engineered by retroviral transduction to stably co-express both firefly luciferase (ffLuc) and the red fluorescent protein, tandem dimer (td)Tomato (LT) (Figure 6-1).

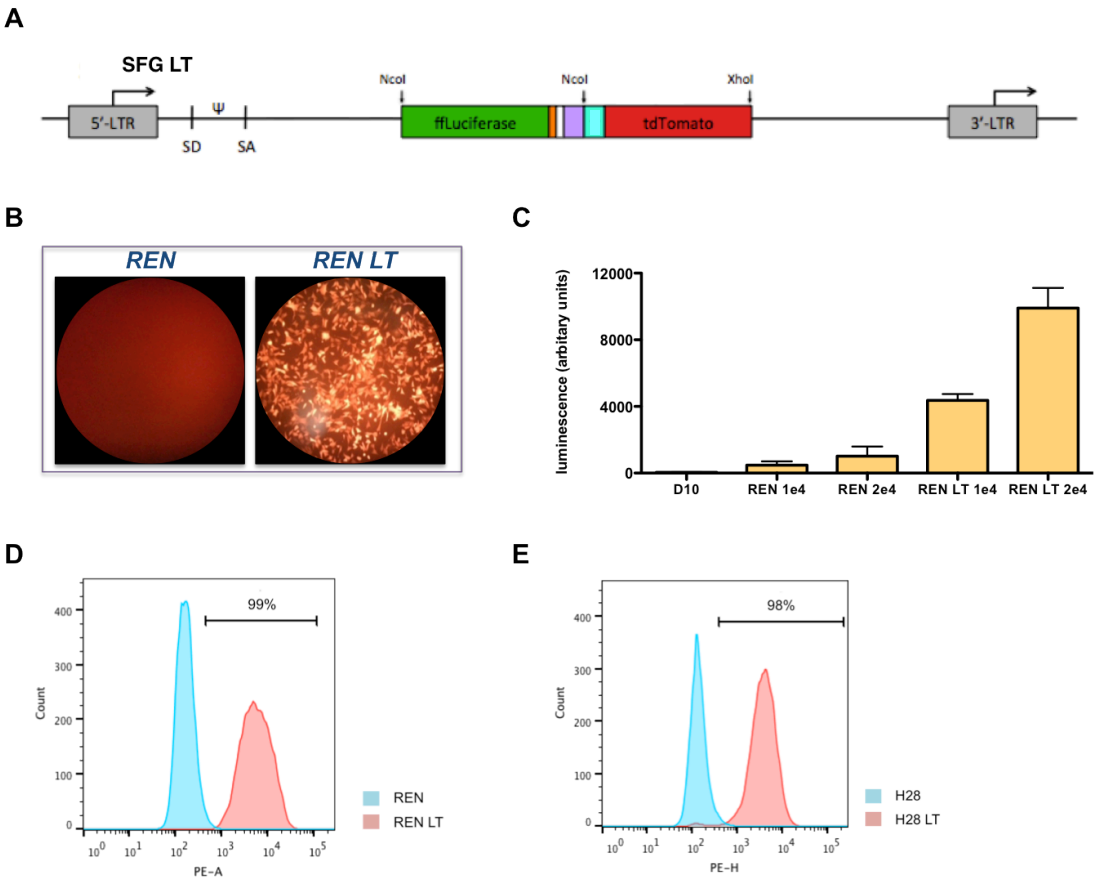

Figure 6-1. Stable expression of the SFG LT construct in mesothelioma cell lines
(**A**) Structure of the SFG LT retroviral vector. Stoichiometric co-expression of firefly luciferase (ffLuc) and tdTomato was achieved through the use of a T2A ribosomal skip sequence. LTR: long terminal repeats; SD: splice donor; Ψ: packaging signal; SA: splice acceptor; *Note: size of the blocks is not representative of the sizes of individual elements*. (**B**) Transduced REN LT cells were visualised by fluorescence microscopy (representative images showing parental REN and REN LT cells). (**C**) Function of ffLuc in tumour cells was confirmed by luciferase assay, making comparison between medium alone, parental REN cells and REN LT cells seeded at $1x10^4$ or $2x10^4$ and read after 24 hours. Representative of two independent repeats. Following transduction, mesothelioma cell lines were flow sorted for tdTomato expression, yielding Ren LT (**D**) and H28 LT cell lines (**E**), which were used to establish xenografts in NSG mice.

6.2.2 Developing a clinically relevant c-Met expressing xenograft model of MPM

Since the most potent *in vitro* anti-tumour activity of c-Met re-targeted CAR T-cells was observed using H28 MPM cells, I first set out to develop a xenograft model using ffLuc-expressing H28 cells. NSG mice were inoculated with tumour cell doses of between 0.5 to 10 x 10^6 tumour cells using the intraperitoneal (i.p.) route. Despite the detection of signal after tumour cell inoculation, tumour progression was not achieved with this model however (Figure 6-2A). Similarly, subcutaneous (s.c.) inoculation of H28 tumour cells alone or supplemented with matrigel [375, 376] did not achieve robust tumour engraftment (Figure 6-2B).

Next, I decided to switch models to investigate xenograft formation by ffLuc-expressing REN LT MPM cells (REN LT). NSG mice (three mice per group) were inoculated with 0.5 and 2 x 10^6 tumour cells. An initial pilot study identified REN LT xenograft was developed aggressively with animals developing very high tumour burden within two weeks (Figure 6-3).

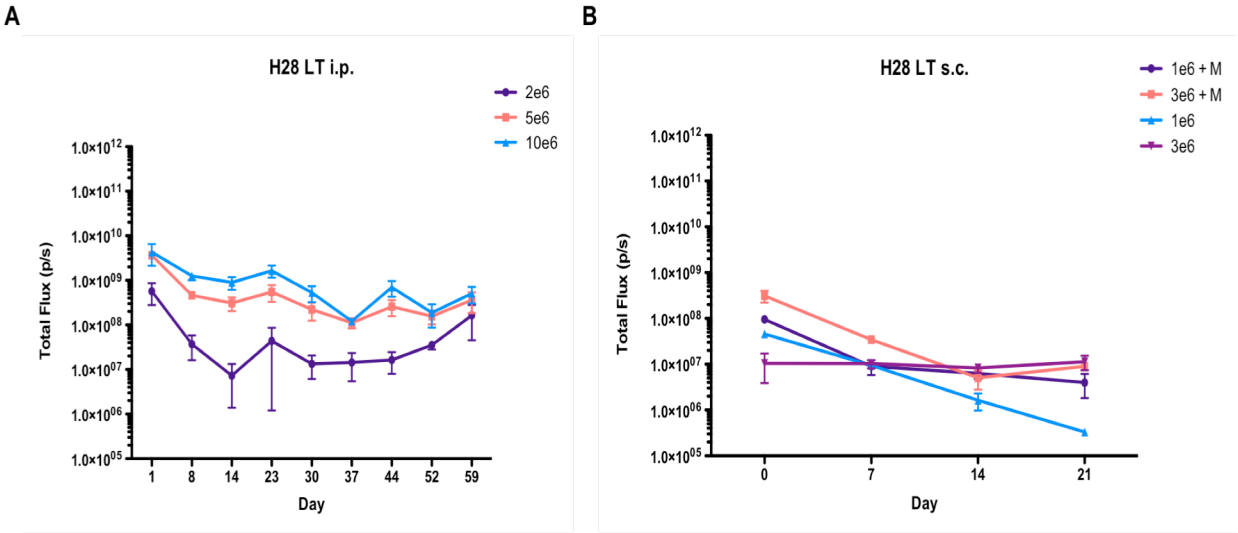

Figure 6-2. Developing an *in vivo* MPM xenograft model: H28 cells
NSG mice (n=3 per dose) were inoculated with the indicated dose of ffLuc-expressing H28 cells, either into the peritoneal cavity (**A**) or subcutaneously (**B**). Tumour growth was monitored at the indicated intervals using bioluminescence imaging. Quantification of luminescence signal released by individual mice was determined by drawing a region of interest (ROI) around each specific mouse. Using Living Image 4.1 software, photon release within the ROI was calculated and standardised to account for the scan duration. The data is expressed as mean total photon flux (photons/s) ± SEM. M- matrigel.

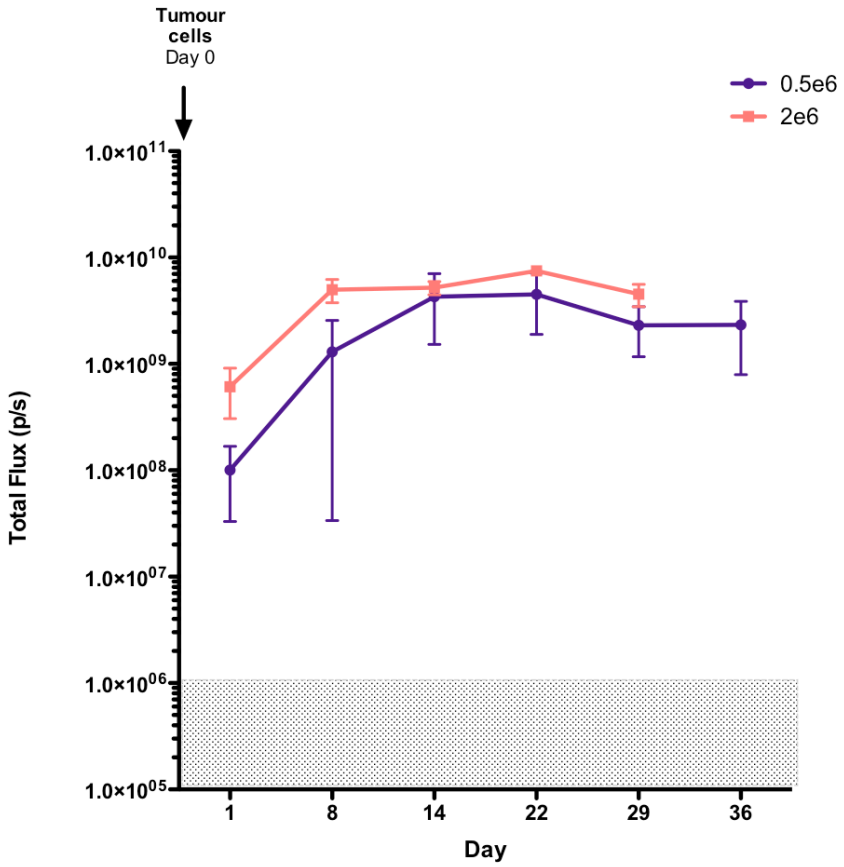

Figure 6-3. Developing an *in vivo* MPM xenograft model: REN LT cells pilot study 1

NSG mice (n=3 per dose) were inoculated with the indicated dose of ffLuc-expressing REN LT cells into the peritoneal cavity. Quantification of luminescence signal released by individual mice was determined by drawing a region of interest (ROI) around each specific mouse. Using Living Image 4.1 software, photon release within the ROI was calculated and standardised to account for the scan duration. The data is expressed as mean total photon flux (photons/s) ± SEM.

In light of the rapid pace of tumour progression seen, I decided to further optimise this model. The number of administered tumour cells was titrated to determine the lowest number that reproducibly engrafted within NSG mice, thereby potentially extending the therapeutic window for adoptive CAR$^+$ T-cell transfer. Tumour cell doses of 0.5 x 10^6, 1.5 x 10^5 and 5 x 10^4 tumour cells were injected i.p. into NSG mice. All three doses resulted in reproducible tumour engraftment within a reasonable time frame (35 days; Figure 6-4). An exponential growth phase was observed in all three dose-groups between day 22 and day 35, at which point all animals were sacrificed. A dose of 5 x 10^4 REN LT cells was chosen for all subsequent experiments.

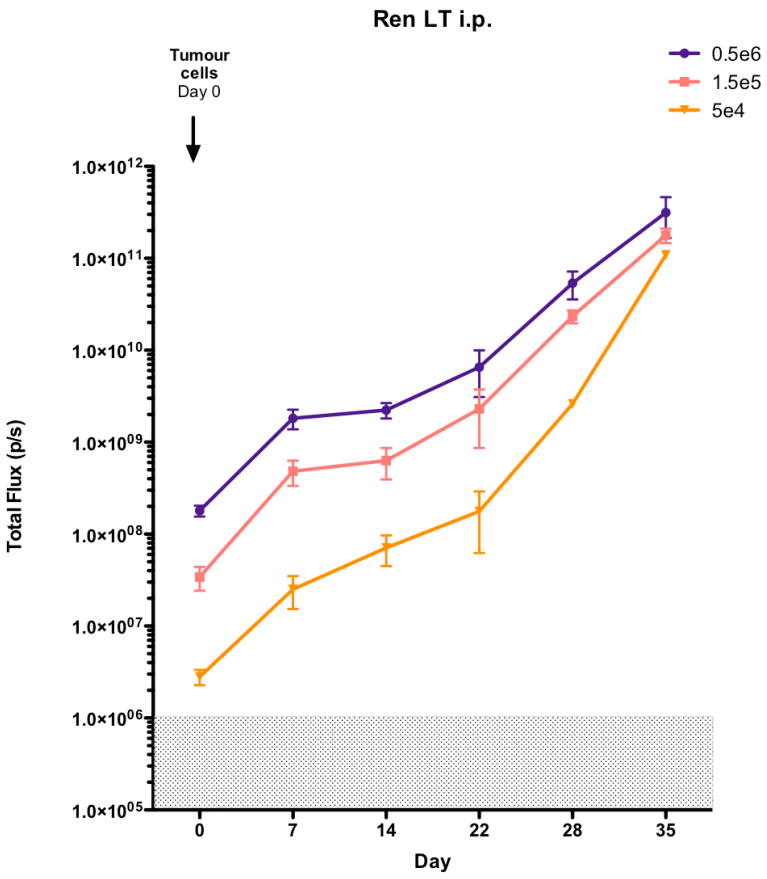

Figure 6-4. Developing an *in vivo* MPM xenograft model: REN LT cells pilot study 2
NSG mice (n=3 per dose) were inoculated with the indicated dose of ffLuc-expressing REN LT cells into the peritoneal cavity. Quantification of luminescent signal released by individual mice was determined by drawing a region of interest (ROI) around each specific mouse. Using Living Image 4.1 software, photon release within the ROI was calculated and standardised to account for the scan duration. The data is expressed as mean total photon flux (photons/s) ± SEM.

6.2.3 Assessing the anti-tumour efficacy of c-Met re-targeted CAR$^+$ T-cells

Next, I investigated anti-tumour activity of c-Met re-targeted CAR$^+$ T-cells *in vivo*, following adoptive transfer into NSG mice with established REN LT xenografts. Mice were imaged using BLI and were weighed regularly throughout the study, in order to monitor for possible toxicity. A schematic overview of experimental design is shown in Figure 6-5.

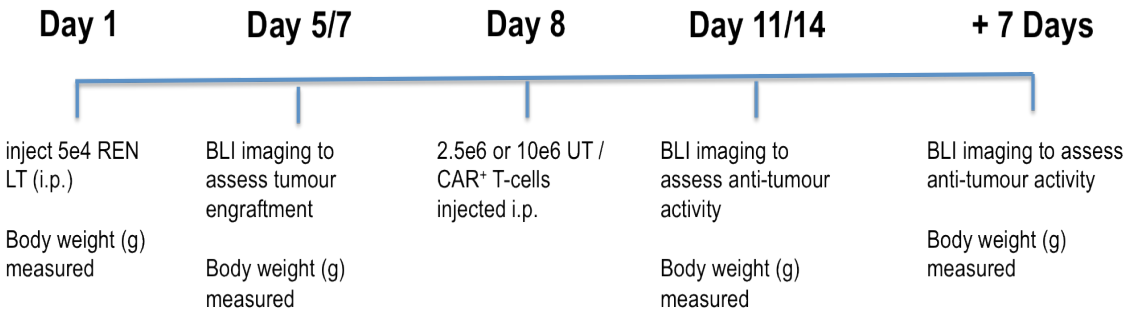

Figure 6-5. MPM tumour inoculation and treatment protocol timeline for *in vivo* studies
This figure shows a schematic overview of how experiments shown in Figure 6-6 and 6-7 were undertaken.

In a randomised study, 55 mice were inoculated i.p. with 5 x 10^4 REN LT tumour cells. Treatment groups were assigned numbers and all treatment and imaging was carried out in a blinded fashion. Five days post tumour cell administration; the mice were imaged using BLI to confirm tumour engraftment. Mice were re-imaged on day 7 to quantify baseline tumour burden prior to being treated the following day with N4$^+$, M4$^+$, cM4$^+$ or V4$^+$ T-cells that had been cultured in IL-4 for 12 days. Prior to infusion, the T-cells were analysed for surface expression of the CAR constructs (Figure 6-6). CAR T-cells were administered i.p. at a dose of either 2.5 or 10 x 10^6 cells (total T-cell dose, not corrected for transduction efficiency). Untransduced (UT) T-cells that had been cultured in IL-2 were injected at the highest dose (10 x 10^6). To quantify tumour progression in the absence of therapeutic intervention, one cohort of mice was received PBS.

At the lower T-cell dose, only $N4^+$ and $CM4^+$ T-cells elicited a modest and transient therapeutic response, when compared to those receiving UT T-cells, $V4^+$ T-cells or PBS. Anti-tumour activity was evident for 7 days following treatment, after which tumour burden increased, mirroring control groups (Figure 6-7). Plots of BLI data for individual mice are shown in Figure 6-8.

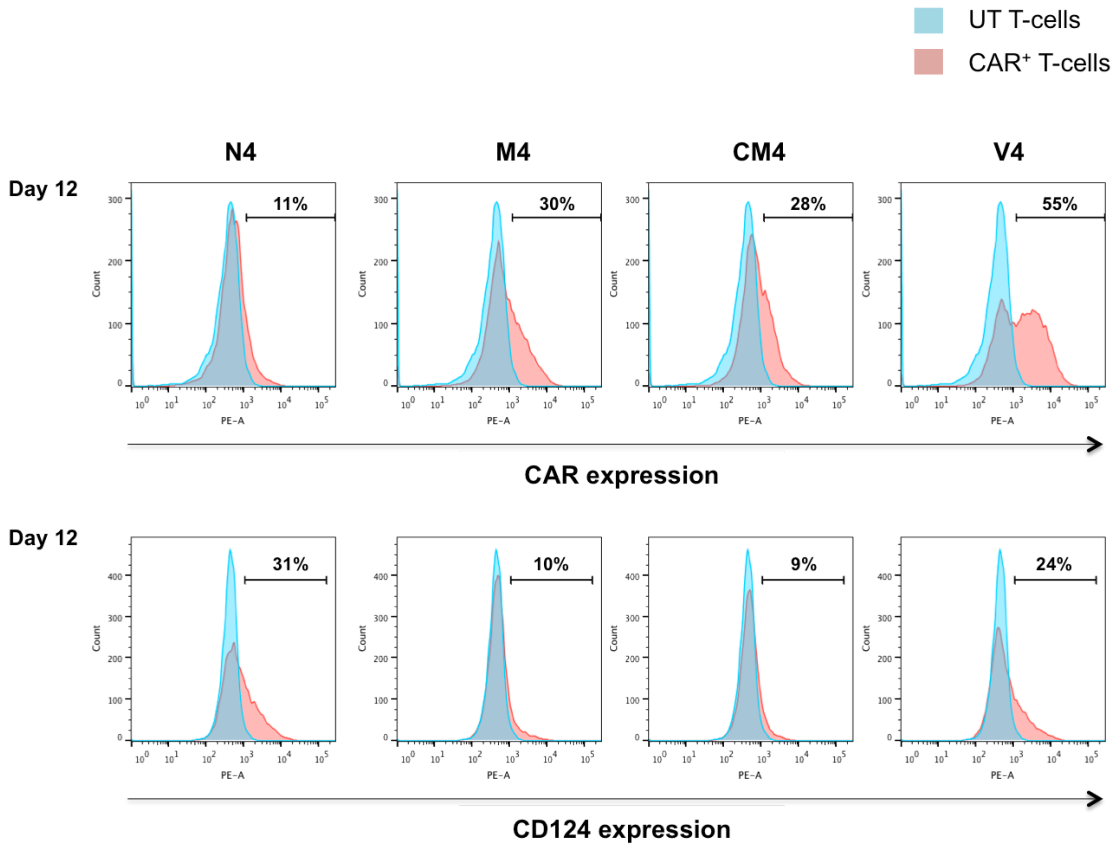

Figure 6-6. c-Met re-targeted CAR^+ T-cell transduction efficiencies used for *in vivo* treatment study
Flow cytometric analysis to show (**A**) transduction efficiency of c-Met re-targeted and V4 CAR^+ T-cells 12 days post retroviral transduction (CAR^+ T-cells cultured in IL-4 supplemented medium, whilst UT cultured in IL-2 supplemented medium). T-cells were stained for CAR expression using the 9e10 antibody which recognises a myc epitope tag in the CAR ectodomain (red histograms). Untransduced (UT) T-cells were similarly stained to generate the negative control (blue histograms). Panel (**B**) shows the same CAR^+ T-cells 12 days post retroviral transduction probed for CD124 cell surface expression, indicating the level of surface expression of the 4αβ chimeric cytokine receptor.

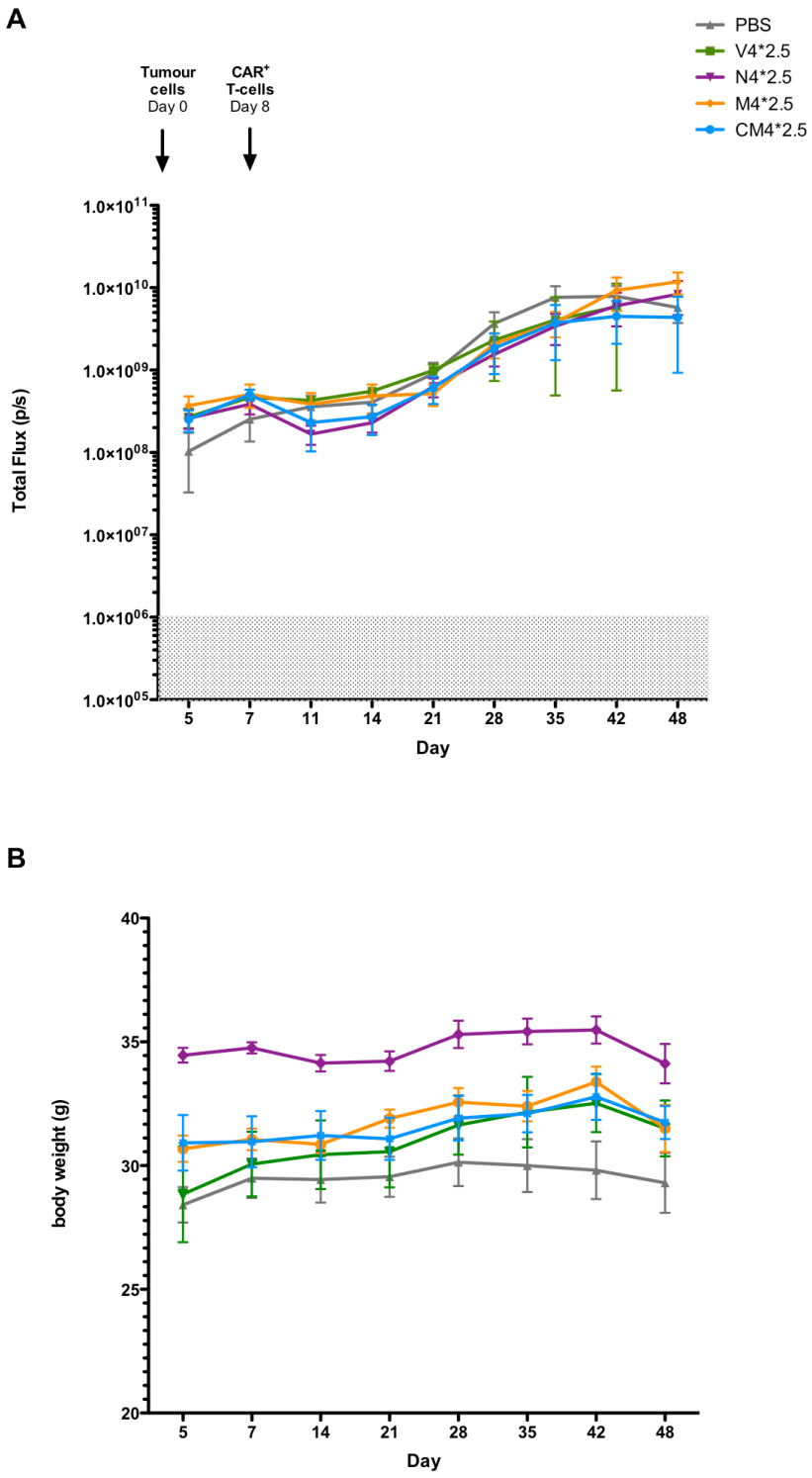

Figure 6-7. Anti-tumour activity of c-Met re-targeted CAR T-cells in mice with established expressing REN LT MPM tumour xenografts (low treatment dose).

Mice were inoculated with 5 x 10^4 ffLuc expressing REN LT tumour cells (i.p.). Engraftment of tumour cells was confirmed using BLI imaging. $N4^+$, $M4^+$, $cM4^+$ and $V4^+$ T-cells (cultured in IL-4) (not corrected for transduction efficiency) were injected i.p. at a dose of 2.5 x 10^6 T-cells. **(A)** Serial BLI imaging was conducted throughout the study to assess baseline tumour growth and anti-tumour activity. **(B)** Body weight (g) was measured throughout the study to monitor for potential toxicity. Data show mean ± SEM for n=5 mice per group (n=8 for PBS group).

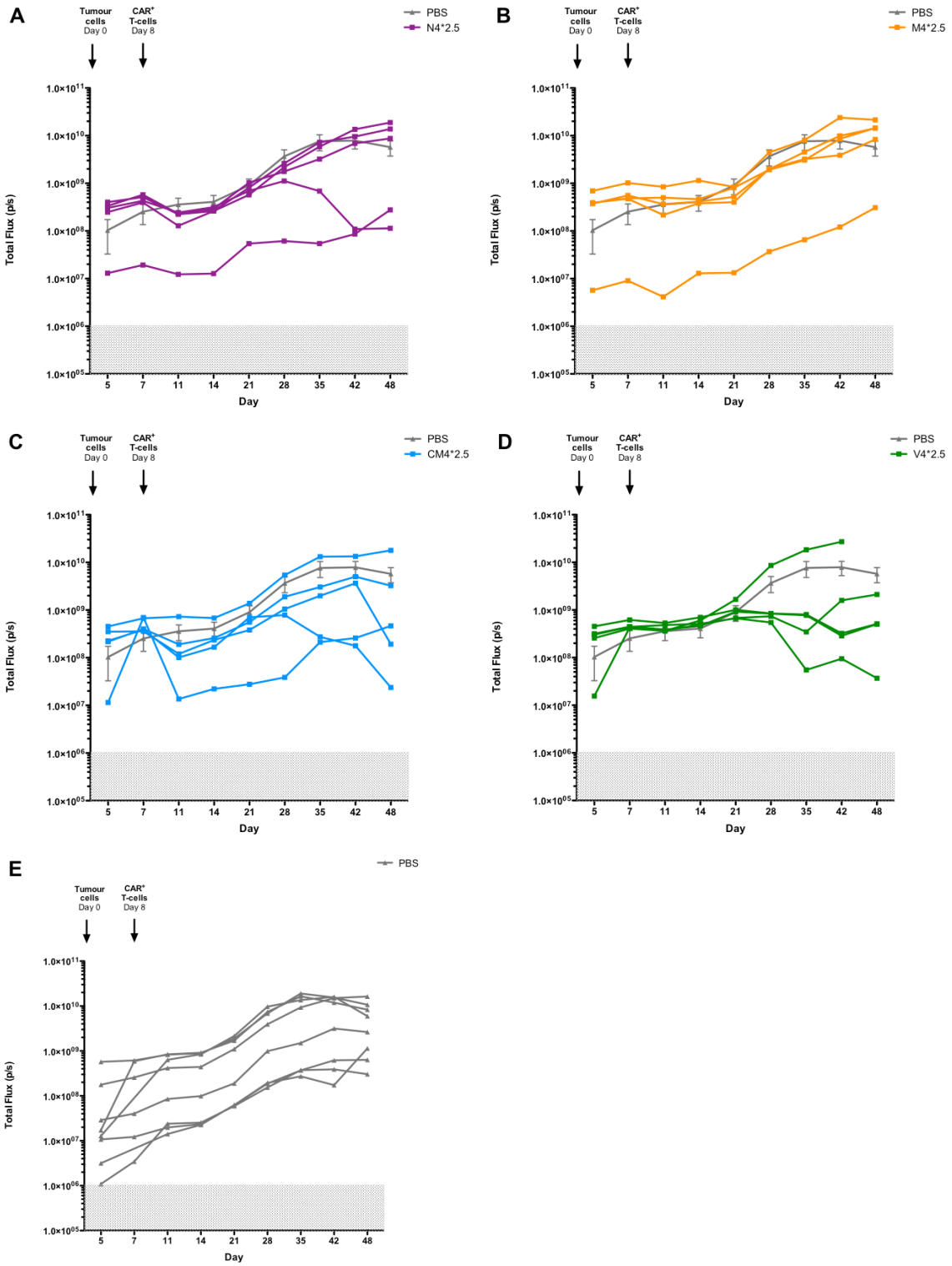

Figure 6-8. Bioluminescence imaging data for individual mice shown in Figure 6-7.
Total flux (p/s) emitted from each individual animal from treatment groups are plotted.

By contrast, treatment with the higher dose of 10 x 10^6 $N4^+$, $M4^+$ and $cM4^+$ CAR T-cells resulted in rapid and more pronounced anti-tumour activity (Figure 6-9; plots of individual mice shown in Figure 6-10). *In vivo* efficacy was only maintained by $cM4^+$ CAR T-cells, which exhibited a significant decrease in tumour burden compared to PBS only animals. Notably, a second phase of anti-tumour activity was observed with a number of the infused T-cell populations with onset between day 21 to day 28. This effect was most marked with $cM4^+$ CAR T-cells, leading to a steady and progressive decrease in tumour burden through to day 48 of the study. Similar albeit less pronounced and ill-sustained tumour regression activity was seen with UT and V4 T-cells, which is contrary to results observed *in vitro*.

Irrespective of the treatment T-cell population and dose administered, the average weight of each group was maintained or steadily increased over the course of the study, indicative of no serious toxicity (Figure 6-7 and Figure 6-9). However, animals from control groups and c-Met re-targeted CAR T-cell groups were euthanised upon symptoms potentially associated with GvHD, such as piloerection and physical hunching (Figure 6-11). However, similar clinical symptoms were also observed in control animals' euthanised due to tumour burden (Figure 6-11) therefore further assessment is required. Techniques such as H&E and IHC staining for immune cell infiltration, in addition to FACS analysis for CAR T-cells within the circulation would be essential before a weighted statement may be generated.

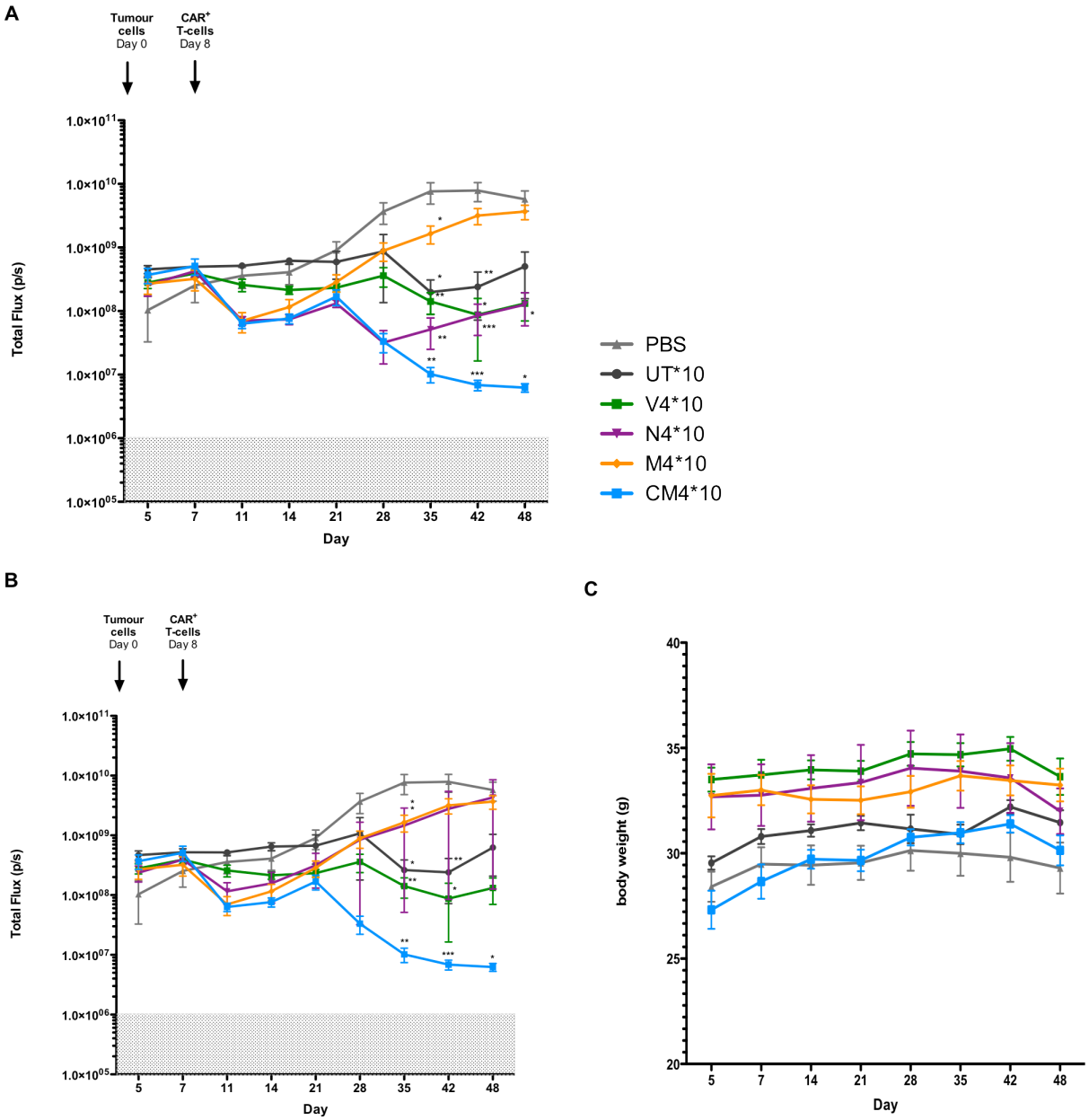

Figure 6-9. Anti-tumour activity of c-Met re-targeted CAR T-cells in mice with established REN LT MPM tumour xenografts (high treatment dose).
Mice were inoculated with 5 x 10^4 ffLuc expressing REN LT tumour cells i.p. Engraftment of tumour cells was confirmed via BLI imaging one day prior to T-cell transfer. $N4^+$, $M4^+$, $cM4^+$ and $V4^+$ T-cells (cultured in IL-4) (not corrected for transduction efficiency) were injected i.p. at a dose of 10 x 10^6 T-cells. **(A)** Serial BLI imaging was conducted throughout the study to assess baseline tumour growth and anti-tumour activity. Important – one animal from N4 group was excluded from data shown in this panel due to a presumed failed T-cell injection. Panel **(B)** shows all of the data with inclusion of the mouse in the N4 treatment group in which T-cell injection failure occurred. **(C)** Body weight (g) of all animals was measured throughout the study to monitor for potential toxicity. Data show mean ± SEM for n=5 mice per group (n=8 for PBS group).

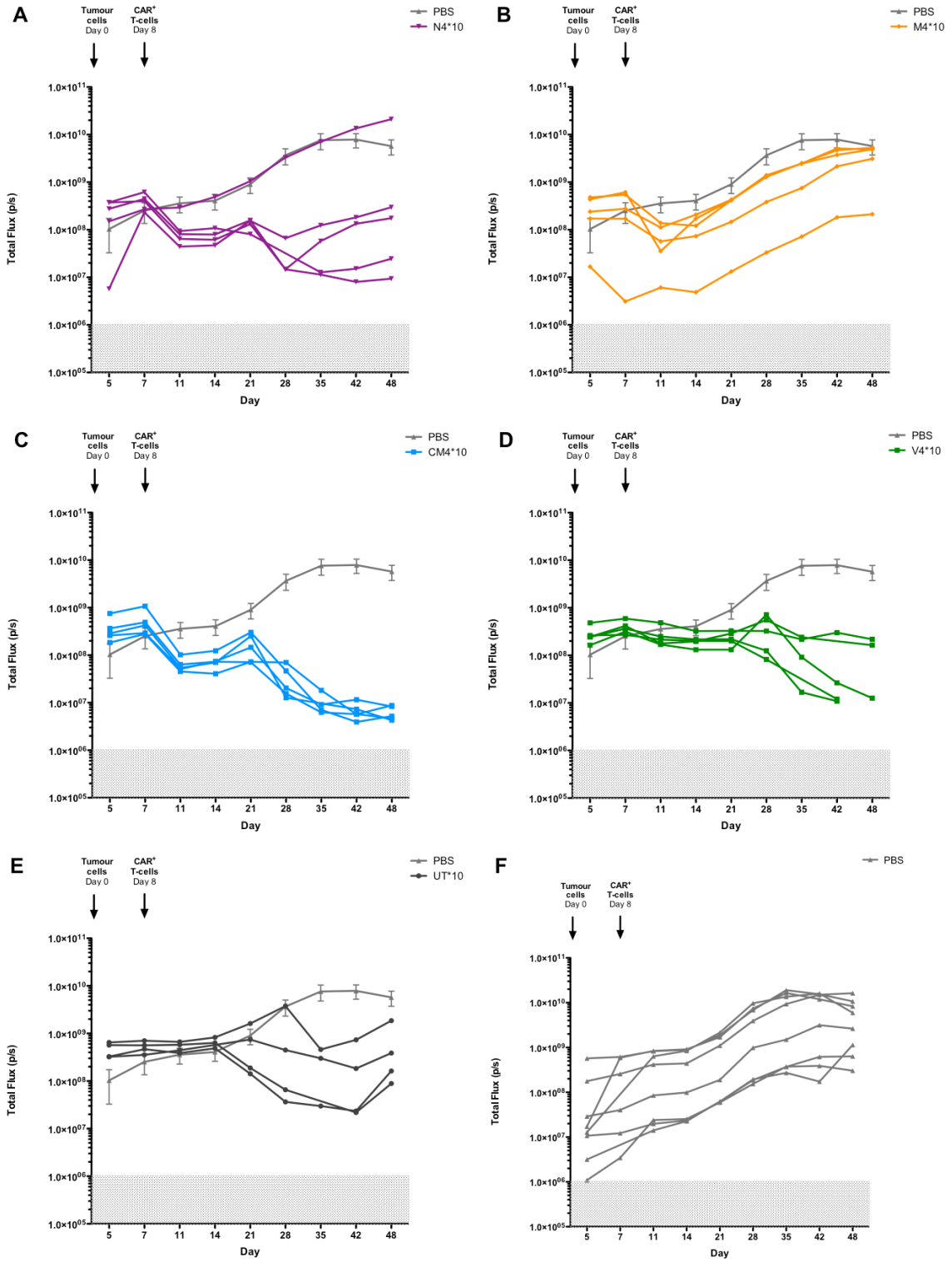

Figure 6-10. Bioluminescence imaging data for individual mice shown in Figure 6-9.
Total flux (p/s) for individual animals from each treatment groups are plotted.

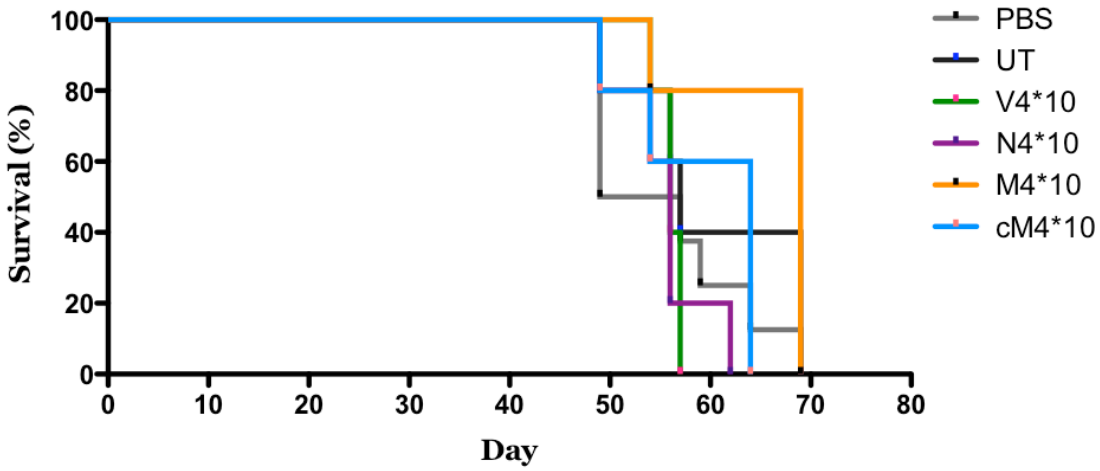

Figure 6-11. Kaplan – Meier survival curve for mice with established REN LT MPM tumour xenografts administered high treatment dose of c-Met re-targeted CAR$^+$ and control T-cells shown in Figure 6-9 and 6-10.
Mice were inoculated with 5 x 10^4 ffLuc expressing REN LT tumour cells i.p. N4$^+$, M4$^+$, cM4$^+$ and V4$^+$ T-cells (cultured in IL-4) (not corrected for transduction efficiency) were injected i.p. at a dose of 10 x 10^6 T-cells. Kaplan – Meier analysis determined using Graphpad Prism software. The x-axis shows days post tumour inoculation. Treatment was administered on Day 8.

6.3 Discussion

The overall aim of the work presented in this chapter was to evaluate the therapeutic activity of c-Met re-targeted CAR$^+$ T-cells following adoptive transfer to mice harbouring established c-Met expressing MPM xenografts. Consequently, the development of a suitable xenograft MPM mouse model was the first step required to undertake this work. To balance the need for experimental feasibility and clinical relevance, I explored the development of intraperitoneal (i.p.) xenograft models. Of the two (H28 LT and REN LT) MPM cell lines tested, only REN LT tumour cells engrafted stably. Similar i.p. models have previously been established in NSG mice in the pre-clinical development of a CAR targeted against Fibroblast Activation Protein (FAP) for treatment of MPM [377].

To investigate *in vivo* efficacy, N4, M4 and cM4$^+$ T-cells were adoptively transferred into NSG mice bearing established i.p. tumours and their subsequent effect upon tumour growth was investigated. T-cells were delivered directly to the peritoneal cavity since regional delivery means that T-cells are provided direct to the site of disease, maximising potential for efficacy and minimising risk of toxicity. The delayed administration of CAR T-cells, one week post tumour inoculation, meant that animals within each of the treatment groups had a similar established tumour burden. Using bioluminescence imaging, I monitored the evolution of tumour burden mice treated with c-Met re-targeted or control CAR T-cells, making comparison with UT T-cells, or PBS alone. At the lower treatment does of 2.5 x 10^6 T-cells (Figure 6-7 and 6-8), an initial modest decrease in signal was observed in both N4 and cM4 treatment groups. However, this reduction did not reach statistical significance. By contrast, at the higher treatment dose (Figure 6-9 and 6-10), c-Met re-targeted T-cells demonstrated rapid and significant anti-tumour activity compared to PBS, control CAR-engineered and UT T-cells treatment groups. The lowest level of tumour burden was observed in mice receiving cM4$^+$ T-cells in which progressive reduction in disease burden was seen over the duration of the study. This result contrasts with *in vitro* comparison of these CARs, which did not unmask any significant or reproducible difference between their anti-tumour activities.

Data presented in Chapter 4 of this thesis repeatedly demonstrate that neither UT nor V28z$^+$ T-cells mediate anti-tumour activity against MPM cells *in vitro*, indicated by failure to induce tumour cell killing or cytokine release. However, the *in vivo* study presented here clearly shows a significant delay in tumour progression in mice treated with V4$^+$ T-cells (day 14/21 onwards) and UT T-cells (day 28 onwards) when compared

to those receiving PBS (Figure 6-9 and Figure 6-10). The exact reason for this unexpected activity is unclear at this stage. When investigating the anti-tumour potential of MUC-1 retargeted [378] or ErbB retargeted CAR T-cells [241], truncated signalling constructs did cause delay in tumour growth. Such an effect could have been mediated by the ability of the control CAR to promote co-localisation of the T-cells and tumour cells. However, this would not be expected with untransduced T-cells or with V4 CAR engineered T-cells, in which the targeting moiety lacks any known binding activity. Alternatively, one could speculate that alloreactivity of these control T-cell groups might have contributed importantly to anti-tumour activity. It is well known that human T-cells can engraft in NSG mice and that xenogeneic graft versus host disease may occur after several weeks. Consequently, it can be speculated that recognition of human alloantigens in the MPM tumour xenograft could have selected for alloreactive T-cells within the untransduced and V4-engineered control groups. Such an effect could also have contributed to efficacy of $cM4^+$ and $N4^+$ T-cell groups, perhaps explaining the second wave of therapeutic activity seen after day 21. It is unclear why this effect was not seen with $M4^+$ T-cells. Irrespective of mechanism, this result highlights the differences that may be observed between *in vitro* and *in vivo* studies, thereby clearly demonstrating the importance for relevant animal xenograft models.

There are a number of possible explanation for the superior activity of $cM4^+$ T-cells compared to the other c-Met re-targeted CAR T-cell groups. First, it would be interesting to investigate the *in vivo* survival and expansion of these T-cells, making comparison with appropriate control groups. A second possibility relates to the stability of the cM4 targeting peptide, which has been reported to be increased compared to the IK1 parental peptide. Enhanced stability of CAR expression within transduced T-cells *in vivo* may have contributed to increased anti-tumour activity in a manner that was not seen in short-term *in vitro* studies. Third, it is possible that cM28z T-cells are more resistant to activation-induced cell death or to induction of anergy, upon repeated *in vivo* stimulation with tumour. These possibilities could be studied by repeated *in vitro* stimulation of c-Met re-targeted CAR T-cells on MPM tumour cell monolayers and by *in vivo* imaging of these CAR T-cells in tumour-bearing mice. The latter could be accomplished by dual bioluminescence imaging, whereby a luciferase that employs a distinct substrate (e.g. renilla luciferase) is co-expressed with the CAR in adoptively infused T-cells. Such an approach would allow separate BLI analysis of tumour and CAR T-cell status following administration of the relevant substrates (coelenterazine and d-luciferin respectively) (Whilding & Maher, unpublished data).

CHAPTER 7 General Discussion

7.1 Overview and synthesis

The overall aim of this PhD was to investigate whether primary human T-cells could be genetically re-targeted against c-Met and whether this approach could be developed as a novel therapy for MPM.

A panel of three c-Met re-targeted CARs were engineered. Targeting was achieved using stabilised derivatives of NK1, the smallest splice variant of HGF that is known to bind to c-Met. A second generation CAR signalling framework was used, comprising a fusion of the CD28 co-stimulatory endodomain placed upstream of that derived from human CD3ζ [261].

A fundamental starting point in the *in vitro* characterisation of these CARs was the demonstration that they could be stably expressed at the cell surface of primary human T-cells. Next, targeting specificity for c-Met was validated using a panel of aAPC murine fibroblast NIH 3T3 cells that had been genetically engineered to express c-Met and/or its best characterised co-factor, CD44v6. Specificity of targeting was confirmed by the demonstration that all three candidate CARs could enable human T-cells to elicit specific destruction of Met-expressing target cells in co-cultures. Cell lysis was accompanied by CAR T-cell activation as indicated by cytokine production (IL-2 and IFN-γ).

Next, I evaluated the cytotoxic potential of these candidate CARs against immortalised MPM tumour cell lines. Variance in activation and cytotoxicity of CAR T-cells against a panel of four c-Met-expressing MPM cell lines was evident. This may reflect intrinsic differences in the susceptibility of these tumour cells to cytotoxic destruction since all four cell lines expressed readily detectable levels of c-Met. Although enhanced activation was seen when c-Met and CD44v6 were co-expressed by NIH3T3 cells, this was not observed when stimulation was provided by c-Met expressing tumour cells. While all four cell lines were negative for CD44v6, they did express alternative co-factors such as Syndecan-1 and ICAM-1, which may have compensated for this. Enhanced anti-tumour activity of c-Met re-targeted CAR T-cells was clearly observed when higher efficiency gene transfer was attained, manifesting as destruction of MPM cells derived from both epithelioid and sarcomatoid mesotheliomas.

In light of the variability in tumour cell destruction observed, I next investigated if cisplatin and/or pemetrexed chemotherapy could enhance sensitivity of MPM tumour cells to killing by c-Met re-targeted CAR T-cells. These cytotoxic agents were selected since they are commonly used in combination to treat patients with MPM. Furthermore, platinum-based chemotherapy has recently been shown to sensitise ovarian tumour cells to destruction by ErbB re-targeted CAR T-cells [350]. In keeping with that earlier study, an increase in the activation of c-Met re-targeted T-cells was not observed following chemotherapy pre-treatment. Nonetheless, a modest increase in the lysis of some MPM cell lines was detected after their exposure to poorly cytotoxic doses of cisplatin and pemetrexed. This finding encouraged me to investigate alternative combinatorial approaches that might prove more effective upon *in vitro* testing. The use of checkpoint inhibitors targeting CTLA-4 and PD-1/PD-L1 has yielded impressive results in certain solid tumours, providing an opportunity for combinatorial therapy with CAR T-cells [109, 351, 379]. Pembrolizumab is a PD-1 inhibitor that achieved promising preliminary results in a small phase I study of MPM patients (76% overall disease control and 28% partial response), supporting the potential combined use of this agent with c-Met re-targeted CAR T-cells [112]. During this PhD, no significant increase in activation of c-Met re-targeted CAR^+ T-cells was observed in the presence of pembrolizumab. By contrast, a modest but significant enhancement of killing of one intrinsically unresponsive MPM cell line (epithelial) by c-Met re-targeted CAR T-cells was observed in the presence of pembrolizumab. Further studies analysing c-Met re-targeted CAR T-cell activation upon repeated exposure to target antigen, including an analysis of differentiation and exhaustion marker expression by c-Met re-targeted CAR T-cells in addition to suitable *in vivo* modelling would broaden the analytical scope of this approach. Additional studies targeting PD-L2 and other checkpoint molecules such as LAG-3 and TIM-3 would also lay the foundation for selecting the optimal combination therapies for MPM.

The final aim of this thesis was to characterise the therapeutic potential of c-Met re-targeted CAR T-cells in an *in vivo* setting. In light of the modest effect of chemotherapy pre-sensitisation and immune checkpoint blockade when combined with c-Met re-targeted CAR T-cells *in vitro*, I elected to move to *in vivo* studies using CAR T-cells alone. A crucial observation in the evaluation of these engineered T-cells was that $N4^+$ and $cM4^+$ T-cells retain their anti-tumour activity *in vivo*. Using a xenograft model based upon the REN MPM cell line, tumour regression was observed in both $N4^+$ and $cM4^+$ T-cell treated mice. $cM4^+$ T-cell treated animals showed the most significant reduction of tumour burden. This contrasts with the result of *in vitro* studies that did not discriminate between the anti-tumour activity of all three candidate c-Met-specific CARs. The superior anti-tumour activity by $cM4^+$ T-cells compared to $N4^+$ and $M4^+$ T-cells warrants further investigation. Although beyond the scope of this thesis, it would be of interest to

undertake *in vivo* T-cell imaging studies to investigate whether differences in longevity between the panel of c-Met re-targeted CARs was of relevance to this observation. Blood analysis for circulating CAR$^+$ T-cells in addition to enhanced sensitivity qPCR analysis would also provide further insight into this possibility.

7.1 Previous attempts to engineer c-Met re-targeted CAR$^+$ T-cells

The targeting strategy employed in this PhD to engineer c-Met re-targeted CAR$^+$ T-cells involved the use of a derivative of HGF, the sole natural ligand for c-Met. Recently, an alternative approach using an scFv derived c-Met re-targeted CAR was described by Frigault *et al* [327]. CAR expression was achieved in human T-cells either using transient mRNA transfection or lentiviral transduction, enabling the authors to test a variety of co-stimulatory domains (CD28, 4-1BB and ICOS). Using cytotoxicity assays, they demonstrated that scFv re-targeted c-Met re-targeted CAR T-cells could mediate target-dependent tumour cell lysis *in vitro*. Unexpectedly however, when the CAR contained a CD28/CD3ζ second-generation endodomain, it exhibited constitutive activity that resulted in accelerated T-cell differentiation, expression of exhaustion markers and impaired anti-tumour activity. This constitutive activity could be circumvented by expression of the CAR at lower levels in T-cells, using a weaker promoter system. Nonetheless, even with the implementation of this solution, the CAR performed poorly when evaluated *in vivo* in mice bearing a c-Met-expressing ovarian Skov-3 xenograft. The non-constitutively active CAR T-cells achieved comparable anti-tumour activity to control CD19-targeted CAR T-cells, while the constitutively active CAR performed considerably less well than the control [327]. Infiltration of tumours by c-Met re-targeted (non-constitutive CAR) and CD19 re-targeted control T-cells were similar, while poorer infiltration was seen with the constitutively active c-Met re-targeted CAR$^+$ T-cells. These data indicate that a strong alloreactive effect was operative in this model, without any significant further enhancement of anti-tumour activity by the c-Met re-targeted CAR. Such a finding resonates with the evidence presented in chapter 6 of this thesis that alloreactivity may contribute to anti-tumour activity of CAR engineered T-cells against tumour xenografts that have been established in NSG mice. Nonetheless, I observed a significant further decrease in tumour burden when N4$^+$ or cM4$^+$ CAR$^+$ T-cells were administered to NSG mice engrafted with a REN LT MPM tumour xenograft, making comparison with control CAR or untransduced T-cells. Consequently, these data represent the first evidence that c-Met re-targeted CAR$^+$ T-cells can mediate specific anti-tumour activity *in vivo*.

7.2 Alternative CAR T-cell targets in mesothelioma

7.2.1 Mesothelin

There have been a number of other studies that have investigated the development of CAR T-cell immunotherapy for MPM. Adusumilli *et al.* reported potent anti-tumour activity with an scFv-derived mesothelin (MSLN) targeted second generation CAR (CD28/CD3ζ) [235]. Impressively, the authors established an intra-pleural mouse model of MPM, enabling accurate assessment of systemic and regional delivery of CAR T-cells. The latter overcame barriers to tumour homing that otherwise limit CAR T-cell immunotherapy of solid tumours. Systemic delivery resulted in CAR T-cells being sequestered in the lungs, delaying entry to the pleural tumour. By contrast, MSLN CAR T-cells administered intrapleurally eradicated established MPM tumours at 30-fold lower doses compared to systemic CAR T-cell delivery [235]. This approach is currently under evaluation in a phase I clinical trial (NCT02414269). The use of a similar orthotopic model was not selected in this PhD for the reasons outlined in section 6.1.2. Similarly, a clinical trial using SS1-antibody-derived MSLN CAR T-cells is currently being evaluated in a Phase I study at the University of Pennsylvania (NCT02159716), in patients with solid malignancies, some of which are MPM^{+}.

7.2.2 Fibroblast activation protein-α

The tumour-associated stroma has been reported to occupy up to 90% of the tumour volume and its role in initiating and sustaining tumour growth is the subject of great interest from the perspective of possible therapeutic intervention [380]. Cancer-associated fibroblasts (CAFs) are a key component of the tumour-associated stroma, significantly influencing the formation of a highly pro-tumourigenic and immunosuppressive microenvironment [381]. Fibroblast-activation protein-α (FAP) is predominantly expressed on the surface of reactive tumour-associated fibroblasts and is also expressed by MPM tumour cells [382]. Additionally, expression has recently also been reported by tumour-associated macrophages (TAMs) [383]. CAR T-cells targeting tumour-associated antigens (TAA) often fail to eradicate CAFs, which may potentiate tumour progression directly via paracrine secretion of cytokines and growth factors. Following acceptable pre-clinical functionality with a second-generation (CD28/CD3ζ) CAR, the clinical evaluation of FAP CAR T-cells in MPM patients is currently ongoing (NCT01722149). This Phase I study is assessing the safety and feasibility of delivering FAP CAR T-cells directly into the pleural cavity via a pleural catheter [384]. Results from the first patient treated with this approach were reported. In combination with three

cycles of chemotherapy, 1 x 10^6 $CD8^+$ FAP CAR T-cells were injected and no adverse events due to CAR T-cells were observed [384].

7.3 Limitations of c-Met re-targeted CAR^+ T-cell immunotherapy of mesothelioma and possible next steps

7.3.1 Loss of efficacy through antigen loss

Recent clinical data has highlighted the risk of antigen escape leading to disease relapse following CD19 CAR T-cell immunotherapy of acute lymphoblastic leukaemia [298]. Theoretically, this risk also applies to use of CAR T-cells that are directed against other single targets, such as c-Met, FAP or mesothelin. Countering this is the fact that c-Met contributes to disease pathogenesis in MPM (section 1.4) and consequently it would expected to be subject to selective pressure within the tumour for maintained expression. A number of alternative approaches have also been proposed which may help to minimise this risk further. For example, a recent study has described the design of a dual-specific "TanCAR", which recognises two distinct target antigens independently. Engagement of either antigen results in CAR T-cell activation, although greater activation is reported when both antigens are bound simultaneously [385].

7.3.2 Risk of toxicity

An alternative risk associated with the use of c-Met re-targeted CAR^+ T-cell immunotherapy is the risk of on-target off tumour toxicity. This reflects the fact that c-Met is expressed at lower levels in healthy tissues, such as the liver. Previous experience with systemic delivery of CAR T-cells for solid tumours (CAIX- and HER2- targeted) has resulted in serious [304] and lethal [300] toxicity respectively. As alluded to above, since MPM spreads mainly by loco-regional progression in the pleural or peritoneal cavity, regional delivery systems provide a theoretically attractive approach to maximise delivery to the site of disease while minimising risk of toxicity. Human HGF exerts biological activity on mouse cells that express the c-Met receptor [386, 387]. Consequently, it is possible that the CARs described in this project are also able to engage the mouse orthologue of c-Met. Further studies are warranted to investigate this possibility, since confirmation of strong biological activity against mouse c-Met would support the undertaking of safety testing of human c-Met re-targeted CAR^+ T-cells in immune compromised mice. Such an approach has been used to obtain regulatory approval to treat patients with head and neck cancer using an ErbB-specific CAR [299].

In additional to regional delivery, an alternative approach that may reduce risk of toxicity involves the separation of signalling domains between dual-expressed CARs targeting different antigens. Such systems can be designed to ensure that maximal activation of CAR T-cells occurs when both targets are engaged simultaneously, thereby increasing precision of tumour targeting. This strategy was initially exemplified by Wilkie *et al.*, with an ErbB2- and MUC1- specific CAR that signalled through CD3ζ and CD28, respectively [280]. Functional co-expression was demonstrated against target cells expressing multiple combinations and densities of the respective antigens. *In vitro* tumour cell lysis and efficient T-cell proliferation was only achieved upon interaction with target cells expressing both target antigens. However, significant cytotoxicity was observed when target cells expressed ErbB2 alone. This limitation was subsequently overcome by Kloss *et al.*, who developed a dual targeting CAR with similar signalling domains and targeted against two prostate cancer antigens, namely prostate-specific membrane antigen and prostate-specific stem cell antigen. [281]. They exploited a low affinity targeting moiety that was coupled to CD3ζ alone, meaning that cytotoxicity was not seen unless the second fusion receptor (coupled to CD28) was bound simultaneously. In MPM, dual targeting strategies can be envisioned in which targeting of c-Met and mesothelin or FAP is titrated to maximise immune attack within the tumour while minimising risk of toxicity to healthy tissues.

7.4 Conclusions

Taken together, the data presented in this thesis show that CAR-modified T-cells can be successfully re-directed against c-Met, achieving sustained anti-tumour activity both *in vitro* and *in vivo*. This is accompanied by greater cytokine secretion (IL-2 and IFN-γ). Furthermore, *in vivo* assessment of c-Met CARs has suggested that cM4 CAR^+ T-cells are superior in comparison to N4 and M4 CAR^+ T-cells resulting in a decrease in tumour burden. These encouraging findings warrant further investigation into the translational application of this technology against the unmet need of patients with mesothelioma.

CHAPTER 8 REFERENCES

1. *Pleural Mesothelioma.* http://www.mesothelioma.com/mesothelioma/types/pleural.htm, updated 2016.
2. McDonald, J.C. and A.D. McDonald, *The epidemiology of mesothelioma in historical context.* Eur Respir J, 1996. **9**(9): p. 1932-42.
3. Selikoff, I.J., E.C. Hammond, and H. Seidman, *Latency of asbestos disease among insulation workers in the United States and Canada.* Cancer, 1980. **46**(12): p. 2736-40.
4. Mott, F.E., *Mesothelioma: a review.* Ochsner J, 2012. **12**(1): p. 70-9.
5. Robinson, B.M., *Malignant pleural mesothelioma: an epidemiological perspective.* Ann Cardiothorac Surg, 2012. **1**(4): p. 491-6.
6. Henley, S.J., et al., *Mesothelioma incidence in 50 states and the District of Columbia, United States, 2003-2008.* Int J Occup Environ Health, 2013. **19**(1): p. 1-10.
7. http://www.hse.gov.uk/Statistics/causdis/mesothelioma/index.htm.
8. Peto, J., et al., *The European mesothelioma epidemic.* Br J Cancer, 1999. **79**(3-4): p. 666-72.
9. Hodgson, J.T., et al., *The expected burden of mesothelioma mortality in Great Britain from 2002 to 2050.* Br J Cancer, 2005. **92**(3): p. 587-93.
10. World Health Organisation (WHO). Elimination of asbestos-related diseases. Geneva: WHO, h.w.w.i.h.W.S.O.e.p.A.N., http://whqlibdoc.who.int/hq/2006/WHO_SDE_OEH_06.03_eng.pdf *Accessed November 10th, 2013.* .
11. Testa, J.R., et al., *Germline BAP1 mutations predispose to malignant mesothelioma.* Nat Genet, 2011. **43**(10): p. 1022-5.
12. Goodman, J.E., M.A. Nascarella, and P.A. Valberg, *Ionizing radiation: a risk factor for mesothelioma.* Cancer Causes Control, 2009. **20**(8): p. 1237-54.
13. Jasani, B. and A. Gibbs, *Mesothelioma not associated with asbestos exposure.* Arch Pathol Lab Med, 2012. **136**(3): p. 262-7.
14. Cacciotti, P., et al., *SV40 replication in human mesothelial cells induces HGF/Met receptor activation: a model for viral-related carcinogenesis of human malignant mesothelioma.* Proc Natl Acad Sci U S A, 2001. **98**(21): p. 12032-7.
15. Cristaudo, A., et al., *SV40 enhances the risk of malignant mesothelioma among people exposed to asbestos: a molecular epidemiologic case-control study.* Cancer Res, 2005. **65**(8): p. 3049-52.
16. Hammond, E.C., I.J. Selikoff, and H. Seidman, *Asbestos exposure, cigarette smoking and death rates.* Ann N Y Acad Sci, 1979. **330**: p. 473-90.
17. Sakamoto, Y., et al., *Induction of mesothelioma by a single intrascrotal administration of multi-wall carbon nanotube in intact male Fischer 344 rats.* J Toxicol Sci, 2009. **34**(1): p. 65-76.
18. Jaurand, M.C., A. Renier, and J. Daubriac, *Mesothelioma: Do asbestos and carbon nanotubes pose the same health risk?* Part Fibre Toxicol, 2009. **6**: p. 16.
19. Mossman, B.T., et al., *New insights into understanding the mechanisms, pathogenesis, and management of malignant mesotheliomas.* Am J Pathol, 2013. **182**(4): p. 1065-77.
20. Sekido, Y., *Molecular pathogenesis of malignant mesothelioma.* Carcinogenesis, 2013. **34**(7): p. 1413-9.
21. Carbone, M. and H. Yang, *Molecular pathways: targeting mechanisms of asbestos and erionite carcinogenesis in mesothelioma.* Clin Cancer Res, 2012. **18**(3): p. 598-604.
22. Sekido, Y., *Genomic abnormalities and signal transduction dysregulation in malignant mesothelioma cells.* Cancer Sci, 2010. **101**(1): p. 1-6.
23. Ou, W.B., et al., *Targeted inhibition of multiple receptor tyrosine kinases in mesothelioma.* Neoplasia, 2011. **13**(1): p. 12-22.

24. Miettinen, M., et al., *Vascular endothelial growth factor receptor 2 as a marker for malignant vascular tumors and mesothelioma: an immunohistochemical study of 262 vascular endothelial and 1640 nonvascular tumors.* Am J Surg Pathol, 2012. **36**(4): p. 629-39.
25. Liu, G., P. Cheresh, and D.W. Kamp, *Molecular basis of asbestos-induced lung disease.* Annu Rev Pathol, 2013. **8**: p. 161-87.
26. Dostert, C., et al., *Innate immune activation through Nalp3 inflammasome sensing of asbestos and silica.* Science, 2008. **320**(5876): p. 674-7.
27. Wang, Y., et al., *Interleukin-1beta and tumour necrosis factor-alpha promote the transformation of human immortalised mesothelial cells by erionite.* Int J Oncol, 2004. **25**(1): p. 173-8.
28. Chow, M.T., et al., *NLRP3 promotes inflammation-induced skin cancer but is dispensable for asbestos-induced mesothelioma.* Immunol Cell Biol, 2012. **90**(10): p. 983-6.
29. Yang, H., et al., *Programmed necrosis induced by asbestos in human mesothelial cells causes high-mobility group box 1 protein release and resultant inflammation.* Proc Natl Acad Sci U S A, 2010. **107**(28): p. 12611-6.
30. Heintz, N.H., Y.M. Janssen-Heininger, and B.T. Mossman, *Asbestos, lung cancers, and mesotheliomas: from molecular approaches to targeting tumor survival pathways.* Am J Respir Cell Mol Biol, 2010. **42**(2): p. 133-9.
31. *Mesothelioma Histology - cell types.* http://www.asbestos.com/mesothelioma/histology.php.
32. Husain, A.N., et al., *Guidelines for pathologic diagnosis of malignant mesothelioma: 2012 update of the consensus statement from the International Mesothelioma Interest Group.* Arch Pathol Lab Med, 2013. **137**(5): p. 647-67.
33. Yaziji, H., et al., *Evaluation of 12 antibodies for distinguishing epithelioid mesothelioma from adenocarcinoma: identification of a three-antibody immunohistochemical panel with maximal sensitivity and specificity.* Mod Pathol, 2006. **19**(4): p. 514-23.
34. Wittekind CH, G.F., Hutter RVP et al, ed. Illustrated Guide to the TMN Classification of and S.B.-. Malignant Tumours. 5th ed. TNM Atlas2004.
35. Edge, S.B. and C.C. Compton, *The American Joint Committee on Cancer: the 7th edition of the AJCC cancer staging manual and the future of TNM.* Ann Surg Oncol, 2010. **17**(6): p. 1471-4.
36. Steele, J.P., *Prognostic factors for mesothelioma.* Hematol Oncol Clin North Am, 2005. **19**(6): p. 1041-52, vi.
37. Herndon, J.E., et al., *Factors predictive of survival among 337 patients with mesothelioma treated between 1984 and 1994 by the Cancer and Leukemia Group B.* Chest, 1998. **113**(3): p. 723-31.
38. Curran, D., et al., *Prognostic factors in patients with pleural mesothelioma: the European Organization for Research and Treatment of Cancer experience.* J Clin Oncol, 1998. **16**(1): p. 145-52.
39. Hasenclever, D. and V. Diehl, *A prognostic score for advanced Hodgkin's disease. International Prognostic Factors Project on Advanced Hodgkin's Disease.* N Engl J Med, 1998. **339**(21): p. 1506-14.
40. Ray-Coquard, I., et al., *Lymphopenia as a prognostic factor for overall survival in advanced carcinomas, sarcomas, and lymphomas.* Cancer Res, 2009. **69**(13): p. 5383-91.
41. Ceze, N., et al., *Pre-treatment lymphopenia as a prognostic biomarker in colorectal cancer patients receiving chemotherapy.* Cancer Chemother Pharmacol, 2011. **68**(5): p. 1305-13.
42. Chanmee, T., et al., *Tumor-associated macrophages as major players in the tumor microenvironment.* Cancers (Basel), 2014. **6**(3): p. 1670-90.
43. Schmidt, H., et al., *Elevated neutrophil and monocyte counts in peripheral blood are associated with poor survival in patients with metastatic melanoma: a prognostic model.* Br J Cancer, 2005. **93**(3): p. 273-8.

44. Lee, Y.Y., et al., *Prognostic value of pre-treatment circulating monocyte count in patients with cervical cancer: comparison with SCC-Ag level.* Gynecol Oncol, 2012. **124**(1): p. 92-7.
45. Koh, Y.W., et al., *Absolute monocyte count predicts overall survival in mantle cell lymphomas: correlation with tumour-associated macrophages.* Hematol Oncol, 2014. **32**(4): p. 178-86.
46. Nishijima, T.F., et al., *Prognostic value of lymphocyte-to-monocyte ratio in patients with solid tumors: A systematic review and meta-analysis.* Cancer Treat Rev, 2015. **41**(10): p. 971-8.
47. Yamagishi, T., et al., *Prognostic significance of the lymphocyte-to-monocyte ratio in patients with malignant pleural mesothelioma.* Lung Cancer, 2015. **90**(1): p. 111-7.
48. Tanrikulu, A.C., et al., *Prognostic value of the lymphocyte-to-monocyte ratio and other inflammatory markers in malignant pleural mesothelioma.* Environ Health Prev Med, 2016.
49. Hoda, M.A., et al., *Circulating activin A is a novel prognostic biomarker in malignant pleural mesothelioma - A multi-institutional study.* Eur J Cancer, 2016. **63**: p. 64-73.
50. Roncella, S., et al., *CTLA-4 in mesothelioma patients: tissue expression, body fluid levels and possible relevance as a prognostic factor.* Cancer Immunol Immunother, 2016.
51. Lang-Lazdunski, L., *Surgery for malignant pleural mesothelioma: why, when and what?* Lung Cancer, 2014. **84**(2): p. 103-9.
52. Treasure, T., et al., *Extra-pleural pneumonectomy versus no extra-pleural pneumonectomy for patients with malignant pleural mesothelioma: clinical outcomes of the Mesothelioma and Radical Surgery (MARS) randomised feasibility study.* Lancet Oncol, 2011. **12**(8): p. 763-72.
53. Vogelzang, N.J., et al., *Phase III study of pemetrexed in combination with cisplatin versus cisplatin alone in patients with malignant pleural mesothelioma.* J Clin Oncol, 2003. **21**(14): p. 2636-44.
54. van Meerbeeck, J.P., et al., *Randomized phase III study of cisplatin with or without raltitrexed in patients with malignant pleural mesothelioma: an intergroup study of the European Organisation for Research and Treatment of Cancer Lung Cancer Group and the National Cancer Institute of Canada.* J Clin Oncol, 2005. **23**(28): p. 6881-9.
55. Haas, A.R. and D.H. Sterman, *Novel intrapleural therapies for malignant diseases.* Respiration, 2012. **83**(4): p. 277-92.
56. Hassan, R., et al., *Major cancer regressions in mesothelioma after treatment with an anti-mesothelin immunotoxin and immune suppression.* Sci Transl Med, 2013. **5**(208): p. 208ra147.
57. Hegmans, J.P., et al., *Consolidative dendritic cell-based immunotherapy elicits cytotoxicity against malignant mesothelioma.* Am J Respir Crit Care Med, 2010. **181**(12): p. 1383-90.
58. O'Brien, M.E., et al., *Phase II study of first-line bortezomib and cisplatin in malignant pleural mesothelioma and prospective validation of progression free survival rate as a primary end-point for mesothelioma clinical trials (European Organisation for Research and Treatment of Cancer 08052).* Eur J Cancer, 2013. **49**(13): p. 2815-22.
59. Buikhuisen, W.A., et al., *Thalidomide versus active supportive care for maintenance in patients with malignant mesothelioma after first-line chemotherapy (NVALT 5): an open-label, multicentre, randomised phase 3 study.* Lancet Oncol, 2013. **14**(6): p. 543-51.
60. Garland, L.L., et al., *Phase II study of cediranib in patients with malignant pleural mesothelioma: SWOG S0509.* J Thorac Oncol, 2011. **6**(11): p. 1938-45.
61. Nowak, A.K., et al., *A phase II study of intermittent sunitinib malate as second-line therapy in progressive malignant pleural mesothelioma.* J Thorac Oncol, 2012. **7**(9): p. 1449-56.
62. Papa, S., et al., *Phase 2 study of sorafenib in malignant mesothelioma previously treated with platinum-containing chemotherapy.* J Thorac Oncol, 2013. **8**(6): p. 783-7.
63. Porpodis, K., et al., *Malignant pleural mesothelioma: current and future perspectives.* J Thorac Dis, 2013. **5**(Suppl 4): p. S397-S406.

64. Sugarbaker, D.J., et al., *Resection margins, extrapleural nodal status, and cell type determine postoperative long-term survival in trimodality therapy of malignant pleural mesothelioma: results in 183 patients.* J Thorac Cardiovasc Surg, 1999. **117**(1): p. 54-63; discussion 63-5.
65. Flores, R.M., et al., *Extrapleural pneumonectomy versus pleurectomy/decortication in the surgical management of malignant pleural mesothelioma: results in 663 patients.* J Thorac Cardiovasc Surg, 2008. **135**(3): p. 620-6, 626 e1-3.
66. van Thiel, E. and J.P. van Meerbeeck, *European guidelines for the management of malignant pleural mesothelioma.* Pol Arch Med Wewn, 2010. **120**(12): p. 503-10.
67. Scherpereel, A., et al., *Guidelines of the European Respiratory Society and the European Society of Thoracic Surgeons for the management of malignant pleural mesothelioma.* Eur Respir J, 2010. **35**(3): p. 479-95.
68. Treasure, T., et al., *The MARS trial: mesothelioma and radical surgery.* Interact Cardiovasc Thorac Surg, 2006. **5**(1): p. 58-9.
69. Treasure, T., et al., *The Mesothelioma and Radical surgery randomized controlled trial: the Mars feasibility study.* J Thorac Oncol, 2009. **4**(10): p. 1254-8.
70. Kao, S.C., et al., *Patterns of care for malignant pleural mesothelioma patients compensated by the Dust Diseases Board in New South Wales, Australia.* Intern Med J, 2013. **43**(4): p. 402-10.
71. Ryan, C.W., J. Herndon, and N.J. Vogelzang, *A review of chemotherapy trials for malignant mesothelioma.* Chest, 1998. **113**(1 Suppl): p. 66S-73S.
72. Kindler, H.L., *Systemic treatments for mesothelioma: standard and novel.* Curr Treat Options Oncol, 2008. **9**(2-3): p. 171-9.
73. Muers, M.F., et al., *Active symptom control with or without chemotherapy in the treatment of patients with malignant pleural mesothelioma (MS01): a multicentre randomised trial.* Lancet, 2008. **371**(9625): p. 1685-94.
74. Zalcman, G., Mazieres, J., Margery, J., Greillier, L.,, C. Audigier-Valette, Moro-Siblot, D. et al., and *Bevacizumab 15mg/kg Plus cisplatin-pemetrexed (CP) triplet versus CP doublet in malignant pleural mesothelioma (MPM): results of the IFCTGFPC-0701 MAPS randomized phase 3 trial.* J Clin Oncol 33(Suppl.): abstract 7500., 2015.
75. Zalcman, G., et al., IFCT-GFPC-0701 MAPS trial, a multicenter randomized phase III trial of pemetrexed-cisplatin with or without bevacizumab in patients with malignant pleural mesothelioma (MPM). Journal of Clinical Oncology, 2012. 30(15).
76. Sorensen, J.B., et al., *Pemetrexed as second-line treatment in malignant pleural mesothelioma after platinum-based first-line treatment.* J Thorac Oncol, 2007. **2**(2): p. 147-52.
77. Jassem, J., et al., *Phase III trial of pemetrexed plus best supportive care compared with best supportive care in previously treated patients with advanced malignant pleural mesothelioma.* J Clin Oncol, 2008. **26**(10): p. 1698-704.
78. Ramalingam, S.S. and C.P. Belani, *Recent advances in the treatment of malignant pleural mesothelioma.* J Thorac Oncol, 2008. **3**(9): p. 1056-64.
79. Rusch, V.W., et al., *A phase II trial of surgical resection and adjuvant high-dose hemithoracic radiation for malignant pleural mesothelioma.* J Thorac Cardiovasc Surg, 2001. **122**(4): p. 788-95.
80. Komaki, R., et al., *Fatal pneumonitis associated with intensity-modulated radiation therapy for mesothelioma: in regard to Allen et al. (Int J Radiat Oncol Biol Phys 2006;65:640-645).* Int J Radiat Oncol Biol Phys, 2006. **66**(5): p. 1595-6; author reply 1596.
81. Kondola, S., D. Manners, and A.K. Nowak, *Malignant pleural mesothelioma: an update on diagnosis and treatment options.* Ther Adv Respir Dis, 2016.
82. Hanahan, D. and R.A. Weinberg, *Hallmarks of cancer: the next generation.* Cell, 2011. **144**(5): p. 646-74.
83. Janne, P.A., et al., *Inhibition of epidermal growth factor receptor signaling in malignant pleural mesothelioma.* Cancer Res, 2002. **62**(18): p. 5242-7.

84. Okuda, K., et al., *Epidermal growth factor receptor gene mutation, amplification and protein expression in malignant pleural mesothelioma.* J Cancer Res Clin Oncol, 2008. **134**(10): p. 1105-11.
85. Cortese, J.F., et al., *Common EGFR mutations conferring sensitivity to gefitinib in lung adenocarcinoma are not prevalent in human malignant mesothelioma.* Int J Cancer, 2006. **118**(2): p. 521-2.
86. Mezzapelle, R., et al., *Mutation analysis of the EGFR gene and downstream signalling pathway in histologic samples of malignant pleural mesothelioma.* Br J Cancer, 2013. **108**(8): p. 1743-9.
87. Kotova, S., R.M. Wong, and R.B. Cameron, *New and emerging therapeutic options for malignant pleural mesothelioma: review of early clinical trials.* Cancer Manag Res, 2015. **7**: p. 51-63.
88. Govindan, R., et al., *Gefitinib in patients with malignant mesothelioma: a phase II study by the Cancer and Leukemia Group B.* Clin Cancer Res, 2005. **11**(6): p. 2300-4.
89. Garland, L.L., et al., *Phase II study of erlotinib in patients with malignant pleural mesothelioma: a Southwest Oncology Group Study.* J Clin Oncol, 2007. **25**(17): p. 2406-13.
90. Jackman, D.M., et al., *Erlotinib plus bevacizumab in previously treated patients with malignant pleural mesothelioma.* Cancer, 2008. **113**(4): p. 808-14.
91. Masood, R., et al., *Malignant mesothelioma growth inhibition by agents that target the VEGF and VEGF-C autocrine loops.* Int J Cancer, 2003. **104**(5): p. 603-10.
92. Bagia, M. and A.K. Nowak, *Novel targeted therapies and vaccination strategies for mesothelioma.* Curr Treat Options Oncol, 2011. **12**(2): p. 149-62.
93. Cornelissen, R., et al., *New roads open up for implementing immunotherapy in mesothelioma.* Clin Dev Immunol, 2012. **2012**: p. 927240.
94. Izzi, V., et al., *Immunity and malignant mesothelioma: from mesothelial cell damage to tumor development and immune response-based therapies.* Cancer Lett, 2012. **322**(1): p. 18-34.
95. Yamada, N., et al., *CD8+ tumor-infiltrating lymphocytes predict favorable prognosis in malignant pleural mesothelioma after resection.* Cancer Immunol Immunother, 2010. **59**(10): p. 1543-9.
96. Leigh, R.A. and I. Webster, *Lymphocytic infiltration of pleural mesothelioma and its significance for survival.* S Afr Med J, 1982. **61**(26): p. 1007-9.
97. Anraku, M., et al., *Impact of tumor-infiltrating T cells on survival in patients with malignant pleural mesothelioma.* J Thorac Cardiovasc Surg, 2008. **135**(4): p. 823-9.
98. Mudhar, H.S., P.M. Fisher, and W.A. Wallace, *No relationship between tumour infiltrating lymphocytes and overall survival is seen in malignant mesothelioma of the pleura.* Eur J Surg Oncol, 2002. **28**(5): p. 564-5.
99. Hodi, F.S., et al., *Improved survival with ipilimumab in patients with metastatic melanoma.* N Engl J Med, 2010. **363**(8): p. 711-23.
100. Lesterhuis, W.J., et al., *Synergistic effect of CTLA-4 blockade and cancer chemotherapy in the induction of anti-tumor immunity.* PLoS One, 2013. **8**(4): p. e61895.
101. Wu, L., et al., *CTLA-4 blockade expands infiltrating T cells and inhibits cancer cell repopulation during the intervals of chemotherapy in murine mesothelioma.* Mol Cancer Ther, 2012. **11**(8): p. 1809-19.
102. Calabro, L., et al., *Tremelimumab for patients with chemotherapy-resistant advanced malignant mesothelioma: an open-label, single-arm, phase 2 trial.* Lancet Oncol, 2013. **14**(11): p. 1104-11.
103. Zucali, P.A., et al., *Second-line chemotherapy in malignant pleural mesothelioma: results of a retrospective multicenter survey.* Lung Cancer, 2012. **75**(3): p. 360-7.
104. Calabro, L., et al., *Efficacy and safety of an intensified schedule of tremelimumab for chemotherapy-resistant malignant mesothelioma: an open-label, single-arm, phase 2 study.* Lancet Respir Med, 2015. **3**(4): p. 301-9.

105. Calabro L, M.A., Fonsatti E, Cuataia O, Fazio C, Danielli R, et al. , *A phase 2 single-arm study with tremelimumab at an optimized dosing schedule in second-line mesothelioma patients.* . J Clin Oncol 2014;32.
106. Kindler HL, D.P.A., Robbins PB, Hong S, Shalabi A, Ibrahim R, et al. , *A randomized, double-blind study comparing tremelimumab to placebo in second and third line treatment of subjects with unresectable pleural or peritoneal mesothelioma.* . J Thorac Oncol 2013;8.
107. Mansfield, A.S., et al., *B7-H1 expression in malignant pleural mesothelioma is associated with sarcomatoid histology and poor prognosis.* J Thorac Oncol, 2014. **9**(7): p. 1036-40.
108. Cedres, S., et al., *Analysis of expression of programmed cell death 1 ligand 1 (PD-L1) in malignant pleural mesothelioma (MPM).* PLoS One, 2015. **10**(3): p. e0121071.
109. Marcq, E., et al., *Targeting immune checkpoints: New opportunity for mesothelioma treatment?* Cancer Treat Rev, 2015. **41**(10): p. 914-24.
110. Kindler Hedy Lee, Z.Z., Khattri Arun, Keck Michaela K, Vigneswaran and H.A.N. Wickii, et al. , *T-cell inflamed phenotype and PDL1 expression in malignant mesothelioma.* . J Clin Oncol 2014;32(5s). 2014.
111. Cowan ML, F.P., Taube JM, Illei PB. , *PD-L1 expression in malignant mesothelioma: an immunohistochemical analysis of 33 cases.* . Lab Invest 2014;94., 2014.
112. Alley, E., Molife, R., Satoro, A., Beckey, K., Yuan, S., Cheng, J. et al. , *Clinical safety and efficacy of pembrolizumab (MK-3475) in patients with malignant pleural mesothelioma: preliminary results from KEYNOTE-028.* Proceedings of the 16th annual meeting of the American Association for Cancer Research, 18–22; 2015., (2015).
113. Topalian, S.L., et al., *Safety, activity, and immune correlates of anti-PD-1 antibody in cancer.* N Engl J Med, 2012. **366**(26): p. 2443-54.
114. Chen, Y.B., C.Y. Mu, and J.A. Huang, *Clinical significance of programmed death-1 ligand-1 expression in patients with non-small cell lung cancer: a 5-year-follow-up study.* Tumori, 2012. **98**(6): p. 751-5.
115. Park, M., et al., *Mechanism of met oncogene activation.* Cell, 1986. **45**(6): p. 895-904.
116. Gherardi, E., et al., *Targeting MET in cancer: rationale and progress.* Nat Rev Cancer, 2012. **12**(2): p. 89-103.
117. Gherardi, E., et al., *Structural basis of hepatocyte growth factor/scatter factor and MET signalling.* Proc Natl Acad Sci U S A, 2006. **103**(11): p. 4046-51.
118. Gherardi, E., et al., *The sema domain.* Curr Opin Struct Biol, 2004. **14**(6): p. 669-78.
119. Mizuno, S. and T. Nakamura, *HGF-MET Cascade, a Key Target for Inhibiting Cancer Metastasis: The Impact of NK4 Discovery on Cancer Biology and Therapeutics.* Int J Mol Sci, 2013. **14**(1): p. 888-919.
120. Gandino, L., et al., *Phosphorylation of serine 985 negatively regulates the hepatocyte growth factor receptor kinase.* J Biol Chem, 1994. **269**(3): p. 1815-20.
121. Peschard, P., et al., *A conserved DpYR motif in the juxtamembrane domain of the Met receptor family forms an atypical c-Cbl/Cbl-b tyrosine kinase binding domain binding site required for suppression of oncogenic activation.* J Biol Chem, 2004. **279**(28): p. 29565-71.
122. Longati, P., et al., *Tyrosines1234-1235 are critical for activation of the tyrosine kinase encoded by the MET proto-oncogene (HGF receptor).* Oncogene, 1994. **9**(1): p. 49-57.
123. Rodrigues, G.A. and M. Park, *Autophosphorylation modulates the kinase activity and oncogenic potential of the Met receptor tyrosine kinase.* Oncogene, 1994. **9**(7): p. 2019-27.
124. Ponzetto, C., et al., *A multifunctional docking site mediates signaling and transformation by the hepatocyte growth factor/scatter factor receptor family.* Cell, 1994. **77**(2): p. 261-71.
125. Weidner, K.M., et al., *Interaction between Gab1 and the c-Met receptor tyrosine kinase is responsible for epithelial morphogenesis.* Nature, 1996. **384**(6605): p. 173-6.

126. Saucier, C., et al., *Use of signal specific receptor tyrosine kinase oncoproteins reveals that pathways downstream from Grb2 or Shc are sufficient for cell transformation and metastasis.* Oncogene, 2002. **21**(12): p. 1800-11.
127. Ramos-Nino, M.E., et al., *HGF mediates cell proliferation of human mesothelioma cells through a PI3K/MEK5/Fra-1 pathway.* Am J Respir Cell Mol Biol, 2008. **38**(2): p. 209-17.
128. Cao, X., et al., *Up-regulation of Bcl-xl by hepatocyte growth factor in human mesothelioma cells involves ETS transcription factors.* Am J Pathol, 2009. **175**(5): p. 2207-16.
129. Organ, S.L. and M.S. Tsao, *An overview of the c-MET signaling pathway.* Ther Adv Med Oncol, 2011. **3**(1 Suppl): p. S7-S19.
130. Birchmeier, C. and E. Gherardi, *Developmental roles of HGF/SF and its receptor, the c-Met tyrosine kinase.* Trends Cell Biol, 1998. **8**(10): p. 404-10.
131. Bladt, F., et al., *Essential role for the c-met receptor in the migration of myogenic precursor cells into the limb bud.* Nature, 1995. **376**(6543): p. 768-71.
132. Schmidt, C., et al., *Scatter factor/hepatocyte growth factor is essential for liver development.* Nature, 1995. **373**(6516): p. 699-702.
133. Uehara, Y., et al., *Placental defect and embryonic lethality in mice lacking hepatocyte growth factor/scatter factor.* Nature, 1995. **373**(6516): p. 702-5.
134. Stoker, M., et al., *Scatter factor is a fibroblast-derived modulator of epithelial cell mobility.* Nature, 1987. **327**(6119): p. 239-42.
135. Nakamura, T., et al., *Molecular cloning and expression of human hepatocyte growth factor.* Nature, 1989. **342**(6248): p. 440-3.
136. Naldini, L., et al., *Extracellular proteolytic cleavage by urokinase is required for activation of hepatocyte growth factor/scatter factor.* EMBO J, 1992. **11**(13): p. 4825-33.
137. Stamos, J., et al., *Crystal structure of the HGF beta-chain in complex with the Sema domain of the Met receptor.* EMBO J, 2004. **23**(12): p. 2325-35.
138. Kirchhofer, D., et al., *Utilizing the activation mechanism of serine proteases to engineer hepatocyte growth factor into a Met antagonist.* Proc Natl Acad Sci U S A, 2007. **104**(13): p. 5306-11.
139. Hartmann, G., et al., *Engineered mutants of HGF/SF with reduced binding to heparan sulphate proteoglycans, decreased clearance and enhanced activity in vivo.* Curr Biol, 1998. **8**(3): p. 125-34.
140. Kemp, L.E., B. Mulloy, and E. Gherardi, *Signalling by HGF/SF and Met: the role of heparan sulphate co-receptors.* Biochem Soc Trans, 2006. **34**(Pt 3): p. 414-7.
141. Lietha, D., et al., *Crystal structures of NK1-heparin complexes reveal the basis for NK1 activity and enable engineering of potent agonists of the MET receptor.* EMBO J, 2001. **20**(20): p. 5543-55.
142. Cecchi, F., et al., *Targeted disruption of heparan sulfate interaction with hepatocyte and vascular endothelial growth factors blocks normal and oncogenic signaling.* Cancer Cell, 2012. **22**(2): p. 250-62.
143. Cipriani, N.A., et al., *MET as a target for treatment of chest tumors.* Lung Cancer, 2009. **63**(2): p. 169-79.
144. Harvey, P., et al., *Immunoreactivity for hepatocyte growth factor/scatter factor and its receptor, met, in human lung carcinomas and malignant mesotheliomas.* J Pathol, 1996. **180**(4): p. 389-94.
145. Eagles, G., et al., *Hepatocyte growth factor/scatter factor is present in most pleural effusion fluids from cancer patients.* Br J Cancer, 1996. **73**(3): p. 377-81.
146. Tolnay, E., et al., *Hepatocyte growth factor/scatter factor and its receptor c-Met are overexpressed and associated with an increased microvessel density in malignant pleural mesothelioma.* J Cancer Res Clin Oncol, 1998. **124**(6): p. 291-6.
147. Jagadeeswaran, R., et al., *Functional analysis of c-Met/hepatocyte growth factor pathway in malignant pleural mesothelioma.* Cancer Res, 2006. **66**(1): p. 352-61.
148. Mukohara, T., et al., *Inhibition of the met receptor in mesothelioma.* Clin Cancer Res, 2005. **11**(22): p. 8122-30.

149. Brevet, M., et al., *Coactivation of receptor tyrosine kinases in malignant mesothelioma as a rationale for combination targeted therapy.* J Thorac Oncol, 2011. **6**(5): p. 864-74.
150. Harvey, P., et al., *Expression of HGF/SF in mesothelioma cell lines and its effects on cell motility, proliferation and morphology.* Br J Cancer, 1998. **77**(7): p. 1052-9.
151. Li, Q., et al., *Pleural mesothelioma instigates tumor-associated fibroblasts to promote progression via a malignant cytokine network.* Am J Pathol, 2011. **179**(3): p. 1483-93.
152. Klominek, J., et al., *Hepatocyte growth factor/scatter factor stimulates chemotaxis and growth of malignant mesothelioma cells through c-met receptor.* Int J Cancer, 1998. **76**(2): p. 240-9.
153. Kawaguchi, K., et al., *Combined inhibition of MET and EGFR suppresses proliferation of malignant mesothelioma cells.* Carcinogenesis, 2009. **30**(7): p. 1097-105.
154. Levallet, G., et al., *Plasma cell membrane localization of c-MET predicts longer survival in patients with malignant mesothelioma: a series of 157 cases from the MESOPATH Group.* J Thorac Oncol, 2012. **7**(3): p. 599-606.
155. Ramos-Nino, M.E., et al., *Microarray analysis and RNA silencing link fra-1 to cd44 and c-met expression in mesothelioma.* Cancer Res, 2003. **63**(13): p. 3539-45.
156. Adamson, I.Y. and J. Bakowska, *KGF and HGF are growth factors for mesothelial cells in pleural lavage fluid after intratracheal asbestos.* Exp Lung Res, 2001. **27**(7): p. 605-16.
157. Menges, C.W., et al., *Tumor Suppressor Alterations Cooperate to Drive Aggressive Mesotheliomas with Enriched Cancer Stem Cells via a p53-miR34a-c-Met Axis.* Cancer Res, 2013.
158. Lai, A.Z., J.V. Abella, and M. Park, *Crosstalk in Met receptor oncogenesis.* Trends Cell Biol, 2009. **19**(10): p. 542-51.
159. Rivera, Z., et al., *The relationship between simian virus 40 and mesothelioma.* Curr Opin Pulm Med, 2008. **14**(4): p. 316-21.
160. Altomare, D.A., et al., *Human and mouse mesotheliomas exhibit elevated AKT/PKB activity, which can be targeted pharmacologically to inhibit tumor cell growth.* Oncogene, 2005. **24**(40): p. 6080-9.
161. Harvey, P., et al., *Hepatocyte growth factor/scatter factor enhances the invasion of mesothelioma cell lines and the expression of matrix metalloproteinases.* Br J Cancer, 2000. **83**(9): p. 1147-53.
162. Rong, S., et al., *Tumorigenicity of the met proto-oncogene and the gene for hepatocyte growth factor.* Mol Cell Biol, 1992. **12**(11): p. 5152-8.
163. Tsarfaty, I., et al., *The Met proto-oncogene mesenchymal to epithelial cell conversion.* Science, 1994. **263**(5143): p. 98-101.
164. Fassina, A., et al., *Epithelial-mesenchymal transition in malignant mesothelioma.* Mod Pathol, 2012. **25**(1): p. 86-99.
165. Cecchi F, W.C., Bottaro DP. , *Experimental Cancer Therapeutics Targeting the Hepatocyte Growth Factor/Met Signaling Pathway. Center for Cancer Research, National Cancer Institute, Bethesda, MD 20892 USA. URL: https://ccrod.cancer.gov/confluence/display/CCRHGF/Home.*
166. Steffan, J.J., D.T. Coleman, and J.A. Cardelli, *The HGF-met signaling axis: emerging themes and targets of inhibition.* Curr Protein Pept Sci, 2011. **12**(1): p. 12-22.
167. Ariyawutyakorn, W., S. Saichaemchan, and M. Varella-Garcia, *Understanding and Targeting MET Signaling in Solid Tumors - Are We There Yet?* J Cancer, 2016. **7**(6): p. 633-49.
168. Iveson, T., et al., *Rilotumumab in combination with epirubicin, cisplatin, and capecitabine as first-line treatment for gastric or oesophagogastric junction adenocarcinoma: an open-label, dose de-escalation phase 1b study and a double-blind, randomised phase 2 study.* Lancet Oncol, 2014. **15**(9): p. 1007-18.
169. Spigel DR, E.M., O'Byrne K, et al. , *Onartuzumab plus erlotinib versus erlotinib in previously treated stage IIIb or IV NSCLC: Results from the pivotal phase III randomized, multicenter, placebo-controlled METLung (OAM4971g) global trial.* J Clin Oncol. 2014; 32: 5s(suppl; abstr 8000).

170. Spigel, D.R., et al., *Randomized phase II trial of Onartuzumab in combination with erlotinib in patients with advanced non-small-cell lung cancer.* J Clin Oncol, 2013. **31**(32): p. 4105-14.
171. Koeppen, H., et al., *Biomarker analyses from a placebo-controlled phase II study evaluating erlotinib+/-onartuzumab in advanced non-small cell lung cancer: MET expression levels are predictive of patient benefit.* Clin Cancer Res, 2014. **20**(17): p. 4488-98.
172. Zhang, Y., R. Jain, and M. Zhu, *Recent Progress and Advances in HGF/MET-Targeted Therapeutic Agents for Cancer Treatment.* Biomedicines, 2015. **3**(1): p. 149.
173. Elisei, R., et al., *Cabozantinib in progressive medullary thyroid cancer.* J Clin Oncol, 2013. **31**(29): p. 3639-46.
174. Smith, D.C., et al., *Cabozantinib in patients with advanced prostate cancer: results of a phase II randomized discontinuation trial.* J Clin Oncol, 2013. **31**(4): p. 412-9.
175. Pant, S., et al., *A phase I dose escalation study of oral c-MET inhibitor tivantinib (ARQ 197) in combination with gemcitabine in patients with solid tumors.* Ann Oncol, 2014. **25**(7): p. 1416-21.
176. Goldberg, J.M., et al., *Extended progression-free survival in two patients with alveolar soft part sarcoma exposed to tivantinib.* J Clin Oncol, 2014. **32**(34): p. e114-6.
177. Kang, Y.K., et al., *A phase II trial of a selective c-Met inhibitor tivantinib (ARQ 197) monotherapy as a second- or third-line therapy in the patients with metastatic gastric cancer.* Invest New Drugs, 2014. **32**(2): p. 355-61.
178. Broggini, M., M.C. Garassino, and G. Damia, *Evaluation of safety and efficacy of tivantinib in the treatment of inoperable or recurrent non-small-cell lung cancer.* Cancer Manag Res, 2013. **5**: p. 15-20.
179. Trojan, J. and S. Zeuzem, *Tivantinib in hepatocellular carcinoma.* Expert Opin Investig Drugs, 2013. **22**(1): p. 141-7.
180. Wagner, A.J., et al., *Tivantinib (ARQ 197), a selective inhibitor of MET, in patients with microphthalmia transcription factor-associated tumors: results of a multicenter phase 2 trial.* Cancer, 2012. **118**(23): p. 5894-902.
181. Goldman, J.W., et al., *Phase 1 dose-escalation trial evaluating the combination of the selective MET (mesenchymal-epithelial transition factor) inhibitor tivantinib (ARQ 197) plus erlotinib.* Cancer, 2012. **118**(23): p. 5903-11.
182. Sequist, L.V., et al., *Randomized phase II study of erlotinib plus tivantinib versus erlotinib plus placebo in previously treated non-small-cell lung cancer.* J Clin Oncol, 2011. **29**(24): p. 3307-15.
183. Remsing Rix, L.L., et al., *GSK3 Alpha and Beta Are New Functionally Relevant Targets of Tivantinib in Lung Cancer Cells.* ACS Chem Biol, 2013.
184. Ghatak, S., et al., *Stromal hyaluronan interaction with epithelial CD44 variants promotes prostate cancer invasiveness by augmenting expression and function of hepatocyte growth factor and androgen receptor.* J Biol Chem, 2010. **285**(26): p. 19821-32.
185. Soong, J., et al., *Sema4D, the ligand for Plexin B1, suppresses c-Met activation and migration and promotes melanocyte survival and growth.* J Invest Dermatol, 2012. **132**(4): p. 1230-8.
186. Tu, H., et al., *CXCR4 and SDF-1 production are stimulated by hepatocyte growth factor and promote glioma cell invasion.* Onkologie, 2009. **32**(6): p. 331-6.
187. Giacobini, P., et al., *Hepatocyte growth factor acts as a motogen and guidance signal for gonadotropin hormone-releasing hormone-1 neuronal migration.* J Neurosci, 2007. **27**(2): p. 431-45.
188. Giacobini, P., et al., *Semaphorin 4D regulates gonadotropin hormone-releasing hormone-1 neuronal migration through PlexinB1-Met complex.* J Cell Biol, 2008. **183**(3): p. 555-66.
189. Engelman, J.A., et al., *MET amplification leads to gefitinib resistance in lung cancer by activating ERBB3 signaling.* Science, 2007. **316**(5827): p. 1039-43.

190. Agarwal, V., M.J. Lind, and L. Cawkwell, *Targeted epidermal growth factor receptor therapy in malignant pleural mesothelioma: where do we stand?* Cancer Treat Rev, 2011. **37**(7): p. 533-42.
191. Pinton, G., et al., *Perifosine as a potential novel anti-cancer agent inhibits EGFR/MET-AKT axis in malignant pleural mesothelioma.* PLoS One, 2012. **7**(5): p. e36856.
192. Follenzi, A., et al., *Cross-talk between the proto-oncogenes Met and Ron.* Oncogene, 2000. **19**(27): p. 3041-9.
193. Gray, S., et al., *Expression of the receptor MST1R/RON and its ligand MSP in malignant pleural mesothelioma.* Lung Cancer, 2011. **71**(Suppl 1 S18 Abstract 52).
194. Salian-Mehta, S., M. Xu, and M.E. Wierman, *AXL and MET crosstalk to promote gonadotropin releasing hormone (GnRH) neuronal cell migration and survival.* Mol Cell Endocrinol, 2013. **374**(1-2): p. 92-100.
195. Varkaris, A., et al., *Ligand-independent activation of MET through IGF-1/IGF-1R signaling.* Int J Cancer, 2013. **133**(7): p. 1536-46.
196. Orian-Rousseau, V., et al., *CD44 is required for two consecutive steps in HGF/c-Met signaling.* Genes Dev, 2002. **16**(23): p. 3074-86.
197. Singleton, P.A., et al., *CD44 regulates hepatocyte growth factor-mediated vascular integrity. Role of c-Met, Tiam1/Rac1, dynamin 2, and cortactin.* J Biol Chem, 2007. **282**(42): p. 30643-57.
198. Penno, M.B., et al., *High CD44 expression on human mesotheliomas mediates association with hyaluronan.* Cancer J Sci Am, 1995. **1**(3): p. 196-203.
199. Fischer, O.M., et al., *Reactive oxygen species mediate Met receptor transactivation by G protein-coupled receptors and the epidermal growth factor receptor in human carcinoma cells.* J Biol Chem, 2004. **279**(28): p. 28970-8.
200. Wang, R., R. Kobayashi, and J.M. Bishop, *Cellular adherence elicits ligand-independent activation of the Met cell-surface receptor.* Proc Natl Acad Sci U S A, 1996. **93**(16): p. 8425-30.
201. Liu, Y., et al., *Coordinate integrin and c-Met signaling regulate Wnt gene expression during epithelial morphogenesis.* Development, 2009. **136**(5): p. 843-53.
202. Trusolino, L., A. Bertotti, and P.M. Comoglio, *A signaling adapter function for alpha6beta4 integrin in the control of HGF-dependent invasive growth.* Cell, 2001. **107**(5): p. 643-54.
203. Cagnoni, G. and L. Tamagnone, *Semaphorin receptors meet receptor tyrosine kinases on the way of tumor progression.* Oncogene, 2013.
204. Giordano, S., et al., *The semaphorin 4D receptor controls invasive growth by coupling with Met.* Nat Cell Biol, 2002. **4**(9): p. 720-4.
205. Matzke, A., et al., *A five-amino-acid peptide blocks Met- and Ron-dependent cell migration.* Cancer Res, 2005. **65**(14): p. 6105-10.
206. Porcel, J.M., et al., *The use of pleural fluid sCD44v6/std ratio for distinguishing mesothelioma from other pleural malignancies.* J Thorac Oncol, 2011. **6**(1): p. 190-4.
207. Olaku, V., et al., *c-Met recruits ICAM-1 as a coreceptor to compensate for the loss of CD44 in Cd44 null mice.* Mol Biol Cell, 2011. **22**(15): p. 2777-86.
208. Ruco, L.P., et al., *Expression of ICAM-1 and VCAM-1 in human malignant mesothelioma.* J Pathol, 1996. **179**(3): p. 266-71.
209. Lindahl, U., M. Kusche-Gullberg, and L. Kjellen, *Regulated diversity of heparan sulfate.* J Biol Chem, 1998. **273**(39): p. 24979-82.
210. Bernfield, M., et al., *Functions of cell surface heparan sulfate proteoglycans.* Annu Rev Biochem, 1999. **68**: p. 729-77.
211. Derksen, P.W.B., et al., *Cell surface proteoglycan syndecan-1 mediates hepatocyte growth factor binding and promotes Met signaling in multiple myeloma.* Blood, 2002. **99**(4): p. 1405-1410.
212. Kumar-Singh, S., et al., *Syndecan-1 expression in malignant mesothelioma: correlation with cell differentiation, WT1 expression, and clinical outcome.* J Pathol, 1998. **186**(3): p. 300-5.

213. Dhodapkar, M.V., et al., *Syndecan-1 Is a Multifunctional Regulator of Myeloma Pathobiology: Control of Tumor Cell Survival, Growth, and Bone Cell Differentiation.* Blood, 1998. **91**(8): p. 2679-2688.
214. Borset, M., et al., *Hepatocyte growth factor and its receptor c-met in multiple myeloma.* Blood, 1996. **88**(10): p. 3998-4004.
215. Sakata, H., et al., *Heparin binding and oligomerization of hepatocyte growth factor/scatter factor isoforms. Heparan sulfate glycosaminoglycan requirement for Met binding and signaling.* J Biol Chem, 1997. **272**(14): p. 9457-63.
216. Swann, J.B. and M.J. Smyth, *Immune surveillance of tumors.* J Clin Invest, 2007. **117**(5): p. 1137-46.
217. Ahmad, A.S., N. Ormiston-Smith, and P.D. Sasieni, *Trends in the lifetime risk of developing cancer in Great Britain: comparison of risk for those born from 1930 to 1960.* Br J Cancer, 2015. **112**(5): p. 943-7.
218. Ayala, A., et al., *Mechanisms of immune resolution.* Crit Care Med, 2003. **31**(8 Suppl): p. S558-71.
219. Vinay, D.S., et al., *Immune evasion in cancer: Mechanistic basis and therapeutic strategies.* Semin Cancer Biol, 2015. **35 Suppl**: p. S185-98.
220. Yokokawa, J., et al., *Enhanced functionality of CD4+CD25(high)FoxP3+ regulatory T cells in the peripheral blood of patients with prostate cancer.* Clin Cancer Res, 2008. **14**(4): p. 1032-40.
221. Gasparoto, T.H., et al., *Patients with oral squamous cell carcinoma are characterized by increased frequency of suppressive regulatory T cells in the blood and tumor microenvironment.* Cancer Immunol Immunother, 2010. **59**(6): p. 819-28.
222. Curiel, T.J., et al., *Specific recruitment of regulatory T cells in ovarian carcinoma fosters immune privilege and predicts reduced survival.* Nat Med, 2004. **10**(9): p. 942-9.
223. Lee, I., et al., *Recruitment of Foxp3+ T regulatory cells mediating allograft tolerance depends on the CCR4 chemokine receptor.* J Exp Med, 2005. **201**(7): p. 1037-44.
224. Zou, W., *Regulatory T cells, tumour immunity and immunotherapy.* Nat Rev Immunol, 2006. **6**(4): p. 295-307.
225. Murdoch, C., et al., *The role of myeloid cells in the promotion of tumour angiogenesis.* Nat Rev Cancer, 2008. **8**(8): p. 618-31.
226. Shojaei, F., et al., *Role of myeloid cells in tumor angiogenesis and growth.* Trends Cell Biol, 2008. **18**(8): p. 372-8.
227. Munn, D.H., et al., *Potential regulatory function of human dendritic cells expressing indoleamine 2,3-dioxygenase.* Science, 2002. **297**(5588): p. 1867-70.
228. Baban, B., et al., *A minor population of splenic dendritic cells expressing CD19 mediates IDO-dependent T cell suppression via type I IFN signaling following B7 ligation.* Int Immunol, 2005. **17**(7): p. 909-19.
229. Mellor, A.L., et al., *Specific subsets of murine dendritic cells acquire potent T cell regulatory functions following CTLA4-mediated induction of indoleamine 2,3 dioxygenase.* Int Immunol, 2004. **16**(10): p. 1391-401.
230. Maher, J., *Clinical immunotherapy of B-cell malignancy using CD19-targeted CAR T-cells.* Curr Gene Ther, 2014. **14**(1): p. 35-43.
231. Whilding, L.M. and J. Maher, *CAR T-cell immunotherapy: The path from the by-road to the freeway?* Mol Oncol, 2015. **9**(10): p. 1994-2018.
232. Sun, M., et al., *Construction and evaluation of a novel humanized HER2-specific chimeric receptor.* Breast Cancer Res, 2014. **16**(3): p. R61.
233. Zhao, Y., et al., *A herceptin-based chimeric antigen receptor with modified signaling domains leads to enhanced survival of transduced T lymphocytes and antitumor activity.* J Immunol, 2009. **183**(9): p. 5563-74.
234. Johnson, L.A., et al., *Rational development and characterization of humanized anti-EGFR variant III chimeric antigen receptor T cells for glioblastoma.* Sci Transl Med, 2015. **7**(275): p. 275ra22.

235. Adusumilli, P.S., et al., *Regional delivery of mesothelin-targeted CAR T cell therapy generates potent and long-lasting CD4-dependent tumor immunity.* Sci Transl Med, 2014. **6**(261): p. 261ra151.
236. Kuwana, Y., et al., *Expression of chimeric receptor composed of immunoglobulin-derived V regions and T-cell receptor-derived C regions.* Biochem Biophys Res Commun, 1987. **149**(3): p. 960-8.
237. Gross, G., T. Waks, and Z. Eshhar, *Expression of immunoglobulin-T-cell receptor chimeric molecules as functional receptors with antibody-type specificity.* Proc Natl Acad Sci U S A, 1989. **86**(24): p. 10024-8.
238. Eshhar, Z., et al., *Specific activation and targeting of cytotoxic lymphocytes through chimeric single chains consisting of antibody-binding domains and the gamma or zeta subunits of the immunoglobulin and T-cell receptors.* Proc Natl Acad Sci U S A, 1993. **90**(2): p. 720-4.
239. Pameijer, C.R., et al., *Conversion of a tumor-binding peptide identified by phage display to a functional chimeric T cell antigen receptor.* Cancer Gene Ther, 2007. **14**(1): p. 91-7.
240. Sharifzadeh, Z., et al., *Genetically engineered T cells bearing chimeric nanoconstructed receptors harboring TAG-72-specific camelid single domain antibodies as targeting agents.* Cancer Lett, 2013. **334**(2): p. 237-44.
241. Davies, D.M., et al., *Flexible targeting of ErbB dimers that drive tumorigenesis by using genetically engineered T cells.* Mol Med, 2012. **18**: p. 565-76.
242. Altenschmidt, U., et al., *Cytolysis of tumor cells expressing the Neu/erbB-2, erbB-3, and erbB-4 receptors by genetically targeted naive T lymphocytes.* Clin Cancer Res, 1996. **2**(6): p. 1001-8.
243. Muniappan, A., et al., *Ligand-mediated cytolysis of tumor cells: use of heregulin-zeta chimeras to redirect cytotoxic T lymphocytes.* Cancer Gene Ther, 2000. **7**(1): p. 128-34.
244. Sadelain, M., *T-cell engineering for cancer immunotherapy.* Cancer J, 2009. **15**(6): p. 451-5.
245. Chmielewski, M., et al., *T cell activation by antibody-like immunoreceptors: increase in affinity of the single-chain fragment domain above threshold does not increase T cell activation against antigen-positive target cells but decreases selectivity.* J Immunol, 2004. **173**(12): p. 7647-53.
246. Kershaw, M.H., et al., *A phase I study on adoptive immunotherapy using gene-modified T cells for ovarian cancer.* Clin Cancer Res, 2006. **12**(20 Pt 1): p. 6106-15.
247. Maus, M.V., et al., *T cells expressing chimeric antigen receptors can cause anaphylaxis in humans.* Cancer Immunol Res, 2013. **1**(1): p. 26-31.
248. Guest, R.D., et al., *The role of extracellular spacer regions in the optimal design of chimeric immune receptors: evaluation of four different scFvs and antigens.* J Immunother, 2005. **28**(3): p. 203-11.
249. Hudecek M, S.A., Kosasih PL, Chen YY, Turtle CJ, Jensen MC, et al. , *The Non-Signaling Extracellular Spacer Domain of CD19-Specific Chimeric Antigen Receptors Is Decisive for in Vivo Anti-Tumor Activity.* 54th ASH Annual Meeting and Exposition, December 8 11,2012; Atlanta, GA2012.
250. James, S.E., et al., *Antigen sensitivity of CD22-specific chimeric TCR is modulated by target epitope distance from the cell membrane.* J Immunol, 2008. **180**(10): p. 7028-38.
251. Almasbak, H., et al., *Inclusion of an IgG1-Fc spacer abrogates efficacy of CD19 CAR T cells in a xenograft mouse model.* Gene Ther, 2015. **22**(5): p. 391-403.
252. Hudecek, M., et al., *The nonsignaling extracellular spacer domain of chimeric antigen receptors is decisive for in vivo antitumor activity.* Cancer Immunol Res, 2015. **3**(2): p. 125-35.
253. Jonnalagadda, M., et al., *Chimeric antigen receptors with mutated IgG4 Fc spacer avoid fc receptor binding and improve T cell persistence and antitumor efficacy.* Mol Ther, 2015. **23**(4): p. 757-68.

254. Bridgeman, J.S., et al., *The optimal antigen response of chimeric antigen receptors harboring the CD3zeta transmembrane domain is dependent upon incorporation of the receptor into the endogenous TCR/CD3 complex.* J Immunol, 2010. **184**(12): p. 6938-49.
255. Borst, J., et al., *The delta- and epsilon-chains of the human T3/T-cell receptor complex are distinct polypeptides.* Nature, 1984. **312**(5993): p. 455-8.
256. Howard, F.D., et al., *The CD3 zeta cytoplasmic domain mediates CD2-induced T cell activation.* J Exp Med, 1992. **176**(1): p. 139-45.
257. Weissman, A.M., et al., *Molecular cloning and chromosomal localization of the human T-cell receptor zeta chain: distinction from the molecular CD3 complex.* Proc Natl Acad Sci U S A, 1988. **85**(24): p. 9709-13.
258. Haynes, N.M., et al., *Redirecting mouse CTL against colon carcinoma: superior signaling efficacy of single-chain variable domain chimeras containing TCR-zeta vs Fc epsilon RI-gamma.* J Immunol, 2001. **166**(1): p. 182-7.
259. Irving, B.A. and A. Weiss, *The cytoplasmic domain of the T cell receptor zeta chain is sufficient to couple to receptor-associated signal transduction pathways.* Cell, 1991. **64**(5): p. 891-901.
260. Finney, H.M., et al., *Chimeric receptors providing both primary and costimulatory signaling in T cells from a single gene product.* J Immunol, 1998. **161**(6): p. 2791-7.
261. Maher, J., et al., *Human T-lymphocyte cytotoxicity and proliferation directed by a single chimeric TCRzeta /CD28 receptor.* Nat Biotechnol, 2002. **20**(1): p. 70-5.
262. Brentjens, R.J., et al., *Genetically targeted T cells eradicate systemic acute lymphoblastic leukemia xenografts.* Clin Cancer Res, 2007. **13**(18 Pt 1): p. 5426-35.
263. Finney, H.M., A.N. Akbar, and A.D. Lawson, *Activation of resting human primary T cells with chimeric receptors: costimulation from CD28, inducible costimulator, CD134, and CD137 in series with signals from the TCR zeta chain.* J Immunol, 2004. **172**(1): p. 104-13.
264. Imai, C., et al., *Chimeric receptors with 4-1BB signaling capacity provoke potent cytotoxicity against acute lymphoblastic leukemia.* Leukemia, 2004. **18**(4): p. 676-84.
265. Song, D.G., et al., *In vivo persistence, tumor localization, and antitumor activity of CAR-engineered T cells is enhanced by costimulatory signaling through CD137 (4-1BB).* Cancer Res, 2011. **71**(13): p. 4617-27.
266. Song, D.G., et al., *CD27 costimulation augments the survival and antitumor activity of redirected human T cells in vivo.* Blood, 2012. **119**(3): p. 696-706.
267. Duong, C.P., et al., *Engineering T cell function using chimeric antigen receptors identified using a DNA library approach.* PLoS One, 2013. **8**(5): p. e63037.
268. Milone, M.C., et al., *Chimeric receptors containing CD137 signal transduction domains mediate enhanced survival of T cells and increased antileukemic efficacy in vivo.* Mol Ther, 2009. **17**(8): p. 1453-64.
269. Kofler, D.M., et al., *CD28 costimulation Impairs the efficacy of a redirected t-cell antitumor attack in the presence of regulatory t cells which can be overcome by preventing Lck activation.* Mol Ther, 2011. **19**(4): p. 760-7.
270. Carpenito, C., et al., *Control of large, established tumor xenografts with genetically retargeted human T cells containing CD28 and CD137 domains.* Proc Natl Acad Sci U S A, 2009. **106**(9): p. 3360-5.
271. Guedan, S., et al., *ICOS-based chimeric antigen receptors program bipolar TH17/TH1 cells.* Blood, 2014. **124**(7): p. 1070-80.
272. Brentjens, R.J., et al., *CD19-targeted T cells rapidly induce molecular remissions in adults with chemotherapy-refractory acute lymphoblastic leukemia.* Sci Transl Med, 2013. **5**(177): p. 177ra38.
273. Porter, D.L., et al., *Chimeric antigen receptor-modified T cells in chronic lymphoid leukemia.* N Engl J Med, 2011. **365**(8): p. 725-33.
274. van der Stegen, S.J., M. Hamieh, and M. Sadelain, *The pharmacology of second-generation chimeric antigen receptors.* Nat Rev Drug Discov, 2015. **14**(7): p. 499-509.

275. Geiger, T.L., et al., *Integrated src kinase and costimulatory activity enhances signal transduction through single-chain chimeric receptors in T lymphocytes.* Blood, 2001. **98**(8): p. 2364-71.
276. Pule, M.A., et al., *A chimeric T cell antigen receptor that augments cytokine release and supports clonal expansion of primary human T cells.* Mol Ther, 2005. **12**(5): p. 933-41.
277. Tammana, S., et al., *4-1BB and CD28 signaling plays a synergistic role in redirecting umbilical cord blood T cells against B-cell malignancies.* Hum Gene Ther, 2010. **21**(1): p. 75-86.
278. Till, B.G., et al., *CD20-specific adoptive immunotherapy for lymphoma using a chimeric antigen receptor with both CD28 and 4-1BB domains: pilot clinical trial results.* Blood, 2012. **119**(17): p. 3940-50.
279. Krause, A., et al., *Antigen-dependent CD28 signaling selectively enhances survival and proliferation in genetically modified activated human primary T lymphocytes.* J Exp Med, 1998. **188**(4): p. 619-26.
280. Wilkie, S., et al., *Dual targeting of ErbB2 and MUC1 in breast cancer using chimeric antigen receptors engineered to provide complementary signaling.* J Clin Immunol, 2012. **32**(5): p. 1059-70.
281. Kloss, C.C., et al., *Combinatorial antigen recognition with balanced signaling promotes selective tumor eradication by engineered T cells.* Nat Biotechnol, 2013. **31**(1): p. 71-5.
282. Lanitis, E., et al., *Chimeric antigen receptor T Cells with dissociated signaling domains exhibit focused antitumor activity with reduced potential for toxicity in vivo.* Cancer Immunol Res, 2013. **1**(1): p. 43-53.
283. Brentjens, R.J., et al., *Eradication of systemic B-cell tumors by genetically targeted human T lymphocytes co-stimulated by CD80 and interleukin-15.* Nat Med, 2003. **9**(3): p. 279-86.
284. Maher, J., *Immunotherapy of malignant disease using chimeric antigen receptor engrafted T cells.* ISRN Oncol, 2012. **2012**: p. 278093.
285. Davila, M.L., et al., *Efficacy and toxicity management of 19-28z CAR T cell therapy in B cell acute lymphoblastic leukemia.* Sci Transl Med, 2014. **6**(224): p. 224ra25.
286. Lee, D.W., et al., *T cells expressing CD19 chimeric antigen receptors for acute lymphoblastic leukaemia in children and young adults: a phase 1 dose-escalation trial.* Lancet, 2015. **385**(9967): p. 517-28.
287. Maude, S.L., et al., *Chimeric antigen receptor T cells for sustained remissions in leukemia.* N Engl J Med, 2014. **371**(16): p. 1507-17.
288. Brentjens, R.J., et al., *Safety and persistence of adoptively transferred autologous CD19-targeted T cells in patients with relapsed or chemotherapy refractory B-cell leukemias.* Blood, 2011. **118**(18): p. 4817-28.
289. Savoldo, B., et al., *CD28 costimulation improves expansion and persistence of chimeric antigen receptor-modified T cells in lymphoma patients.* J Clin Invest, 2011. **121**(5): p. 1822-6.
290. Lamers, C.H., et al., *Treatment of metastatic renal cell carcinoma with autologous T-lymphocytes genetically retargeted against carbonic anhydrase IX: first clinical experience.* J Clin Oncol, 2006. **24**(13): p. e20-2.
291. Park, J.R., et al., *Adoptive transfer of chimeric antigen receptor re-directed cytolytic T lymphocyte clones in patients with neuroblastoma.* Mol Ther, 2007. **15**(4): p. 825-33.
292. Pule, M.A., et al., *Virus-specific T cells engineered to coexpress tumor-specific receptors: persistence and antitumor activity in individuals with neuroblastoma.* Nat Med, 2008. **14**(11): p. 1264-70.
293. Louis, C.U., et al., *Antitumor activity and long-term fate of chimeric antigen receptor-positive T cells in patients with neuroblastoma.* Blood, 2011. **118**(23): p. 6050-6.
294. Riddell, S.R., et al., *Adoptive therapy with chimeric antigen receptor-modified T cells of defined subset composition.* Cancer J, 2014. **20**(2): p. 141-4.
295. Cieri, N., et al., *IL-7 and IL-15 instruct the generation of human memory stem T cells from naive precursors.* Blood, 2013. **121**(4): p. 573-84.

296. Gattinoni, L. and N.P. Restifo, *Moving T memory stem cells to the clinic.* Blood, 2013. **121**(4): p. 567-8.
297. Kochenderfer, J.N., et al., *Donor-derived CD19-targeted T cells cause regression of malignancy persisting after allogeneic hematopoietic stem cell transplantation.* Blood, 2013. **122**(25): p. 4129-39.
298. Grupp, S.A., et al., *Chimeric antigen receptor-modified T cells for acute lymphoid leukemia.* N Engl J Med, 2013. **368**(16): p. 1509-18.
299. van der Stegen, S.J., et al., *Preclinical in vivo modeling of cytokine release syndrome induced by ErbB-retargeted human T cells: identifying a window of therapeutic opportunity?* J Immunol, 2013. **191**(9): p. 4589-98.
300. Morgan, R.A., et al., *Case report of a serious adverse event following the administration of T cells transduced with a chimeric antigen receptor recognizing ERBB2.* Mol Ther, 2010. **18**(4): p. 843-51.
301. Lee, D.W., et al., *Current concepts in the diagnosis and management of cytokine release syndrome.* Blood, 2014. **124**(2): p. 188-95.
302. Heslop, H.E., *Safer CARS.* Mol Ther, 2010. **18**(4): p. 661-2.
303. Ahmed, N., et al., *Human Epidermal Growth Factor Receptor 2 (HER2) -Specific Chimeric Antigen Receptor-Modified T Cells for the Immunotherapy of HER2-Positive Sarcoma.* J Clin Oncol, 2015. **33**(15): p. 1688-96.
304. Lamers, C.H., et al., *Treatment of metastatic renal cell carcinoma with CAIX CAR-engineered T cells: clinical evaluation and management of on-target toxicity.* Mol Ther, 2013. **21**(4): p. 904-12.
305. Lamers, C.H., et al., *Immune responses to transgene and retroviral vector in patients treated with ex vivo-engineered T cells.* Blood, 2011. **117**(1): p. 72-82.
306. Dai, H., et al., *Chimeric Antigen Receptors Modified T-Cells for Cancer Therapy.* J Natl Cancer Inst, 2016. **108**(7).
307. Sambrook! J, R.D., *Molecular Cloning A Laboratory Manual.* Third Edition ed.New York: Cold Spring Harbor Laboratory Press;, 2001.
308. Birnboim, H.C. and J. Doly, *A rapid alkaline extraction procedure for screening recombinant plasmid DNA.* Nucleic Acids Res, 1979. **7**(6): p. 1513-23.
309. Melzak KA, S.C., Turner RFB, Haynes CA. , *Driving Forces for DNA Adsorption to Silica in Perchlorate Solutions. .* Journal of Colloid and Interface Science. 1996(181):635I44.
310. Lenschow, D.J., T.L. Walunas, and J.A. Bluestone, *CD28/B7 system of T cell costimulation.* Annu Rev Immunol, 1996. **14**: p. 233-58.
311. Wilkie, S., et al., *Selective expansion of chimeric antigen receptor-targeted T-cells with potent effector function using interleukin-4.* J Biol Chem, 2010. **285**(33): p. 25538-44.
312. Vogt PK. In: Varmus HE, e., *Retroviral virions and genomes.* Retroviruses. New York:Cold Spring Harbor Laboratory Press; 1997.p.27I70.
313. Schwartzberg, P., J. Colicelli, and S.P. Goff, *Construction and analysis of deletion mutations in the pol gene of Moloney murine leukemia virus: a new viral function required for productive infection.* Cell, 1984. **37**(3): p. 1043-52.
314. Rein, A., et al., *Myristylation site in Pr65gag is essential for virus particle formation by Moloney murine leukemia virus.* Proc Natl Acad Sci U S A, 1986. **83**(19): p. 7246-50.
315. Gorelick, R.J., et al., *Point mutants of Moloney murine leukemia virus that fail to package viral RNA: evidence for specific RNA recognition by a "zinc finger-like" protein sequence.* Proc Natl Acad Sci U S A, 1988. **85**(22): p. 8420-4.
316. Oshima, M., et al., *Effects of blocking individual maturation cleavages in murine leukemia virus gag.* J Virol, 2004. **78**(3): p. 1411-20.
317. Alberts B, B.D., Hopkin K, Johnson A, Lewis J, Raff M, et al., *Essential Cell Biology.* 2009. **3rd Edition ed:Garland Science;** .
318. Swanstrom R, W.J.I.E.V.H., *Synthesis,! assembly! and! processing! of! viral! proteins.* Retroviruses. New York:Cold Spring Harbor Laboratory Press; 1997.p.27I70.
319. Graham, F.L., et al., *Characteristics of a human cell line transformed by DNA from human adenovirus type 5.* J Gen Virol, 1977. **36**(1): p. 59-74.

320. Ory, D.S., B.A. Neugeboren, and R.C. Mulligan, *A stable human-derived packaging cell line for production of high titer retrovirus/vesicular stomatitis virus G pseudotypes.* Proc Natl Acad Sci U S A, 1996. **93**(21): p. 11400-6.
321. Gossen, M. and H. Bujard, *Tight control of gene expression in mammalian cells by tetracycline-responsive promoters.* Proc Natl Acad Sci U S A, 1992. **89**(12): p. 5547-51.
322. Miller, A.D., et al., *Construction and properties of retrovirus packaging cells based on gibbon ape leukemia virus.* J Virol, 1991. **65**(5): p. 2220-4.
323. Riviere, I., K. Brose, and R.C. Mulligan, *Effects of retroviral vector design on expression of human adenosine deaminase in murine bone marrow transplant recipients engrafted with genetically modified cells.* Proc Natl Acad Sci U S A, 1995. **92**(15): p. 6733-7.
324. Hanenberg, H., et al., *Colocalization of retrovirus and target cells on specific fibronectin fragments increases genetic transduction of mammalian cells.* Nat Med, 1996. **2**(8): p. 876-82.
325. Hoeffel, J.C., et al., *Persistence of the common pulmonary vein in a child.* AJR Am J Roentgenol, 1979. **133**(1): p. 121-2.
326. Mosmann, T., *Rapid colorimetric assay for cellular growth and survival: application to proliferation and cytotoxicity assays.* J Immunol Methods, 1983. **65**(1-2): p. 55-63.
327. Frigault, M.J., et al., *Identification of chimeric antigen receptors that mediate constitutive or inducible proliferation of T cells.* Cancer Immunol Res, 2015. **3**(4): p. 356-67.
328. Davies DM, V.d.S.S., Parente ACP, Chiapero-Stanke L, Delinassios G, Burbridge SE, Kao V, Liu Z, Bosshard-Carter L, van Schalkwyk MCI, Box C, Eccles SA, Mather SJ, Wilkie S, Maher J, *Flexible targeting of ErbB dimers that drive tumorigenesis using genetically engineered T-cells. .* Molecular Medicine, 2012. **18:**((1)): p. 565-76.
329. Lokker, N.A. and P.J. Godowski, *Generation and characterization of a competitive antagonist of human hepatocyte growth factor, HGF/NK1.* J Biol Chem, 1993. **268**(23): p. 17145-50.
330. Cioce, V., et al., *Hepatocyte growth factor (HGF)/NK1 is a naturally occurring HGF/scatter factor variant with partial agonist/antagonist activity.* J Biol Chem, 1996. **271**(22): p. 13110-5.
331. Jones, D.S., 2nd, P.C. Tsai, and J.R. Cochran, *Engineering hepatocyte growth factor fragments with high stability and activity as Met receptor agonists and antagonists.* Proc Natl Acad Sci U S A, 2011. **108**(32): p. 13035-40.
332. Latouche, J.-B. and M. Sadelain, *Induction of human cytotoxic T lymphocytes by artificial antigen-presenting cells.* Nat Biotech, 2000. **18**(4): p. 405-409.
333. Papanicolaou, G.A., et al., *Rapid expansion of cytomegalovirus-specific cytotoxic T lymphocytes by artificial antigen-presenting cells expressing a single HLA allele.* Blood, 2003. **102**(7): p. 2498-505.
334. Dupont, J., et al., *Artificial antigen-presenting cells transduced with telomerase efficiently expand epitope-specific, human leukocyte antigen-restricted cytotoxic T cells.* Cancer Res, 2005. **65**(12): p. 5417-27.
335. Gong, M.C., et al., *Cancer patient T cells genetically targeted to prostate-specific membrane antigen specifically lyse prostate cancer cells and release cytokines in response to prostate-specific membrane antigen.* Neoplasia, 1999. **1**(2): p. 123-7.
336. Zhong, X.S., et al., *Chimeric antigen receptors combining 4-1BB and CD28 signaling domains augment PI3kinase/AKT/Bcl-XL activation and CD8+ T cell-mediated tumor eradication.* Mol Ther, 2010. **18**(2): p. 413-20.
337. Rivière, I., K. Brose, and R.C. Mulligan, *Effects of retroviral vector design on expression of human adenosine deaminase in murine bone marrow transplant recipients engrafted with genetically modified cells.* Proc Natl Acad Sci U S A, 1995. **92**(15): p. 6733-7.
338. Swanstrom R, W.J., Varmus HE, *Synthesis, assembly and processing of viral proteins.* Retrviruses - New York: Cold Spring Harbor Laboratory Press, 1997.
339. Schwall, R.H., et al., *Heparin induces dimerization and confers proliferative activity onto the hepatocyte growth factor antagonists NK1 and NK2.* J Cell Biol, 1996. **133**(3): p. 709-18.

340. Maulik, G., et al., *Role of the hepatocyte growth factor receptor, c-Met, in oncogenesis and potential for therapeutic inhibition.* Cytokine Growth Factor Rev, 2002. **13**(1): p. 41-59.
341. Kurre, P., et al., *Envelope fusion protein binding studies in an inducible model of retrovirus receptor expression and in CD34(+) cells emphasize limited transduction at low receptor levels.* Gene Ther, 2001. **8**(8): p. 593-9.
342. Orian-Rousseau, V., *CD44, a therapeutic target for metastasising tumours.* Eur J Cancer, 2010. **46**(7): p. 1271-7.
343. Thirkettle, I., et al., *Immunoreactivity for cadherins, HGF/SF, met, and erbB-2 in pleural malignant mesotheliomas.* Histopathology, 2000. **36**(6): p. 522-8.
344. Bois, M.C., et al., *c-Met expression and MET amplification in malignant pleural mesothelioma.* Annals of Diagnostic Pathology, 2016. **23**: p. 1-7.
345. Manning, L.S., et al., *Establishment and characterization of five human malignant mesothelioma cell lines derived from pleural effusions.* Int J Cancer, 1991. **47**(2): p. 285-90.
346. Chavez, A.R., et al., *Pharmacologic administration of interleukin-2.* Ann N Y Acad Sci, 2009. **1182**: p. 14-27.
347. Burt, B.M., et al., *Expression of interleukin-4 receptor alpha in human pleural mesothelioma is associated with poor survival and promotion of tumor inflammation.* Clin Cancer Res, 2012. **18**(6): p. 1568-77.
348. van Schalkwyk, M.C., et al., *Design of a Phase I Clinical Trial to Evaluate Intratumoral Delivery of ErbB-Targeted Chimeric Antigen Receptor T-Cells in Locally Advanced or Recurrent Head and Neck Cancer.* Hum Gene Ther Clin Dev, 2013. **24**(3): p. 134-42.
349. Kochhar, K.S., et al., *Evidence for autocrine basis of transformation in NIH-3T3 cells transfected with met/HGF receptor gene.* Growth Factors, 1995. **12**(4): p. 303-13.
350. Parente-Pereira, A.C., et al., *Synergistic Chemoimmunotherapy of Epithelial Ovarian Cancer Using ErbB-Retargeted T Cells Combined with Carboplatin.* J Immunol, 2013. **191**(5): p. 2437-45.
351. John, L.B., et al., *Anti-PD-1 antibody therapy potently enhances the eradication of established tumors by gene-modified T cells.* Clin Cancer Res, 2013. **19**(20): p. 5636-46.
352. Suarez, E.R., et al., *Chimeric antigen receptor T cells secreting anti-PD-L1 antibodies more effectively regress renal cell carcinoma in a humanized mouse model.* Oncotarget, 2016.
353. Lake, R.A. and B.W. Robinson, *Immunotherapy and chemotherapy--a practical partnership.* Nat Rev Cancer, 2005. **5**(5): p. 397-405.
354. Zitvogel, L., et al., *Immunological aspects of cancer chemotherapy.* Nat Rev Immunol, 2008. **8**(1): p. 59-73.
355. Shurin, G.V., et al., *Chemotherapeutic agents in noncytotoxic concentrations increase antigen presentation by dendritic cells via an IL-12-dependent mechanism.* J Immunol, 2009. **183**(1): p. 137-44.
356. Su, L., et al., *Death receptor 5 and cellular FLICE-inhibitory protein regulate pemetrexed-induced apoptosis in human lung cancer cells.* Eur J Cancer, 2011. **47**(16): p. 2471-8.
357. Collins, J.L. and M.S. Kao, *The anticancer drug, cisplatin, increases the naturally occurring cell-mediated lysis of tumor cells.* Cancer Immunol Immunother, 1989. **29**(1): p. 17-22.
358. Stewart, J.H.t., et al., *Induction of apoptosis in malignant pleural mesothelioma cells by activation of the Fas (Apo-1/CD95) death-signal pathway.* J Thorac Cardiovasc Surg, 2002. **123**(2): p. 295-302.
359. Abate-Daga, D., et al., *Expression profiling of TCR-engineered T cells demonstrates overexpression of multiple inhibitory receptors in persisting lymphocytes.* Blood, 2013. **122**(8): p. 1399-410.
360. Kalos, M., et al., *T cells with chimeric antigen receptors have potent antitumor effects and can establish memory in patients with advanced leukemia.* Sci Transl Med, 2011. **3**(95): p. 95ra73.

361. Moon, E.K., et al., *Multifactorial T-cell hypofunction that is reversible can limit the efficacy of chimeric antigen receptor-transduced human T cells in solid tumors.* Clin Cancer Res, 2014. **20**(16): p. 4262-73.
362. Squibb, P.R.B.-M., *Study Comparing Opdivo (nivolumab) to Chemotherapy in Treatment Naïve Advanced Melanoma Patients Marks First PD-1 Immune Checkpoint Inhibitor to Demonstrate a Survival Benefit in a Phase 3 Trial.* http://investor.bms.com/investors/news-and-events/press-releases/press-release-details/2014/Study-Comparing-Opdivo-nivolumab-to-Chemotherapy-in-Treatment-Nave-Advanced-Melanoma-Patients-Marks-First-PD-1-Immune-Checkpoint-Inhibitor-to-Demonstrate-a-Survival-Benefit-in-a-Phase-3-Trial/default.aspx, 2014.
363. Shin, J.H., et al., *Positive conversion of negative signaling of CTLA4 potentiates antitumor efficacy of adoptive T-cell therapy in murine tumor models.* Blood, 2012. **119**(24): p. 5678-87.
364. Ankri, C., et al., *Human T cells engineered to express a programmed death 1/28 costimulatory retargeting molecule display enhanced antitumor activity.* J Immunol, 2013. **191**(8): p. 4121-9.
365. Liu, X., et al., *A Chimeric Switch-Receptor Targeting PD1 Augments the Efficacy of Second-Generation CAR T Cells in Advanced Solid Tumors.* Cancer Res, 2016. **76**(6): p. 1578-90.
366. Gross, G. and Z. Eshhar, *Therapeutic Potential of T Cell Chimeric Antigen Receptors (CARs) in Cancer Treatment: Counteracting Off-Tumor Toxicities for Safe CAR T Cell Therapy.* Annu Rev Pharmacol Toxicol, 2016. **56**: p. 59-83.
367. Cleo Robinson, J.N.S., YC Gary Lee, Richard A Lake & W Joost Lesterhuis,, *Mouse models of mesothelioma: strengths, limitations and clinical translation.* October 2014 ,Vol. 3, No. 5, Pages 397-410 , DOI 10.2217/lmt.14.27 (doi:10.2217/lmt.14.27), 2014.
368. McCoy, M.J., A.K. Nowak, and R.A. Lake, *Chemoimmunotherapy: an emerging strategy for the treatment of malignant mesothelioma.* Tissue Antigens, 2009. **74**(1): p. 1-10.
369. Devaud, C., et al., *Tissues in different anatomical sites can sculpt and vary the tumor microenvironment to affect responses to therapy.* Mol Ther, 2014. **22**(1): p. 18-27.
370. Miselis, N.R., et al., *Targeting tumor-associated macrophages in an orthotopic murine model of diffuse malignant mesothelioma.* Mol Cancer Ther, 2008. **7**(4): p. 788-99.
371. Spugnini, E.P., et al., *Piroxicam and cisplatin in a mouse model of peritoneal mesothelioma.* Clin Cancer Res, 2006. **12**(20 Pt 1): p. 6133-43.
372. Martarelli, D., et al., *Characterization of human malignant mesothelioma cell lines orthotopically implanted in the pleural cavity of immunodeficient mice for their ability to grow and form metastasis.* BMC Cancer, 2006. **6**: p. 130.
373. Colt, H.G., et al., *Clinical course of human epithelial-type malignant pleural mesothelioma replicated in an orthotopic-transplant nude mouse model.* Anticancer Res, 1996. **16**(2): p. 633-9.
374. Yanagihara, K., et al., *An orthotopic implantation mouse model of human malignant pleural mesothelioma for in vivo photon counting analysis and evaluation of the effect of S-1 therapy.* Int J Cancer, 2010. **126**(12): p. 2835-46.
375. Bonfil, R.D., et al., *Stimulation of angiogenesis as an explanation of Matrigel-enhanced tumorigenicity.* Int J Cancer, 1994. **58**(2): p. 233-9.
376. Topley, P., et al., *Effect of reconstituted basement membrane components on the growth of a panel of human tumour cell lines in nude mice.* Br J Cancer, 1993. **67**(5): p. 953-8.
377. Schuberth, P.C., et al., *Treatment of malignant pleural mesothelioma by fibroblast activation protein-specific re-directed T cells.* J Transl Med, 2013. **11**: p. 187.
378. Wilkie, S., et al., *Retargeting of human T cells to tumor-associated MUC1: the evolution of a chimeric antigen receptor.* J Immunol, 2008. **180**(7): p. 4901-9.
379. John, L.B., M.H. Kershaw, and P.K. Darcy, *Blockade of PD-1 immunosuppression boosts CAR T-cell therapy.* Oncoimmunology, 2013. **2**(10): p. e26286.

380. Santos, A.M., et al., *Targeting fibroblast activation protein inhibits tumor stromagenesis and growth in mice.* J Clin Invest, 2009. **119**(12): p. 3613-25.
381. Kakarla, S., et al., *Antitumor effects of chimeric receptor engineered human T cells directed to tumor stroma.* Mol Ther, 2013. **21**(8): p. 1611-20.
382. Petrausch, U., et al., *Re-directed T cells for the treatment of fibroblast activation protein (FAP)-positive malignant pleural mesothelioma (FAPME-1).* BMC Cancer, 2012. **12**: p. 615.
383. Arnold, J.N., et al., *Tumoral immune suppression by macrophages expressing fibroblast activation protein-alpha and heme oxygenase-1.* Cancer Immunol Res, 2014. **2**(2): p. 121-6.
384. Magdalena Pircher, c.a.P.S., 1 Pratiksha Gulati,1 Simon Sulser,2 Walter Weder,3 Alessandra Curioni,1 Christoph Renner,4 and Ulf Petrausch4, *FAP-specific re-directed T cells first in-man study in malignant pleural mesothelioma: experience of the first patient treated.* J Immunother Cancer. 2015; 3(Suppl 2): P120. doi: 10.1186/2051-1426-3-S2-P120.
385. Grada, Z., et al., *TanCAR: A Novel Bispecific Chimeric Antigen Receptor for Cancer Immunotherapy.* Mol Ther Nucleic Acids, 2013. **2**: p. e105.
386. Francone, T.D., et al., *Novel xenograft model expressing human hepatocyte growth factor shows ligand-dependent growth of c-Met-expressing tumors.* Mol Cancer Ther, 2007. **6**(4): p. 1460-6.
387. Wu, M.H., et al., *Hepatocyte growth factor both prevents and ameliorates the symptoms of dermal sclerosis in a mouse model of scleroderma.* Gene Ther, 2004. **11**(2): p. 170-80.

CHAPTER 9 APPENDIX

9.1 CAR Sequences

9.1.1 N28z

ATGGCATGGGTGACCAAGCTGCTGCCTGCCCTGCTGCTGCAGCACGTGCTGCTGCACCT
GCTGCTGCTGCCCATCGCCATCCCCTACGCTGAGGGCCAGCGGAAGAGGCGGAACACC
ATCCACGAGTTCAAGAAGAGCGCCAAGACCACCCTGATCAAGATCGACCCTGCCCTGAA
GATCAAGACCAAGAAGGTGAACACCGCTGACCAGTGCGCCAACCGGTGCACCCGGAAC
AAGGGCCTGCCCTTCACCTGCAAGGCCTTCGTGTTCGACAAGGCTCGGAAGCAGTGCCT
GTGGTTCCCCTTCAACAGCATGAGCAGCGGCGTGAAGAAGGAGTTCGGCCACGAGTTC
GACCTGTACGAGAACAAGGACTACATCCGGAACTGCATCATCGGCGAAGGCGAAAGCT
ACAAGGGCACCGTGAGCATCACCAAGAGCGGCATCAAGTGCCAGCCCTGGAGCAGCAT
GATCCCTCACGAGCACAGCTTCCTGCCCAGCAGCTACAGGGGCAAGGACCTGCAGGAG
AACTACTGCCGGAACCCTCGGGGCGAGGAAGGCGGCCCTTGGTGCTTCACCAGCAACC
CTGAGGTGCGGTACGAGGTGTGCGACATCCCTCAGTGCAGCGAGGGCAAGgcGGCCGC
TATCGAGGTGGAGCAGAAGCTGATCAGCGAGGAGGACCTGCTAGACAATGAGAAGAGC
AATGGAACCATTATCCATGTGAAAGGGAAACACCTTTGTCCAAGTCCCCTATTTCCCGG
ACCTTCTAAGCCCTTTTGGGTGCTGGTGGTGGTTGGTGGAGTCCTGGCTTGCTATAGCT
TGCTAGTAACAGTGGCCTTTATTATTTTCTGGGTGAGGAGTAAGAGGAGCAGGCTCCT
GCACAGTGACTACATGAACATGACTCCCCGCCGCCCCGGGCCCACCCGCAAGCATTACC
AGCCCTATGCCCCACCACGCGACTTCGCAGCCTATCGCTCCAGAGTGAAGTTCAGCAGG
AGCGCAGACGCCCCCGCGTACCAGCAGGGCCAGAACCAGCTCTATAACGAGCTCAATCT
AGGACGAAGAGAGGAGTACGATGTTTTGGACAAGAGACGTGGCCGGGACCCTGAGAT
GGGGGGAAAGCCGAGAAGGAAGAACCCTCAGGAAGGCCTGTACAATGAACTGCAGAA
AGATAAGATGGCGGAGGCCTACAGTGAGATTGGGATGAAAGGCGAGCGCCGGAGGGG
CAAGGGGCACGATGGCCTTTACCAGGGTCTCAGTACAGCCACCAAGGACACCTACGAC
GCCCTTCACATGCAGGCCCTGCCCCCTCGCTAA

9.1.2 N4

ATGGGCTGGCTGTGTTCCGGCCTGCTGTTTCCTGTGTCCTGTCTGGTGCTGCTGCAGGT
GGCCAGCTCCGGGAACATGAAAGTGCTGCAGGAGCCCACATGTGTGTCCGACTACATG
TCCATCTCTACATGTGAGTGGAAGATGAACGGCCCCACAAACTGCTCTACCGAGCTGCG
GCTGCTGTACCAGCTGGTGTTTCTGCTGAGCGAGGCCCACACCTGTATCCCAGAAAATA
ATGGCGGGGCCGGGTGTGTGTGCCACCTGCTGATGGATGACGTGGTGTCTGCCGACAA
TTACACCCTGGACCTGTGGGCCGGACAGCAGCTGCTGTGGAAGGGGTCCTTCAAACCC

TCTGAGCACGTGAAGCCAAGGGCCCCCGGCAACCTGACAGTGCACACCAACGTGTCTG
ATACACTGCTGCTGACATGGAGCAATCCATACCCTCCTGACAACTACCTGTACAACCAC
CTGACCTACGCCGTGAATATCTGGAGCGAAAATGATCCTGCCGACTTTCGGATTTACAA
TGTGACCTATCTGGAGCCCTCCCTGAGAATTGCCGCCTCTACCCTGAAATCTGGAATCT
CCTACCGCGCCAGGGTGCGGGCCTGGGCCCAGTGTTACAACACCACCTGGTCTGAGTG
GAGCCCAAGCACCAAGTGGCACAATTCTTATCGGGAGCCTTTTGAGCAGCACCTGATCC
CCTGGCTGGGACACCTGCTGGTGGGGCTGTCTGGCGCCTTTGGCTTCATCATTCTGGTG
TACCTGCTGATCAACTGTAGGAATACAGGCCCTTGGCTGAAGAAGGTGCTGAAGTGTA
ACACCCCCGACCCCTCTAAGTTCTTCAGCCAGCTGTCCTCTGAACACGGGGGAGATGTG
CAGAAGTGGCTGTCCAGCCCTTTCCCATCCAGCTCCTTTAGCCCCGGGGGCCTGGCCCC
TGAGATCTCTCCACTGGAAGTGCTGGAGCGGGACAAGGTGACCCAGCTGCTGCTGCAG
CAGGACAAGGTGCCAGAACCCGCCTCCCTGAGCTCCAACCACAGCCTGACATCTTGCTT
TACAAATCAGGGATACTTCTTCTTCCACCTGCCCGATGCCCTGGAGATCGAGGCCTGCC
AGGTGTACTTCACCTACGATCCCTACTCTGAGGAAGACCCAGATGAGGGCGTGGCCGG
GGCCCCAACCGGGTCCAGCCCACAGCCACTGCAGCCACTGTCCGGCGAAGATGACGCC
TACTGCACATTCCCTTCCAGGGATGACCTGCTGCTGTTCAGCCCATCTCTGCTGGGCGG
ACCCTCTCCTCCAAGCACAGCCCCAGGGGGATCCGGCGCCGGGGAAGAGAGGATGCCC
CCTAGCCTGCAGGAGCGCGTGCCCAGAGACTGGGACCCCCAGCCCCTGGGCCCTCCAA
CCCCTGGGGTGCCCGACCTGGTGGACTTCCAGCCTCCACCCGAGCTGGTGCTGAGGGA
GGCCGGCGAAGAGGTGCCCGACGCCGGCCCCCGGGAGGGCGTGTCCTTCCCTTGGTCC
AGACCTCCAGGACAGGGCGAGTTCCGCGCCCTGAACGCCAGGCTGCCTCTGAACACCG
ATGCCTACCTGTCTCTGCAGGAACTGCAGGGCCAGGACCCAACCCACCTGGTGCGGAG
AAAGCGCAGCGGCTCCGGCGAGGGCCGGGGCAGCCTGCTGACCTGCGGCGACGTGGA
AGAGAACCCCGGACCCATGGCATGGGTGACCAAGCTGCTGCCTGCCCTGCTGCTGCAG
CACGTGCTGCTGCACCTGCTGCTGCTGCCCATCGCCATCCCCTACGCTGAGGGCCAGCG
GAAGAGGCGGAACACCATCCACGAGTTCAAGAAGAGCGCCAAGACCACCCTGATCAAG
ATCGACCCTGCCCTGAAGATCAAGACCAAGAAGGTGAACACCGCTGACCAGTGCGCCA
ACCGGTGCACCCGGAACAAGGGCCTGCCCTTCACCTGCAAGGCCTTCGTGTTCGACAAG
GCTCGGAAGCAGTGCCTGTGGTTCCCCTTCAACAGCATGAGCAGCGGCGTGAAGAAGG
AGTTCGGCCACGAGTTCGACCTGTACGAGAACAAGGACTACATCCGGAACTGCATCATC
GGCGAAGGCGAAAGCTACAAGGGCACCGTGAGCATCACCAAGAGCGGCATCAAGTGCC
AGCCCTGGAGCAGCATGATCCCTCACGAGCACAGCTTCCTGCCCAGCAGCTACAGGGG
CAAGGACCTGCAGGAGAACTACTGCCGGAACCCTCGGGGCGAGGAAGGCGGCCCTTGG
TGCTTCACCAGCAACCCTGAGGTGCGGTACGAGGTGTGCGACATCCCTCAGTGCAGCG
AGGGCAAGgcGGCCGCTATCGAGGTGGAGCAGAAGCTGATCAGCGAGGAGGACCTGCT
AGACAATGAGAAGAGCAATGGAACCATTATCCATGTGAAAGGGAAACACCTTTGTCCA
AGTCCCCTATTTCCCGGACCTTCTAAGCCCTTTTGGGTGCTGGTGGTGGTTGGTGGAGT
CCTGGCTTGCTATAGCTTGCTAGTAACAGTGGCCTTTATTATTTTCTGGGTGAGGAGTA
AGAGGAGCAGGCTCCTGCACAGTGACTACATGAACATGACTCCCCGCCGCCCCGGGCC

CACCCGCAAGCATTACCAGCCCTATGCCCCACCACGCGACTTCGCAGCCTATCGCTCCA
GAGTGAAGTTCAGCAGGAGCGCAGACGCCCCCGCGTACCAGCAGGGCCAGAACCAGCT
CTATAACGAGCTCAATCTAGGACGAAGAGAGGAGTACGATGTTTTGGACAAGAGACGT
GGCCGGGACCCTGAGATGGGGGGAAAGCCGAGAAGGAAGAACCCTCAGGAAGGCCTG
TACAATGAACTGCAGAAAGATAAGATGGCGGAGGCCTACAGTGAGATTGGGATGAAAG
GCGAGCGCCGGAGGGGCAAGGGGCACGATGGCCTTTACCAGGGTCTCAGTACAGCCAC
CAAGGACACCTACGACGCCCTTCACATGCAGGCCCTGCCCCCTCGCTAA

9.1.3 M28z

ATGGCCTGGGTGACCAAGCTGCTGCCTGCCCTGCTGCTCCAGCACGTGCTGCTGCACCT
GCTGCTGCTGCCCATCGCCATCCCCNNNTACGCCGAGGGCCAGCGGAAGCGGCGGAAC
ACCATCCACGAGTTCAAGAAGAGCGCCAAGACCACCCTGATCAAGATCGACCCTGCCCT
GAAGATCAAGACCGAGAAGGTGAACACCGCCGACCAGTGCGCCAACCGGTGCACCCGG
AACAAGGGCCTGCCCTTCACCTGCAAGGCCTTCGTGTTCGACAAGGCTCGGAAGCGGT
GCCTGTGGTTCCCCTTCAACAGCATGAGCAGCGGCGTGAAGAAGGAGTTCGGCCACGA
GTTCGACCTGTACGAGAACAAGGACTACATCCGGAACTGCATCATCGGCAACGGCAGG
AGCTACCGGGGCACCGTGAGCATCACCAAGAGCGGCATCAAGTGCCAGCCCTGGAGCA
GCATGATCCCTCACGAGCACAGCTTCCTGCCCAGCAGCTACAGAGGCGAGGACCTGCG
GGAGAACTACTGCCGGAACCCCAGGGGCGAAGAGGGAGGCCCCTGGTGCTTCACCAGC
GACCCCGAGGTGCGGTACGAGGTGTGCGACATCCCCCAGTGCAGCGAGGTGGAGGCG
GCCGCTATCGAGGTGGAGCAGAAGCTGATCAGCGAGGAGGACCTGCTAGACAATGAGA
AGAGCAATGGAACCATTATCCATGTGAAAGGGAAACACCTTTGTCCAAGTCCCCTATTT
CCCGGACCTTCTAAGCCCTTTTGGGTGCTGGTGGTGGTTGGTGGAGTCCTGGCTTGCTA
TAGCTTGCTAGTAACAGTGGCCTTTATTATTTTCTGGGTGAGGAGTAAGAGGAGCAGG
CTCCTGCACAGTGACTACATGAACATGACTCCCCGCCGCCCCGGGCCCACCCGCAAGCA
TTACCAGCCCTATGCCCCACCACGCGACTTCGCAGCCTATCGCTCCAGAGTGAAGTTCA
GCAGGAGCGCAGACGCCCCCGCGTACCAGCAGGGCCAGAACCAGCTCTATAACGAGCT
CAATCTAGGACGAAGAGAGGAGTACGATGTTTTGGACAAGAGACGTGGCCGGGACCCT
GAGATGGGGGGAAAGCCGAGAAGGAAGAACCCTCAGGAAGGCCTGTACAATGAACTG
CAGAAAGATAAGATGGCGGAGGCCTACAGTGAGATTGGGATGAAAGGCGAGCGCCGG
AGGGGCAAGGGGCACGATGGCCTTTACCAGGGTCTCAGTACAGCCACCAAGGACACCT
ACGACGCCCTTCACATGCAGGCCCTGCCCCCTCGCTAA

9.1.4 M4

ATGGGCTGGCTGTGTTCCGGCCTGCTGTTTCCTGTGTCCTGTCTGGTGCTGCTGCAGGT
GGCCAGCTCCGGGAACATGAAAGTGCTGCAGGAGCCCACATGTGTGTCCGACTACATG
TCCATCTCTACATGTGAGTGGAAGATGAACGGCCCCACAAACTGCTCTACCGAGCTGCG
GCTGCTGTACCAGCTGGTGTTTCTGCTGAGCGAGGCCCACACCTGTATCCCAGAAAATA
ATGGCGGGGCCGGGTGTGTGTGCCACCTGCTGATGGATGACGTGGTGTCTGCCGACAA
TTACACCCTGGACCTGTGGGCCGGACAGCAGCTGCTGTGGAAGGGGTCCTTCAAACCC
TCTGAGCACGTGAAGCCAAGGGCCCCCGGCAACCTGACAGTGCACACCAACGTGTCTG
ATACACTGCTGCTGACATGGAGCAATCCATACCCTCCTGACAACTACCTGTACAACCAC

CTGACCTACGCCGTGAATATCTGGAGCGAAAATGATCCTGCCGACTTTCGGATTTACAA
TGTGACCTATCTGGAGCCCTCCCTGAGAATTGCCGCCTCTACCCTGAAATCTGGAATCT
CCTACCGCGCCAGGGTGCGGGCCTGGGCCCAGTGTTACAACACCACCTGGTCTGAGTG
GAGCCCAAGCACCAAGTGGCACAATTCTTATCGGGAGCCTTTTGAGCAGCACCTGATCC
CCTGGCTGGGACACCTGCTGGTGGGGCTGTCTGGCGCCTTTGGCTTCATCATTCTGGTG
TACCTGCTGATCAACTGTAGGAATACAGGCCCTTGGCTGAAGAAGGTGCTGAAGTGTA
ACACCCCCGACCCCTCTAAGTTCTTCAGCCAGCTGTCCTCTGAACACGGGGGAGATGTG
CAGAAGTGGCTGTCCAGCCCTTTCCCATCCAGCTCCTTTAGCCCCGGGGGCCTGGCCCC
TGAGATCTCTCCACTGGAAGTGCTGGAGCGGGACAAGGTGACCCAGCTGCTGCTGCAG
CAGGACAAGGTGCCAGAACCCGCCTCCCTGAGCTCCAACCACAGCCTGACATCTTGCTT
TACAAATCAGGGATACTTCTTCTTCCACCTGCCCGATGCCCTGGAGATCGAGGCCTGCC
AGGTGTACTTCACCTACGATCCCTACTCTGAGGAAGACCCAGATGAGGGCGTGGCCGG
GGCCCCAACCGGGTCCAGCCCACAGCCACTGCAGCCACTGTCCGGCGAAGATGACGCC
TACTGCACATTCCCTTCCAGGGATGACCTGCTGCTGTTCAGCCCATCTCTGCTGGGCGG
ACCCTCTCCTCCAAGCACAGCCCCAGGGGGATCCGGCGCCGGGGAAGAGAGGATGCCC
CCTAGCCTGCAGGAGCGCGTGCCCAGAGACTGGGACCCCCAGCCCCTGGGCCCTCCAA
CCCCTGGGGTGCCCGACCTGGTGGACTTCCAGCCTCCACCCGAGCTGGTGCTGAGGGA
GGCCGGCGAAGAGGTGCCCGACGCCGGCCCCCGGGAGGGCGTGTCCTTCCCTTGGTCC
AGACCTCCAGGACAGGGCGAGTTCCGCGCCCTGAACGCCAGGCTGCCTCTGAACACCG
ATGCCTACCTGTCTCTGCAGGAACTGCAGGGCCAGGACCCAACCCACCTGGTGCGGAG
AAAGCGCAGCGGCTCCGGCGAGGGCCGGGGCAGCCTGCTGACCTGCGGCGACGTGGA
AGAGAACCCCGGACCcATGGCCTGGGTGACCAAGCTGCTGCCTGCCCTGCTGCTCCAGC
ACGTGCTGCTGCACCTGCTGCTGCTGCCCATCGCCATCCCCNNNTACGCCGAGGGCCA
GCGGAAGCGGCGGAACACCATCCACGAGTTCAAGAAGAGCGCCAAGACCACCCTGATC
AAGATCGACCCTGCCCTGAAGATCAAGACCGAGAAGGTGAACACCGCCGACCAGTGCG
CCAACCGGTGCACCCGGAACAAGGGCCTGCCCTTCACCTGCAAGGCCTTCGTGTTCGAC
AAGGCTCGGAAGCGGTGCCTGTGGTTCCCCTTCAACAGCATGAGCAGCGGCGTGAAGA
AGGAGTTCGGCCACGAGTTCGACCTGTACGAGAACAAGGACTACATCCGGAACTGCAT
CATCGGCAACGGCAGGAGCTACCGGGGCACCGTGAGCATCACCAAGAGCGGCATCAAG
TGCCAGCCCTGGAGCAGCATGATCCCTCACGAGCACAGCTTCCTGCCCAGCAGCTACAG
AGGCGAGGACCTGCGGGAGAACTACTGCCGGAACCCCAGGGGCGAAGAGGGAGGCCC
CTGGTGCTTCACCAGCGACCCCGAGGTGCGGTACGAGGTGTGCGACATCCCCCAGTGC
AGCGAGGTGGAGGCGGCCGCTATCGAGGTGGAGCAGAAGCTGATCAGCGAGGAGGAC
CTGCTAGACAATGAGAAGAGCAATGGAACCATTATCCATGTGAAAGGGAAACACCTTT
GTCCAAGTCCCCTATTTCCCGGACCTTCTAAGCCCTTTTGGGTGCTGGTGGTGGTTGGT
GGAGTCCTGGCTTGCTATAGCTTGCTAGTAACAGTGGCCTTTATTATTTTCTGGGTGAG
GAGTAAGAGGAGCAGGCTCCTGCACAGTGACTACATGAACATGACTCCCCGCCGCCCC
GGGCCCACCCGCAAGCATTACCAGCCCTATGCCCCACCACGCGACTTCGCAGCCTATCG
CTCCAGAGTGAAGTTCAGCAGGAGCGCAGACGCCCCCGCGTACCAGCAGGGCCAGAAC

CAGCTCTATAACGAGCTCAATCTAGGACGAAGAGAGGAGTACGATGTTTTGGACAAGA
GACGTGGCCGGGACCCTGAGATGGGGGGAAAGCCGAGAAGGAAGAACCCTCAGGAAG
GCCTGTACAATGAACTGCAGAAAGATAAGATGGCGGAGGCCTACAGTGAGATTGGGAT
GAAAGGCGAGCGCCGGAGGGGCAAGGGGCACGATGGCCTTTACCAGGGTCTCAGTACA
GCCACCAAGGACACCTACGACGCCCTTCACATGCAGGCCCTGCCCCCTCGCTAA

9.1.5 cM28z

ATGGCCTGGGTGACCAAGCTGCTGCCTGCCCTGCTGCTCCAGCACGTGCTGCTGCACCT
GCTGCTGCTGCCCATCGCCATCCCCTGCTACGCCGAGGGCCAGCGGAAGCGGCGGAAC
ACCATCCACGAGTTCAAGAAGAGCGCCAAGACCACCCTGATCAAGATCGACCCTGCCCT
GAAGATCAAGACCGAGAAGGTGAACACCGCCGACCAGTGCGCCAACCGGTGCACCCGG
AACAAGGGCCTGCCCTTCACCTGCAAGGCCTTCGTGTTCGACAAGGCTCGGAAGCGGT
GCCTGTGGTTCCCCTTCAACAGCATGAGCAGCGGCGTGAAGAAGGAGTTCGGCCACGA
GTTCGACCTGTACGAGAACAAGGACTACATCCGGAACTGCATCATCGGCAACGGCAGG
AGCTACCGGGGCACCGTGAGCATCACCAAGAGCGGCATCAAGTGCCAGCCCTGGAGCA
GCATGATCCCTCACGAGCACAGCTTCCTGCCCAGCAGCTACAGAGGCGAGGACCTGCG
GGAGAACTACTGCCGGAACCCCAGGGGCGAAGAGGGAGGCCCCTGGTGCTTCACCAGC
GACCCCGAGGTGCGGTACGAGGTGTGCGACATCCCCCAGTGCAGCGAGGTGGAGGCG
GCCGCTATCGAGGTGGAGCAGAAGCTGATCAGCGAGGAGGACCTGCTAGACAATGAGA
AGAGCAATGGAACCATTATCCATGTGAAAGGGAAACACCTTTGTCCAAGTCCCCTATTT
CCCGGACCTTCTAAGCCCTTTTGGGTGCTGGTGGTGGTTGGTGGAGTCCTGGCTTGCTA
TAGCTTGCTAGTAACAGTGGCCTTTATTATTTTCTGGGTGAGGAGTAAGAGGAGCAGG
CTCCTGCACAGTGACTACATGAACATGACTCCCCGCCGCCCCGGGCCCACCCGCAAGCA
TTACCAGCCCTATGCCCCACCACGCGACTTCGCAGCCTATCGCTCCAGAGTGAAGTTCA
GCAGGAGCGCAGACGCCCCCGCGTACCAGCAGGGCCAGAACCAGCTCTATAACGAGCT
CAATCTAGGACGAAGAGAGGAGTACGATGTTTTGGACAAGAGACGTGGCCGGGACCCT
GAGATGGGGGGAAAGCCGAGAAGGAAGAACCCTCAGGAAGGCCTGTACAATGAACTG
CAGAAAGATAAGATGGCGGAGGCCTACAGTGAGATTGGGATGAAAGGCGAGCGCCGG
AGGGGCAAGGGGCACGATGGCCTTTACCAGGGTCTCAGTACAGCCACCAAGGACACCT
ACGACGCCCTTCACATGCAGGCCCTGCCCCCTCGCTAA

9.1.6 cM4

ATGGGCTGGCTGTGTTCCGGCCTGCTGTTTCCTGTGTCCTGTCTGGTGCTGCTGCAGGT
GGCCAGCTCCGGGAACATGAAAGTGCTGCAGGAGCCCACATGTGTGTCCGACTACATG
TCCATCTCTACATGTGAGTGGAAGATGAACGGCCCCACAAACTGCTCTACCGAGCTGCG
GCTGCTGTACCAGCTGGTGTTTCTGCTGAGCGAGGCCCACACCTGTATCCCAGAAAATA
ATGGCGGGGCCGGGTGTGTGTGCCACCTGCTGATGGATGACGTGGTGTCTGCCGACAA
TTACACCCTGGACCTGTGGGCCGGACAGCAGCTGCTGTGGAAGGGGTCCTTCAAACCC
TCTGAGCACGTGAAGCCAAGGGCCCCCGGCAACCTGACAGTGCACACCAACGTGTCTG
ATACACTGCTGCTGACATGGAGCAATCCATACCCTCCTGACAACTACCTGTACAACCAC
CTGACCTACGCCGTGAATATCTGGAGCGAAAATGATCCTGCCGACTTTCGGATTTACAA

TGTGACCTATCTGGAGCCCTCCCTGAGAATTGCCGCCTCTACCCTGAAATCTGGAATCT
CCTACCGCGCCAGGGTGCGGGCCTGGGCCCAGTGTTACAACACCACCTGGTCTGAGTG
GAGCCCAAGCACCAAGTGGCACAATTCTTATCGGGAGCCTTTTGAGCAGCACCTGATCC
CCTGGCTGGGACACCTGCTGGTGGGGCTGTCTGGCGCCTTTGGCTTCATCATTCTGGTG
TACCTGCTGATCAACTGTAGGAATACAGGCCCTTGGCTGAAGAAGGTGCTGAAGTGTA
ACACCCCCGACCCCTCTAAGTTCTTCAGCCAGCTGTCCTCTGAACACGGGGGAGATGTG
CAGAAGTGGCTGTCCAGCCCTTTCCCATCCAGCTCCTTTAGCCCCGGGGGCCTGGCCCC
TGAGATCTCTCCACTGGAAGTGCTGGAGCGGGACAAGGTGACCCAGCTGCTGCTGCAG
CAGGACAAGGTGCCAGAACCCGCCTCCCTGAGCTCCAACCACAGCCTGACATCTTGCTT
TACAAATCAGGGATACTTCTTCTTCCACCTGCCCGATGCCCTGGAGATCGAGGCCTGCC
AGGTGTACTTCACCTACGATCCCTACTCTGAGGAAGACCCAGATGAGGGCGTGGCCGG
GGCCCCAACCGGGTCCAGCCCACAGCCACTGCAGCCACTGTCCGGCGAAGATGACGCC
TACTGCACATTCCCTTCCAGGGATGACCTGCTGCTGTTCAGCCCATCTCTGCTGGGCGG
ACCCTCTCCTCCAAGCACAGCCCCAGGGGGATCCGGCGCCGGGGAAGAGAGGATGCCC
CCTAGCCTGCAGGAGCGCGTGCCCAGAGACTGGGACCCCCAGCCCCTGGGCCCTCCAA
CCCCTGGGGTGCCCGACCTGGTGGACTTCCAGCCTCCACCCGAGCTGGTGCTGAGGGA
GGCCGGCGAAGAGGTGCCCGACGCCGGCCCCCGGGAGGGCGTGTCCTTCCCTTGGTCC
AGACCTCCAGGACAGGGCGAGTTCCGCGCCCTGAACGCCAGGCTGCCTCTGAACACCG
ATGCCTACCTGTCTCTGCAGGAACTGCAGGGCCAGGACCCAACCCACCTGGTGCGGAG
AAAGCGCAGCGGCTCCGGCGAGGGCCGGGGCAGCCTGCTGACCTGCGGCGACGTGGA
AGAGAACCCCGGACCcATGGCCTGGGTGACCAAGCTGCTGCCTGCCCTGCTGCTCCAGC
ACGTGCTGCTGCACCTGCTGCTGCTGCCCATCGCCATCCCCTGCTACGCCGAGGGCCAG
CGGAAGCGGCGGAACACCATCCACGAGTTCAAGAAGAGCGCCAAGACCACCCTGATCA
AGATCGACCCTGCCCTGAAGATCAAGACCGAGAAGGTGAACACCGCCGACCAGTGCGC
CAACCGGTGCACCCGGAACAAGGGCCTGCCCTTCACCTGCAAGGCCTTCGTGTTCGACA
AGGCTCGGAAGCGGTGCCTGTGGTTCCCCTTCAACAGCATGAGCAGCGGCGTGAAGAA
GGAGTTCGGCCACGAGTTCGACCTGTACGAGAACAAGGACTACATCCGGAACTGCATC
ATCGGCAACGGCAGGAGCTACCGGGGCACCGTGAGCATCACCAAGAGCGGCATCAAGT
GCCAGCCCTGGAGCAGCATGATCCCTCACGAGCACAGCTTCCTGCCCAGCAGCTACAGA
GGCGAGGACCTGCGGGAGAACTACTGCCGGAACCCCAGGGGCGAAGAGGGAGGCCCC
TGGTGCTTCACCAGCGACCCCGAGGTGCGGTACGAGGTGTGCGACATCCCCCAGTGCA
GCGAGGTGGAGGCGGCCGCTATCGAGGTGGAGCAGAAGCTGATCAGCGAGGAGGACC
TGCTAGACAATGAGAAGAGCAATGGAACCATTATCCATGTGAAAGGGAAACACCTTTGT
CCAAGTCCCCTATTTCCCGGACCTTCTAAGCCCTTTTGGGTGCTGGTGGTGGTTGGTGG
AGTCCTGGCTTGCTATAGCTTGCTAGTAACAGTGGCCTTTATTATTTTCTGGGTGAGGA
GTAAGAGGAGCAGGCTCCTGCACAGTGACTACATGAACATGACTCCCCGCCGCCCCGG
GCCCACCCGCAAGCATTACCAGCCCTATGCCCCACCACGCGACTTCGCAGCCTATCGCT
CCAGAGTGAAGTTCAGCAGGAGCGCAGACGCCCCCGCGTACCAGCAGGGCCAGAACCA
GCTCTATAACGAGCTCAATCTAGGACGAAGAGAGGAGTACGATGTTTTGGACAAGAGA

CGTGGCCGGGACCCTGAGATGGGGGGAAAGCCGAGAAGGAAGAACCCTCAGGAAGGC
CTGTACAATGAACTGCAGAAAGATAAGATGGCGGAGGCCTACAGTGAGATTGGGATGA
AAGGCGAGCGCCGGAGGGGCAAGGGGCACGATGGCCTTTACCAGGGTCTCAGTACAGC
CACCAAGGACACCTACGACGCCCTTCACATGCAGGCCCTGCCCCCTCGCTAA

9.1.7 T28z (TMY28z)

ATGGCTCTCCCAGTGACTGCCCTACTGCTTCCCCTAGCGCTTCTCCTGCATGCAGTGGT
GTCGCACTTCAATGACTGTCCACTGTCGCACGATGGATACTGCCTCCATGATGGTGTGT
GCATGTACATCGAGGCATTGGACAAGTATGCATGCAACTGTGTCGTCGGCTACATCGG
AGAGCGATGTCAGTACCGAGACCTGAAGTGGTGGGAACTGAGAGCGGCCGCCATCGAG
GTGGAGCAGAAGCTGATCAGCGAGGAGGACCTGCTGGACAACGAGAAGAGCAACGGC
ACCATCATCCACGTGAAGGGCAAGCACCTGTGCCCCAGCCCCCTGTTCCCCGGCCCCAG
CAAGCCCTTCTGGGTGCTGGTGGTGGTGGGCGGCGTGCTGGCCTGCTACAGCCTGCTG
GTGACCGTGGCCTTCATCATCTTCTGGGTGCGGAGCAAGCGGAGCCGGCTGCTGCACA
GCGACTACATGAACATGACCCCCCGGCGGCCTGGGCCCACCCGCAAGCATTACCAGCCC
TATGCCCCACCACGCGACTTCGCAGCCTATCGCTCCAGAGTGAAGTTCAGCAGGAGCGC
AGAGCCCCCCGCGTACCAGCAGGGCCAGAACCAGCTCTATAACGAGCTCAATCTAGGAC
GAAGAGAGGAGTACGATGTTTTGGACAAGAGACGTGGCCGGGACCCTGAGATGGGGG
GAAAGCCGAGAAGGAAGAACCCTCAGGAAGGCCTGTACAATGAACTGCAGAAAGATAA
GATGGCGGAGGCCTACAGTGAGATTGGGATGAAAGGCGAGCGCCGGAGGGGCAAGGG
GCACGATGGCCTTTACCAGGGTCTCAGTACAGCCACCAAGGACACCTACGACGCCCTTC
ACATGCAGGCCCTGCCCCCTCGCTAA

9.1.8 V28z

ATGGGGTGGCTCTGTTCCGGGCTCCTCTTTCCTGTCTCCTGTCTCGTCCTCCTCCAAGTC
GCTTCCTCCGGGAATAATGCTGTCCCTAATCTCGCCGCCGCCGCCCAAGTCCTCGCTCA
AAAAGTCGCTAGGACAGGCGCGGCCGCTATCGAGGTGGAGCAGAAGCTGATCAGCGAG
GAGGACCTGCTAGACAATGAGAAGAGCAATGGAACCATTATCCATGTGAAAGGGAAAC
ACCTTTGTCCAAGTCCCCTATTTCCCGGACCTTCTAAGCCCTTTTGGGTGCTGGTGGTG
GTTGGTGGAGTCCTGGCTTGCTATAGCTTGCTAGTAACAGTGGCCTTTATTATTTTCTG
GGTGAGGAGTAAGAGGAGCAGGCTCCTGCACAGTGACTACATGAACATGACTCCCCGC
CGCCCCGGGCCCACCCGCAAGCATTACCAGCCCTATGCCCCACCACGCGACTTCGCAGC
CTATCGCTCCAGAGTGAAGTTCAGCAGGAGCGCAGACGCCCCCGCGTACCAGCAGGGC
CAGAACCAGCTCTATAACGAGCTCAATCTAGGACGAAGAGAGGAGTACGATGTTTTGG
ACAAGAGACGTGGCCGGGACCCTGAGATGGGGGGAAAGCCGAGAAGGAAGAACCCTC
AGGAAGGCCTGTACAATGAACTGCAGAAAGATAAGATGGCGGAGGCCTACAGTGAGAT
TGGGATGAAAGGCGAGCGCCGGAGGGGCAAGGGGCACGATGGCCTTTACCAGGGTCT
CAGTACAGCCACCAAGGACACCTACGACGCCCTTCACATGCAGGCCCTGCCCCCTCGCT
AA

9.1.9 V4

ATGGGCTGGCTGTGTTCCGGCCTGCTGTTTCCTGTGTCCTGTCTGGTGCTGCTGCAGGT
GGCCAGCTCCGGGAACATGAAAGTGCTGCAGGAGCCCACATGTGTGTCCGACTACATG
TCCATCTCTACATGTGAGTGGAAGATGAACGGCCCCACAAACTGCTCTACCGAGCTGCG
GCTGCTGTACCAGCTGGTGTTTCTGCTGAGCGAGGCCCACACCTGTATCCCAGAAAATA
ATGGCGGGGCCGGGTGTGTGTGCCACCTGCTGATGGATGACGTGGTGTCTGCCGACAA
TTACACCCTGGACCTGTGGGCCGGACAGCAGCTGCTGTGGAAGGGGTCCTTCAAACCC
TCTGAGCACGTGAAGCCAAGGGCCCCCGGCAACCTGACAGTGCACACCAACGTGTCTG
ATACACTGCTGCTGACATGGAGCAATCCATACCCTCCTGACAACTACCTGTACAACCAC
CTGACCTACGCCGTGAATATCTGGAGCGAAAATGATCCTGCCGACTTTCGGATTTACAA
TGTGACCTATCTGGAGCCCTCCCTGAGAATTGCCGCCTCTACCCTGAAATCTGGAATCT
CCTACCGCGCCAGGGTGCGGGCCTGGGCCCAGTGTTACAACACCACCTGGTCTGAGTG
GAGCCCAAGCACCAAGTGGCACAATTCTTATCGGGAGCCTTTTGAGCAGCACCTGATCC
CCTGGCTGGGACACCTGCTGGTGGGGCTGTCTGGCGCCTTTGGCTTCATCATTCTGGTG
TACCTGCTGATCAACTGTAGGAATACAGGCCCTTGGCTGAAGAAGGTGCTGAAGTGTA
ACACCCCCGACCCCTCTAAGTTCTTCAGCCAGCTGTCCTCTGAACACGGGGGAGATGTG
CAGAAGTGGCTGTCCAGCCCTTTCCCATCCAGCTCCTTTAGCCCCGGGGGCCTGGCCCC
TGAGATCTCTCCACTGGAAGTGCTGGAGCGGGACAAGGTGACCCAGCTGCTGCTGCAG

CAGGACAAGGTGCCAGAACCCGCCTCCCTGAGCTCCAACCACAGCCTGACATCTTGCTT
TACAAATCAGGGATACTTCTTCTTCCACCTGCCCGATGCCCTGGAGATCGAGGCCTGCC
AGGTGTACTTCACCTACGATCCCTACTCTGAGGAAGACCCAGATGAGGGCGTGGCCGG
GGCCCCAACCGGGTCCAGCCCACAGCCACTGCAGCCACTGTCCGGCGAAGATGACGCC
TACTGCACATTCCCTTCCAGGGATGACCTGCTGCTGTTCAGCCCATCTCTGCTGGGCGG
ACCCTCTCCTCCAAGCACAGCCCCAGGGGGATCCGGCGCCGGGGAAGAGAGGATGCCC
CCTAGCCTGCAGGAGCGCGTGCCCAGAGACTGGGACCCCCAGCCCCTGGGCCCTCCAA
CCCCTGGGGTGCCCGACCTGGTGGACTTCCAGCCTCCACCCGAGCTGGTGCTGAGGGA
GGCCGGCGAAGAGGTGCCCGACGCCGGCCCCCGGGAGGGCGTGTCCTTCCCTTGGTCC
AGACCTCCAGGACAGGGCGAGTTCCGCGCCCTGAACGCCAGGCTGCCTCTGAACACCG
ATGCCTACCTGTCTCTGCAGGAACTGCAGGGCCAGGACCCAACCCACCTGGTGCGGAG
AAAGCGCAGCGGCTCCGGCGAGGGCCGGGGCAGCCTGCTGACCTGCGGCGACGTGGA
AGAGAACCCCGGACcCATGGGGTGGCTCTGTTCCGGGCTCCTCTTTCCTGTCTCCTGTC
TCGTCCTCCTCCAAGTCGCTTCCTCCGGGAATAATGCTGTCCCTAATCTCGCCGCCGCC
GCCCAAGTCCTCGCTCAAAAAGTCGCTAGGACAGGCGCGGCCGCTATCGAGGTGGAGC
AGAAGCTGATCAGCGAGGAGGACCTGCTAGACAATGAGAAGAGCAATGGAACCATTAT
CCATGTGAAAGGGAAACACCTTTGTCCAAGTCCCCTATTTCCCGGACCTTCTAAGCCCTT
TTGGGTGCTGGTGGTGGTTGGTGGAGTCCTGGCTTGCTATAGCTTGCTAGTAACAGTG
GCCTTTATTATTTTCTGGGTGAGGAGTAAGAGGAGCAGGCTCCTGCACAGTGACTACAT
GAACATGACTCCCCGCCGCCCCGGGCCCACCCGCAAGCATTACCAGCCCTATGCCCCAC
CACGCGACTTCGCAGCCTATCGCTCCAGAGTGAAGTTCAGCAGGAGCGCAGACGCCCC
CGCGTACCAGCAGGGCCAGAACCAGCTCTATAACGAGCTCAATCTAGGACGAAGAGAG
GAGTACGATGTTTTGGACAAGAGACGTGGCCGGGACCCTGAGATGGGGGGAAAGCCG
AGAAGGAAGAACCCTCAGGAAGGCCTGTACAATGAACTGCAGAAAGATAAGATGGCGG
AGGCCTACAGTGAGATTGGGATGAAAGGCGAGCGCCGGAGGGGCAAGGGGCACGATG
GCCTTTACCAGGGTCTCAGTACAGCCACCAAGGACACCTACGACGCCCTTCACATGCAG
GCCCTGCCCCCTCGCTAA

9.2 Chimeric Antigen Receptor Plasmid Schematics

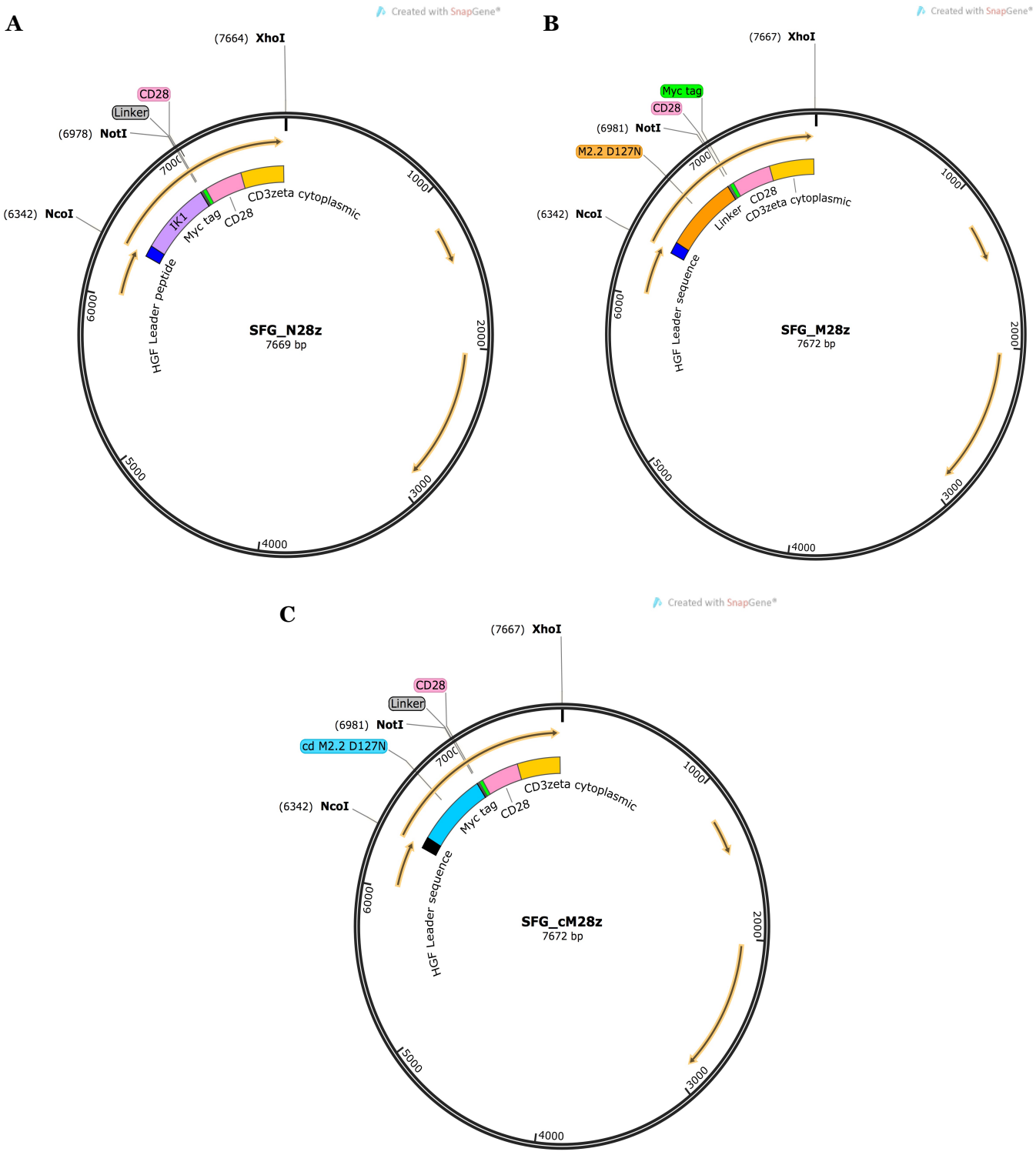

Figure 9-1. Circular plasmid maps of SFG c-Met chimeric antigen receptors. Schematic depicting **(A)** SFG N28z, **(B)** SFG M28z and **(C)** SFG cM28z. Key individual modules are shown along with unique restriction enzymes.

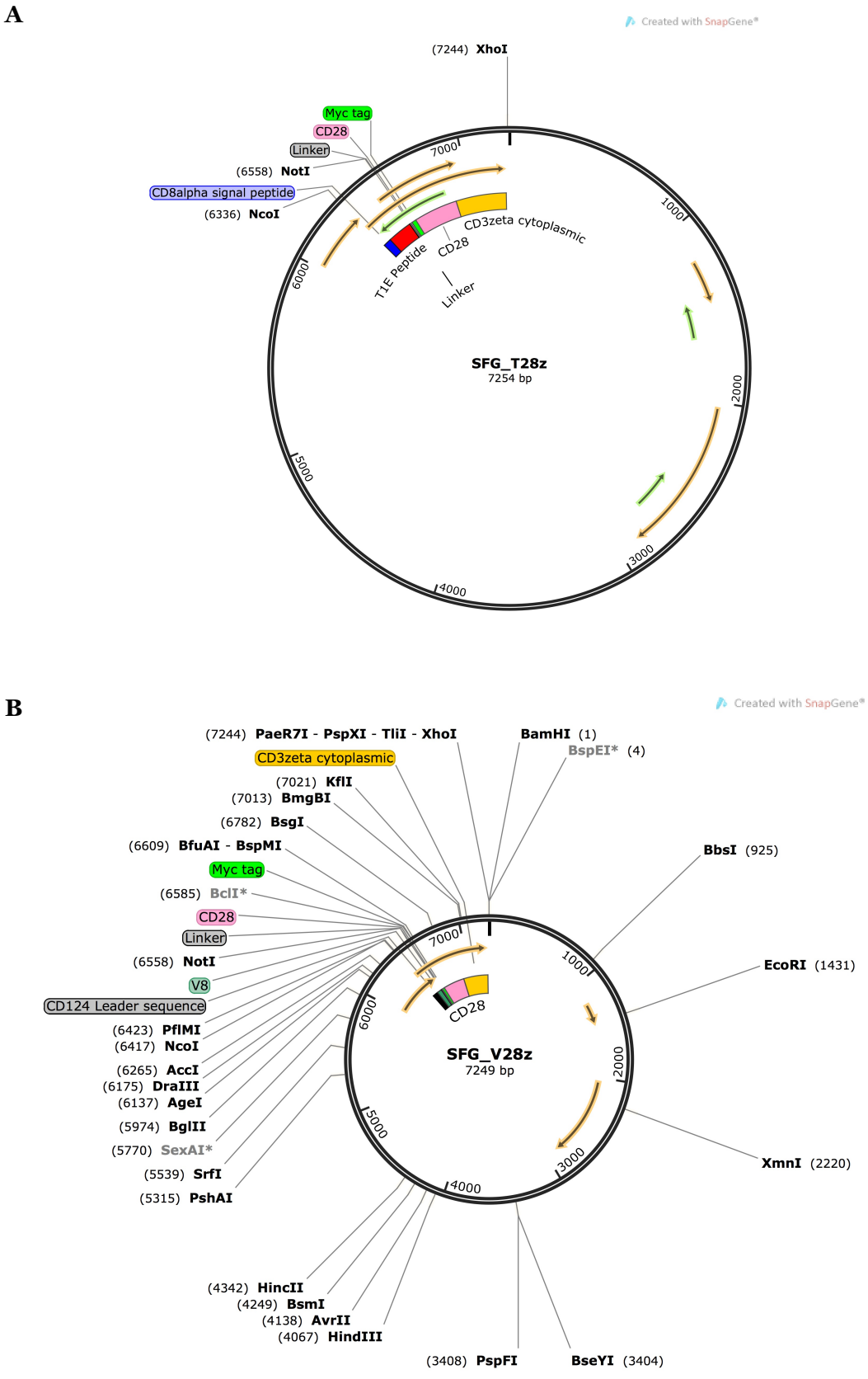

Figure 9-2. Circular plasmid maps of SFG T28z and V28z chimeric antigen receptors.
(A) Schematic depicting SFG T28z. **(B)** Schematic of SFG V28z. Key individual modules are shown along with unique restriction enzymes.

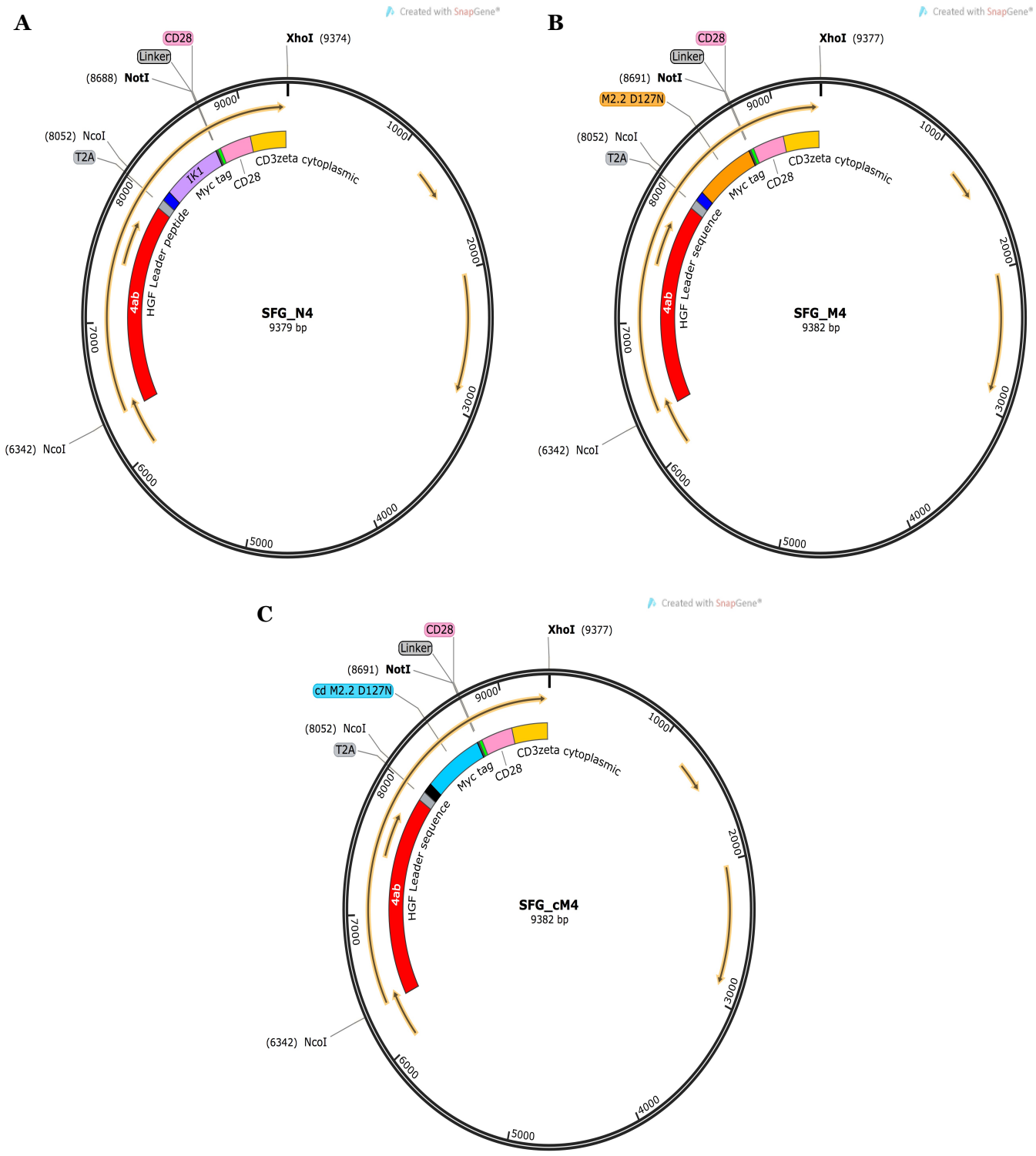

Figure 9-3. Circular plasmid maps of SFG 4αβ c-Met chimeric antigen receptors.
Schematic depicting **(A)** SFG N4, **(B)** SFG M4 and **(C)** SFG cM4. Key individual modules are shown along with unique restriction enzymes.

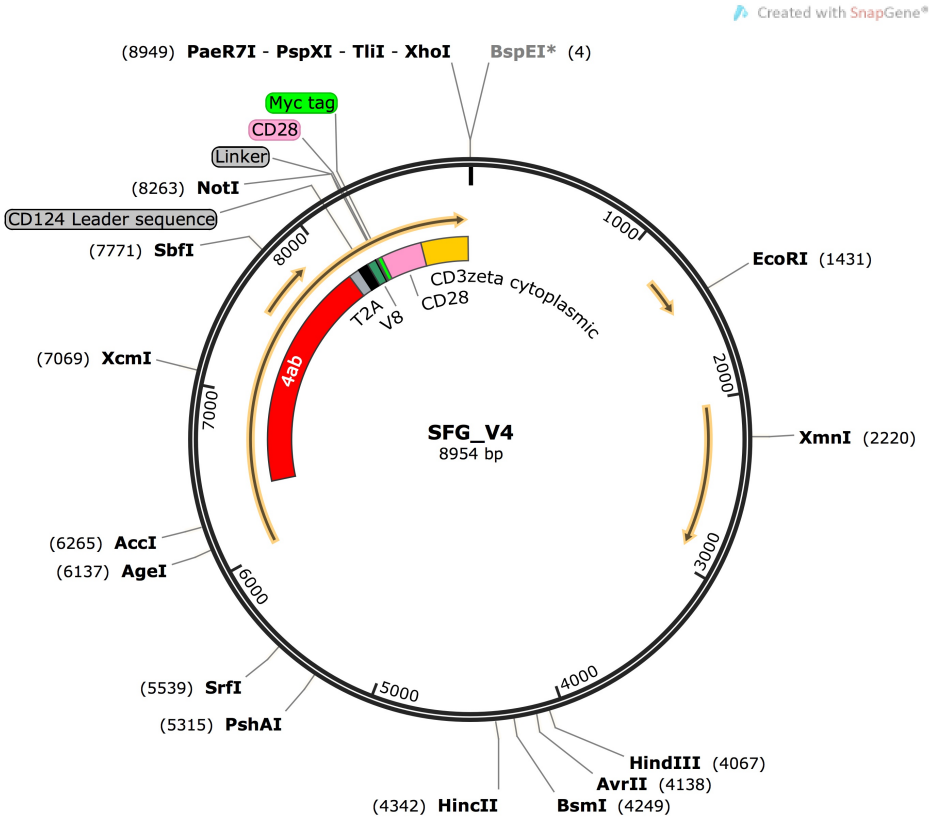

Figure 9-4. Circular plasmid map of SFG V4 chimeric antigen receptor. Key individual modules are shown along with unique restriction enzymes.

9.3 BLI images - *in vivo* therapeutic study

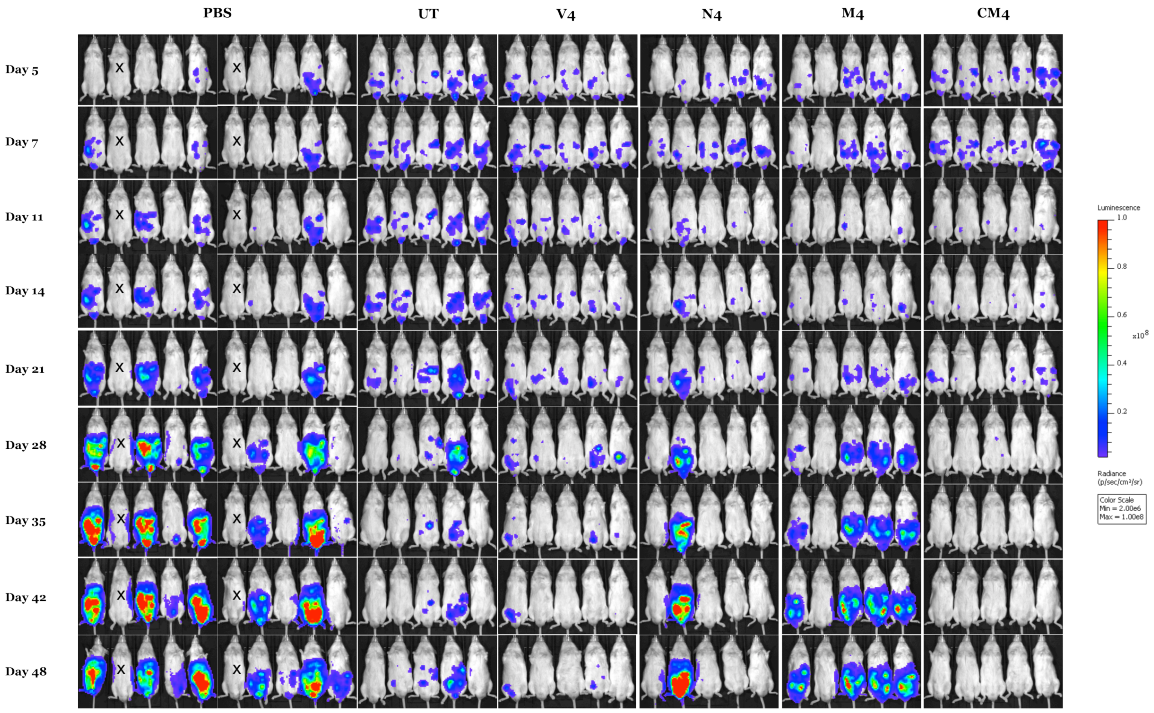

Figure 9-5. Bioluminescence imaging data for individual mice shown in Figure 6-9 – *in vivo* therapeutic study.
NSG mice were inoculated with 5 x 10^4 REN tumour cells intraperitonealy (IP) in 200µL PBS and tumours were allowed to grow over a time period of 7 days prior to T-cell administration (IP) of Day 8. Mice (each group n=5 except for PBS (n=8)) were treated with 10 x 10^6 UT, V4, N4, M4 or CM4 transduced T-cells. Control animals (PBS) were administered 200µL PBS to identify baseline tumour growth. Sequential BLI of tumour size (as total flux (p/s)) prior to (Day 5 and Day 7) and after (Day 11 onwards) T-cell administration. The data from each group over every given time point is presented on the same scale. x indicates mouse devoid of tumour. The luciferase enzyme present within the tumour cells allowed tumour growth to be monitored over the indicated timeframe by bioluminescence imaging (BLI). The images gained for each time point were analysed using Living Image 3.1 software. The level of luminescent signal released by each mouse was calculated by drawing a region of interest (ROI). The software automatically calculated the level of photon release within the ROI and this was standardised to account for the size of ROI and scan duration.